UNIVERSITE SULTAN MOULAY SLIMANE

Faculté des Sciences et Techniques

Béni-Mellal

Centre d'Études Doctorales : Sciences et Techniques

Formation Doctorale : **Mathématique et Physique appliquées**

THÈSE

Présentée par

BELBSIR HAMZA

Pour l'obtention du grade de
DOCTEUR

Spécialité : **SCIENCES POUR L'INGENIEUR**

Option : ***Matériaux et*** **MECANIQUE DES FLUIDES**

Rheology and modeling the flow behavior of phosphate slurry, transported via Pipeline and its derivatives products

Soutenue le Samedi 05 Septembre 2020 à 10h30mn devant la commission d'examen :

Pr.MOHAMED TALEA	Professeur, Université Hassan II Ben M'Sik, Casablanca, Maroc.	Président
Pr.AHMED ERRKIK	Professeur, Université Hassan1er F.S.T.Settat , Maroc	Rapporteur
Pr. ASSIA BAKALI	Professeur, Ecole Royale Navale de Casablanca, Maroc	Rapporteur
Pr.SANAA HAYANI-MOUNIR	Professeur, Université Sultan Moulay Slimane, F.P Khouribga, Maroc	Rapporteur
Pr.HAMID MAZOUZ	Docteur, Office Chérifien de Phosphate, EL Jadida, Maroc	Invité
Pr.ABDELAZIZ SOUFI	Professeur, Université Sultan Moulay Slimane, E.N.S.A Kouribga, Maroc	Co-Directeur de thèse
Pr.KHALIL EL HAMI	Professeur,Université Sultan Moulay Slimane, F.P Khouribga, Maroc	Directeur de thèse

Acknowledgement

I would like to express my most sincere gratitude and my deepest appreciation to my advisor Prof. Dr. Khalil EL-HAMI who has guided and supported me in both research and life through my Phd program. He has never stopped giving me advices and fruitful discussion that held me through all the difficulties during my years pursuing Ph.D.

Many thanks go to my co-supervisor Prof. Dr. Aziz SOUFI for his advices and guidelines.

I wish to thank my dear parents who have supported me throughout my academic career; I thank them for their support and for their encouragement from the beginning to this success.

I express my gratitude to Dr. Hamid MAZOUZ, Senior researcher in the Group (OCP) in Eljadida city, for accepting me to do my training of six months in his department.

I do not forget to thank all persons contributed either near or far to the success of this thesis.

Table of contents

CHAPTER 4: EXPERIMENTAL AND MODELING STUDIES OF THE RHEOLOGICAL BEHAVIOR OF THE PHOSPHATE-WATER SLURRY, WITH AND WITHOUT ADDITIVES, FOR A SUITABLE MODEL DESCRIPTION

CHAPTER 5: CHARACTERIZATION AND RHEOLOGY OF MOROCCAN PHOSPHATE'S DERIVATIVES: PHOSPHOGYPSUM SLURRY AND SLUDGES

List of tables

Chapter 1

Chapter 2

Chapter 3

Chapter 4

Chapter 5

Chapter 6

List of figures

Chapter 1

Chapter 2

Chapter 3

Chapter 4

Chapter 5

Chapter 6

General Introduction

The transport of materials through pipelines has recently undergone a great evolution due to the economic and environmental advantages offer. This mode of transport requires a lot of studies and research to fully understand and control the mechanisms related to the transport of slurries through pipelines. Those slurries or pulps are generally mixtures of fine solid particles and a carrier solvent (generally water). For this purpose, we carried out extensive bibliographical research on the flow of ore-based slurries in pipelines and, also, research on the rheological studies of various existing slurries the literature. This to reach certain synthesis and methods that may inspired us to carry out theoretical and experimental studies on the flow and rheology of phosphate slurry and its derivatives products, which are the Phosphogypsum slurry, Phosphoric sludges and Phosphoric acids. The first step with which we started is a modeling of the head losses behavior along the Khouribga-Jorf-Lasfar pipeline, in order to have a theoretical model of modeling and simulation. This theoretical model, will allow us thereafter to present perfectly the impact of the Pipeline operating Parameters and the physical properties of the phosphate slurry on the behavior of the flow.

The second step is the physical characterization and the rheological study of the phosphate slurry, and this by elaborating an in-depth study on the impact of physicochemical parameters on the viscosity and on the flow profile of the phosphate slurry. During this study, we carried out investigations on the effect of solid concentration of the slurry, the particle size distribution and the temperature on the rheology of the phosphate slurry. We performed studies on the effect of additives such as flocculants, Esters, Amines and dispersants on the rheological behavior of the slurry. Concerning the modeling of the rheological behavior of phosphate slurry, we tried to adjust the rheological profiles obtained experimentally to the rheological empirical model of Casson, Bingham, Power Law and Hershel-Buckley in order to identify the most accurate model to describe the rheological behavior of the phosphate slurry, for the purpose to identify the values of viscosity and yield stress relative to each model.

The phosphate slurry when it reached Jorf-Lasfar industrial platform, the processes started the chemical valorization to manufacture the phosphoric acid and fertilizers. Firstly, this slurry undergoes attack with sulfuric acid to dissociate the Fluorapatite contained in the phosphate and release the phosphorus in the form of phosphoric acid. This attack generates a “Phosphogypsum-Slurry”, which is a mixture between crystals of dehydrated calcium sulfate ($Ca.SO_4.2H_2O$) and phosphoric acids 29% in P_2O_5. This effect aroused our curiosity to conduct rheological studies on

the mentioned mixture which is, also, called "Phosphogypsum-slurry". In the reaction medium (attack thank) the viscosity of the Phosphogypsum-slurry should be minimal to facilitate the mobility of sulfate ions (SO_4^{2-}) and calcium ions (Ca^{2+}) to form calcium sulfate well. If the viscosity is minimal, it will facilitate the development of ($Ca.SO_4.2H_2O$) nucleons into large size gypsum crystals and this to make the phosphoric acid-Phosphogypsum filtration operation easy. Through the completed experiments, we explored the effects of the solids concentration, the size of the crystals, the temperature and the chemical composition on the rheology of the Phosphogypsum-slurry without neglecting the generated sludge. A modeling of the rheological profiles was, also, obtained experimentally via empirical rheological models.

The phosphoric acids, the Phosphogypsum-slurry and their sludges, undergo flows in pipes as suspensions. The knowledge of their rheological behaviors is primordial. In general, rheological studies applied to this type of materials still not study and there are no much reports in the literature. This gave us the privilege of being the first who's carried out studies on the flow of phosphate slurry and its by-products. Those products are, for examples, the "Phosphogypsum-Slurry", the phosphoric acids in various types and the phosphoric sludges which are the precipitates generated during the storage and concentration of phosphoric acid.

Introduction générale

Le transport des matériaux à travers les pipelines à connue récemment une grande évolution grâce aux avantages économiques et environnementaux dont ils disposent. Ce mode de transport nécessite énormément d'études et de recherches pour bien comprendre et contrôler les mécanismes relatifs au transport des pulpes à travers les pipelines. Ces pulpes sont en général des mélanges entre les particules solides très fines et un solvant porteur (en général l'eau). Pour cela, nous avons réalisé des recherches bibliographiques approfondies sur les écoulements des pulpes à base de minerais dans les pipelines. Des recherches sur des études rhéologiques de certaines pulpes existantes dans la littérature ont été ainsi effectuées. L'objectif est d'aboutir à certaines synthèses et méthodes, qui peuvent nous inspirer d'effectuer des études théoriques et expérimentales sur l'écoulement et la rhéologie de la pulpe de phosphate et de ses produits dérivés à savoir : la bouillie ″Phosphogypse″, les boues phosphoriques et les acides phosphoriques.

La première étape s'intéresse à la modélisation du comportement des pertes de charges le long du pipeline liant la zone minière de Khouribga à la Plateforme industrielle Jorf-Lasfar. Nous avons pu obtenir un modèle théorique de modélisation et de simulation, qui nous permettra par la suite de bien présenter l'impact des paramètres de marches et des propriétés physiques de la pulpe de phosphate sur le comportement de l'écoulement.

La deuxième étape est consacrée à la caractérisation physicochimique et à l'étude rhéologique de la pulpe de phosphate. Nous avons mené une étude approfondie des paramètres physicochimiques influençant la viscosité et le profil d'écoulement de la pulpe de phosphate. De plus, nous avons étudié l'effet de la concentration en solides dans la pulpe, la distribution granulométrique des particules et la température sur la rhéologie de la pulpe de phosphate. Nous avons réalisé ainsi des études sur l'effet des additifs tel que le floculant, les esters, les amines et les dispersants sur le comportement rhéologique de la pulpe. Concernant la modélisation du comportement rhéologique de la pulpe de phosphate, nous avons ajusté les profils rhéologiques obtenus expérimentalement aux modèles empiriques rhéologiques de Casson, Bingham, Power Law et Hershel-Buckley pour identifier le modèle adéquat à la description du comportement rhéologique de la pulpe de phosphate. Cette modélisation nous a permis d'élaborer les valeurs de viscosité et le seuil d'écoulement correspondants à chaque modèle.

La pulpe de phosphate, lorsqu'elle atteint la plateforme industrielle de Jorf-Lasfar, elle rentre dans des procédés de valorisation chimique pour fabriquer l'acide phosphorique et les engrais à partir de cette pulpe. La première étape que subit cette pulpe est l'attaque par l'acide

sulfurique pour dissocier la Fluorapatite contenu dans le phosphate. Cette attaque permet de libérer le phosphore sous forme d'acide phosphorique en générant une bouillie, qui est un mélange des cristaux de sulfate de calcium di-hydratée ($Ca.SO_4.2H_2O$) et d'acide phosphorique 29% en P_2O_5. Cela a éveillé notre curiosité pour effectuer des études rhéologiques sur ce mélange appelé aussi « Bouillie de Phosphogypse ». Dans le milieu réactionnel s'agissant de la cuve d'attaque, la viscosité de la bouillie doit être minimale pour faciliter la mobilité des ions sulfate (SO_4^{2-}) et des ions Calcium (Ca^{2+}), et la formation de sulfate de calcium. La viscosité doit être minimale pour favoriser le développement des nucléons de ($Ca.SO_4.2H_2O$) en cristaux de gypse de grosses tailles, pour faciliter l'opération de filtration d'acide phosphorique du phosphogypse. Nous avons réalisé des expériences pour déceler l'effet la concentration en solides, la taille des cristaux, la température et la composition chimique sur la rhéologie de la bouillie et des boues générées. Des modélisations des profils rhéologiques obtenus via les modèles empiriques ont été ainsi élaborées.

Les suspensions, à savoir, les acides phosphoriques, leurs boues et bouillies, subissent des écoulements dans des conduites. La connaissance de leurs comportements rhéologiques et primordiale. En général, des études rhéologiques appliquées à ce type de matériaux sont dépourvues dans la littérature, ce qui nous a donné le privilège d'être les premiers à entamer la recherche scientifique sur l'écoulement et la rhéologie de la pulpe de phosphate et de ses dérivés. Ces produits sont la bouillie « Phosphogypsum-Slurry », les boues et les acides phosphoriques avec toutes ses compositions.

Chapter 1

TRANSPORT OF MATERIALS IN THE FORM OF SLURRIES THROUGH PIPELINES

1. Introduction on transport through Pipelines

The pipeline is generally in the form of a cylindrical pipe made of a robust material to resist wear and friction during the flow, it allows the transport of fluid materials over great distances, this mode of transport is carried out by means of pressurized tubes and accessories, constituting a system often in a network.

The products often transported by pipelines are fuels (petroleum, hydrocarbons, natural gas ...), chemicals and food products, and ores in the form of slurries (combustible coal slurry, sand slurry, limestone slurry and phosphate slurry which we have interest in this thesis. Without forgetting the gravitational evacuation of effluents (wastewater, rainwater, ...) or the supply of water in a hydraulic structure, this is also done through pipelines.

Nomenclatures are associated to pipelines according to the nature of the products they transport, for gas pipelines it is called ‘gazoduc’, oil pipelines are called ‘oleoduc’, ore pipelines are called ‘mineroduc’.

2. Definitions

2. 1. Slurry

A slurry is a mixture or suspension of any liquid combined with solid particles in various rate. When slurry reaches its destination, the material is separated from the water before further processing. Some key elements are the size, nature of the solids in the liquid shape and quantity of the particles together with the nature of transporting liquid determine the exact characteristics and flow properties of the slurry.

Depending on the particle size, distribution, concentration, and character of solids, the slurry can be broadly divided into the two general groups:

* non-settling for very fine particles which can form stable homogeneous mixtures. When fine solids are present in the slurry in sufficient quantity to cause this change in behavior away from a normal liquid, they are referred to as being non-Newtonian.

* settling slurries are formed by coarser particles and tend to form an unstable mixture and have higher wearing properties. These coarser particles and form the majority.

2. 2. Slurry pump

A slurry pump is equipment for pumping liquid containing solid particles. There is a large number of differing pump types used for pumping of slurries designed and constructed for each kind of slurry. The most common slurry pump is the centrifugal pump which uses the centrifugal

force generated by a rotating impeller to impact kinetic energy to the slurry, similar to how a water-like liquid would move through a standard centrifugal pump.

3. Examples of materials transport in pipelines

3.1 - Oil pipeline

Oil pipelines or "Oleoduc" are intended for the transportation of crude oil from the places of exploitation to refineries or ports, and may also be dedicated for the transportation of other petroleum-derived hydrocarbons **[100]**. This mode of transport of oil is generally over long distances. Figure (1) shows a photo of the Prudhoe Bay ('Alaska' USA) and Valdez ('Alaska' USA) oil pipeline over a length of 1300 km.

Figure 1: Pipeline linking Prudhoe Bay to Valdez, (Alaska).

3.2 – Gaz pipeline

As their name implies, gas pipelines or "gazoduc" are dedicated to the transport of gaseous materials. The gaseous products transported through the "pipelines" are numerous, but the transport of natural gas fuel via pipeline is most frequently. Figure (2) shows the distribution network of Algerian natural gas to Morocco, and to Spain and Italy crossing the Mediterranean Sea, it is known under the name "Trans-Mediterranean Pipeline".

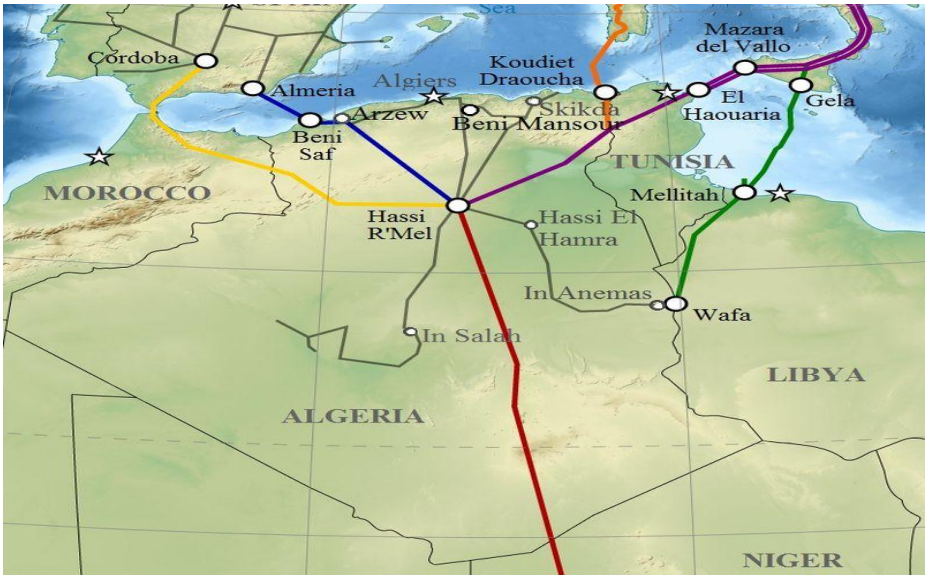

Figure 2: Algerian natural gas distribution network "Trans-Mediterranean Pipeline".

3.3 - Ore Pipeline

"Mineroduc" are pipelines designed for the transport of ores in the form of slurry (water-ore mixture), this mode of transport has undergone a great evolution at the world level because of their economic, logistical and environmental advantage.

Among the mining substances transported through pipelines in the form of slurry, we can mention the coal-water slurry (CWS), the limestone slurry, the sand slurry and the phosphate slurry which is the subject of this thesis. Figure (3) shows the pipeline for transporting phosphate-water slurry from the Khouribga mine (Morocco) to the industrial platform of Jorf-Lasfar (Morocco) over a length of 187 km.

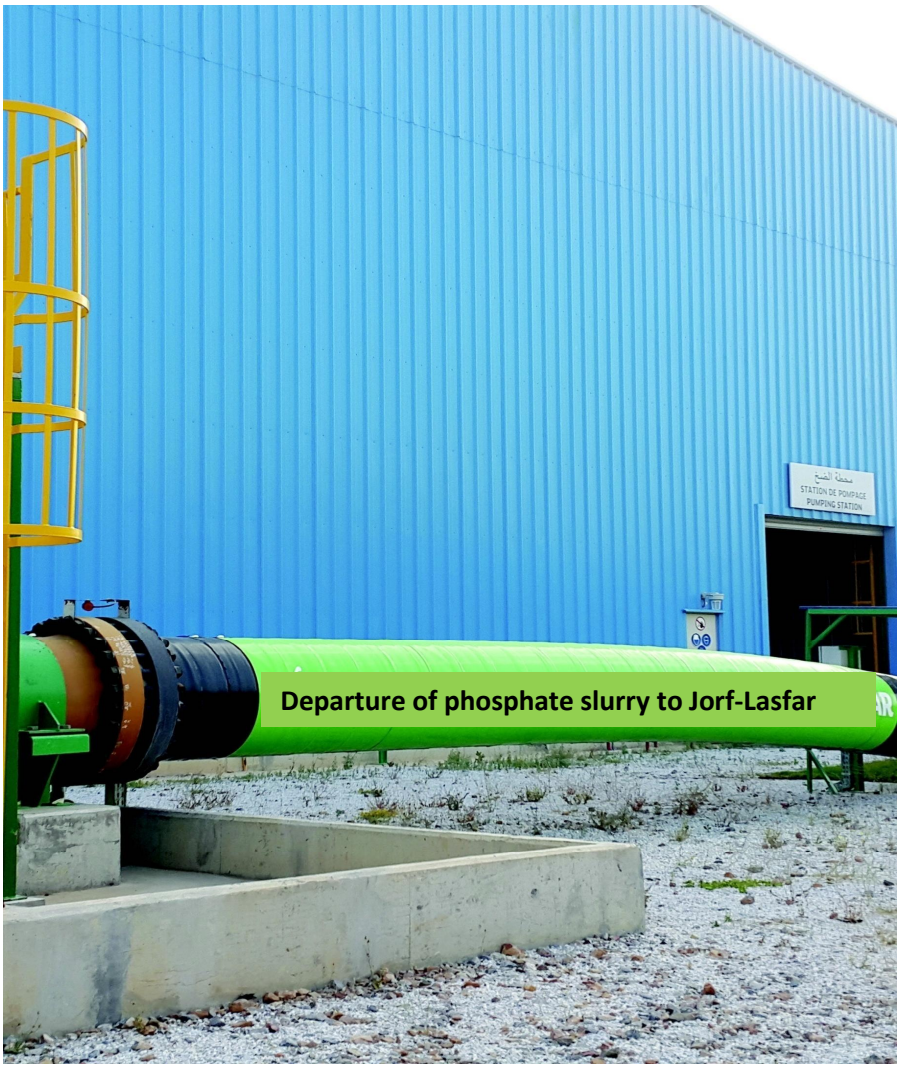

Figure 3: pipeline of transport of the phosphate slurry (Group OCP)

4. Case of Phosphate slurry Transport in Pipeline

4.1. Presentation of the Slurry Pipeline project

The leader in its field (OCP) has invested 4.5 billion dirhams on this hydraulic installation to increase current production from 18 million tons / year to 38 million tons / year, while reducing transportation costs, a drop costs of 90% (the cost of loading for transport by the (Oncf) without forgetting the installation congestion.).

The installation, which consists of transporting the phosphate slurry from the washing plants, will result in the following gains for the group:

- An energy gain of 1000GWH (the progression of the pulp is favored by the natural gravity).
- Nearly 3 to 4 million m3 of water per year (elimination of the drying phase).

● Significant environmental benefits by avoiding the emission of 900,000 tons of CO2 / year (15 furnaces: 8 in services + 3 reserves with a fuel by heat (Coke-Fuel) and a hot air oven).

● The pipeline will allow, in addition to the export from Jorf Lasfar, the release of tonnage transiting to the port of Casablanca.

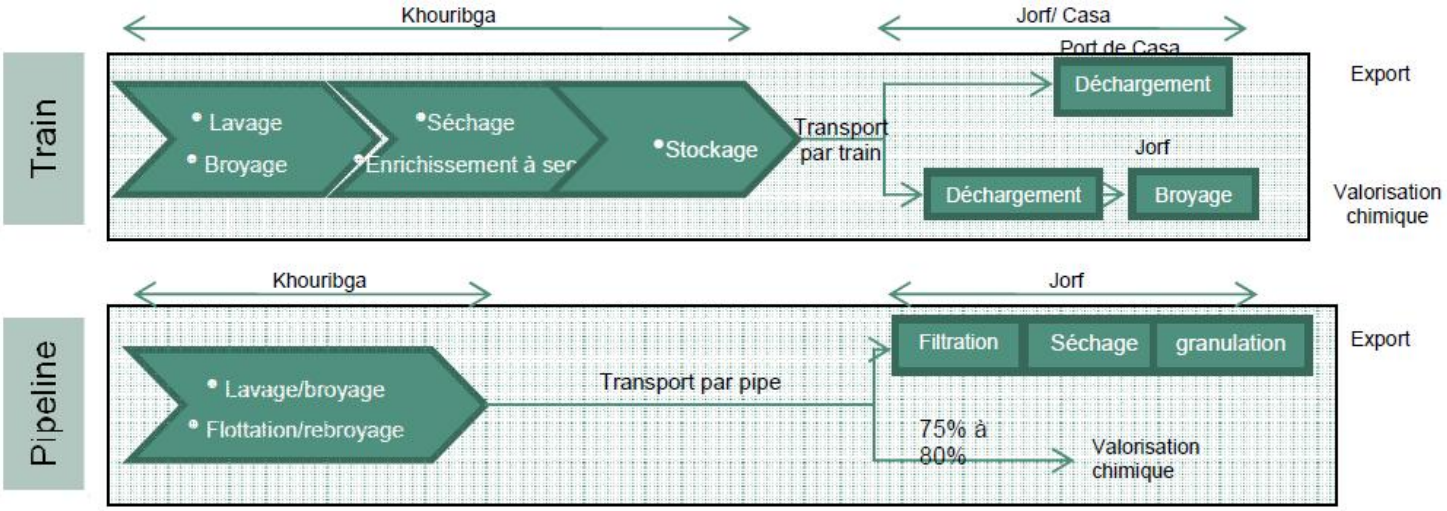

Figure 4: Phosphate Transport by Train & Pipeline

4. 2. Pipeline System Components

The rugged stainless steel pipeline is protected by internal and external lining in addition to cathodic protection against corrosion. It crosses 3 provinces Khouribga, Settat and Jorf Lasfar, 23 rural communes and an urban commune, with a length of 235 kilometers (including secondary pipelines) and a right of approximately 150,8 ha of which:

- 187 km for the main axis with a diameter of 900mm buried to a depth of 2m in order to transport the phosphate pulp from the head station to Khouribga to the terminal station in Jorf Lasfar.
- 4 secondary pipelines of 48 km linking the washing plants to the Khouribga head station for the transport of slurry including:
  • 22km between the 'Daoui' washing plant and the head station with 450mm diameter.
  • 2km between 'Mea' washing plant and Head Station with 300mm diameter for high grade and 2km with 400mm diameter for low grade.
  • 15km between El Halassa laundry and the head station with 500mm diameter.
  • 10km between the head station and Ouled Fares with 500mm diameter. (in progress)
- Washing plants whose function is to enrich the phosphate and prepare it for transport via (Slurry Pipeline):

• MRAH / MEA (12Mt / year) already in production.

• DAOUI (6Mt / year) already in production.

• OULAD FARES (14Mt / year) under construction.

• HALASSA (12Mt / year) already in production.

- The installation of a pumping station to overcome the slope of the first 30 km, and guarantee the flow of slurry to Jorf lasfar.

- Three storage tanks for the slurry at the exit of the Daoui and El Halassa washing plants with a capacity of 6,300 m3 each.

- A valve station and 4 other intermediate pressure control stations installed every 40 km to provide live pressure data needed by the control system.

- A head station located near the MEA washing plant linked directly to the 4 washing plants by the secondary pipeline system of 48 km and 187 km at the terminal station in Jorf Lasfar. The latter has 4 tanks in addition to the main pumping station. This station, whose function is to liaise with the terminal station of Jorf Lasfar.

- A terminal station in Jorf Lasfar to complete the distribution of the slurry. It consists of 8 tanks with a control system.

- A treatment system consisting of filtration, drying and pelleting units for the slurry intended for export at Jorf Lasfar, called: Downstream

- A Control and Data Acquisition System -SCADA-.

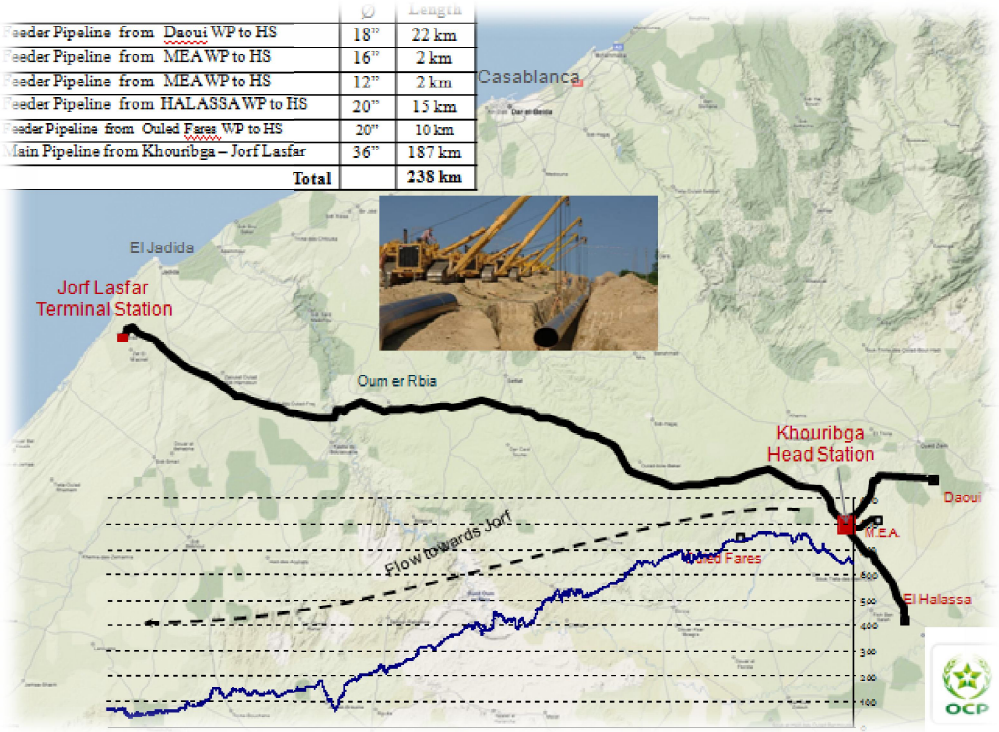

Figure 5: Map and Basic Components of the Pipeline System

We recall that these installations and these large-scale projects are carried out over a total area of 235 linear kms linking Khouribga to Jorf Lasfar. It was necessary to deal with multiple interfaces (ONCF, ADM, ONEP, ONEE, Watershed Agency and landowners) for its realization.

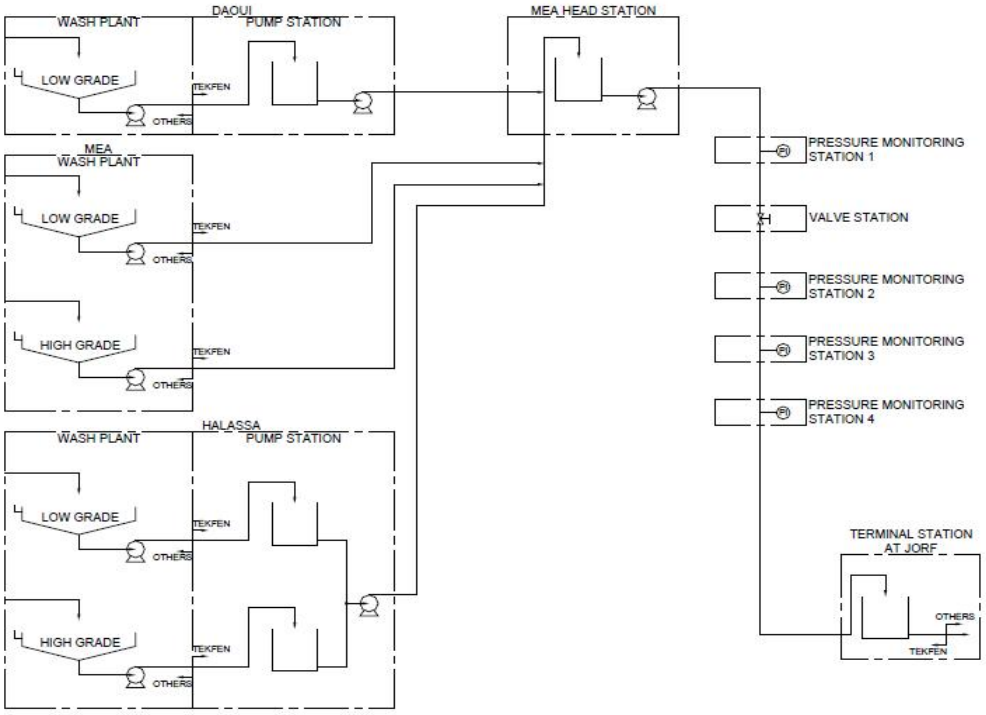

Figure 6: Basic Components and Links of the Pipeline System

4. 2. 1. The tanks

The tanks, contains at the bottom agitators so that the slurry always remains in movement; because the phosphate grains and the water do not interact chemically (the phosphate is insoluble in water), then the phosphate grains sediment downwards and the water will stabilize at the top, then without agitator we will have a clogging at the tank level, the capacity of each tank is 6300 m^3.

Figure 7: photo of the agitator at the bottom of the tank

4. 2. 2. Centrifugal slurry pumps

Centrifugal slurry pumps work in the same way as water pumps; the slurry pumps have been modified to handle abrasive solids and to provide adequate wear resistance.

Figure 8: photo of centrifugal slurry pumps

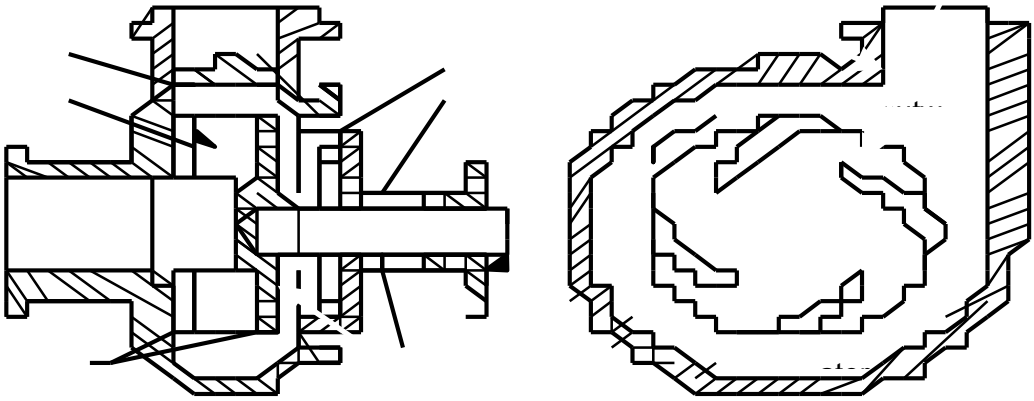

Figure 9: Centrifugal pump

The maximum technical data written on the nameplates of centrifugal slurry pumps:

Flow rate: 5000 m^3/H ; pressure: 56 bar

Manometric height (Head): 51,5 m ; velocity of rotation : 406 tr/min

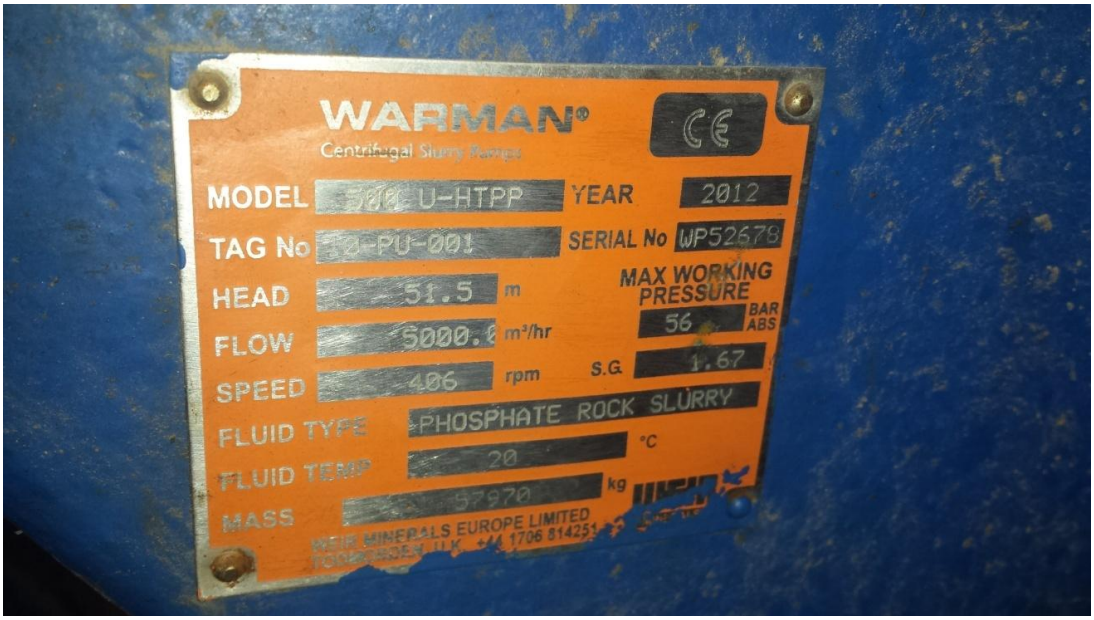

Figure 9: Nameplate of the centrifugal pump

For high pressure, a pump alone is not enough, that is why several pumps are then put in series in a pumping station. Multiple pump stations may be needed where pressures are very high. High pressure pumps can be used to increase the output of a single pump station.

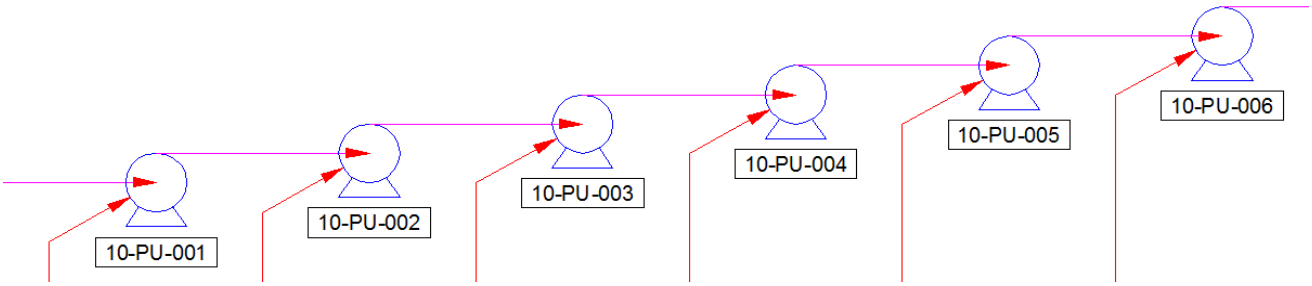

Figure 10: The six centrifugal pumps mounted in series

Results	***Discharge pressure of the slurry pump***					
	stage1	*stage 2*	*stage 3*	*stage 4*	*stage 5*	*stage 6*
Maximum result	785 kPa	1570 kPa	2355 kPa	3140 kPa	3925 kPa	4710 kPa
Min Result	500 kPa	1000 kPa	1000 kPa	1000 kPa	1000 kPa	1500 kPa

Table 1: Table showing the pressure that each pump associates to the slurry

Pipeline	Longueur en Km	Débit en m^3/h	Acier	Diamètre extérieur	Epaisseur	HDPE	Pression	Nbre de pompes (+ réserve)
Daoui à St de tête	22	932	API 5L B35	16''	0.25''	0.375''	27 Bar	3+3
MEA à St de tête (low grade)	0.8	982	API 5L B35	16''	0.25''	0.375''	5 Bar	1+1
MEA à St de tête (high grade)	0.8	517	API 5L B35	12''	0.25''	0.25''	5 Bar	1+1
O.Fares à St de tête	10	1642	API 5L B35	20''	0.25''	0.375''	24 Bar	3+3
Halassa à St de tête	15	1420	API 5L B35	20''	0.25''	0.375''	42 Bar	5+5
Pipeline Principal	187	5023	API 5L X70	36''	0.434''	0.875''	49 Bar	6+6

Table 2: OCP Pipeline Technical Characteristics

- The washing plants

Phosphate slurry milled, thickened and stored in laundries; it is then pumped via secondary pipelines to the slurry collection station (head station). These pipes feed the main pipeline before it arrives at the Jorf Lasfar industrial site and in particular at the terminal station. The latter is equipped with storage tanks implemented for the reception and distribution of the phosphate slurry.

4. 2. 3. Head station

At the head station, the ore is received through the Daoui feed line, the two MEA feed lines and the El Halassa feed line. In the future, the ore will also be received through the Oulad Fares feed line.

Figure 11: Pipelines from washing plants

The Daoui line goes through the throttling station which aims to regulate the pressure (Increase or Decrease) before going to Tanks.

Figure 12: Throttling station (choke station)

The ore in each pipeline is diverted to one of the two groups of tanks by opening or closing the corresponding valves in a pipe collector system. At the head station, the ore received is stored in two groups of tanks. From the head station, different grades of ore are pumped neatly through the main pipeline to the Jorf Lasfar terminal station. The ore received from the feed stations can be directed to each of the two manifolds, by opening or closing the corresponding valves in a pipe collector system. The operation of the head station is based on the actual contents of the tank. The emptying of the tanks is prioritized according to the levels and the flow arriving towards the head station. Generally, emptying begins only when a tank is full and continues as much as possible. This maximizes the phosphate batch time and minimizes the need for water buffers (batch). The batches in each category are separated by a 5-minute water buffer.

Figure 13: Phosphate slurry stirred in a tank

The discharge line of each tank is connected to the suction head of the pump. The suction head sends the ore to each of the two pumping trains.

A test loop is installed to determine the hydraulic gradient (head losses), whether the slurry should be pumped or not, if the hydraulic gradient measured at the test loop is very high, that says that the slurry is not in the standards to be pumped into the pipeline and it can caused clogging.

Figure 14: Photo of test loupe

Once the slurry passed through the test loop, it is found in the main pump station equipped with 12 large horizontal centrifugal pumps (6 running at a time) connected in series.

The main ore pumps through which the slurry passes before the discharge serve to overcome the pressure drop along the main pipeline. They ensure a pumping rate between 3800 and 4400 m^3 / h and a starting pressure of 3758 Kpa. The pumping station consists of two ore pumping trains. Only train runs at any time whereas the others are paused. Each train includes six high-power ore pumps installed in series.

Figure 15: Centrifugal pumps in series

4. 2. 4. Control and Data Acquisition System (SCADA)

For the entire pipeline route, the main telecommunication leg is provided by an optical fiber link installed along the pipeline. This fiber optic link provides remote data, telephony, data and video images for all installations. Automatic, manual and maintenance modes, and local or remote control of equipment. To enable operators to manage, monitor and operate all operations, the pipeline is equipped with a control and data acquisition system (SCADA).

4. 3. Identification of the flow mode

The studied fluid is in the form of phosphate slurry, which is a mixture between very fine grains of phosphate and water. The mixture remains heterogeneous since the solid and liquid phases do not interact chemically.

Paramètre	Valeur
Densité solides	3.0 t/m^3
Concentration	60%m
Densité de la pulpe	1.7 t/m^3
pH de la pulpe	8.0
Porosité	20%
P80 P20	160 µm 44 µm
Distribution des particules par dimension	-250 µm 100% -210 µm 96.6% -150 µm 74.0% -74 µm 30.8% -53 µm 21.9% -44 µm 20.4% -37 µm 16.8%
Élasticité	55%m 1.56 Pa 58%m 2.67 Pa 60%m 3.8 Pa
Viscosité plastique	55%m 6.6 x 10^{-3} Pa.s 58%m 8.5 x 10^{-3} Pa.s 60%m 10.2 x 10^{-3} Pa.s

Table 3: Physical Characteristic of the Phosphate slurry

The problem that exists is the need for the slurry to remain always agitated (in movement) so that the slurry does not sediment down, the sedimentation of the solid particles downwards will cause a creation of a bed in the pipeline. To avoid the sedimentation of phosphate, turbulent flow must be used to suspend solids so that they can be carried away by the flow of the liquid.

In case of low speed, the solid bodies are deposited at the bottom of the pipe: formation of a stationary deposit ("established bed"):

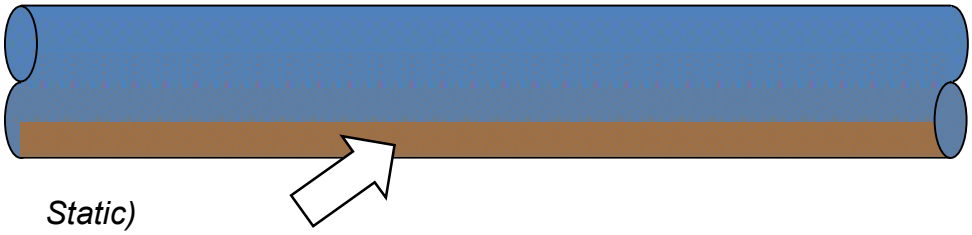

If the speed becomes even lower, the thickness of the established bed increases:

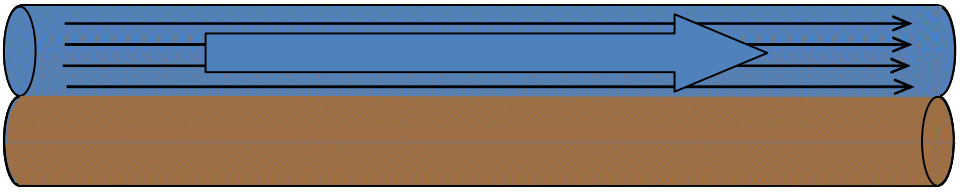

Laminar

Hence the need to operate pipeline in turbulent mode, turbulence keeps the solid grains in suspension:

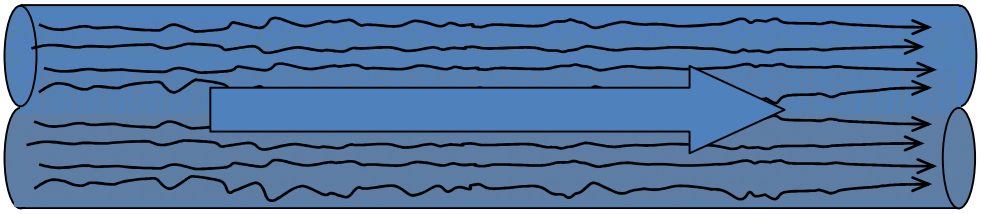

Turbulent

The velocity must be large enough that the intensity of the turbulence is able to keep the solid grains of phosphate in suspension and in motion.

Experimental studies have been conducted to establish the flow velocity at which phosphate grains begin to settle. This study consists of varying the concentration of solid phosphate in the slurry. Thus, we can mark the flow velocity at which grains are deposited for each concentration. The results of these studies are represented on the following curve:

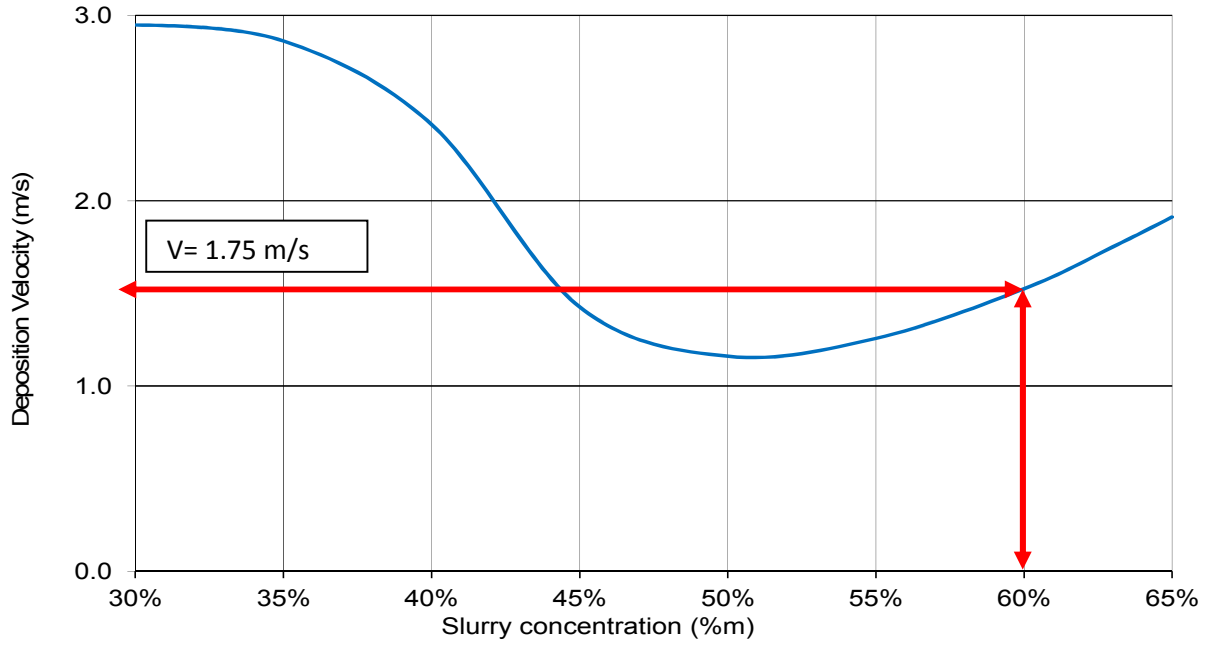

Figure 16: Characteristic curve of deposition of phosphate grains during flow.

The phosphate slurry transported by the pipeline has a concentration of **60%** solids. This corresponds to a minimum specific deposition flow velocity of **V = 1.75 m / s**.

This velocity is equivalent to a volume flow of: **Q = S × V**.

S = πD² / 4: surface of the pipeline crossed by the slurry.

D: diameter of the main pipeline which are of the order **D = 855 mm**.

The velocity of V = 1.75 m / s corresponds to a flow rate of **Q = 3560 m3 / h** and which represents the minimum flow rate so that there will be no deposition of the phosphate grains.

This flow rate corresponds to a Reynolds number: **Re = (ρVD / μ) = 234705**

Knowing that the dynamic viscosity μ = 0.0102 Pa.s and the density ρ = 1600 Kg / m3.

The Reynolds number **Re = 234705 >> 5000** therefore the turbulence is very intense, which is normal to keep the solid particles of phosphate in suspension.

5. Fluid mechanics applied to transport through pipelines

5. 1. Bernoulli's theorem

Considering the schema of the fluid vein with the following assumptions:

- The fluid is perfect and incompressible.
- The flow is permanent.
- The flow is in a perfectly smooth pipe. We consider a vertical Z axis directed upwards.

We denote Z_1, Z_2 and Z respectively the altitudes of the centers of gravity of masses dm_1, dm_2 and M.

F_1 and F_2 respectively denote the norms of the pressure forces of the fluid acting at sections S_1 and S_2.

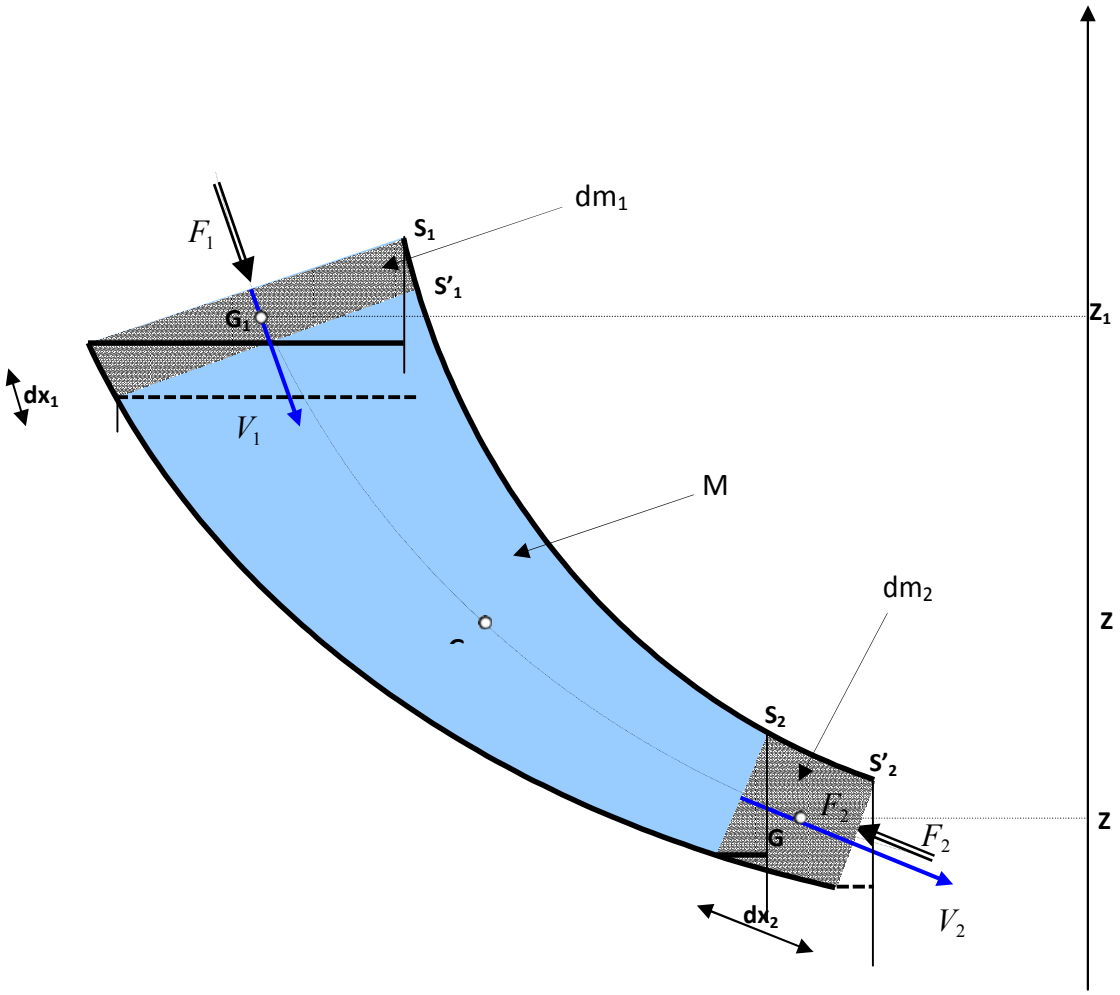

Figure 17: Schema of the fluid vein

At the instant (t) the fluid mass ($dm_1 + M$) is between S_1 and S_2. Its mechanical energy is:

$$E_{méc} = E_{pot} + E_{cin} = (dm_1.g.Z_1 + MgZ) + \frac{1}{2}.dm_1.V_1^2 + \int_{S1}^{S2} \frac{dm.V^2}{2}$$

At instant (t') the fluid mass ($dm_2 + M$) is between S'_1 and S'_2. Its mechanical energy is:

$$E'_{méc} = E'_{pot} + E'_{cin} = (dm_2.g.Z_2 + MgZ) + \frac{1}{2}.dm_2.V_2^2 + \int_{S1'}^{S2'} \frac{dm.V^2}{2}$$

The theorem of mechanical energy is applied to the fluid between t and t ': "The variation of the mechanical energy is equal to the sum of the work of the external forces"

$E'_{méc} - E_{méc} = W_{Forces\ de\ pression} = F_1.dx_1 - F_2.dx_2 \leftrightarrow E'_{méc} - E_{méc} = P_1.S_1.dx_1 - P_2.S_2.dx_2 = P_1.dV_1 - P_2.dV_2$

We simplify we get: $dm_2.g.Z_2 + \frac{1}{2}.dm_2.V_2^2 - dm_1.g.Z_1 - \frac{1}{2}.dm_1.V_1^2 = \frac{P1}{\rho 1}.dm_1 - \frac{P2}{\rho 2}.dm_2$

By conservation of the mass: $dm_1 = dm_2 = dm$ and since the fluid is incompressible $\rho_1 = \rho_2 = \rho$, we succeed to the Bernoulli equation:

$$\frac{V1^2 - V2^2}{2} + \frac{P2 - P1}{\rho} + g.(Z_2 - Z_1) = 0$$

We can write it also in the following form :

$$\frac{V2^2}{2} + \frac{P2}{\rho} + gZ_2 = \frac{V1^2}{2} + \frac{P1}{\rho} + gZ_1$$

5. 2. Conservation Law of the momentum and Navier-Stokes equation

We consider a homogeneous fluid, incompressible, with density ρ. The incompressibility of the fluid is presented by:

$$\vec{\nabla} \cdot \vec{u} = 0$$

Where $\vec{u}$ is the field of velocity.

Using the summation convention on repeated indices, the conservation of momentum is written as follow:

$$\frac{d\rho ui}{dt} = \frac{\partial \rho ui}{\partial t} + \frac{\partial \rho ui}{\partial xj}.u_j = \frac{\partial \sigma ij}{\partial xj} + f\,i$$

Where (σij) is the tensor of the stresses and (f i) the ith component of the resultant of the voluminal forces.

The fluid is assumed Newtonian, so that the stress tensor is a linear function of the velocity gradient (Shear rate). Taking into account the incompressibility, the constitutive law of the fluid is then written as follow:

$$\sigma ij = -p\delta ij + 2\mu\varepsilon ij(u)$$

Where μ is the dynamic viscosity coefficient and εij is the tensor of the strain rates defined by:

$$\varepsilon ij(u) = \frac{1}{2}\left(\frac{\partial ui}{\partial xj} + \frac{\partial uj}{\partial xi}\right)$$

We then obtain:

$$\left(\frac{\partial ui}{\partial t} + \frac{\partial ui}{\partial xj}.\mathrm{u_j}\right) = -\frac{\partial p\delta ij}{\partial xj} + 2\mu\frac{\partial \varepsilon ij(u)}{\partial xi} + f\,i$$

$$\left(\frac{\partial ui}{\partial t} + \frac{\partial ui}{\partial xj}.\mathrm{u_j}\right) = -\frac{\partial p}{\partial xi} + \mu\frac{\partial^2 ui}{\partial xj^2} + \mu\frac{\partial^2 uj}{\partial xj.\partial xi} + f\,i$$

By using the incompressibility of the fluid, it comes:

$$\rho\left(\frac{\partial ui}{\partial t} + \frac{\partial ui}{\partial xj}.\mathrm{u_j}\right) = -\frac{\partial p}{\partial xi} + \mu\sum_j \frac{\partial^2 ui}{\partial xj^2} + \mu\frac{\partial}{\partial xi}\sum_j \frac{\partial ui}{\partial xj} + f\,i$$

What is still written in tensorial form (Navier-Stokes equation):

$$\rho\left(\frac{\partial \vec{u}}{\partial t} + (\vec{u}.\vec{\nabla}).\vec{u}\right) = -\vec{\nabla}P + \rho\nu\Delta\,\vec{u} + \vec{f}$$

Where we put ν = μ / ρ, called kinematic viscosity [95-98].

5. 3. Calculation of the regular head losses and concept of piezometric line

The piezometric line (hydraulic grade line) is the linear function characterizing the hydraulic pressure losses along a pipe, these pressure losses are due to friction, and they are energy losses. This line describes the pressure drop depending on the distance.

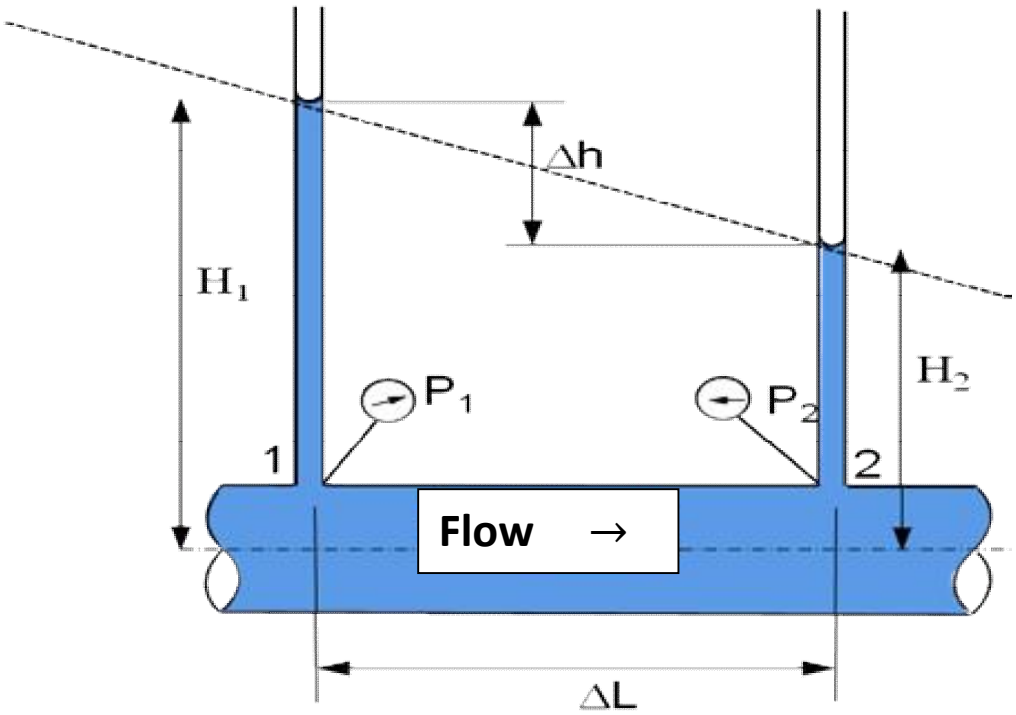

Figure 18: Head losses in a pipe

Bernoulli's theorem states that the relation between pressure and hydraulic head is:

Head (H) = P (Pressure) ÷ ρ (liquid density) × g (acceleration caused by gravity)

$$\mathbf{H} = \frac{P}{\rho \times g}$$ (with P is relative pressure)

The pressure drop between points 1 and 2 is: $\Delta P = P1 - P2$

The head losses between points 1 and 2 is: $\Delta h = H1 - H2$

The hydraulic gradient is the head losses divided by the distance traveled by the fluid : $\frac{\Delta h}{\Delta L}$

and : $$\frac{\Delta P}{\Delta L} = \frac{\Delta h}{\Delta L} \times (\rho \times g)$$

The coefficient $\frac{\Delta h}{\Delta L}$ represents the slope of the piezometric line, also called hydraulic gradient.

The slope of the piezometric line does not depend on the slope of the pipeline.

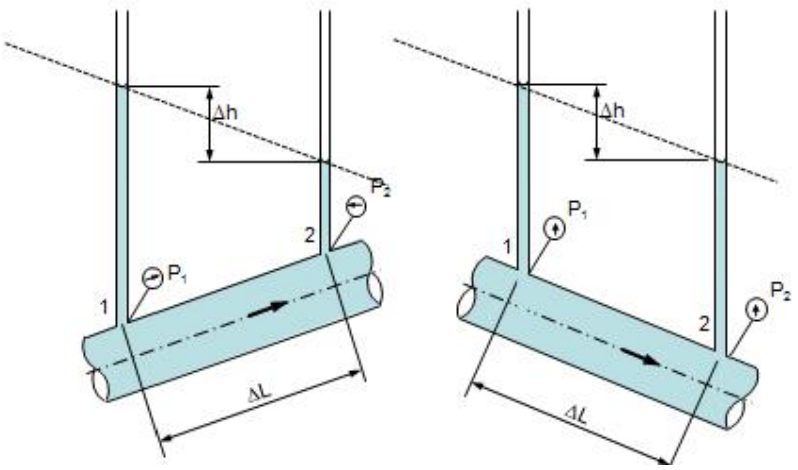

Figure 19: The hydraulic gradient does not depend on the inclination of the pipe.

In general the regular head losses depend on the type of flow, therefore it depend on the Reynolds number.

5. 3. 1. Coefficient of friction

$$\Delta P = f \frac{L}{D} \frac{1}{2} \rho V^2$$

To account for this energy loss, the corresponding pressure loss is introduced.

- L is the pipe length,
- D is the internal diameter of the pipe,
- ½.ρV^2 is the kinetic energy of the fluid
- f is the coefficient of friction of the pipe.

$$h = f \frac{L}{D} \frac{V^2}{2g}$$

The pressure drop is often used in equivalent fluid height, with $\Delta P = \rho g \Delta h$.

5. 3. 2. Laminar flow

For a laminar flow in a horizontal cylindrical pipe, the coefficient of friction is written as follow:

$$f = 64/Re$$

5. 3. 3. Turbulent flow

For turbulent flow, the Colebrook empirical equation allows the calculation of the coefficient f.

$$\frac{1}{\sqrt{f}} = -2\log_{10}\left[\frac{\varepsilon/D}{3.7} + \frac{2.51}{Re\sqrt{f}}\right]$$

This equation is an implicit equation that is not easy to manipulate; we will instead use the Moody diagram, drawn from the previous equation.

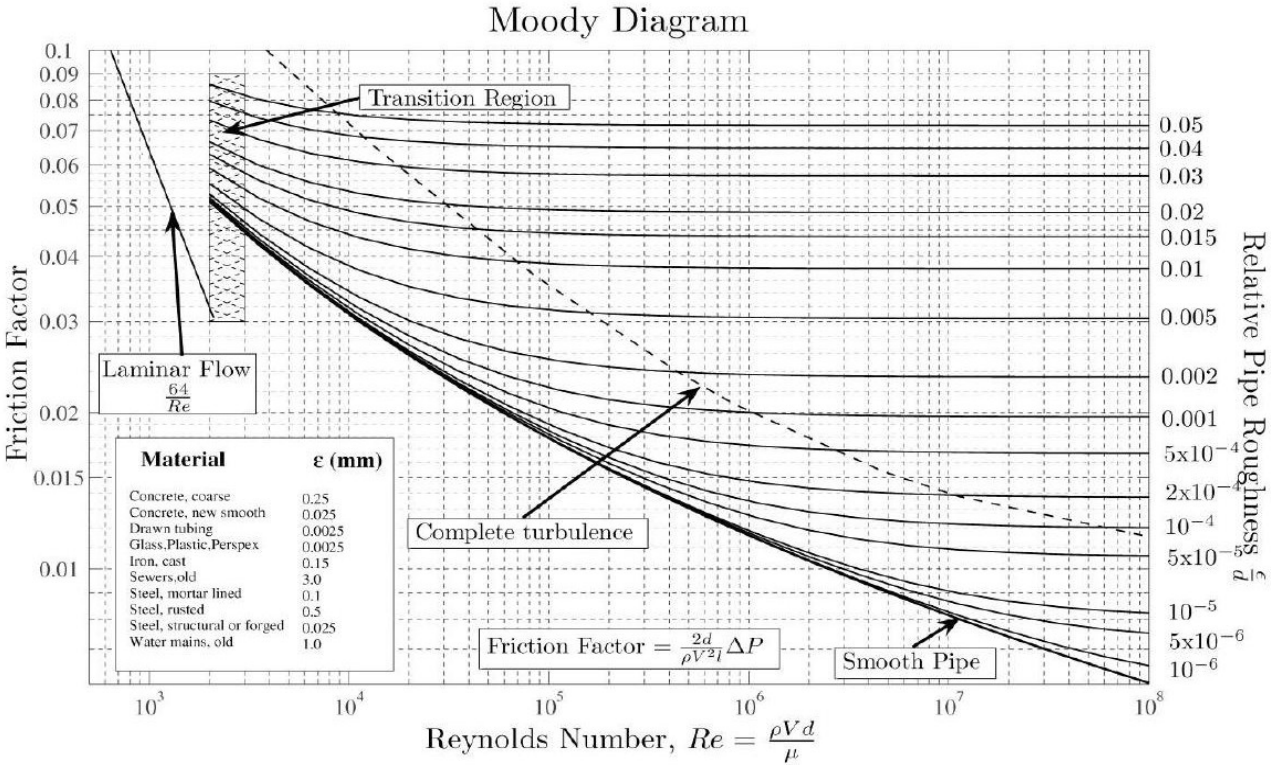

Figure 20 : Moody Diagram

5. 3. 4. Impact of Flow rate on Regular head Losses

For a flow index Q1, corresponding to a hydraulic gradient i_1:

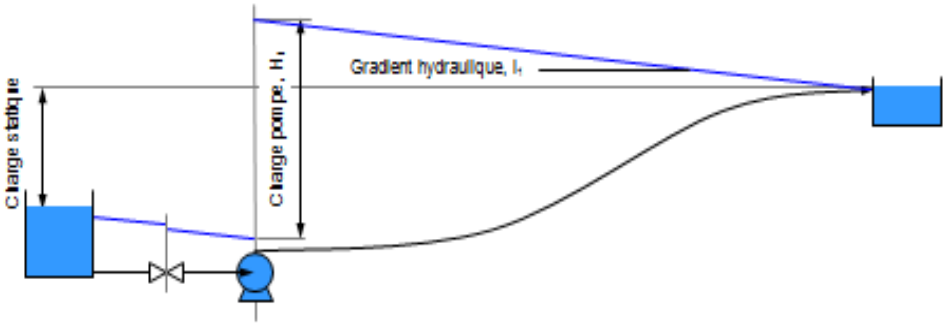

Figure 21: Hydraulic head associated by the pump to the fluid for a low hydraulic gradient

The charge H1 delivered by the pump corresponds to a discharge pressure P1 (P1 = ρgH1)

For a flow index Q2> Q1, corresponding to a hydraulic gradient i_2 higher than i_1.

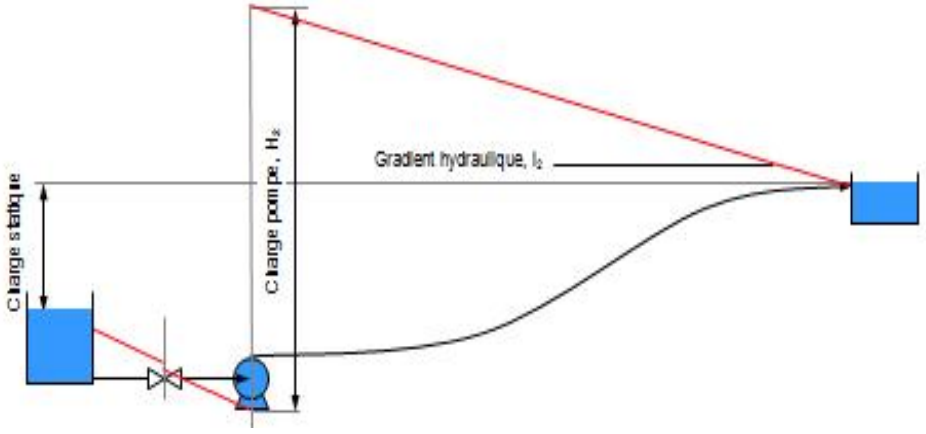

Figure 22: Hydraulic head associated by the pump to the fluid for a large hydraulic gradient

The hydraulic gradient depends on flow rate, density and viscosity. The greater the hydraulic gradient, the greater the pressure delivered by the pumps and exerted on the fluid.

6. Literature reviews on the flow of sediments in pipelines

6. 1. Studies on the internal mechanism of sediments transport

Ismail [46] published an article in 1952 on the transport of sediments through a closed rectangular channel, in the experiments he used grains of sand of average diameter between 0.10 mm and 0.16 mm. The experiment consists in varying the flow velocity in 4 speed levels. The quantities to measure are; the pressure drops, the flow rate, the velocity profiles, the sediment concentration and the temperature.

Ismail studied the effect of sediments on the momentum transfer coefficient (ε_m), the sediment transfer coefficient (ε_s), the Darcy-Weisbach resistance coefficient (**f**), and the Karman constant (**K**), and it has reached the following 4 conclusions:

• The universal Von-karman constant (K) decreases as sediment load in suspension increases. The minimum value obtained for (K) was 0.20 when the total concentration C_T was 43 g / l.

• The Van-Karman constant (K) varies from section to section, but maintains a constant value on the surface of the section.

• The momentum transfer coefficient value (ε_m) is affected by the presence of sediment only through changes in (K).

• The Darcy-Weisbach (f) coefficient of friction is unaffected by the presence of sediment to a point where the sediment load is large enough to form dunes at the bottom of the channel.

Vanoni [47], published a research article in 1946, usually his research work is based on experiments. The experimental distribution of sediments in the vertical was compared to the theoretical distribution:

$$\frac{C}{C_a} = \left[\frac{D_1 - y}{y} \cdot \frac{a}{D_1 - a}\right]^z \qquad z = \frac{\omega}{K\sqrt{gDs}}$$

Whith: (D_1) Depth of flow, (a) distance measured from bed of channel where Ca is measured, (y) Depth of flow, (C) Local concentration in per cent by weight, (Ca) Local concentration in per cent by weight at distance a from the bed of channel, S : the energy gradient. (D) Diameter of the pipe, (g) Gravitational acceleration and (ω) is Settling velocity of the sediment particle. We consider these same conventions in the following.

This equation is obtained under the assumption that $\varepsilon_s \sim \varepsilon_m$; from this comparison he came to conclusions:

• The distribution of the relative concentration of the suspended charge is given by the equation above, but the value of Z given by the theory is not in agreement with the value of Z which corresponds to the experimental data.

• The above disagreement is attributed to the action of random turbulent fluctuations in suspended sediments and slippage between fluid and sediment as the sediment accelerates. This makes that ε_s differs from ε_m.

• For fine materials, the sediment transfer coefficient tends to exceed the momentum transfer coefficient, for large sediments the opposite trend is found.

• The suspended load decreases the value of K, which characterizes the efficiency of the turbulence in momentum transfer. The reduction of K means that the mixture is less efficient and would indicate that the sediment tends to suppress or attenuate the turbulence.

Chamberlain [48] in 1955 studied the mechanism of transport of sediments with a diameter of 0.20 mm in pipelines. Concentration profiles were measured on the horizontal and vertical diameters of the pipe. The horizontal concentration profiles revealed that the concentration was constant along horizontal diameters for corrugated tubes, smooth and standard. For the helical corrugated pipeline, there was a large concentration deviation near the wall compared to the average concentration across the section. The value of the concentration varies between 0.21 and 0.34 for the smooth pipe and between 0.34 and 1.33 for the standard corrugated pipe.

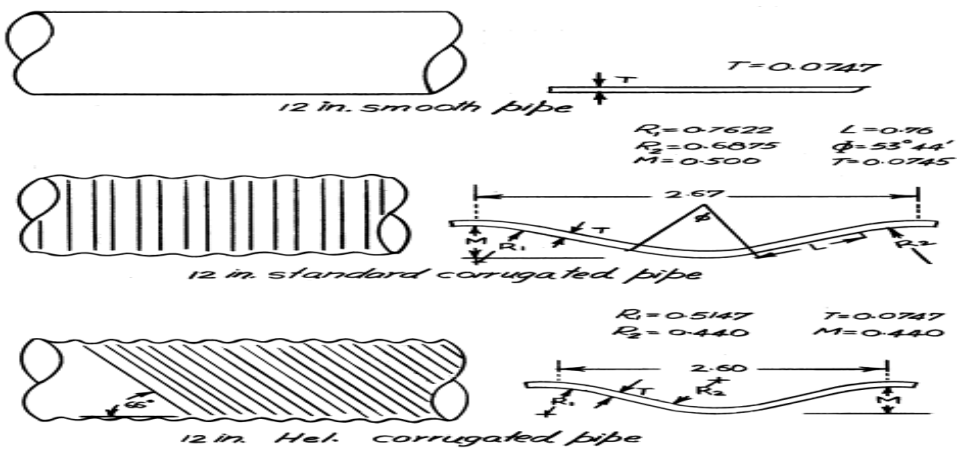

Figure 23: Pipe with smooth wall and corrugated wall

6. 2. Theoretical Approach of the Sediment Transport Mechanism

In this approach we consider that the mixture (water-sediments) is homogeneous and continuous, u, v, w, are respectively the components of the mean velocity along the x, y, z axes. Because the flow is turbulent, velocity fluctuations u ', v', w 'appear [47].

The average of these velocities over a long time domain T or a large area A is zero.

$$\frac{1}{T}\int_0^T u'dT = 0 = \frac{1}{A}\int_0^A u'dA$$

By taking a unit horizontal plane, it can be shown that the tangential stress resulting from the momentum exchange due to velocity fluctuations is given by:

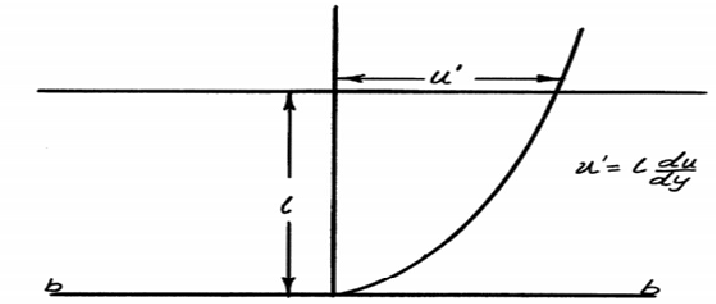

Figure 24: Relationship between the velocity fluctuation and the velocity gradient.

$$\tau = \rho\, u'\, v'$$

$$\tau = \rho\, l^2 \left(\frac{du}{dy}\right)^2 = \rho \left[l^2 \frac{du}{dy}\right] \frac{du}{dy} = \rho \epsilon_m \frac{du}{dy}$$

With : (ρ) Mass density of mixture, (l) Mixing length in theory of turbulence.

In the case where the sediments are in suspension, the sediment transfer can be compared to momentum transfer, an equation similar to the previous equation can be written as follow:

$$g_1 = \rho\, \epsilon_s \frac{dC}{dy}$$

g1 represents the amount of sediment that moves upward through a unit of area and time. If ω is the particle sedimentation rate, then the amount of sediment falling down through a unit area per unit of time will be (C.ω) where C is the concentration at that depth. Given equilibrium conditions the sum of these terms must be zero [47].

$$\omega C + \epsilon_s \frac{dC}{dy} = 0$$

This is the fundamental equation for sediment transport through pipelines. By solving this equation we ended up:

$$\frac{C}{C_a} = \left[\frac{D_1 - y}{y} \cdot \frac{a}{D_1 - a}\right]^z \qquad z = \frac{\omega}{K\sqrt{gDs}}$$

6. 3. Study of the required energy and the coefficient of resistance (friction)

Willson [49] in 1942 approached the problem of sediment transport assuming that the total pressure drop equals the pressure drop for a flow of pure water at the same speed + the load required for sediment transport:

$$J = \frac{fV^2}{2gD} + \frac{\gamma_s - \gamma_w}{\gamma_w}(1 + A_1)\frac{C_T \omega}{V}$$

With: γ_s Unit weight of sediment, γ_w Unit weight of water.

In 1945 Willson introduced a new dimensionless parameter to describe the energy required for sediment transport:

$$E = \frac{J}{\frac{C_T}{100}} \equiv \text{Energy required per foot of pipe per pound of sediment transported.}$$

O'brien et Folsom [50] have published an article on sand transport in the pipeline, in which they discussed the results of experiments using wrought iron pipes of 5.08 cm and 7.62 cm in diameter, with three different sizes of sand included between 0.16 mm and 1.27 mm in diameter. Data analysis revealed that the Darcy-Weisbach equation is adequate for studying the flow of homogeneous and inhomogeneous mixtures.

$$J = \frac{fV^2}{2gD}$$

Craven [51] in 1952 studied sediment transport through pipes and the range of sediment deposition.

The diameter of the pipe being 14.09 cm the sediments studied being sand grain size of (0.25 mm, 0.58 mm and 1.62 mm). Craven claims that the majority of sediment bed load equations have the form:

$$J \propto \frac{\Delta\gamma}{\gamma_w} (C_T)^n$$

Where n varies from ½ to 2/3, it has been found that a similar relation is valid for the flow in the pipeline, the equation has the form:

$$J \approx 0.606 \frac{\Delta\gamma}{\gamma_w} (C_T)^{2/3}$$

Durand [52] published in 1953 its results of experiment carried out in pipes of diameter which varies between 3.81 cm and 71.12 cm, the sediment diameter varies between 20 microns and 100 microns. The study revealed the need to classify sediment mixtures according to grain size into homogeneous and heterogeneous classes:

Homogeneous mixtures: clay, fine ash and finely pulverized coals (between 20 and 30 microns).

Intermediate mixtures: silt (between 25 and 50 microns)

Mixtures heterogeneous: Mixed heterogeneous transported in suspension: Fine sand, coal, slurries (between 50 microns and 0.2 mm) .Category of transition: coarse sand and fine-grained coal (from 0.2 mm to 2mm). Heterogeneous mixtures transported by salting: gravel, pebbles, and pieces of coal (above 2 mm).

The importance of the (V^2 / gD) parameter has also been shown and it has been possible to establish a sediment transport function for a no-deposit regime in terms of (V^2 / gD),

((J-Je) / Je.C1) and other variables describing liquid sediments, where C1 is the relative absolute volume of sediments.

Ambrose [53] in 1952 studied free-surface flow in pipes with a water-sediment mixture; using dimensional analysis, 2 functions have been established:

Transport function:

$$\frac{Q/D^2}{\left(\frac{\gamma_s}{\gamma_w}-1\right)^{2/5} Q_s^{1/5} g^{2/5}}$$

Discharge function:

$$\frac{Q}{g^{1/2} s^{1/2} D^{5/2}}$$

With: Q Discharge of water sediment mixture, Qs is absolute volume rate of transport.

6. 4. Study of the effect of boundaries

Chamberlain [54], in 1955, he studied the flow of sediments of 0.20 mm diameter in a 30.48 cm diameter pipe. He studied the case of smooth-boundaries pipes with corrugated helical boundaries and standard corrugated walls.

He reached the following conclusions:

● The resistance coefficient of Darcy-Weisbach (f) is not affected by the presence of sediments in the mode studied.

● The average speed at which the deposition begins becomes less dependent on the magnitude of the total load as velocities have increased. This velocity was higher in the smooth pipe than in the standard or helical corrugated pipe.

● By taking the minimum point in the J(V) curve in a constant C_T as the operating point, the helical corrugated pipe required less power for a fixed total sediment load than the standard corrugated pipe.

● Helical corrugated pipes and Standard corrugated pipes provided more sediment for a given amount of flow (water-sediment) than smooth pipe.

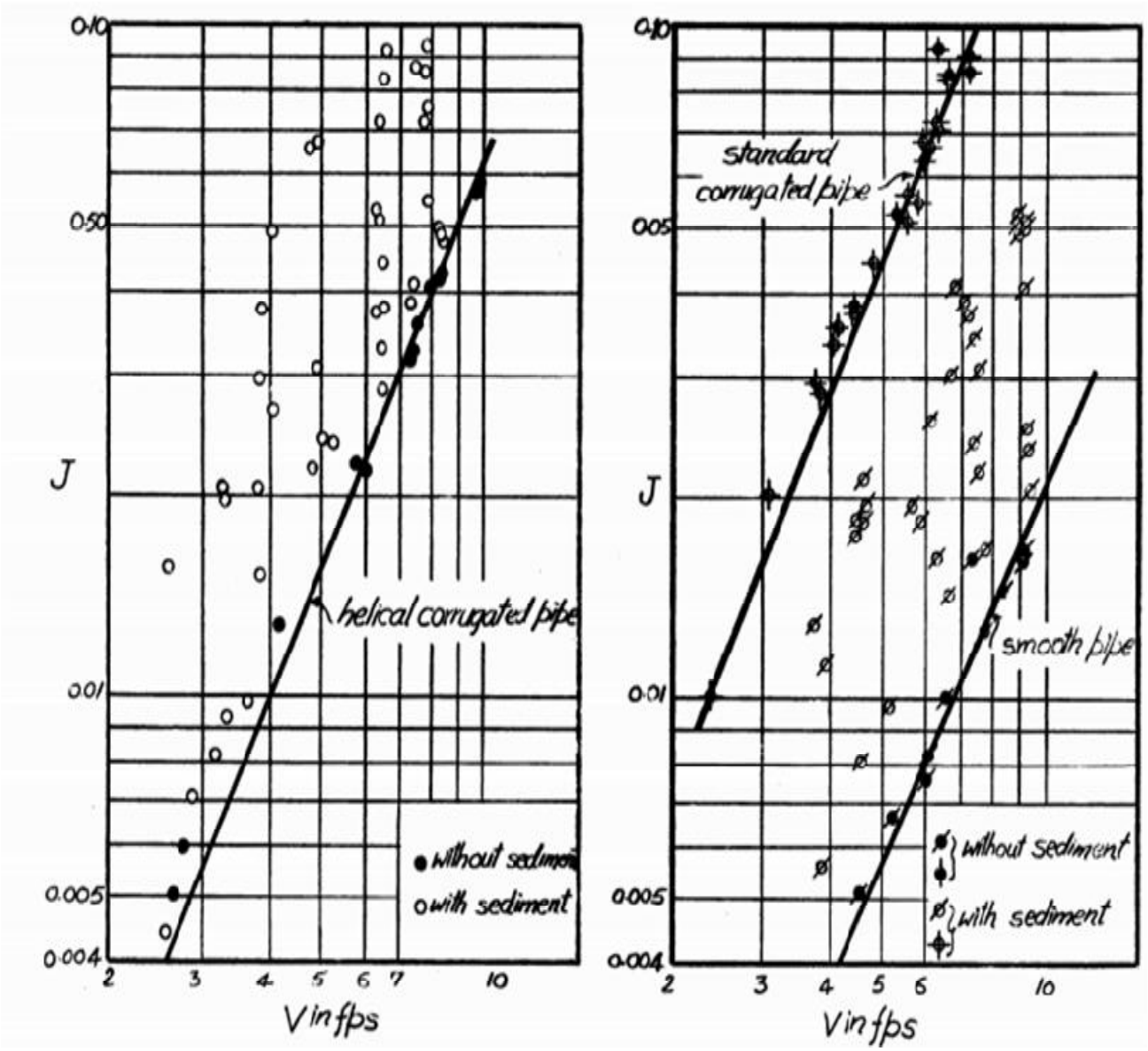

Figure 25: Variation of J with V and Ct for all boundaries

7 – Conclusion

In this chapter, we have defined the mode of transport of various substances through pipelines, focusing on the case of phosphate slurry transport through the pipeline (OCP) from Khouribga mining pole to the industrial platform of Jorf-Lasfar. We presented the different components and tools related to the process of transporting phosphate slurry by pipeline, the slurry pumping system, the feeding system from the washing plants, etc ... We thus elaborated some physicochemical parameters of phosphate slurry. Information related to the phosphate grains critical flow velocity of deposition at the bottom of the pipeline was also elaborated.

We presented theorems of fluid mechanics applied to the transport of slurries through the pipes, which are Bernoulli's theorem, Navier-Stokes theorem, and some mathematical formula for the calculation of the head losses during the flow. These theorems are used to model the flow behavior as a function of the physical parameters (pressure, velocity field, viscosity, density ...).

A literature review was discussed in this chapter about the studies of some researchers on the flow of slurries through different types of pipes. We presented research findings on the study of the internal sediment transport mechanism with its experimental and theoretical aspects. Studies on the required energy, coefficient of friction and effect of boundaries on the flow were also discussed. All this research is to be able to synthesize some methods and theories that will help us to model the behavior of phosphate slurry flow in the following chapters.

Chapter 2

RHEOLOGY AND FLOW OF NEWTONIAN AND NON-NEWTONIAN COMPLEX FLUIDS

1. Overview of the rheology of complex fluids

Most consumer products today are formulated products, ie complex mixtures of constituents such as macromolecules, lipids, minerals, vitamins, flavors, thickeners ..., their applications are in very varied fields such as agri-food, cosmetics, pharmacy, detergency, ... The diversity of the functional properties of these constituents, the physicochemical properties of the mixtures and the industrial processes used for their preparation allow prepare a range of formulated products whose use properties meet consumer demand.

In addition, most of these products are composed of constituents that interact at the molecular level; interactions that can produce the formation of particulate structures whose dynamic mechanism of aggregation or separation represents considerable challenges in understanding their behavior under flow. Consequently, because of these trans-scale couplings between the physicochemistry of the constituents, the microstructures they form and the macroscopic flows, rheology is a central tool in the context of the development of these complex products. This chapter is devoted to a rather general descriptive study of complex fluids and their main behavioral laws.

1.1. The complex fluids

A fluid can be said complex when it has an internal structure of characteristic size between the molecular scale and that of the sample. These mesoscopic sizes give the fluids a microstructure that will give them very particular properties. These properties are intermediate between those of a simple fluid and the purely elastic solid. Due to their special properties, these products are used in everyday life, but also as finished or intermediate products in most process industries. Citing all industrial sectors in which complex fluids are implemented is a challenge; however, from heavy industries to the finest industries, the areas most particularly concerned are: drilling muds in the exploitation of oil deposits, cements and mortars, ore processing in extractive metallurgy, molten polymers, pasta paper, mastics, paints and varnishes, food industries (ketchup, mayonnaise ....), cosmetics and pharmaceuticals.

1. 2. Examples of complex fluids

1. 2. 1. Slurries

The slurries are mixtures of solid particles and a liquid (generally water), these suspensions have a very great application in the mining field and in particular for the transport of ores via pipelines. Slurries are suspensions where the particles have a size generally greater than 1 µm and they can reach 500 microns, against colloidal suspensions whose particle sizes are between 1 nm and 1 micron. The phosphates slurry, the coal slurry, the Limston slurry are suspensions which we could cite as examples.

Those slurries are a complex nature because the particles are different from one another at the level of the sizes and at the level of natures.

1. 2. 2. Complex molecular or macromolecular systems

They are molecular systems of mesoscopic size that are constructed from real chemical bonds (polymers) or through strong molecular interactions (micelles, liquid crystals). Take the example of liquid crystals which are anisotropic molecules. They are often assimilated, from the steric and / or electrical point of view, to sticks, ellipsoids or elongated revolution. They associate the anisotropy of crystals with the fluidity of liquids and thus constitute intermediate states of matter between the liquid and solid phases, hence the denomination of mesomorphic states or mesophases. A purely orientational order defines the nematic phase. In addition to this order, the high class of smectics presents a position order.

It is conceivable that steric and dipolar interactions tend to generate an order of orientation and possibly of position, whereas thermal agitation tends to average orientations and positions in a homogeneous and isotropic manner. At high temperature, the system is isotropic. When the temperature decreases, ordered phases appear. However, it is important to distinguish anisotropy at the molecular level and macroscopic behavior. Indeed, a thermotropic liquid crystal is composed of molecules whose mesogenic nature can induce a large-scale organization.

By lowering the temperature, such a system can pass from an isotropic phase i.e. without order at great distance, to a nematic phase, for which the characteristic axes of these mesogenic molecules are aligned in a particular direction. The existence of this preferred direction induces the appearance of a second optical refractive index, the medium is said to be birefringent. In addition, under the action of shear, some molecules acquire new dynamic properties. Thus, starting from a thermodynamically stable isotropic phase, the shear can sometimes induce the appearance of a

nematic phase. This isotropic-nematic transition has often been observed on giant micelle solutions [1].

1. 2. 3. Suspensions or glassy systems

These are systems called Soft Glassy Materials. In this class of materials, we find the concentrated suspensions of Brownian or non-Brownian particles, concentrated emulsions, foams... They consist of one phase dispersed in another. They are amorphous systems that can be characterized by a very slow evolution of their physical properties: they are never at thermodynamic equilibrium. Among these complex fluids, emulsions occupy a very important place. An emulsion is a special case of colloid. The discontinuous "liquid" phase is dispersed in the continuous phase which is also a liquid. Emulsions are often composed of an aqueous phase, similar to water, and an oily phase.

To make an emulsion stable over time, it is necessary to reduce the particle size of the discontinuous phase (Stockes law). The smaller the desired size, the more energy it will take to get it. There are several devices capable of producing such emulsions. The areas where emulsions are encountered are extremely numerous, for example during the exploitation of oil deposits. However, the emulsions formulated are mainly finished products or commonly used products in a wide variety of domestic or industrial application sectors [2-3].

Take the example of concentrated suspensions. These highly concentrated dispersions of particles, which we will describe as pasta, appear as intermediates between fluids and solids. It is generally accepted that pasta is a concentrated suspension of solid particles in a fluid [4]; however, pasty behavior can be achieved with molten polymers or highly concentrated polymeric solutions. Whatever the composition of the paste, its behavior is comparable to that of an equivalent homogeneous fluid, the biphasic nature of the medium may possibly be taken into account to evaluate the dynamic viscosity of the equivalent fluid. A paste will be defined as a dispersion of particles, brownian or not, in which the average free volume per particle is small, typically less than the intrinsic volume of a particle [5].

From the rheological point of view, the most striking characteristic of pasta is probably its ability to undergo large plastic deformations, with a constant stress, once a stress threshold (the plasticity threshold) has been reached. Such behavior is well demonstrated in an experiment with increasing imposed deformation. This type of experiment makes it possible to distinguish pastes from gels. The latter also have a stress threshold before the flow, but unlike the pasta, exceeding

the elastic limit deformation leads to a significant drop in the stress level. This difference is due to the difference in the structures.

Unlike pasta, which is a dense pile, gels are hollow networks. Putting them in flow involves the rupture, if not the collapse, of the network. Like liquids, in the vicinity of the flow threshold, pasta deforms by a deeply collective phenomenon. A local displacement of the order of a particle size generally implies concerted displacements of a larger or smaller number of other particles. From the rheological point of view, this leads to a behavior similar to that of dry granular media, with, in particular, significant normal forces related to the excluded volume (dilatancy), slow kinetics of rearrangement, under vibration for example [6], and a frictional contribution to the yield point and the viscosity [4], [6].

Granular materials are not part of the soft matter, but many situations encountered in non-equilibrium complex fluids (concentrated emulsions, foams, colloidal pastes) pose very similar problems to those encountered in dry granular systems. They are very out of equilibrium systems in which the fluctuations are not thermodynamic: the spontaneous reorganizations are very slow; we talk about aging. Many experimental results have been obtained, but the theoretical description remains very phenomenological. Let's mention a theme such as "jamming", which concerns materials as different as vitreous polymers, colloids or dry granular materials.

2. Law of behavior

To identify the behavior of the fluid and the movement of the elements of a fluid with respect to each other, one places oneself within the framework of the mechanics of the continuous mediums which expresses the law of behavior, that is to say the relation between applied stress fields and tensor deformations. The Cauchy stress tensor, σ, represents the surface forces exerted by the fluid. The tangential terms σ ij are at the origin of the shear. The diagonal terms σ_{ii} are at the origin of compressions and elongations. The shear σ_{ij} is the stress applied in direction i on a surface normal to j. Its general expression in the landmark (1,2,3) representing the directions of flow, gradient, and vorticity is given by :

$$\sigma = \begin{pmatrix} \sigma 11 & \sigma 12 & \sigma 13 \\ \sigma 21 & \sigma 22 & \sigma 23 \\ \sigma 31 & \sigma 32 & \sigma 33 \end{pmatrix}$$

When the fluid is at rest, the stresses are normal and isotropic. The diagonal terms are identical and opposite to the hydrostatic pressure. The stress tensor can then decompose into a portion representing the pressure forces and a portion representing the viscous forces.

$$\boldsymbol{\sigma} = -p\,\mathbf{I} + \boldsymbol{\tau} \quad with \quad p = \frac{1}{3}tr(\boldsymbol{\sigma})$$

$\boldsymbol{\tau}$ represents the viscous stress tensor. This tensor exists on the condition that the fluid undergoes a deformation.

2. 1. Case of simple shear

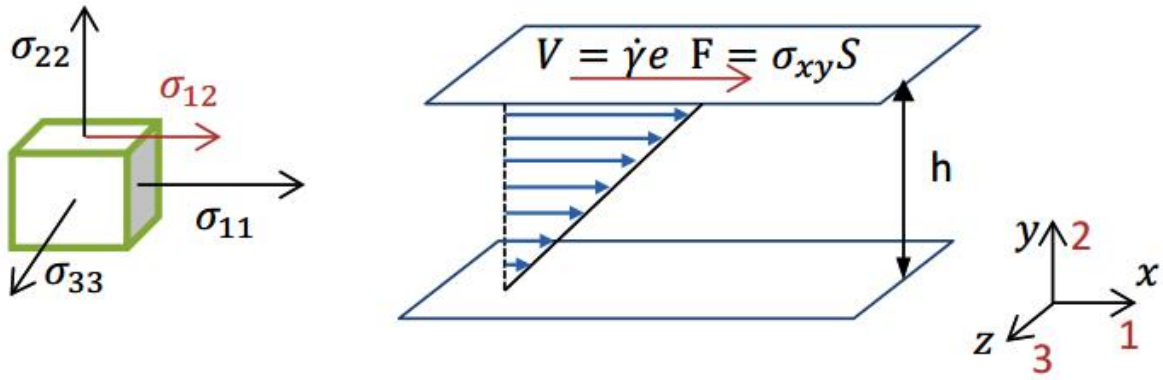

Figure 1: Schematic representation of the principle of a rheology experiment. The sample is placed between two infinite plates whose one of the top is animated with a velocity V, and a force F.

To determine the stress tensor it is necessary to apply to the fluid a deformation. The deformation is expressed by the strain tensor **E**. To obtain **E**, we are interested in the simplest flow, namely the flow between two infinite plates. In such a case the shear rate $\dot{\gamma}$ is defined as the derivative of the velocity in the normal direction of the flow *y*. It corresponds to the velocity gradient and is equal to the ratio of the maximum velocity (that of the upper plane) by the thickness *e*.

$$\dot{\gamma} = \frac{\partial u}{\partial y} = \frac{V}{e}$$

In these conditions the deformation tensor is expressed:

$$\mathrm{E} = \frac{\dot{\gamma}}{2}\begin{pmatrix} 0 & 1 & 0 \\ 1 & 0 & 0 \\ 0 & 0 & 0 \end{pmatrix}$$

The response of the fluid to this deformation is expressed by the appearance of two tangential components in the stress tensor σ_{12} and its symmetric σ_{21}.

$$\sigma = \begin{pmatrix} -P & \sigma 12 & 0 \\ \sigma 21 & -p & 0 \\ 0 & 0 & -p \end{pmatrix}$$

Still in the case of a simple flow, the stress of each plane in the direction of movement is constant in the thickness. It is then possible to show that the tangential components are directly the forces per unit area.

$$\tau = \sigma_{12} = F/S$$

In the case of a Newtonian fluid, the tensor of the viscous stresses is directly related to the tensor of deformation by the viscosity of the fluid η_f.

$$\tau = 2\eta_f D \quad is \quad \eta_f = \frac{\tau}{\gamma}$$

It is important to note that in the case of non-Newtonian fluids the viscosity may be dependent on the shear rate. The expressions of viscosities are then non-linear. In some cases it is possible to see normal anisotropic forces other than pressure. They are then defined as the first and the second difference of normal stresses N1 and N2, the differences of the diagonal terms:

$$N1 = \sigma_{11} - \sigma_{22} \; ; \; N2 = \sigma_{22} - \sigma_{33}$$

τ, $N1$ and $N2$ characterize the flow of a fluid. If it is possible to measure them in a flow type, it is then possible to predict the flow in more complex geometry.

2. 2. Non-linear rheology

In complex fluids, there is a link between the microstructure of the fluid and the flow. It is this link that is at the root of non-linearity. They are said to be non-Newtonian fluids. The viscosity is therefore not constant and depends on the shear rate applied. There are three main types of behavior.

2. 2. 1. The shear thickening fluids

The viscosity of the fluid increases with the shear rate (Figure 2). The best-known example is Maizena. This fluid, a concentrated mixture of small grains of cornstarch and water, is a pretty telling example. If you want to introduce a spoon in a glass of corn, it is better to go slowly, because in this case the viscosity of the fluid will be smaller because little sheared. This type of fluid is currently very studied because not yet well understood.

2. 2. 2. The shear thinning fluids

This is the inverse behavior of the case of shear thickenning: the viscosity of the fluid decreases with the shear rate (Figure 2). The more the fluid is sheared, the easier it flows: for example shampoos, polymer solutions, ketchup. The curves of such fluids are decomposed into three parts: At the low shear rate, there is a plateau of viscosity η_0, then passed a γc the viscosity decreases with the shear rate, it is the zone of rheofluidification. For higher shear rates, the viscosity is almost constant. The viscosity of the solvent is then measured η_∞.

2. 2. 3. Fluids with yield stress

They flow only when the shear stress applied has exceeded a critical value called threshold stress (yield stress) (Figure 2). Below this value, the viscosity is infinite whatever the applied stress. An example of a threshold fluid is toothpaste. To remove the toothpaste, you must press enough on the tube, otherwise the stress is too low and it does not flow. Such fluids can thus support their own weight or withstand the flow when they are arranged on an inclined plane.

2. 2. 4. Thixotropy

A thixotropic fluid undergoes a decrease of viscosity over time, when subjected to constant shear.

2. 2. 5. Rheopexy

This is essentially the opposite behavior of the thixotropic behavior, in that the viscosity of the fluid increases with time when subjected to a constant shear rate. Both thixotropy and rheopexy can occur in combination with any flow behavior that we have seen so far, or only at some shear rates. The time factor is extremely variable, under constant shear conditions, some fluids can reach their final viscosity value in seconds, while others will take several days.

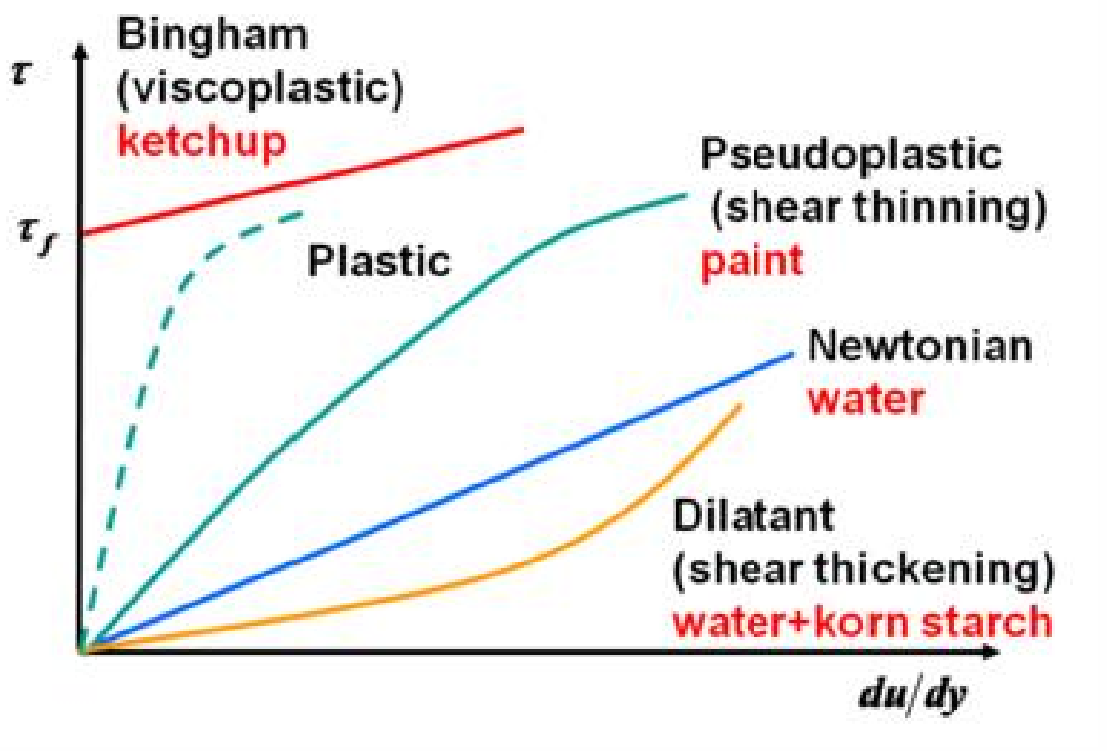

Figure 2: The different natures of rheological behavior of fluids.

3. Measurement of rheological characteristics of fluids

3. 1. Volume Rheology

To characterize the flows in complex fluids, a rotational rheometer consisting of an axis of rotation linked to the motor (at speed or imposed torque) and a measuring cell is generally used. The measuring cell consists of a moving part connected to the axis of rotation (the rotor) and a fixed part (the stator). The fluid is confined between the stator and the rotor (gap). In both cases, the setting in motion of the axis of rotation of the rheometer shears the sample placed in the gap. The simplest geometry for measuring the rheological properties is that generating a simple shear flow, as shown in Figure 3, where the stress is constant throughout the geometry. In practice, the geometries are approximations of this simple geometry, and the most frequently used are the cone-plane geometry, and the Couette cell (Fig 3).

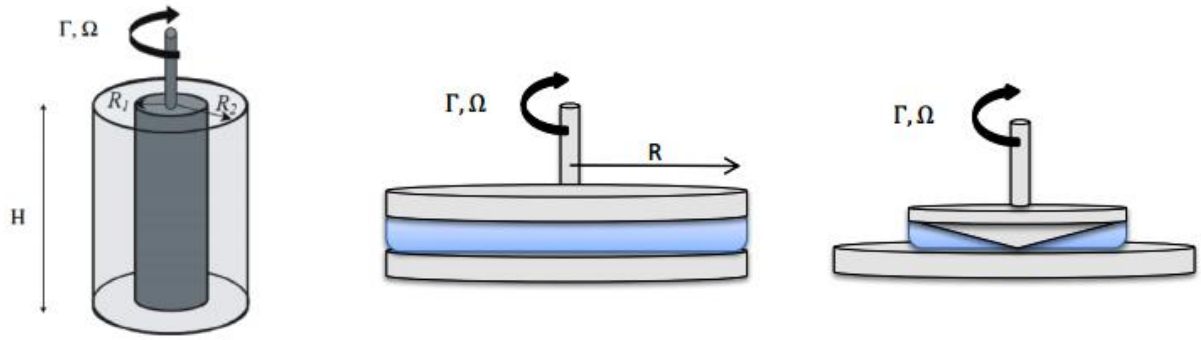

Figure 3: Schematic representation of a cylindrical Couette geometry, plane-plane geometry, plane cone geometry

3. 1. 1. Couette geometry

A Couette cell consists of two concentric cylinders R1 and R2 (R1 <R2) and of height H (see Fig. 3). The rheometer imposes a torque Γ which rotates the inner cylinder (rotor) at the speed of rotation Ω. Given the symmetry of the geometry, the velocity field is of the form $\vec{v} = v\,(r).\vec{\theta}$, and the only non-zero component of the stress tensor is $\sigma_{r\theta}$, given by:

$$\boldsymbol{\sigma_{r\theta}} = \frac{\boldsymbol{\Gamma}}{\boldsymbol{2\pi H r^2}}$$

In this geometry the stress is not constant and varies in $1 / r^2$. In this case the shear also depends on the position in the gap, it is given by:

$$\dot{\boldsymbol{\gamma}}(\boldsymbol{r}) = -\boldsymbol{r}\frac{\boldsymbol{\partial}}{\boldsymbol{\partial r}}\left(\frac{\boldsymbol{v}}{\boldsymbol{r}}\right)$$

For a Newtonian fluid $\sigma_{r\theta}(r) = \eta\dot{\gamma}$. The average values of stress σ and shear ($\dot{\gamma}$) are therefore directly linked by:

$$\boldsymbol{\sigma} = \frac{\boldsymbol{R^2 1 + R^2 2}}{\boldsymbol{4\pi h R^2 1 R^2 2}}\,\Gamma \quad \text{and} \quad \dot{\boldsymbol{\gamma}} = \frac{\mathbf{R^2 1 + R^2 2}}{\mathbf{R^2 1 - R^2 2}}$$

These formulas are used as is, even if the fluid is non-Newtonian. In the case of a non-Newtonian fluid, there may be an offset between the result given by the rheometer and the actual behavior of the fluid.

3. 1. 2. Plane cone geometry

In a cone-plane cell (FIG. 3), the flow is generated by the rotation of the cone of radius R and of angle α between the cone and a flat surface. Within the fluid in the gap, the velocity field is of the form $\vec{v} = v\ (r).\vec{\theta}$. If the angle α is sufficiently small (<5 °), the shear and the stress are homogeneous throughout the air gap, and are given by:

$$\dot{\gamma} = \frac{\Omega}{\tan \alpha} \quad \text{et} \quad \sigma = 3\,\Gamma/(2\pi R^3)$$

3. 1. 3. Plane-plane geometry

In a plane-plane rheometer, the fluid is between two circular discs of radius R coaxial separated by an air gap *e* as shown in Figure (3). The flow in this geometry is generated by the rotation of the upper cylinder. In such geometry the stress and the shear rate depend on the distance to the axis of rotation and are given by:

$$\sigma(r) = 2\Gamma/(\pi r^3) \quad \text{et} \quad \dot{\gamma}(r) = \Omega r/e$$

3.2. The empirical rheological models

3. 2. 1. Casson model

The Casson model has often been used to describe the rheological behavior of concentrated suspensions with pseudoplastic behavior [56].

$$\sigma^{1/2} = (a.\gamma)^{1/2} + b^{1/2}$$

With: viscosity ν = a and (yield stress) = b; γ: shear rate et σ: shear stress.

3. 2. 2. Bingham model

The Bingham model is a model for describing the behavior of suspensions with linear rheological profiles with a yield tress [57].

$$\sigma = a.\gamma + b$$

With: (viscosity) = a ; and (yield stress) = b.

3. 2. 3. Ostwald-Power Law model

The Ostwald model is often used to describe the rheological behavior of suspensions with a dilatant profile or a pseudoplastic without yield [58].

$$\sigma = a.\gamma^{n}$$

With: a, is the coherence parameter, n is the behavior index of the flow.

3. 2. 4. Herschel-Buckley model

The Herschel-Buckley model presents a generalization of all the rheological models that have been cited [59,60].

$$\sigma = a.\gamma^{p} + b$$

4. Interaction between particles in concentrated suspensions

4. 1. The Brownian motion of the particles

A particle suspended in a fluid is subjected to the incessant bombardment of the agitated molecules constituting this fluid. It is not possible to see under the microscope the movement of a particle that has been shocked with a single molecule. On the other hand, the contribution of a large number of molecules can be effective enough for the movement of the particle to be observable. Of course the size of the particle is important:

• The particle and the size of the particles of the fluid: we are in the case of an ordinary solution: the movement of the particles is not observable.

• If the particle is very large, the velocities of the molecules coming to bombard the particle are isotropic and the law of large numbers causes that the impulse on the particle resulting from the shocks of the molecules is null (observation under optical microscope of red blood cells or leucocytes or pollen grain).

• Between these two cases, the smaller the particle, the less it undergoes shocks and the more it is sensitive to deviations from the law of large numbers: the shocks cease to be exactly compensated and produce disordered displacements whose direction changes constantly : it is the Brownian movement. These particles are not directly observable under the microscope. One way to observe them is to use the scattered light: the particles are large enough that the intensity of the light scattered at 90 ° is strong enough to be observed: the particles appear as luminous points without

definite apparent form, but this is enough to observe their movement. Two random phenomena exist in parallel: the movement of the particle itself and the fluctuations of the velocities of the neighboring molecules. The Brownian diffusion coefficient D is the ratio between the agitation and the friction forces acting on the particles. It is given by :

$$D = \frac{KB.T}{6\pi\eta a}$$

Where: η the viscosity of the medium, (KB) the Boltzmann constant and (a) the particle size.

4.2. Interactions between colloidal particles

The attraction, repulsion and friction forces between particles in an aqueous medium are the basic components of the macroscopic mechanical behavior of the colloidal suspensions. We resume here the inventory realized by [Güven (1992)] and summarized by [Besq (2000)] within the framework of the understanding of the different types of interactions between the "leaflets":

• Born repulsion forces: They appear when the particles are separated by short distances (0.1 nm). They result from the impossibility of recovery of the electronic clouds and their role is to prevent too close contact between the particles and, as a result, generate a significant potential for interaction.

• Van der Waals forces: These attractive forces result from thermodynamic fluctuations of the electromagnetic field in and around the particles. They are related to the interactions between fluctuating dipoles. Even non-polar atoms or molecules have an instant dipole created by the movement of electrons. This dipole generates an electric field that polarizes any surrounding atom then becoming an induced dipole. The interaction between these two dipoles creates an instantaneous attractive force whose temporal average is non-zero. The range of this type of force is relatively large (10nm).

• Osmotic forces (repulsion of the double layer): These are repulsive forces coming from the bringing together of two charged surfaces of the same sign (their double layer is of the same sign also). The main parameters of this force are the surface potential (Ψ0), the electrolyte concentration and the valence of the ions. The repulsive energy defined by these parameters leads to an energy barrier limiting the aggregation of particles.

• Solvent forces and steric interactions: Since the classical models used to describe Van der Waals forces and osmotic forces do not take into account the size of the solvent molecules and therefore the discrete nature of the separation medium of particles at short distances, the solvent (water) can

not be considered simply as a continuous phase. Due to its specific structure and properties, water interacts specifically with the surface and ions (steric and physicochemical effects) [Güven and Pollastro (1992)]. A particularly important type of "steric" interaction will be discussed later: it is a dispersion of Laponite in a polymer solution.

4.3. Colloidal stabilization: DLVO theory

The DLVO theory suggests that the stability of a particle in a solution is dependent on the total interaction energy Ut. This theory recognizes that this energy is the equilibrium of several antagonistic contributions: Ut = UA + UR + US; where US represents the potential energy of the solvent, it is generally only a marginal contribution to the total interaction energy over the few nanometers of separation. The balance between UA and UR is much more important, it is the contributions of attractions and repulsions. In the case of a colloidal system, the DLVO theory suggests that stability is determined by the sum of the Van der Waals forces (UA) and the repulsive forces of the electric layer (UR), which exist between particles when they approach one another because of the Brownian motion. This theory states that an energy barrier resulting from repulsive forces prevents two particles from approaching each other and adhering to one another. So to maintain the stability of a colloidal system, repulsion forces must be dominant. Colloidal stabilization can be achieved in two ways:

• Steric repulsions: this implies that the polymers added to the system are adsorbed on the surface of the particles and prohibit any surface contact between particles. If enough polymer is adsorbed, the thickness of the layer is sufficient to keep the particles separated by steric repulsion between the polymer layers, and at these separations, Van der Waals forces are too weak to adhere the particles.

• Electrostatic Stabilization: This is the effect on the interaction of the particle due to the distribution or present of charged elements in the system. With many negative charges on its surface, a colloid in a medium of low ionic strength has a long-range electrostatic repulsion. Thus, the particles will repel each other by the barrier.

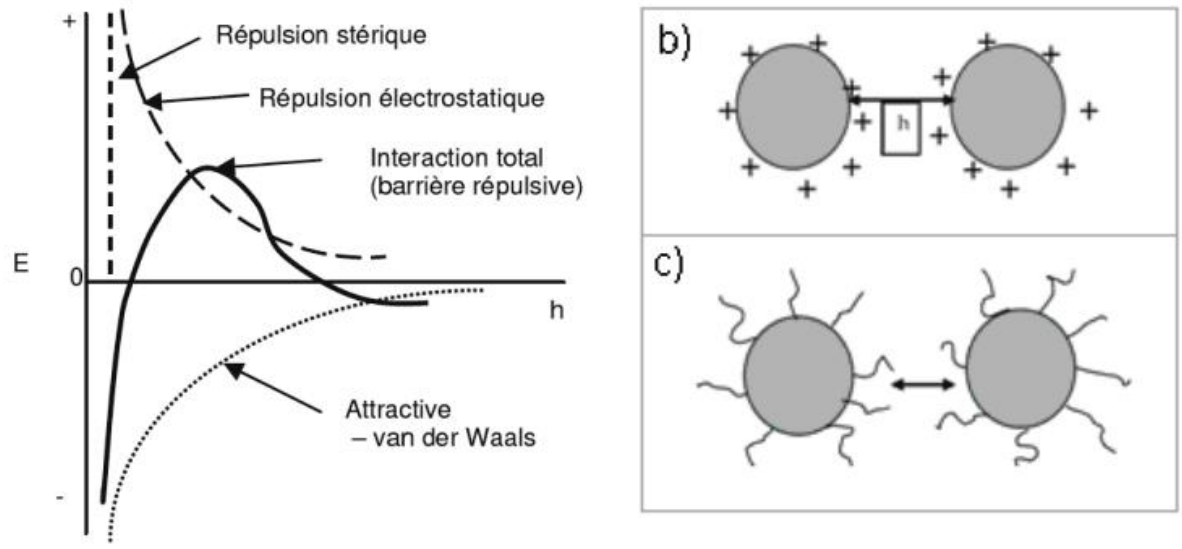

Figure 4: Schematic representations (a) Curves of interaction energies for colloidal particles in suspension. (b) charged particles - electrostatic repulsion (c) particles with adsorbed polymers - steric repulsion.

5. Literature review on the rheology of complex fluids

Several parameters have very remarkable influences on the rheology of complex fluids, these parameters generally related to the physical behavior of the complex fluid. We can cite among these parameters for example, the concentration in solids, the sizes and shapes of the particles, the temperature, the PH … [7-11].

The chemical elements (additives) added to ore slurries during operations of beneficiation or grinding also have a significant impact on the rheology of these slurries.

In this part we will try to develop a literature review on what researchers have found on the impact of all these parameters on the rheological behavior of ore slurries.

5. 1. Effect of solid concentration

Qualitatively, the rheological behaviour of a time-independent suspension has the following characteristics. At low concentrations, it may be Newtonian with the viscosity η independent of the shear rate. As the concentration increases, it will become progressively more strongly non-Newtonian with a steeply increasing viscosity as the shear rate decreases (see Fig. 5), signifying the possible appearance of a yield stress (see Fig. 6) and a remarkable shear-thinning characteristic over the intermediate shear rates (see Fig.7). The rheological behaviours, for dolomite slurries, galena slurries, quartz slurries, coal slurries, respectively, with respect to the effect of solids concentration, are similar to Figs. 5-8. Gao and Forssberg [12] have investigated the influence of

various slurry densities of dolomite on the slurry rheology and ultrafine grinding performance. It was found that by increasing the slurry density from 65 to 75 wt%, the slurry viscosity exponentially increased. This phenomenon was also observed by other researchers in the cases with and without dispersants. The slurry viscosities at different slurry densities did not change (see Fig.8) much as the milling proceeded. [12]

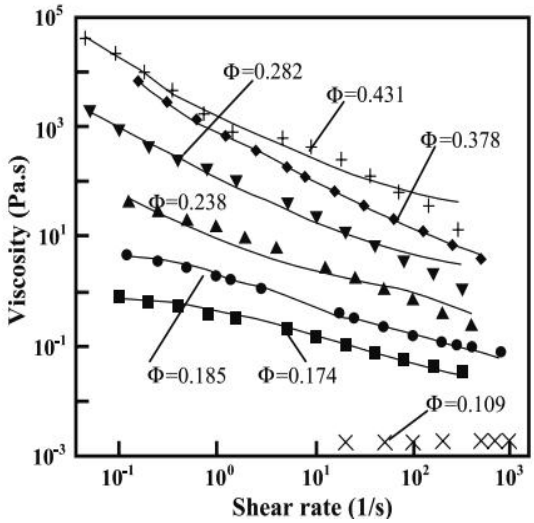

Figure 5 : *Effect of the volume fraction of the solid φ on the apparent viscosity of the titanium dioxide suspensions [12].*

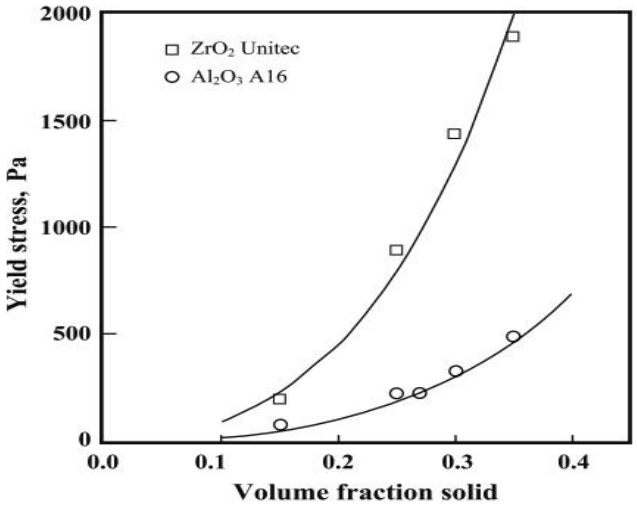

Figure 6 : *The maximum yield stress of alumina A16 and zirconia Unitec suspensions, respectively, as a function of solid loading.*

Bernhardt et al. [32] have studied the effect of the solid concentration of limestone on the slurry rheology for the effective wet ultrafine grinding and the energy utilization. The curves in (Fig.7) showed the typical non-Newtonian behaviour with a yield stress value and remarkable shearthinning characterization, both strongly dependent on the solid concentration (Fig.7,8).

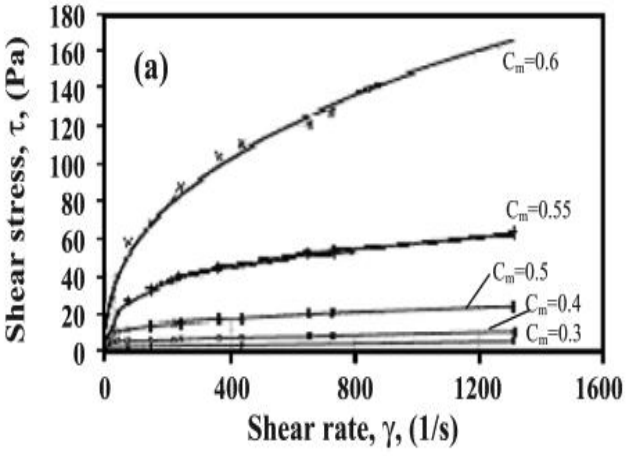

Figure 7 : *The influences of various slurry concentration of limestone on slurry rheology*

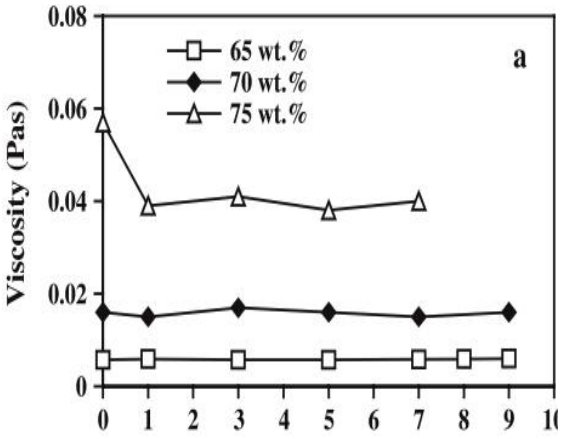

Figure 8 : *Influence of the limstone slurry density on the viscosity*

The physical interactions between particles and operating shear rate ranges are the two main factors that affect the solids concentration when determining the viscosities of the slurry. The viscosity of a suspension will increase with the concentration of solids. This phenomenon is attributed to the physical interactions of particles that occur when a solid is dispersed in a liquid. According to [14], there are three main categories of these physical interactions:

- The interparticle attraction promotes the formation of flocs and aggregates. This phenomenon occurs mainly in suspensions of fine particles
- Hydrodynamic interactions cause viscous dissipation in the liquid
- Particle-particle contact involves frictional interactions.

At a concentration low to medium in solids, the effect of hydrodynamic interactions dominates, whereas at low solids concentration, viscosity appears to increase linearly with increasing solids concentration. However, Rutgers observed that after a certain solids concentration, the slurry viscosity increases significantly with small increments in concentration. According to Cheng, from the medium to high concentration of solids, the frictional contact of the particles dominates and at very high concentration in solids the effect of the particles predominates on the hydrodynamic effects [14].

Studies conducted on the rheological behavior of iron powder (mean particle size was 28.48 μm) with some binders indicate that dynamic viscosity increased with increasing solid content due to strong interaction between particles [15].

P.K.Senapati et al. Carried out invstigations on the effect of solid rates on the rheology of the (Limstone-Water slurry), they found that slurries up to 37.8 vol. % shows the Newtonian behavior beyond this volume percentage, the suspension has a pseudoplastic rheological nature. Therefore, it can be inferred that slurry changes to non-Newtonian behavior above 37.8 vol. % [16].

S.K MISHRA et al worked on (coal water slurry) over a range of solid rates (50% to 57%), they found in this study that the slurry of coal have a pseudoplastic behavior and they become more viscous with a increased ash content and increased solids concentration. [17]

5. 2. Influence of particle size distribution

Tangsathitkulchai and Austin [18] investigated the influence of natural size distributions of ground coal and quartz on the rheological properties of concentrated slurries. They found that the strong influence of characteristic particle size on the slurry rheology was not due to packing or adsorbed layers on the particles. In addition, it was deduced that any rheological theory of concentrated slurries, which does not include a strong dependence of viscosity on particle size, could not be correct. A similar investigation was reported by Logos and Nguyen [19] that by adding a narrow-sized coarse coal fraction (208–279 μm) to the fine (<45 μm) coal slurry, the flow characteristics of the slurry, at a fixed total solids concentration, could be changed significantly with a substantial reduction in the slurry viscosity. It was also found that an optimum coarse-to-fine particle ratio of 40:60 existed at which the slurry was Newtonian with a minimum viscosity of about five times lower than that of a slurry containing only the fine particles at the same solids concentration. Another similar work [20] has presented that the titanium dioxide suspensions with a broad size distribution exhibited a lower yield stress and a smaller viscosity than those with a narrow size distribution at the same solid volume fraction (see Fig. 9)

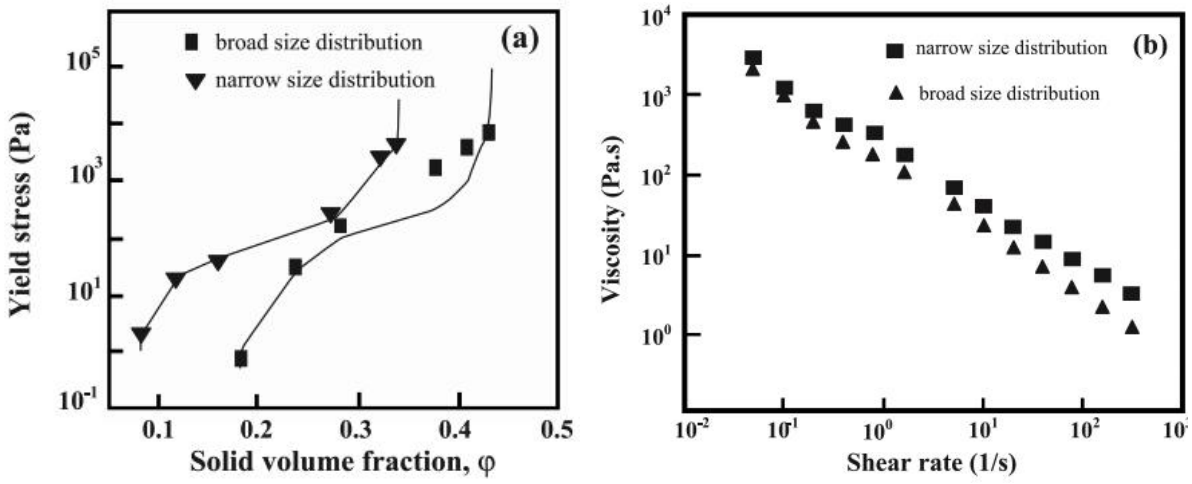

Figure 9 : Effects of particle size distribution on yield stress (a); and viscosity at a solid volume fraction of 0.28 (b).

Other several researchers have reported the effect of particle size and distribution on the flow patterns of the slurries of iron ore [21], quartz [22] and metal [23]. Although these reported results are not in complete agreement with each other, the influence of particle size and distribution on the rheological behavior of slurry is significant (see Fig. 10).

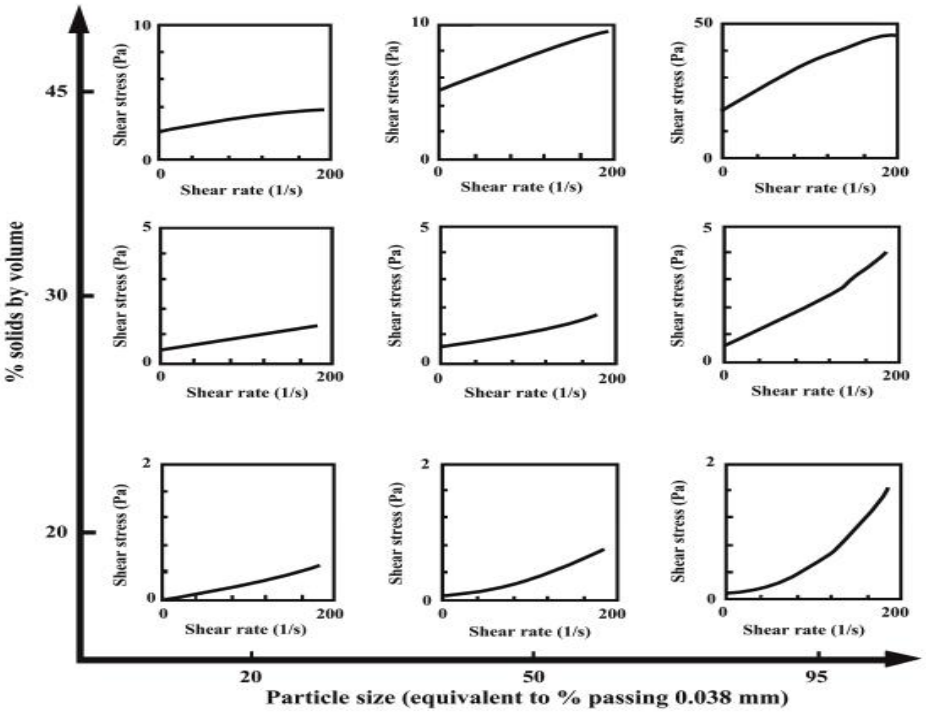

Figure 10: ***Effect of particle size distribution on the rheological behavior of slurries at different volume concentrations.***

Garcia, F et al., worked on the calcite suspension, the rhological behavior of calcite suspensions behaved as a shear thinning fluid with a yield value, and the viscosity increases when the particle size decreases due to attractive interparticle forces [24].

P.K. Senapati et al worked on two Limstone Slurry samples, S-1 and S-2, and found that, the rheological behavior of concentrated slurries is strongly related to the viscosity –dependence on the particle size [15,16]. The ground product becomes finer with increase in grinding time of the ore samples. Fig. depicts the rheological behavior of the two slurry samples S-1 and S-2 having different median sizes at 46 vol. % concentration. The relative viscosity at a given shear rate indicates higher value for sample S-1 It is generally realized that a decreasing particle size (particularly when the particle size distribution is narrow) results in an increase in slurry viscosity, especially at low shear rates. In addition, the inter particle attraction is expected to become stronger as the specific surface area of the particles increases at the same solids volume concentration of the slurry. Also the packing efficiency reduces in a material with a narrower particle size distribution at a fixed solids concentration. It may be mentioned that the fines content (<10 μm) in S-1 is more than twice that of S-2 as indicated in particle size distribution plot.

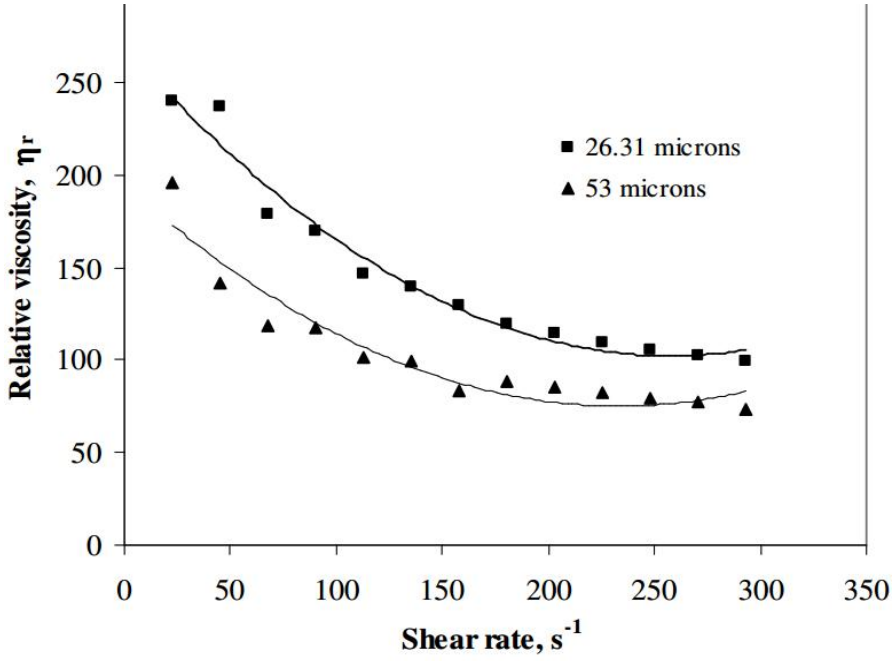

Figure 11 : Effect of particle size distribution on slurry viscosity at 46 vol.% concentration

Irrespective of the solids concentration, the specific surface area of the particles increases due to presence of more finer particles in sample S-1 that leads to the production of new surfaces and the total number of particles increases promoting a decreasing of inter-particle distance. For sample S-2 with larger median particle size and with less proportion of finer particles, the interaction between particles is weak. Hence the relative viscosity indicates higher values for S-1 than S-2 at a specific solids concentration and shear rate [16].

Kawatra and Eisele observed that at a constant solids concentration, a reduction in particle size will result in an increase in (silica sand based suspensions slurry) viscosity (1998). This was attributed to increased surface area, which binds up water molecules and thus increases the effective solids concentration. This is in contradiction with the work of Clarke, (1967) and De Bruijn, (1951) as reported by Thomas, (1965), which revealed that slurry viscosity increases with particle diameter. They attributed this to inertial effects, which resulted in additional energy dissipation. Clarke conducted his investigations on silica sand suspensions in water having particle sizes of up to 211 microns and concentrations of up to 50% by volume. A rotational viscometer was used to determine the rheological measurements of the suspensions [14].

5. 3. Impact of shear rate (rotation)

Viscometric investigations of concentrated aqueous alumina suspensions with particle size smaller than 5 µm have been investigated [26]. In the shear rate interval between 20 and 640 S^{-1}, the experimental flow curves indicated thixotropy, which exhibited a pseudoplastic flow behaviour

in the range smaller than 200 S^{-1} and a dilatants flow behavior in the higher range. The shear rate in a stirred bead mill is closely pertinent to its rotational speed. Thus, the effect of rotational speeds on slurry rheology is important to characterize correctly the flow behavior of slurry and to provide reasonable data for commercial production. However, no methods can accurately predict a real shear rate in a stirred media mill at present. Therefore, the precise evaluation of the shear rate distribution at different points in a stirred media mill with respect to the slurry rheology should be studied by means of computational fluid dynamics [27].

According to Cheng (1980), as the concentration increases from medium to high, non-Newtonian behavior is exhibited. The transition from Newtonian to non-Newtonian is not only dependent on concentration but also on shear rate. The shear rate at which the non-Newtonian behavior starts decreases as concentration increases. As the shear rate increases, the suspension first becomes shear thinning and then shear thickening. Ferreira and Olhero (2003) noted similar observations in studies with silica sand-water suspensions. The experiments were conducted using particle sizes ranging from 2.2 to 19 microns with a solids concentration up to 46% by volume. The rheological measurements were conducted using a rotational controlled stress rheometer. They observed that the shear thinning behavior occurred at low shear rates. This was followed by a shear thickening behavior at intermediate shear rates and a trend to Newtonian behavior at the highest shear rate region. The transition from shear thinning to shear thickening at higher shear rates for narrow particle size distributions was attributed to particle rearrangements and the increasing average distances between layers of particles. Under these conditions the capillary forces oppose to the flow and the suspension thickens [14].

5. 4. Effect of temperature

Temperature is another important factor that strongly affects the apparent viscosity and yield stress of slurries by varying the viscosity of a carrier solvent. Yang et al. [28] have investigated the temperature dependences of viscosity and yield stress for titanium dioxide suspensions. The viscosity decreased with increasing temperature (see Fig. 12), as is consistent with results reported by Mikulasek et al. [29], and the yield stress decreased with increasing temperature in the lower temperature ranges and increased in the high temperature (see Fig. 13). It was also noted that the suspensions underwent a flow transition from shear thinning to shear thickening at a shear rate of about 10 S^{-1} around 50°C (see Fig. 12). The onset of shear thickening was dependent on the balance of hydrodynamic and Brownian contributions. In wet ultrafine grinding, the temperature of ground slurries changes significantly during grinding. For instance, the temperature of various

ground slurries fluctuated from 14 to 60 °C under different conditions in a stirred media mill [30]. It is necessary to take into account the effect of temperature when evaluating the slurry rheology.

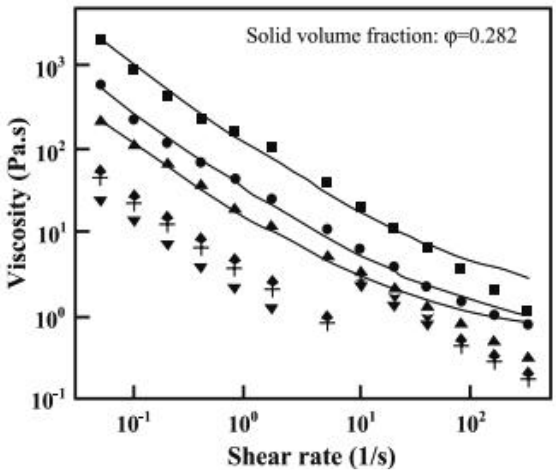

Fig. 12. Relationship between shear viscosity and shear rate at different temperatures.

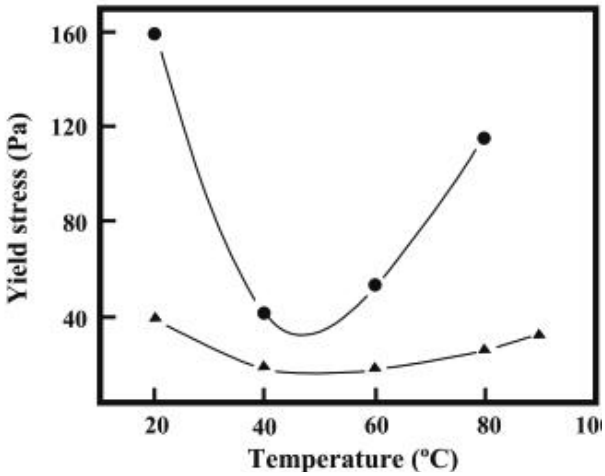

Fig. 13. Yield stress at various temperatures. Solid volume fraction: ● φ=0.282 ,▲ φ =0.238 .

The temperature dependence of viscosity of Coal Water Slurry (CWS) was also investigated by S. K. Mishra and al in the shear rate of 0 to100 S^{-1} [17]. Figure 6 shows the variation of the logarithm of viscosity as a function of the reciprocal temperature for various solids concentration for ROM coal (C) only. As seen in the figure, the temperature dependence of viscosity can be represented in terms of a simple Arrhenius expression for the range of temperature investigated. The relation between viscosity and temperature may be presented as:

$$\eta = A \exp(E/RT)$$

or

$$1n\ \eta = E/RT + 1nA\ ;$$

Where η is the viscosity at a particular shear rate, E is the fluid-flow activation energy, T is the temperature in Kelvin, R is the universal gas constant, and A is a fitting parameter. As is well known, an increase in the temperature of the system leads to an increase in the kinetic energy of the particles, which results in a decrease in the viscosity of the CWS. Table 1 shows the values of fluid-flow activation energy for the CWS of the three different coals at different solids concentration at the shear rate of 100 S^{-1}. It may be noted that there is little variation in the apparent activation energy with shear rate and amount of coal in CWS. Yamaguchi et al. (1979) also conclude that the apparent [31].

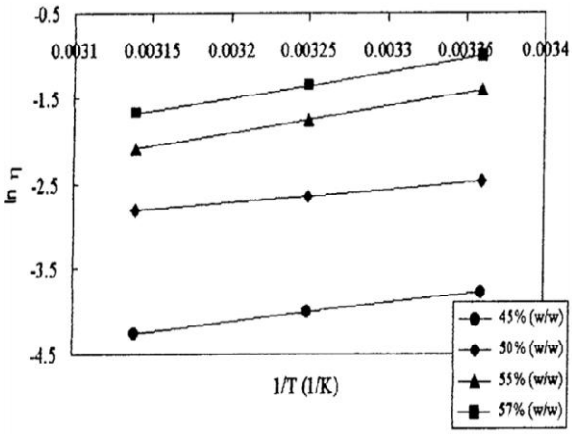

Figure 14. Effect of temperature on apparent viscosity of CWS (coal C) at 100 1/S.

Fluid-flow activation energy as a function of the solid concentration for CWS of different coal samples

Solid Concn. % (w/w)	Activation Energy, kJ mol^{-1}		
	CWS (Coal A)	CWS (Coal B)	CWS (Coal C)
45.0	30.23	18.48	18.37
50.0	41.57	19.19	13.25
55.0	23.62	23.66	27.71
57.0	...	...	26.02

Table 1: Fluid-flow activation energy as a function of the solid concentration for CWS of different coal samples

P.K.Sanapati et al [16] found that; during the process of grinding the limestone slurry samples, the temperature of ground slurry fluctuates between 30 °C to 60 °C depending upon the grinding conditions which affects the slurry rheology [32]. Therefore the temperature dependence of viscosity of lime stone slurry was also investigated in the shear rate range of 1 to 300 S^{-1}. P.K.Sanapati et al were investigated the variation of temperature with relative viscosity of the limestone slurry sample at 40.4 vol.%, 43.1 vol.% and 46.0 vol.% solids concentration respectively. The relative viscosity of the slurry decreases in the range of temperature studied (30°C – 50 °C). The trend of decreasing viscosity at elevated temperatures occurs due to increased kinetic energy of the particles promoting the breakage of intermolecular bond between adjacent layers which results in decrease in viscosity of the limestone slurry.

5. 5. Influence of slurries PH

Some literature shows that the pH value greatly influenced the rheological behaviours of ultrafine sulphide mineral slurries in size below 5 μm, such as sphalerite and galena . It was found that the yield stress was strongly dependent on the pH value due to the significant dependence of the surface properties of ultrafine sulphide mineral particles in slurries on the pH value. Furthermore, the maximum yield stress value occurred in the region of pH values corresponding closely to the isoelectric points (IEP) of various minerals, as is in agreement with the results from the slurry of oxides, and kaolin. Besides, Prestidge studied the effect of pH on the viscosity of galena slurry. The results showed that the plastic viscosity of the slurry was insignificantly dependent on pH, which is similar to the experimental results for alumina suspensions in the pH ranges from 7.3 to 10.8 by Zhou et al. However, some studies on the slurries of titanium dioxide and of ZST ((Zr,Sn)TiO4) and Nb2O5 have shown that the pH of slurry could change the flow pattern of slurry and thus varied the viscosity of slurry (see Figs. 15). These results are not free

from contradictions due to the complexity of the factors influencing slurry rheology, such as particle size/shape and particle surface properties. Besides, the effect of the interactions between or among the pH value and other factors on slurry rheology is unclear [33 – 40].

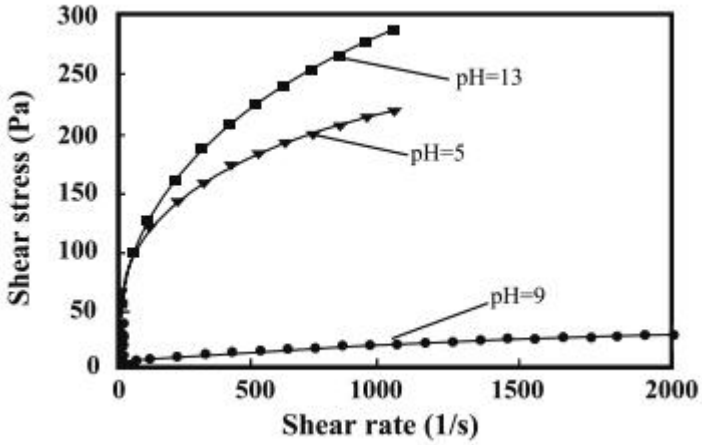

***Figure 15:** Effect of pH on the flow properties of 30 vol.% titanium dioxide dispersions at temperature 20 °C.*

Concerning the impact of PH on the rheology of coal water slurry, it is well known that the surface properties of coal and the ionic strength of the supernatant solution strongly influence the rheology of CWS [17]. Supernatant composition and ionic strength can vary with pH since comparatively large amounts of metal ions are dissolved at low pH, and at pH greater than about 8 the dissolution of the same decreases to trace amounts (Kaji et al., 1985) [41]. The resulting ionic strength has a significant effect on the stability of CWS stabilized by electric charge on the particles against flocculation (Heimenz, 1986) [42]. The oxygen-containing functional groups along with the inorganic minerals contribute to particle surface charge. The oxygen-containing functional groups (carboxylic and carboxylates) with exchangeable cations play a very crucial role in influencing changes in yield stress and apparent viscosity (Boger et al., 1987) [43]. The surface charge is low at low pH, as the functional groups are hydrogen exchanged. The net attractive interaction between the particles results in flocculation. Hence at low pH the apparent viscosity of CWS is high. The surface charge increases with increases in pH. This leads to the formation of a well-dispersed suspension and results in the reduction in apparent viscosity.

Kaji et al. (1987) [43] reported the influence of pH on the apparent viscosity of CWS of an American bituminous coal from the Upper Freeport, Pennsylvania seam (ash 11.5 wt%, VM 30.6 wt%, and moisture 1.9 wt%) in the pH range of 7 to 8.5 only. According to the authors, viscosity of CWS increases with decreasing pH, i.e., with increasing hydrogen ion concentration in the supernatant solution. The present work shows the variation of apparent viscosity with a wide range

of pH, i.e., in the range of 3.0 to 9.0. The apparent viscosity of 50% (*w/w*) slurries of all three types of coal was measured at shear rates ranging from 0 to 100 S21. It may be seen from Figure 4 that apparent viscosity increases from pH 3, attains its peak value in the pH range of 5 to 6, and then decreases with increase in pH. It is interesting to note that viscosity has the highest value near the pHpzc of coal. The pHpzc of ROM coal was determined using the solid addition method (Balistrieri and Murray, 1981) [44] and was found to be 5.5. At pHpzc there is hardly any repulsion between coal particles. It may be seen from Figure 4 that the values of apparent viscosity decrease at pH values below and above pHpzc. The variation of apparent viscosity with pH may be attributed to the partial neutralization of the electrical charge of the particles by the compression of the electrical double layer around them, thus decreasing the repulsive interaction forces caused by the overlap of the double layers (Verwey, 1947) [45].

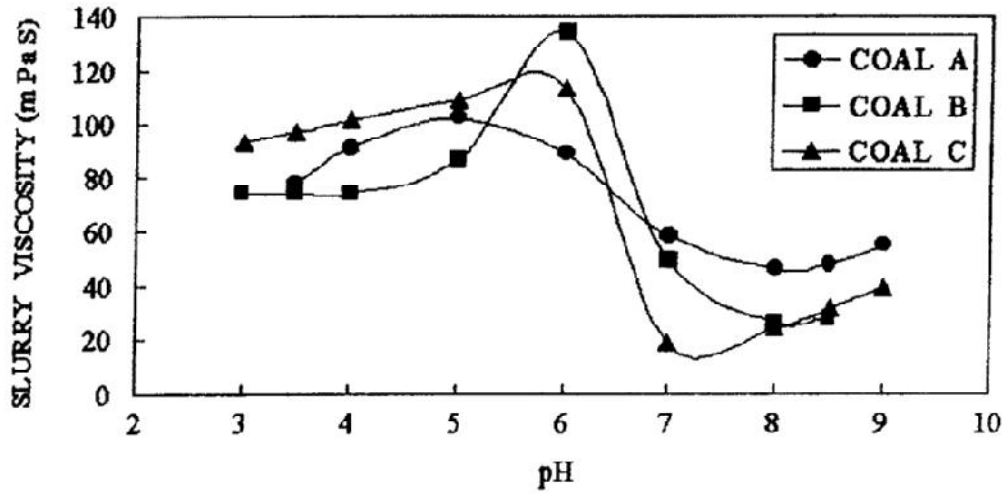

Figure 16: Apparent viscosity of CWS (50% w/w) as a function of pH at a shear rate of 100 (1/S). [17]

The change in the flow behavior of CWS may be illustrated with the help of the power law (Ostwald model), $\sigma=k.\gamma^n$, where *k* is referred to as a fluid consistency and *n* is called a flow index. Figure 5 shows the effect of pH of the CWS on the constants *n* and *k* with pH for 50% (*w/w*) CWS at 25° C (shear rate 100 S^{-1}) for coal C as a typical example. The results show that for CWS involving coal A, the value of *n* increases almost linearly with pH, whereas that of *k* decreases with a similar increase. The situation is little different with the two other varieties of coal. In case of CWS of coal B (25% ash), *n* remains constant in the pH range 3 to 5, decreases to its lowest value at pH 6, attains its peak value at pH 7, and then decreases with increases in pH. The parameter *k* exhibits the opposite trend to that of *n* in the same pH range. For the CWS of coal C (37% ash), initially *n* decreases from pH 2, attains its minimum at pH 5, and then increases

exponentially with pH. The parameter *k* exhibits the opposite behavior of *n* with change in pH as shown in Figure 17 [17].

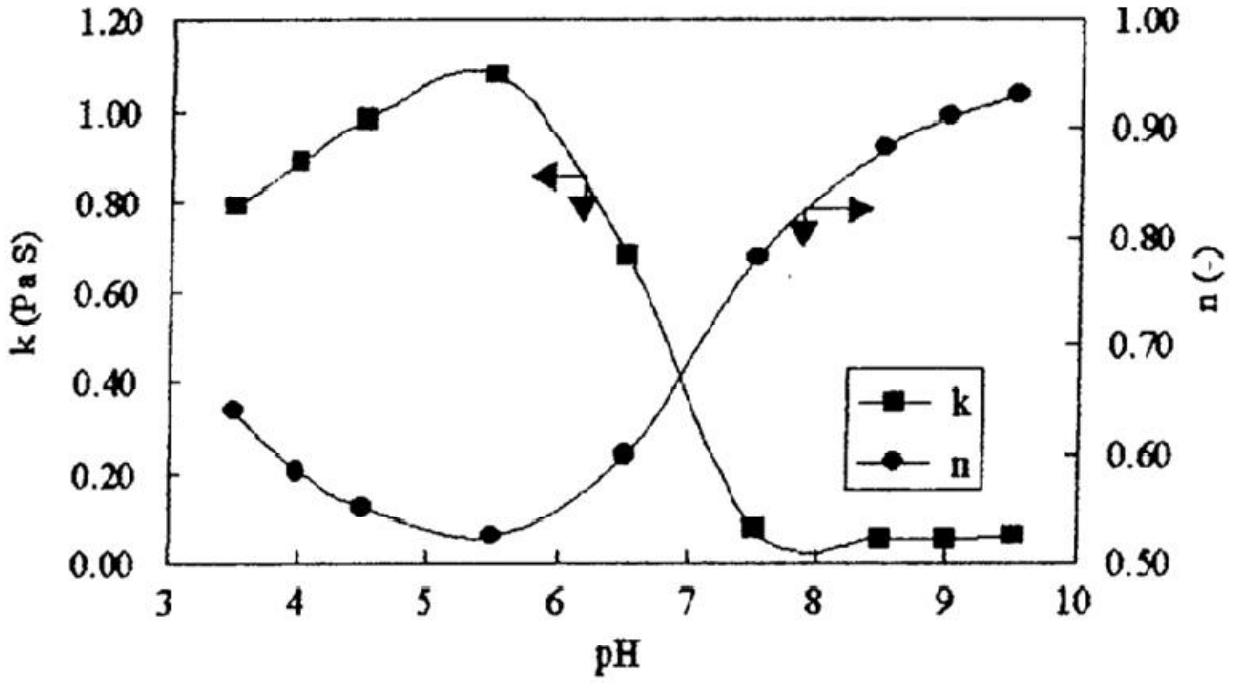

Figure 17: ***Apparent viscosity of the coal slurry (50% solids) as a function of pH at a constant shear rate of 100 (1 / S). Coal (37% ash).*** *[17]*

5. 6. Effect of additives (dispersants)

The effect of a dispersant on wet ultrafine grinding performance is crucial since the solids content of a ground material with an appropriate dispersant in a stirred media mill increases by about 30 wt.% and the fineness of the final product significantly enhances. For the slurry rheology control, the mostly used dispersant as a grinding aid is polyacrylic acid or its salts with a molecular weight in the range of 5000 to 20,000, which appears to be optimal depending on the application. However, there is still little understanding on the mechanism for the effect of molecular weights of a dispersant on the slurry rheology control. The methods to determine the optimum dosage of a dispersant need further be optimized to accurately control a slurry rheology by the use of a dispersant. The influence of the periodic addition of dispersant on slurry rheology is still lack of reason able experimental explanation. These relevant investigations should be studied by means o f some effective characterization methods, such as X-ray photonelectron energy spectrometry (XPS), infrared spectrome try (FT-IR), atomic force microscopy (AFM), and the measurements of rheology with a suitable rheometer and of zeta potential in a concentrated suspension with a reliable technique as well [70].

6 - Conclusion

In this chapter we presented different theoretical and experimental aspects of fluid and complex suspensions rheology concept. Some definitions of the physical natures of the effects between particles in complex suspensions have been briefly discussed.

We have discussed the results of some research carried out on the rheology of some ore-based slurries, that is to say, mixtures between fine particles of ores and water. For example, coal water slurry, Limstone slurry, sand slurry, Titanium dioxide slurry etc ... The effect of physicochemical parameters on the rheological behavior of these slurry was briefly presented in this chapter. These parameters are the concentration in solids, the particle size distribution, the temperature, pH, shear rate and additives.

We have noticed that the physicochemical parameters have very remarkable impacts on the rheology of ore-based slurries. The impact of these parameters varies from each substance to another.

Chapter 3

EXPERIMENTAL AND MODELING THE FLOW BEHAVIOR OF PHOSPHATE SLURRY VIA PIPELINE AND SIMULATING THE IMPACT OF PIPELINE OPERATING PARAMETERS ON THE FLOW

Chapter abstract

In this chapter, we were interested in the flow of phosphate-water slurry into the pipeline linking the Khouribga mine pole (Morocco) and the Eljorf-Lasfar industrial platform in El Jadida (Morocco). We carried out a mathematical modeling on the linear head losses, the hydraulic gradient, the friction factor and the geographic profile followed by the pipeline. The results of the modeling were grouped in a program in MATLAB. The modeling allowed us to know the values of the pressures in all the points of the pipeline according to the operating parameters. The agreement of the experimental results with the results of our modeling pushed us to make simulations through our theoretical model. The simulations focuses on the impact of flow rate, density, viscosity of the slurry and choke on the behavior of head losses. This simulation allowed us to present perfectly the impact of the physical properties of the slurry and the operating parameters of the pipeline on the behavior of head losses. This study includes the case of continuous pumping in slurry and the batch case.

1. Introduction

Between the Khouribga mining basin and the industrial platform of JorfLasfar, the OCP Group built, over 187 km, the Slurry Pipeline to convey phosphate slurry for valorization. This transport infrastructure is revolutionizing both upstream and downstream of phosphate mining in Morocco. The objective of the transport of the phosphate slurry through the pipeline is to reduce the energy bill and to increase the production capacity. This mode of slurry transport essentially depends on two constraints: The geographic profile of the route (Khouribga- Jorflasfar), and the physical properties of the phosphate slurry.

The "Slurry pipeline" project consists of a main line of **187 km** in length and **90 cm** in diameter, linking the head station (pumping station) to the terminal station, and 4 secondary pipelines feeding the head station In slurry from phosphate washing plants [61-64].

The fluid studied is phosphate slurry, which is a mixture of very fine grains of phosphate and water, the mixture consists of **60%** phosphate and **40%** water. In this study, we consider that the phosphate slurry behaves like a pseudo plastic fluid characterized by its density **ρ** and its viscosity **μ** [102], the flow regime of the slurry is always turbulent to avoid the sedimentation of solid aggregates down the pipe.

The main objective of the study in this paper is to establish a theoretical model that simulates the operation of the pipeline's operating parameters. This study uses linear interpolations to model the geographical profile followed by the pipeline, In order to have a function **Z (x)** which manages the behavior of the geographical profile, and we also rely on the formulas of 'Darcy' and 'Swamee and jain' [64-67], to model the linear head losses in order to have a function **H (x)** which manages the head losses and the behavior of the hydraulic grade line during the flow.

We also adopt an experimental approach to compare the real results with the results generated by the theoretical model. We begin with the experimental approach to describe the components of the pipeline installation and to mention experimental values of pressure and hydraulic gradient in the pipeline.

2 - Experimental approach

2.1. Description of the system

2. 1. 1. The hydraulic system

A typical pipeline system consists of a tank, a suction line with a valve, a pump, an exhaust pipe and a tank [101].

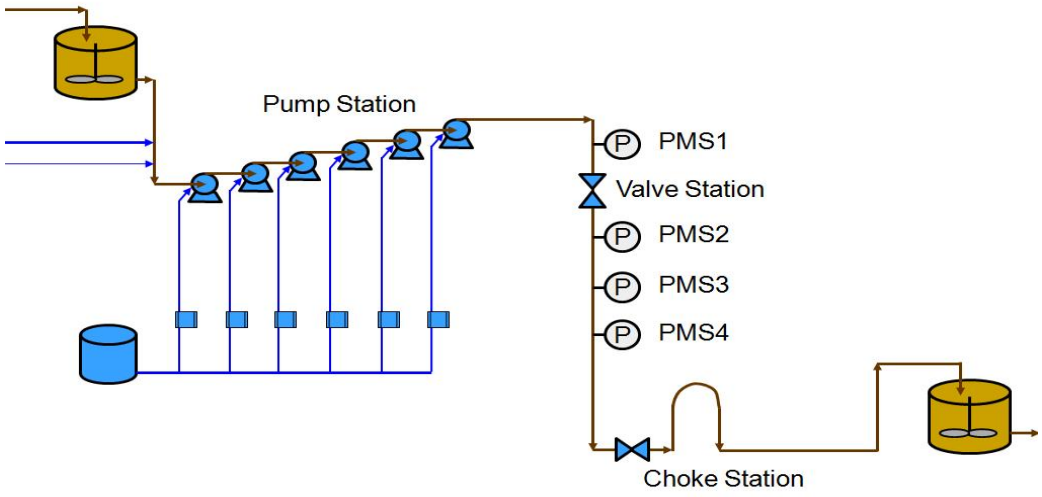

Figure 1: The components of the hydraulic pipeline system [101].

The head station consists of 4 slurry storage tanks and a pumping station, this pumping station is equipped with 6 centrifugal pumps mounted in series, to increase the pressure and keep the same flow. The terminal station is composed of 8 slurry storage tanks and a (choke station), the

role of the choke station is to brake the pipeline from its end to adjust the pressure and flow rate, because of this choke the hydraulic head increases in the pipe. Along the path are installed pressure and monitoring stations (PMS) marked in (Fig. 1). The PMS1 is located 46 km from the head station, the PMS2 is located 101 km from the head station. The PMS3 is located 129 km from the head station, the PMS4 is located 161 km from the head station. For the station of the valves this station is located at 68 km of the head station, it also contains sensors for measurement of pressure.

2. 1. 2. The geographical tracing (pipeline profile)

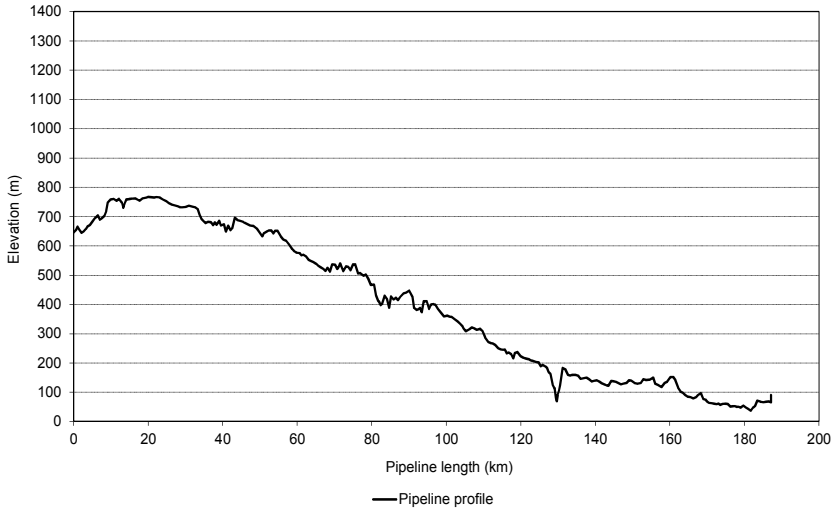

Figure 2: The geographical tracing Khouribga-Jorf Lasfar

The geographical tracing is the path followed by the pipeline, taking into account at sea level height. The geographical tracing represents the profile of the pipeline, linking the head station to the terminal station.

The height of the head station (Khouribga) in relation to sea level is 645m.

The height of the terminal station (jorflasfar) in relation to the sea level is 66m.

The geographical tracing presents the profile of the pipeline over the 187 km (altitude as a function of the distance).

The head station is at the point (x = 0), and the terminal station is at the point (x = 187 km).

We note that this is a slope between the head station and the terminal station, therefore the energy required for the pumping is optimized by the gravity.

2. 1. 3. Measurement of operating parameters and physical properties of the slurry

The head station contains an internal laboratory which aims to measure the plastic viscosity of the slurry; and analyzing the particle size of the particles contained in the mixture (water-phosphate), the diameter of the phosphate particles is always lower to **250µm**, for measuring the density of the slurry. The pipeline is equipped with Sensor with gamma ray, this sensor is permanent, it delivers us the value of the density of the slurry at every moment. Measurement of flow in the pipeline is carried out through an ultrasonic flow meter and pressure measurement through ABB2600T sensors. These pressure and flow sensors are contained in all of the (PMS) mentioned previously [102].

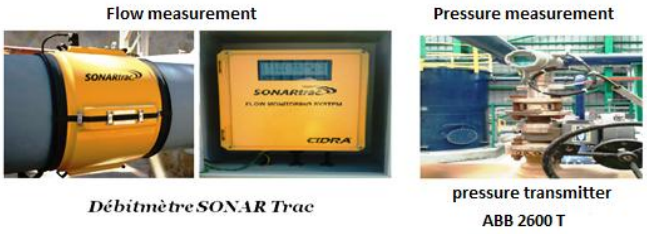

Figure 3: Measuring instruments

All these instruments are linked to a control and data acquisition system (SCADA), which displays in the control room the general behavior of the transport process via pipeline. This allows operators to track, and control the operating parameters. The values measured by all the metrology instruments that we have already mentioned are displayed in an interface in the control room.

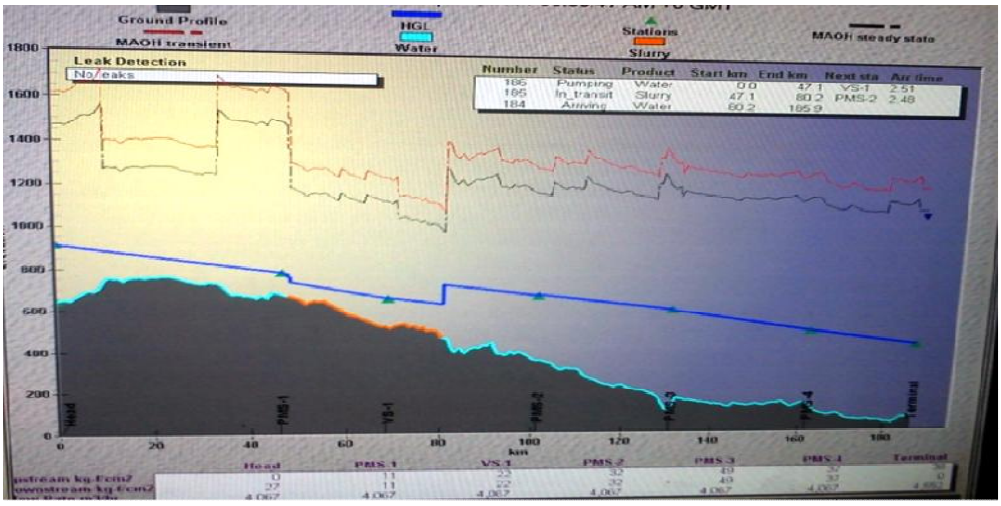

Figure 4: Real supervision system (SCADA)

The information contained in this screenshot (Fig. 4) are the pressures in all (PMS) in bar, flow rate in m^3 / h, hydraulic head of output pumping station, and the drawing of the hydraulic grade line (behavior of the pressure drops), it is the line in dark blue. We notice clearly in (Fig. 4)

that part of the pipeline is colored orange and the other two parts are colored in sky blue, the part colored in orange is the part filled with slurry for the other part is filled with water, this section of slurry is pushed by the water to the terminal station (piston effect), this is the case for (Fig. 4). The slurry section is called a batch.

We also notice that the behavior of the hydraulic grade line for the part filled with slurry is not the same for the part filled with water, which is normal because the head losses are due to the physical properties of the fluid.

The pressure values detected in the case of Fig. 4 are shown in the following table:

Table 2: The pressure values detected by the various pressures measuring stations

	Head station	**PMS 1**	**Vanes station**	**PMS 2**	**PMS 3**	**PMS 4**	**Terminal station**
Pressure (in bar)	27,89	11,07	22,11	32,51	49,92	37,6	38,85

This test was carried out for a flow rate of 4000 m3 / h and a slurry density ρ = 1600 Kg / m3 and a plastic viscosity of slurry μ = 0.0102 Pa.s.

The hydraulic gradient of the flow for the slurry filled part is: J = 0.0038 meter / meter of the pipeline.

Throughout this study, we are interested in the fact that the hydraulic gradient of the flow of the part fills in slurry.

(The plastic viscosity of the phosphate slurry varies in a design range between 0.006 Pa.s and 0.0102 Pa.s.) [103].

3. Theoretical approach

3. 1. Modeling of the geographical profile followed by the pipeline

The problem that exists is that the profile of the pipeline given by the constructor is not continuous; it does not contain all the points of the path between the head station and the terminal

station. It contains only the coordinates of 303 points belonging to the route. This profile is discontinuous.

Table 2: The coordinates of the 303 points belonging to the pipeline profile

Point	**Distance** (m)	**Elevation** (m)
1	0,0	645,8
2	428,5	651,5
3	1094,7	656,7
4	1782,3	649,0
5	2354,1	643,6
↓	↓	↓
302	187252,3	66,4
303	187252,3	93,2

In order to have a continuous pipeline profile we will precede to an interpolation method between the points given in Table (2), this method consists in establishing linear functions of the form,

$$Z(x) = ax + b \qquad (1)$$

between each point and which follows. The **a** and **b** are determined from the coordinates of the points in the table (2). That is, between point 1 of coordinates (0; 645) and point 2 of coordinates (428; 651.5):

$$Z(x) = \left(\frac{651,5 - 645}{428 - 0}\right) x + 645$$

$$= (0, 01330)\, x + 645 \qquad \text{for } x \in [0 ; 428]$$

Between 2 → 3: Z(x) = (0, 00780) x + 648, 1577 for x ϵ [428; 1094.7]

Between 3 → 4: Z(x) = (-0, 01119) x + 668, 9418 for x ϵ [1094.7; 1782.3]

Between 4 → 5: Z(x) = (-0, 00944) x + 665, 8220 for x ϵ [1782.3; 2354.1]

↓ ↓ ↓

Between 302 → 303: Z(x) = (-0.00099) x + 251,7980 for x ϵ [186747.4 ; 187252.3]

Now the geographical profile is continuous over the interval [0; 187252.3], and manage by the function **Z (x)**. The function **Z (x)** is defined by part on the interval [0; 187252.3]. (187252, 3) is the length of the pipeline in meters.

3.2. Modeling the behavior of head losses

3. 2. 1. Case of Continuous pumping in slurry

The hydraulic grade line is the line describing the linear head losses along the pipe; we will determine the function **H (x)** which manages this line. For continuous pumping of the slurry the hydraulic grade line keeps the same inclination along the entire pipeline. In general, for turbulent flows, the friction factor **f** is determined from the MOODY diagram and the COLBROOK-WHITE formula, but for the case where:

(10^{-6}< k/D < 10^{-2} and 5×10^{3}< Re < 1×10^{8}), which is our case; we used the equation "Swamee and Jain". The coefficient of pressure drop **J** or (hydraulic gradient) from Darcy's formula **[101-103]**:

$$J = \left(\frac{\Delta H}{\Delta x} \right) = \frac{2\ f\ V^{2}}{g\ D} \qquad (2)$$

With $$f = \frac{0.33125}{\left[\ln\left(\frac{k}{3.7D} + \frac{5.74}{\mathrm{Re}^{0.9}} \right) \right]^{2}} \qquad (3)$$

f: the friction factor ; **V**: the flow velocity of the fluid. **D**: The internal diameter of the pipeline (D = 0.85 m); **g**: acceleration of gravity; **k**: The roughness of the pipe. The friction factor **f** is related to the Reynolds number **Re** and the roughness **K** by the ratio (k / D) as indicated by the

equation (2) and (3). The inner layer of the pipeline is made of a plastic material (H.D.P.E) having a roughness $k = 2 \times 10^{-5}$.

For an elementary displacement on the pipeline:

$$\lim_{\Delta x \to 0} \frac{\Delta H}{\Delta x} = \frac{dH}{dx} = \frac{2 f V^2}{g D} \qquad (4)$$

So: $dH = \frac{2 f V^2}{g D} \times dx$; Integrating this formula: $\int dH = \int \frac{2 f V^2}{g D} .dx$

We will arrive at: $H(x) = (\frac{2 f V^2}{g D})x + cte$

Determining the integration constant: at x = 0, **cte=H(x=0)**. **H(x=0)** is the head supplied by the pumping station (**hi**) + the head due to the choke (**C**). (**x = 0** is the position of the pumping station).

So the analytical function that manages the hydraulic grade line for the case of continuous pumping in slurry:

$$H(x) = (\frac{2fV^2}{gD}) x + H(x = 0) \qquad \forall x \in [0; 187252] \qquad (5)$$

In this case the pumping is continuous in slurry (the slurry, fills the entire pipeline).

3. 2. 2. Batch Case

For the batch case the pumping is not continuous in slurry, the batch does not cover the entire pipeline, it occupies part of the pipeline and the other parts are occupied by water to keep continuity in the pipeline, and pushed The batch to the terminal station (piston effect). Water assures the separation between the different volumes of slurry in the case of several batches.

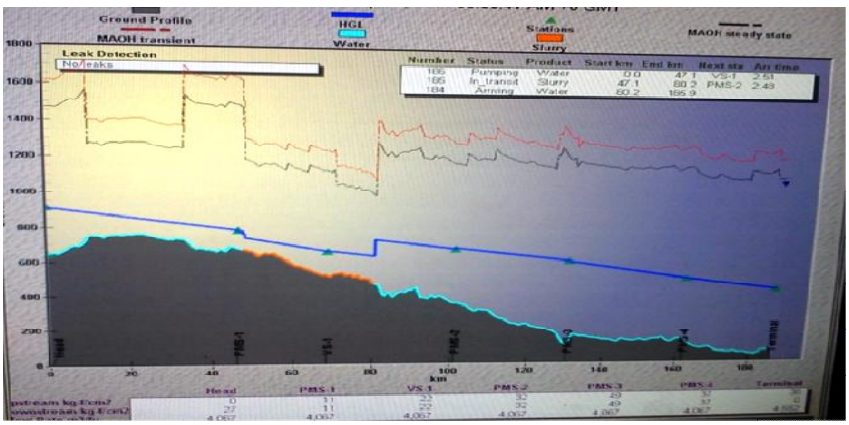

Figure 5: Batch operation

In this case we have two types of functions that manage the hydraulic grade line, function in the part filled by the slurry and function for the water filled parts. The position of the batch tail in the pipeline is (i) and the position of its head is (j).

$$\mathbf{j > i \ \ and \ (i \ ; \ j) \in [0 \ ; 187252]^2}$$

The behavior of the hydraulic grade line along the pipeline in this case is managed in this way:

For $X \in [0 \ ; \ i]$: $$\mathbf{H(x) = \left(\frac{2\, f''\, V^2}{g\, D}\right) x + H(x = 0)} \quad (6)$$

(f " is the friction factor for water flow)

For $x \in [i \ ; \ j]$: $$\mathbf{H(x) = \left(\frac{2\, f\, V^2}{g\, D}\right) x + H(x = 0)} \quad (7)$$

(f is the friction factor for slurry flow)

For $x \in [j \ ; \ 187252]$: $$\mathbf{H(x) = \left(\frac{2\, f''\, V^2}{g\, D}\right) x + H(x = 0)} \quad (8)$$

The friction factor **f** depends on the density **ρ** and on the viscosity **μ** of the fluid, so the inclination of the hydraulic grade line for the water flow does not have the same behavior as for the flow of the slurry.

3. 3. Elaboration of MATLAB program

We have obtained functions to model the behavior of the geographical route (pipeline profile), and to model the head losses (hydraulic grade line) along the pipeline, either for continuous pumping or for batch. And this in order to have a program in MATLAB that provides the value of the pressure in any point of the pipeline, for given conditions of operation. Condition of operation: (flow rate, viscosity,density, pumping station outlet head, ...). The structure of the program is based on the function **Z (x)** which characterizes the behavior of the pipeline profile and on the function **H (x)** which characterizes the hydraulic head losses along the pipeline (hydraulic grade line). Are the functions obtained in the preceding paragraphs, and we will also rely on the method of calculating the pressure at a point (M) belonging to the pipeline.

$\mathbf{P}(M) = [\mathbf{H}(M) - \mathbf{Z}(M)] \times \rho \mathbf{g}$ (Bernoulli's theorem), it is a pressure relative. In this study, we have interest that this pressure. ρ: density of the fluid; g: acceleration of gravity; P (M): the pressure at point (M), H (M): The head in point (M), Z (M): height of (M) with respect to sea level.

4. Results and discussion

4. 1. Comparison of program results with real results

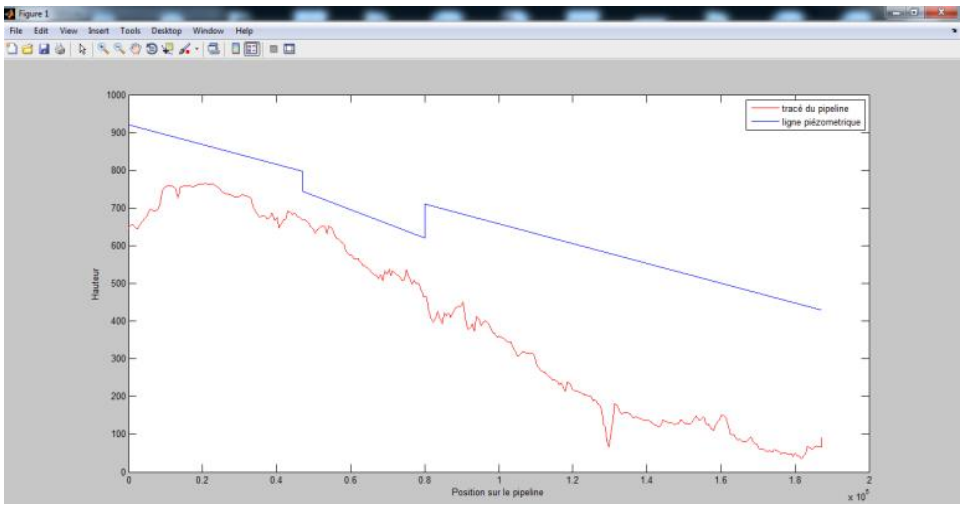

Figure 6: The plot of the geographical profile and hydraulic grade line delivered by the program

The plot displayed by the program is similar to the plot displayed on the real control system in the control room, the difference between the two plots is that the first plot (fig. 6) is based on theoretical calculations and the second plot (fig .5) is based on experimental measurements. The operating conditions in this case are: the position of the batch tail (in km): 47, the position of the batch head (in km): 80, the flow rate (in m3 / h): 4000, the slurry density (in Kg / m3): 1600, plastic viscosity of slurry (in Pa.s): 0.0102, the hydraulic head at pumping station output (in meters): 240, the hydraulic head caused by choke (in meters): 35.

We carried out a series of experiments to compare the actual results with the theoretical results given by the program. These tests consist in comparing the pressure values given by the (PMS) with our model in MATLAB.

The following table shows the result of the test closer to reality, the actual values of the pressures marked in this table are the values already quoted in the paragraph (experimental approach).

TABLE 3: A comparison of real results and results delivered by our model

	Head station	**PMS 1**	**Vanes station**	**PMS 2**	**PMS 3**	**PMS 4**	**Terminal station**
Real results(bar	27,89	11,07	22,11	32,51	49,92	37,6	38,85
Theoretical results(bar	27,18	12,47	22,63	33,11	51,23	37,3	39,41

In this test the position of the tail of the batch was in the kilometer 47 and its head in the kilometer 80. This test was made for a running flow of 4000 m3 / h and a slurry density ρ = 1600 Kg / m3 and a plastic viscosity of slurry μ = 0.0102 Pa.s, the hydraulic gradient for the flow of the slurry in this simulation is: J = 0.0038 meters / meter of the pipeline, it is the same gradient obtained experimentally. We notice the approximate agreement of the real results with the theoretical results, which validates and values our theoretical model.

4. 2. Simulation through our theoretical model

We have proved the validity of our model, and at what level the results of the model are in agreement with the experimental results. It is what encouraged us to do some simulations has shortcoming our program, to know the influence of certain operating parameters on the behavior of the process.

This simulation consists of having all the parameters fixed, and of varying one of them in order to know its impact on the pressures and the head losses. These parameters are: (flow rate, slurry density, slurry viscosity, and the hydraulic head that associates the choke to pipeline).

4. 3. Simulation on the Influence of flow rate, slurry density, slurry viscosity and hydraulic head caused by choke

- Influence of flow rate

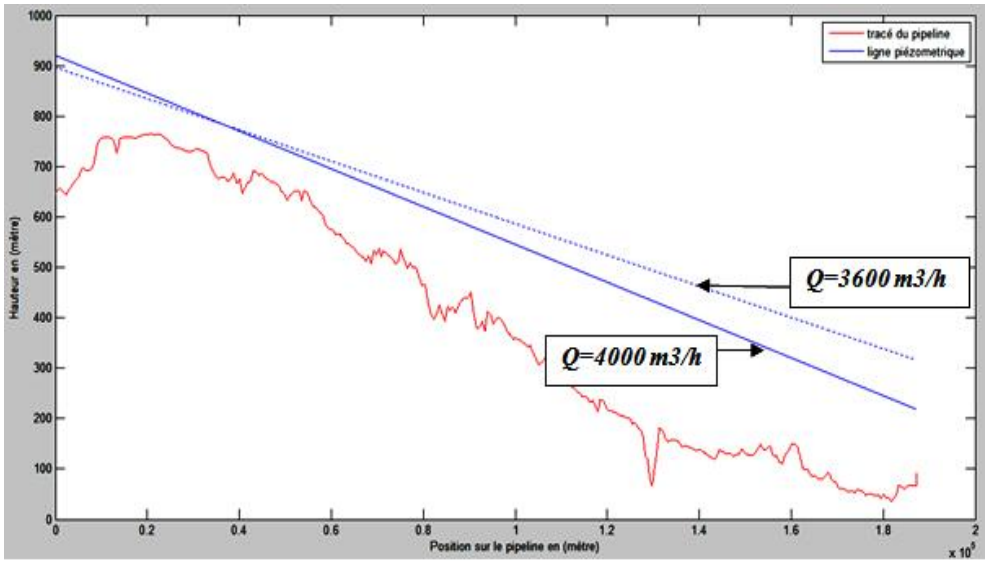

Figure 7: Hydraulic grade line for flow rates 3600 m^3 / h and 4000 m^3 / h , for continuous pumping in slurry

Concerning continuous pumping of slurry, in the case where the flow rate is 4000 m^3 / h, the hydraulic grade line is more inclined at the bottom than the case where the flow rate is 3600 m^3 / h, the head losses for (Q = 4000 m^3 / h) are greater than for (Q = 3600 m^3 / h).It can be concluded that the higher the flow rate increases the greater the head losses.

The hydraulic gradients shown in our program are J = 0.0038 m / m for (Q = 4000 m^3 / h) and J = 0.0031 m / m for (Q = 3600 m^3 / h). The flow rate has the same influences for the case of batch. The red line is the geographical tracing of the pipeline, and the blue line is the hydraulic grade line.

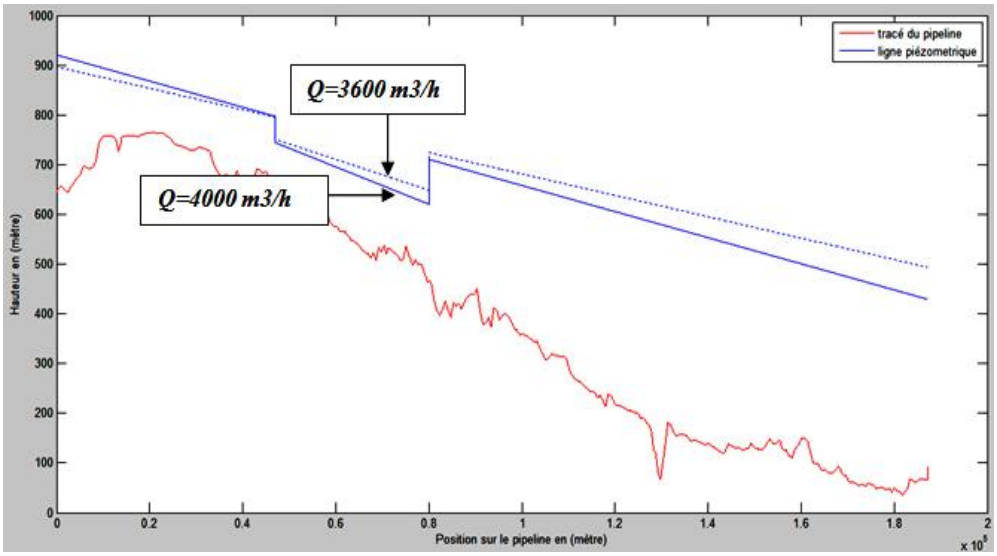

Figure 8: Hydraulic grade line for the flow rates 3600 m^3 / h and 4000 m^3 / h , for the batch case

- Influence of slurry density

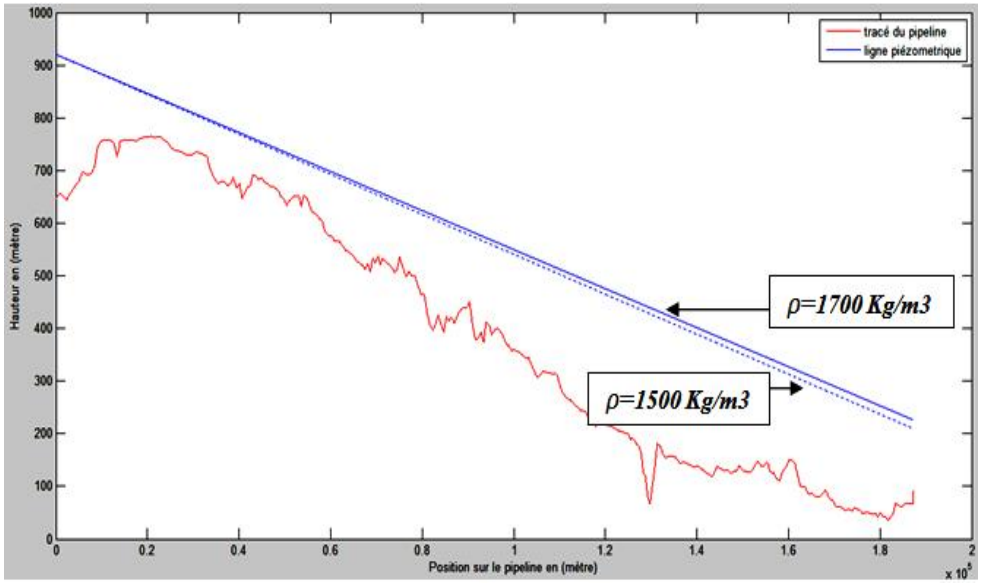

Figure 9: Hydraulic grade line for densities 1700 Kg / m^3 and 1500 Kg / m^3, for continuous pumping

Concerning continuous pumping, in the case where the slurry density is ρ = 1500 Kg / m^3, the hydraulic grade line is more inclined at the bottom than the case where the slurry density is ρ = 1700Kg / m^3, so the head losses of (ρ = 1500 Kg / m^3) are greater than for (ρ = 1700 Kg / m^3), normally we must have the opposite tendency, but here we have to consider that the viscosity is constant between the two cases. In general, we notice from the curves that the slurry density has no significant influence on the behavior of the pressure drops. The hydraulic gradients shown in our program are J = 0.0037 m / m for (ρ = 1500 Kg / m^3) and J = 0.0038 m / m for (ρ = 1700 Kg / m^3). The slurry density has the same influences on the batch case.

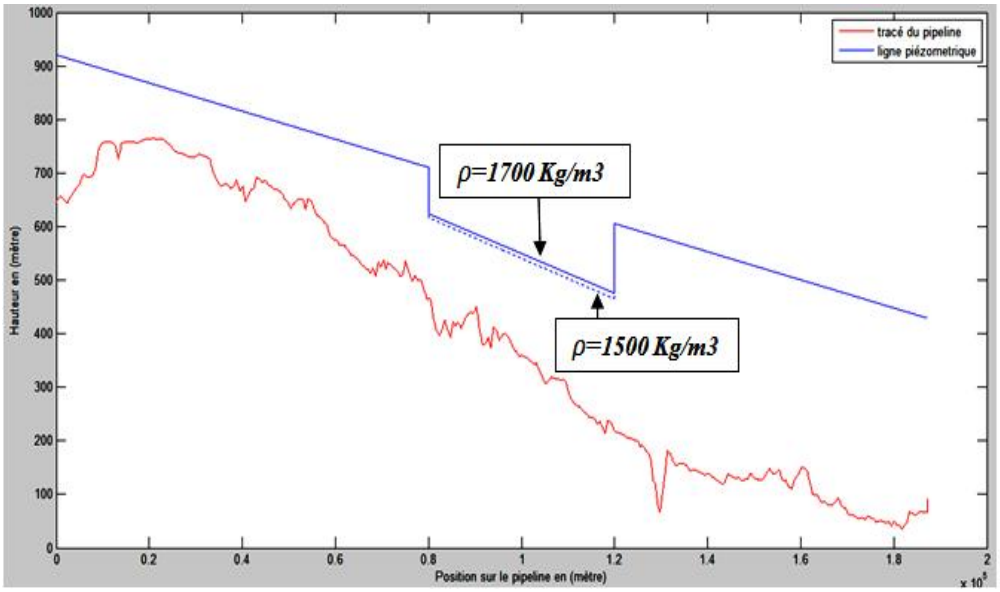

Figure 10: Hydraulic grade line for densities 1700 Kg / m^3 and 1500 Kg / m^3, for the batch case

- Influence of the plastic viscosity of the slurry

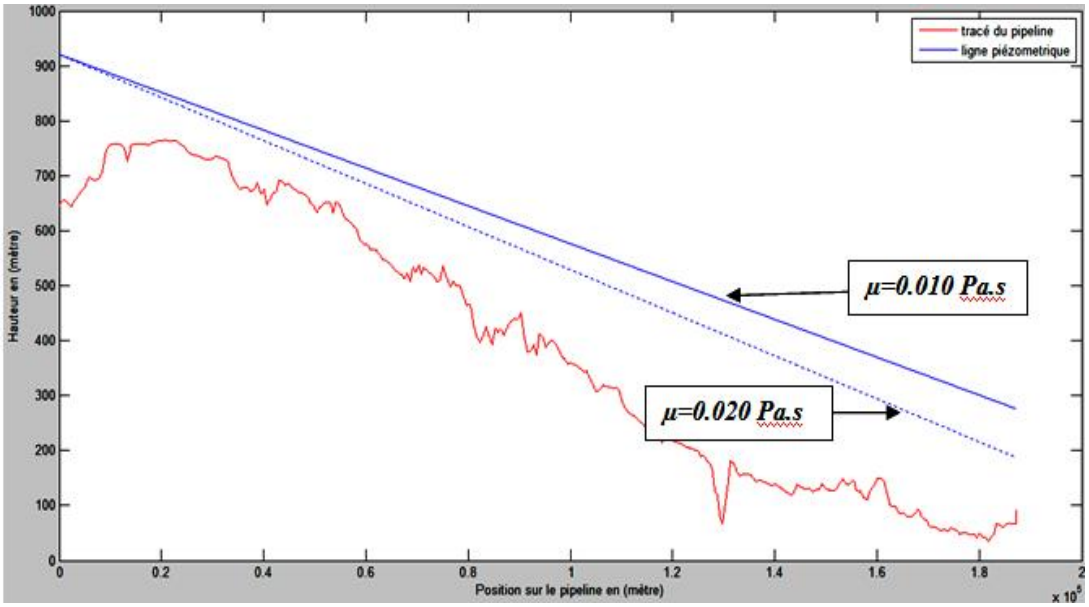

Figure 11: Hydraulic grade line for viscosities 0.010 Pa.s and 0.020 Pa.s for, continuous pumping in slurry.

Concerning continuous pumping, in the case where the slurry viscosity is μ = 0.020 Pa.s, the hydraulic grade line is more inclined at the bottom than the case where the slurry viscosity is μ = 0.010 Pa.s, so the head losses for (μ = 0.020 Pa.s) are greater than for (μ = 0.010 Pa.s). Then it can be concluded that the higher the slurry viscosity increases, the greater head losses. The hydraulic gradients shown in our program are J = 0.0034 m / m for (μ = 0.010 Pa.s) and

J = 0.0039 m / m for (μ = 0.020 Pa.s). The slurry density is assumed constant between the two cases.

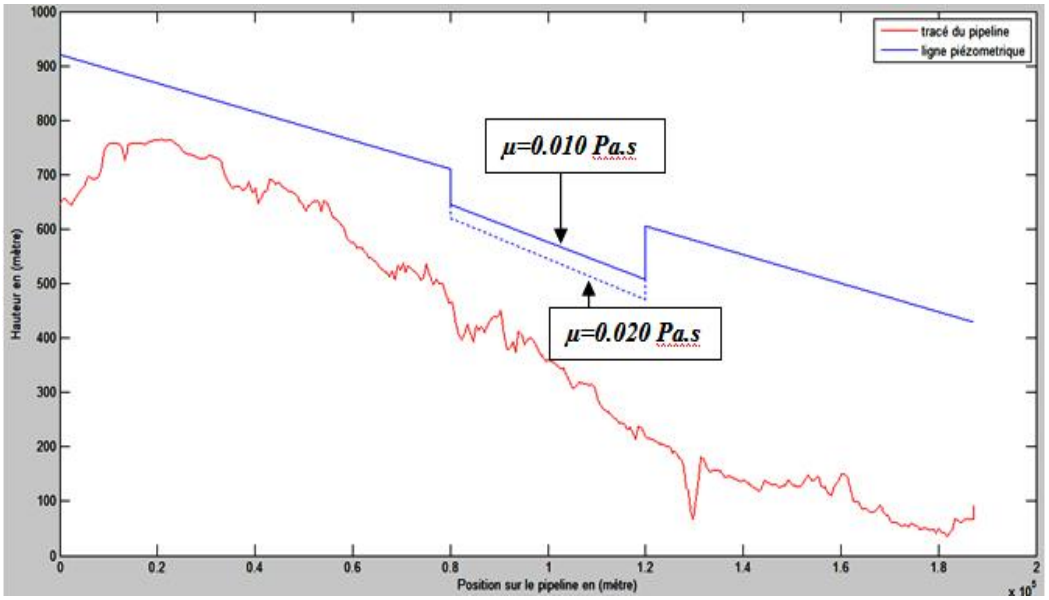

Figure 12: Hydraulic grade line for viscosities 0.010 Pa.s and 0.020 Pa.s, for batch case

- Influence of hydraulic head caused by choke

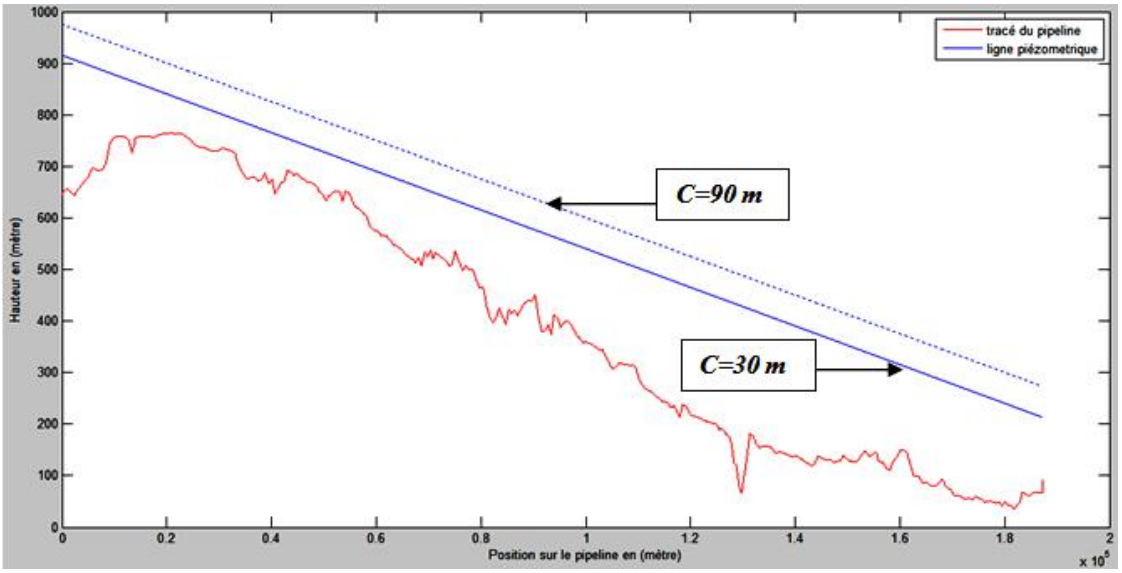

Figure 13: Hydraulic grade line for choke at 30 m and 90 m, for continuous pumping in slurry

Concerning continuous pumping in slurry, in the case where the hydraulic head due to the choke is C = 30 m, the hydraulic grade line retains the same inclination as the case where C = 90 m, so the choke has not Influence on the head losses. The higher the choke level, the more the hydraulic grade line is translated at the top without changing the inclination. It can be

concluded that the choke increases the hydraulic head in the pipeline without influencing the pressure drops. In the case of batch the choke has the same influences.

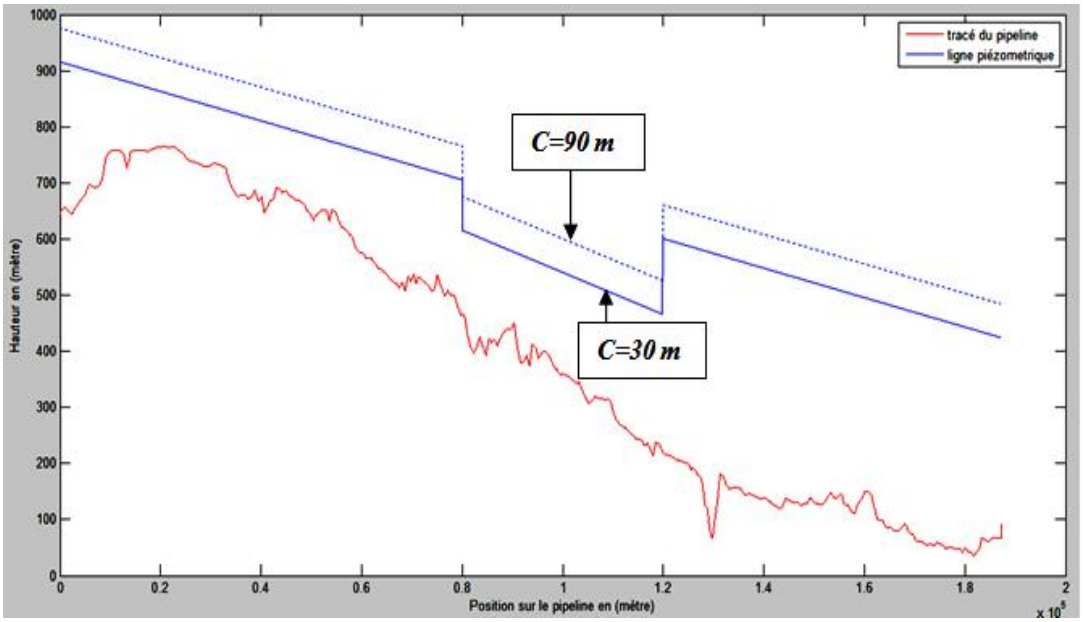

Figure 14: Hydraulic grade line for choke at 30 m and 90 m, for the batch case

5. Conclusion

A mathematical modeling of a number of parameters influencing the process of conducting phosphate through the pipeline was carried out. Thus, linear head losses, hydraulic gradient, friction factor, pipe roughness and fluid mechanics of the phosphate slurry were optimized and the result was grouped into a program in MATLAB.

The simulation allowed us to understand perfectly the work of the pipeline OCP and to know the influence of certain parameters on the operation of the process.

Chapter 4

EXPERIMENTAL AND MODELING STUDIES OF THE RHEOLOGICAL BEHAVIOR OF THE PHOSPHATE-WATER SLURRY, WITH AND WITHOUT ADDITIVES, FOR A SUITABLE MODEL DESCRIPTION

Chapter abstract

The rheological behavior of the phosphate-water slurry depends on several parameters, the density of the slurry, the concentration of solids, the particle size distribution, temperature and additives such as dispersants, flocculants, Ester-Amine…The rheological behavior of the slurry was studied using a rotary viscometer (Anton-Paar). The phosphate slurry consists of solid phosphate and water. We conducted experiments on a solids mass concentration range of (φ = 34.24% at φ = 57.27%) in the shear rate range (1 to 1000 s^{-1}). we have noticed that the phosphate slurry changes its pseudoplastic behavior towards a Bingham behavior from the 46.03% concentration, and changes its Bingham behavior towards a dilatant behavior from the concentration 38.45%. Models of rheological description are numerous, we were interested in this study to four models (Casson, Bingham, Ostwald-Pawer Law, and Herschel-Buckley), Model enables us to adjust and predict the apparent viscosity and yield stress of phosphate-water slurry, and will also allow us to predict dynamic motion of the slurry and understand mechanisms for characteristic rheological behaviors.

1. Introduction

Rheology plays an essential role in the design procedures of the slurry transport system, in general, the rheology of the suspensions is based on the measurement of the shear stress as a function of the shear rate. The relationship between shear stress and shear rate during a single shear defines the rheological behavior of a given fluid, because 'any mechanical system obeys a fundamental equation that establishes a relationship between dynamic quantities responsible for the movement and the kinematic quantities describing this movement' [69]. This mathematical relation describing the flow of a fluid, expresses the law of behavior of the material. Based on fluid behavior, two large groups were identified. These are Newtonian fluids and non-Newtonian fluids. The mathematical models of rheological description of which we have an interest in this study are the models, Casson, Bingham, Ostwald-Pawer Law and Herschel-Buckley. The different physical and chemical properties of slurry have important influences on the rheology of the suspension, because of a change or a modification of the surface property [70,92], these properties are: the particle size distribution, temperature, the concentration in solids, shear rates, etc. The study of the rheological behavior of phosphate water slurry indicated pseudoplastic behavior at high concentrations. In the preparation of phosphate slurry it is required that the solid phosphate concentration should be in the range recommended by the pipeline designer (50% at 60% in solids), but the viscosity should be minimal to facilitate the storage and transport of slurry via pipeline. But the stability of the phosphate slurry becomes mediocre if the viscosity is reduced

and the viscosity of the slurry increases with the concentration of the solid grains in the suspension [71-74].

In this chapter, we studied the rheological behavior of the phosphate-water slurry, and the effect of the variation of the solids mass concentration, the particle size distribution, and the temperature on the rheological behavior of the slurry. And we will carry out a modeling of the rheological behavior of the phosphate slurry, we will search between the 4 models (Casson, Bingham, Ostwald-Pawer Law and HerschelBuckley), the most suitable model for the description of the rheological behavior of the phosphate slurry at each index of concentration, we seek the mathematical model having the curve which passes by the maximum of the experimental points. Adjusting the mathematical models of rheology to experimental data allows us to calculate and predict the values of viscosity and yield stress. **[102].**

2. Experimental study of rheological behavior of phosphate slurry

2. 1. Equipment used for the measurement: Rheometer, Granulometer, desiccator

The phosphate samples used in this study are taken from the Moroccan phosphate extraction zones (Khouribga region). These raw samples were washed and flushed at the laboratory level and were then milled and sieved to give the particle size distribution as shown in Fig.7. The particle size distribution of the granules of the phosphate slurry samples was adjusted using a Tammie Fig.3 and measured using an analyzer (Master-Sizer 3000) Fig.5, and the solids content in the slurry was measured using a desiccator (Mettler TOLEDO) Fig. 2. Phosphate slurry samples are stirred to be consistent prior to rheological measurements Fig. 4. The rheological measurements of phosphate slurry were made using a rotary rheometer (Anton-Paar) coaxial cylinders (Couette geometry (Fig.1)), which is connected to a computer. The rotor is screwed onto the spindle and the sample is poured into the cup. The rheometer also contains a thermostat that adjusts the temperature of the sample to make rheological measurements at any desired temperature. Rotation varies from high to low shear rate. The rheological measurements were carried out at an ambient temperature of 25 ° C. The experimental conditions were as follows: shear rate: (from 1-1000 s^{-1}), temperature variation: 25 ° C, 35 ° C, 45 ° C and 55 ° C, and mass concentrations in solids ranging from 34.24% to 57.27%. The shear stress versus shear rate was obtained from the data collected by the computer.

Figure 1: Rheometer (Anton Paar) with geometry Couette.

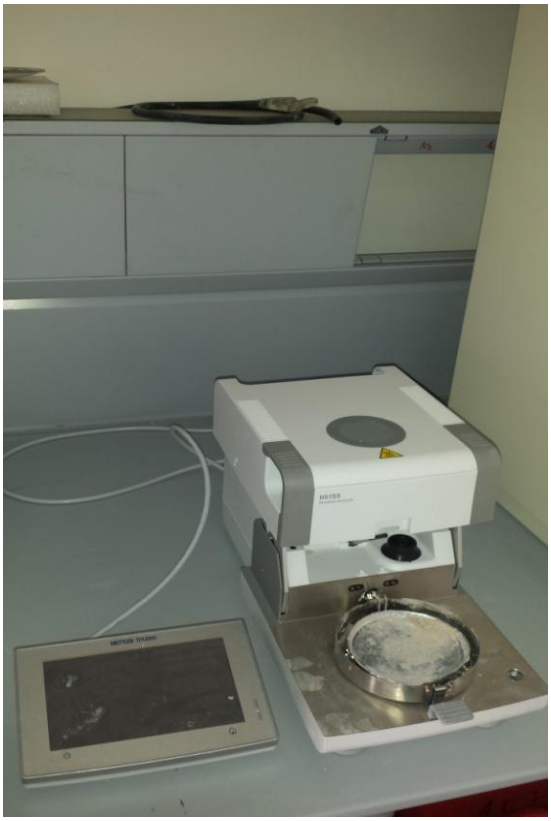

Figure 2: Mettler TOLEDO for solid rate measurement in phosphate slurry samples.

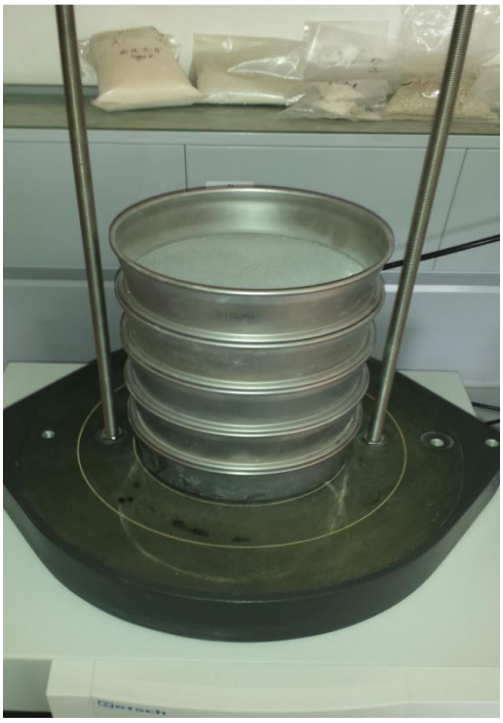

Figure 3: Vibration Tammy to adjust the solid phosphate samples to the desired particle size distribution.

Figure 4: Sample of phosphate slurry prepared stirring before rheological measurements.

Figure 5: Analyzer (Master Sizer 3000) for particle size distribution measurements of phosphate particles.

2. 2. DRX characterization of phosphate

Before carrying out rheological studies, it is necessary to first characterize the phosphate samples on which we are working, and this by identifying the chemical phases to know the types of crystals contained in the phosphate slurry, and thus to know the fractions of each chemical element in the phosphate. For this purpose we subjected the phosphate used in this study to X-ray diffraction and X-ray fluorescence.

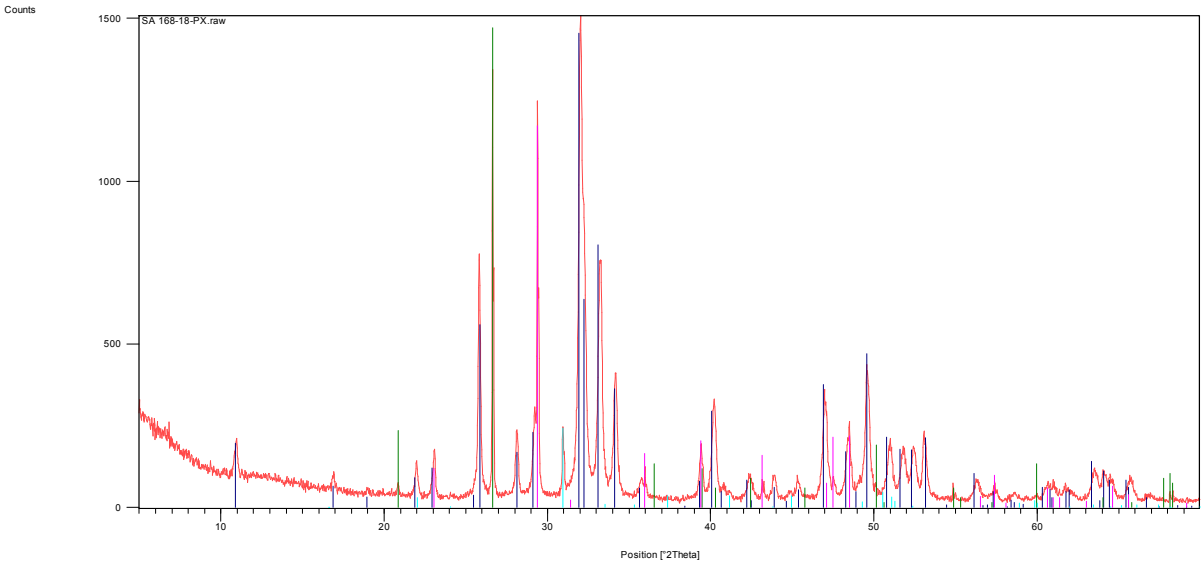

Figure 6: X-ray diffractogram of phosphate used in this study.

Table 1: Phases identified from the diffractogram.

Visible	Compound Name	Chemical Formula
++++	Fluorapatite	Ca5 (P O4)3 F
++++	Quartz, syn	Si O2
++++	Calcite, syn	Ca (C O3)
++++	Dolomite	Ca Mg (C O3)2

We note that the most frequent phases in our phosphate sample are, Fluorapatite $Ca_5(PO)_3F$ (streak in dark blue), silicon dioxide SiO_2 (streak in green), and $Ca(CO_3)$ carbonates (rai en violet), for $CaMg(CO_3)_2$ it is weak in phosphate (streak in sky blue).

2. 3. XRF characterization of phosphate

Table 2: Chemical Analysis of Phosphate Used in this study by X-Ray Fluorescence.

Compound	Conc	Unit
MgO	0,392	%
Al2O3	0,697	%
SiO2	2,056	%
P2O5	29,142	%
SO3	1,05	%
Cl	625,4	ppm
K2O	374,2	ppm
CaO	49,074	%
TiO2	337,4	ppm
V2O5	225,1	ppm
Cr2O3	189,6	ppm
MnO	13,8	ppm
Fe2O3	0,217	%
CuO	44,2	ppm
ZnO	242,3	ppm
As2O3	29,1	ppm
SrO	0,159	%
Y2O3	388,6	ppm
ZrO2	68,3	ppm
Nb2O5	0	ppm
SnO2	182,7	ppm
Nd2O3	133,2	ppm
Sm2O3	0	ppm
Eu2O3	0	ppm
Gd2O3	0	ppm
Yb2O3	34,4	ppm
PbO	11,2	ppm
U	262,3	ppm

2. 4. Result and discussion

Concentrated phosphate slurries generally have Non-Newtonian behavior (pseudoplastic). The impact of solids concentration, particle size distribution and temperature on the rheological properties of the slurry is briefly discussed in the following paragraphs.

2. 4. 1. The effect of solids concentration on the rheological behavior of phosphate slurry

The solids concentration for the viscosity measurement started from 34.24% by mass. The shear stress and shear rate data were computed from the chart recorder for mass concentrations between 34.24% and 57.27%, plotted and given in the fig. 6. We performed this operation on several samples, they gave the same results, and here we take a sample between them that is called B1.

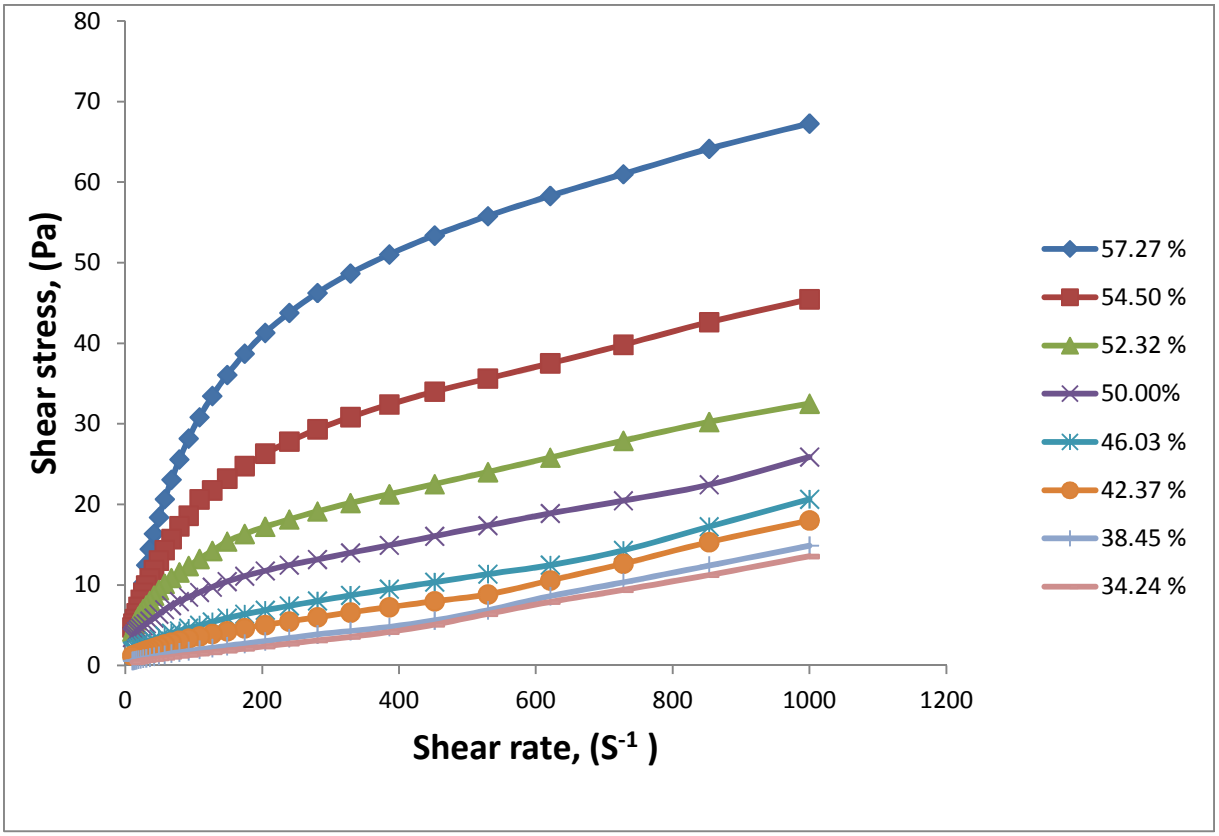

Figure 6 : Rheology of phosphate slurry at different mass concentrations (sample B1)

The shear thinning behavior can be explained as a disturbance of the structure of the applied shear suspension. For high shear rates the fractures predominate the composition of the sample, therefore the cohesion between the particles becomes low due to the applied mechanical stress [75], for low shear rates the suspension structure is close to balance, since the thermal movement dominates the viscous forces. The influence of the solid concentration on the rheology of the phosphate slurry is very remarkable in fig. 6, the higher the solids concentration the higher the

viscosity of the slurry increases, we noticed from figure 6 that with the dilution, the phosphate slurry starts to change are pseudoplastic behavior towards a Bingham behavior from the mass concentration 46.03%. This concentration does not represent a specific point of change in behavior, but it is a point from which the slurry begins to change its behavior. It can be noted that for the phosphate slurry, the mass concentration point 46.03% has a transition point between pseudoplastic behavior with threshold stress (yield) and linear behavior with threshold stress (Bingham), and the mass concentration point 38.45% has a transition point between Bingham behavior and dilatant behavior with yield. **[102]**.

2. 4. 2. Effect of particle size distribution

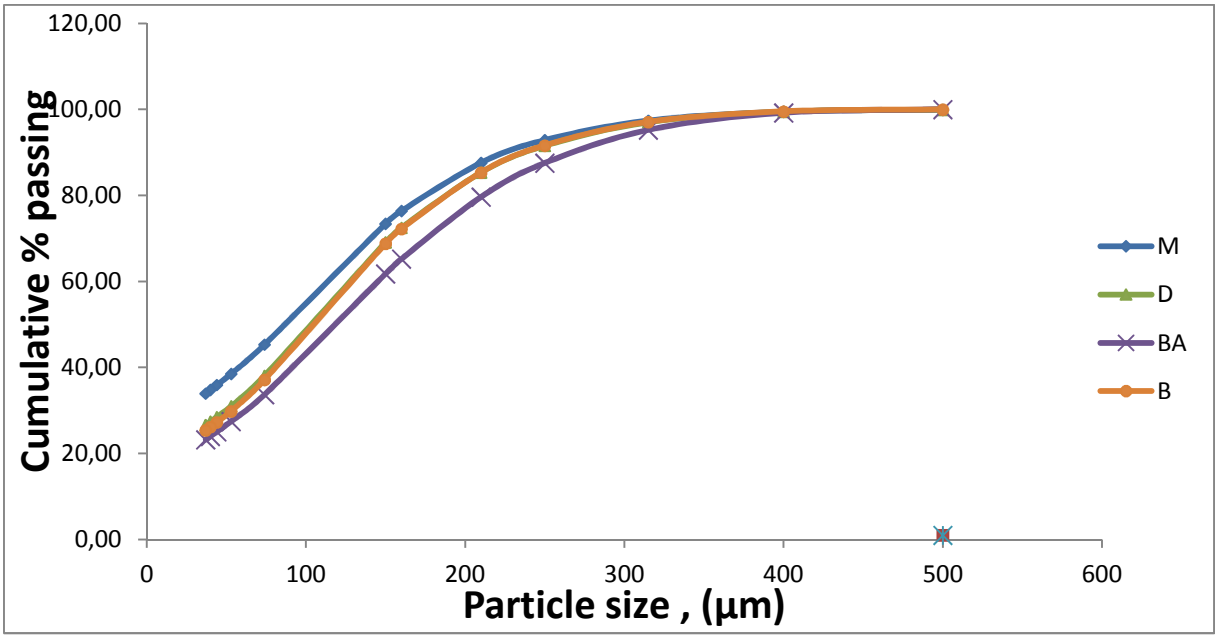

Figure 7: Particle size distribution of phosphate slurry samples.

The rheological profile of the concentrated slurries is strongly related to the size distribution of the particles [76]. Phosphate slurry samples becoming thinner with increasing grinding time. Fig. 7 shows the particle size distributions of the 4 suspension samples having different sizes at a fixed concentration of 50.54%. The viscosity of the slurry at a given shear rate indicates a higher value for the sample (M). It is generally noted that a decreasing particle size results in an increase in suspension viscosity, particularly at low shear rates fig. 8. In addition, the inter-particle attraction is expected to become stronger as the particle surface area increases at the same mass concentration of slurry solids. It can be mentioned that the fines content (<37 µm) in (M) is higher than that of (D), (BA) and (B) as indicated in the particle size distribution diagram fig. 7.

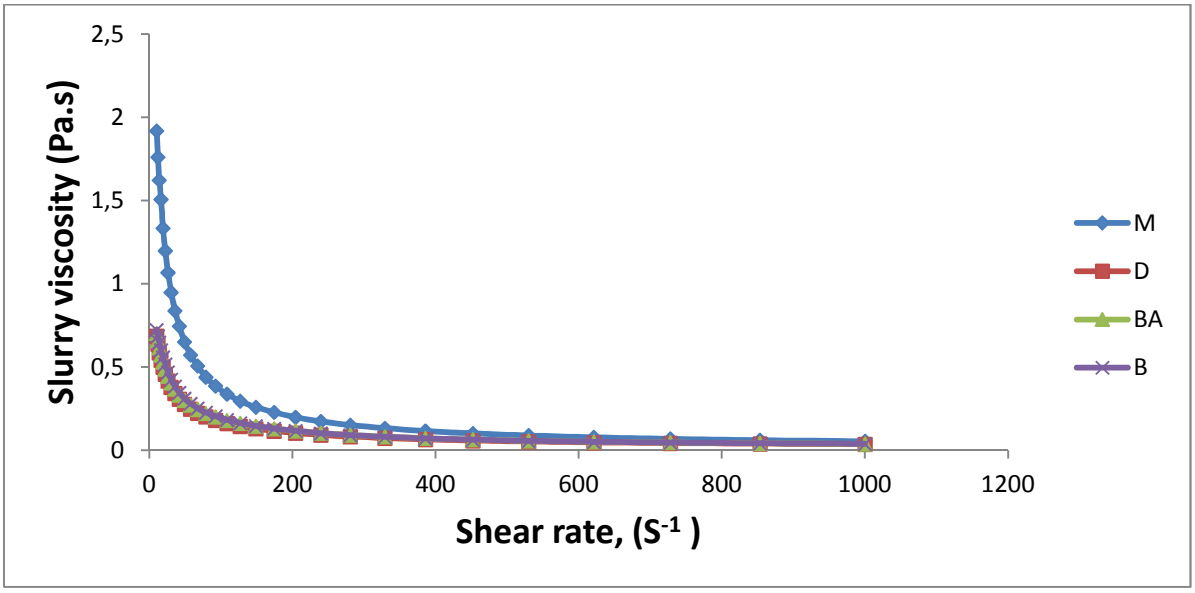

Figure 8: The effect of the shear rate on the viscosity of the phosphate slurry at different particle size distributions.

We can conclude that the higher the content of fine aggregates, the more the slurry becomes viscous. Regardless of the solids concentration, the specific surface area of the particles increases due to the presence of finer particles in the sample (M) which leads to the production of new surfaces and the total number of particles increases by promoting a decrease in the distance between the grains . For samples (D), (BA) and (B) with a larger average particle size and with fewer finer particles, the interaction between the particles is small. As a result, viscosity indicates higher values for (M) than for the other samples at a specific mass concentration and shear rate [16].

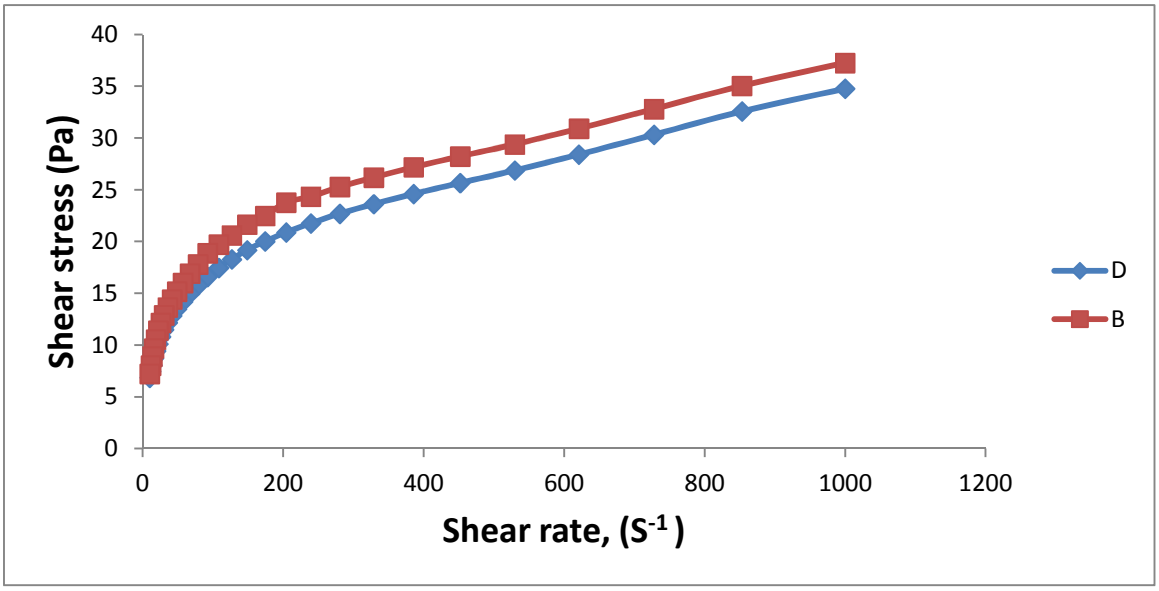

Figure 9: Rheology of samples (D) and (B) at the same concentration and particle size distribution. (50.54%)

It is quite remarkable from the fig. 7 that the samples (D) and (B) have the same particle size distribution, and for the same mass concentration the two samples have a different rheological behavior fig. 9, this is attributed to the porosity aggregates and mineralogy of each sample and also to the content of flocculant and additives in the slurry.

2. 4. 3. Effect of slurry Temperature

The temperature dependence of the viscosity of the phosphate slurry was investigated in the shear rate range of 1 to 1000 s^{-1}. Fig.10 shows the effect of temperature on the rheology of phosphate water slurry at a concentration of 57.27% solids. The viscosity of the slurry decreases in the temperature range studied (25 ° C-55 ° C). The decrease in viscosity at elevated temperatures occurs due to the increase in the kinetic energy of the particles promoting the breaking of the intermolecular bond between the adjacent layers, which causes a decrease in the viscosity of the phosphate slurry. For the temperature 55 ° C, we notice a deformation of the rheological profile especially for low shear rates, this deformation can be attributed to the change of the structure of the slurry with the temperature, with the increase of the temperature, the particles can to be dissolved in the suspension, and one can also have chemical reactions which are provoked with the increase of the temperature. This changes the physicochemical structure of the suspension and therefore affects the rheological behavior of the phosphate slurry. [31].

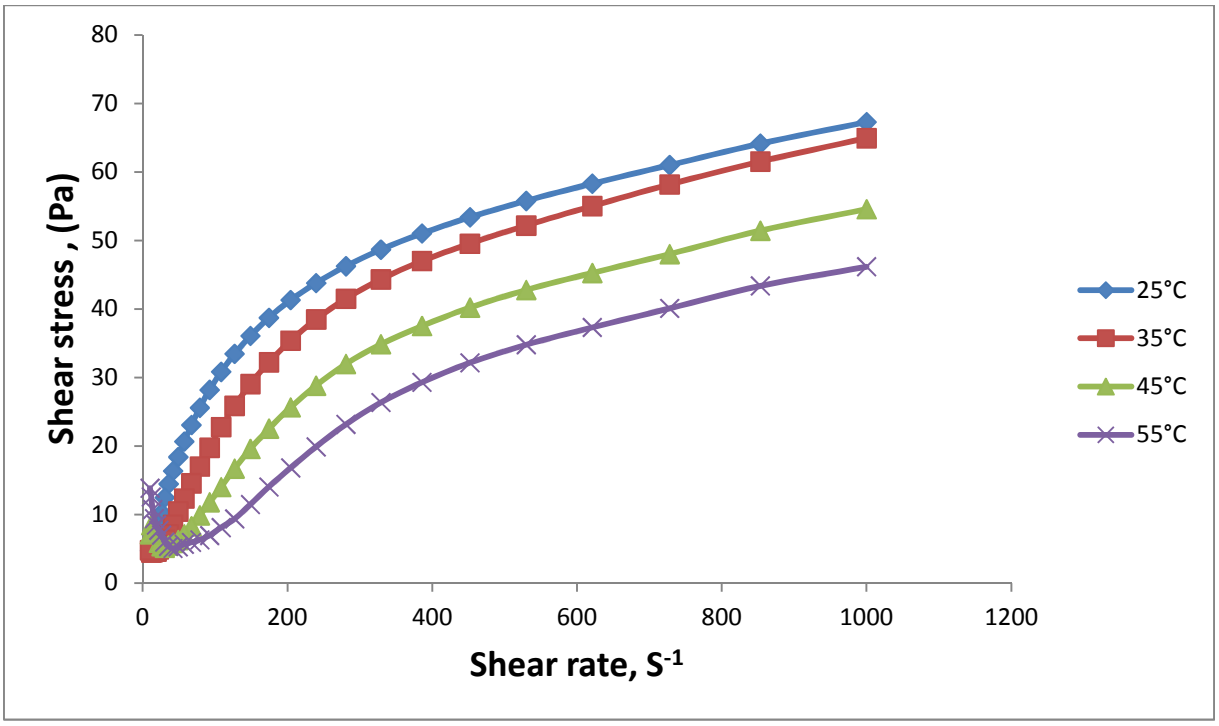

Figure 10: Effect of temperature on the rheology of the phosphate slurry at a concentration of 57.27%. (B1)

2. 4. 4. Fluid flow Activation energy

Activation energy (E) is a parameter that characterizes the stability of a fluid. The temperature dependence of the viscosity can be represented in terms of a simple Arrhenius expression for the temperature range studied, this Arrhenius formula contains the activation energy (E). The relationship between viscosity and temperature can be presented as:

$$\eta = A \exp(E/RT)$$

or

$$1n\ \eta = E/RT + 1nA\ ;$$

Where η is the viscosity at a particular shear rate, E is the activation energy of the fluid flow, T is the temperature in Kelvin, R is the universal gas constant, and A is an adjustment parameter.

Fig. 11 shows the variation of the relative viscosity as a function of temperature in the range (25 ° C-55 ° C), and Fig. 12 shows the variation of the logarithm of the viscosity as a function of the reciprocal temperature phosphate slurry (sample B1 at a solid rate of 57.27%). A simple regression of the experimental data (viscosity as a function of temperature) to the Arrhenius formula allows us to identify the value of the activation energy (E) for the phosphate slurry.

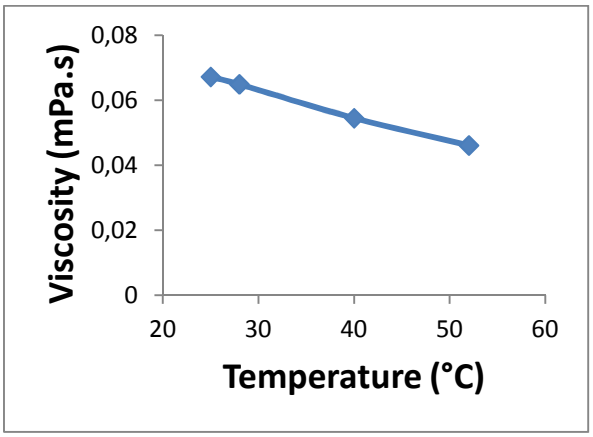

Figure 11: Relative viscosity versus temperature at a fixed shear rate of (1000 S^{-1})

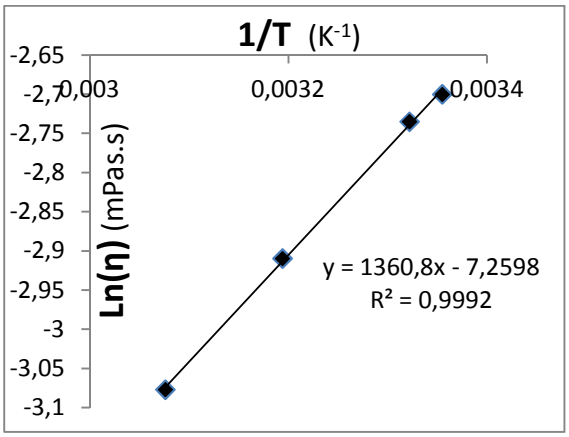

Figure 12: Variation of the logarithm of the viscosity as a function of the reciprocal temperature of the phosphate slurry.

So the value of the fluid flow activation energy of the phosphate slurry is:

E= 11,3 Kj/mol

In general, the suspensions retain almost the same activation energy value even at different solids concentrations [17].

3. Influence of additive compounds on the rheology of phosphate slurry

3. 1. Influence of flocculant for both 60% and 50% solid rates

The goal of adding the flocculant to the phosphate slurry is to combine small particles (<40 µm) to form medium size agglomerates, because the transport of fine aggregates via pipeline is very difficult, these small aggregates present a risk of creation of static bed in the pipeline which can cause clogging. In this part, we will carry out an experimental investigation on the impact of the flocculant content in the phosphate slurry on its rheological behavior. The phosphate samples were prepared using a grinder and a sieve to fit all the samples to the design particle size distribution shown in Table (2). The flocculant used in this study is polyacrylamide $(C_3H_5NO)_n$. Polyacrylamide is a highly absorbent polymer, it is used in phosphate slurry to absorb fine particles and combine them to form agglomerates of medium size. The polyacrylamide is in powder form, it is diluted in water to form a viscous gel after vigorous stirring. Ionic substances, such as sodium chloride, allow the polyacrylamide to release the absorbed substances. Concerning the preparation of the flocculent, we solubilize 2g of solid polyacrylamide in one liter of water.

Paramètre	Valeur
Densité solides	3.0 t/m^3
Concentration	60%m
Densité de la pulpe	1.7 t/m^3
pH de la pulpe	8.0
Porosité	20%
P80 P20	160 µm 44 µm
Distribution des particules par dimension	-250 µm 100% -210 µm 96.6% -150 µm 74.0% -74 µm 30.8% -53 µm 21.9% -44 µm 20.4% -37 µm 16.8%
Élasticité	55%m 1.56 Pa 58%m 2.67 Pa 60%m 3.8 Pa
Viscosité plastique	55%m 6.6 x 10^{-3} Pa.s 58%m 8.5 x 10^{-3} Pa.s 60%m 10.2 x 10^{-3} Pa.s

Table 2: Physical parameters Design of phosphate slurry.

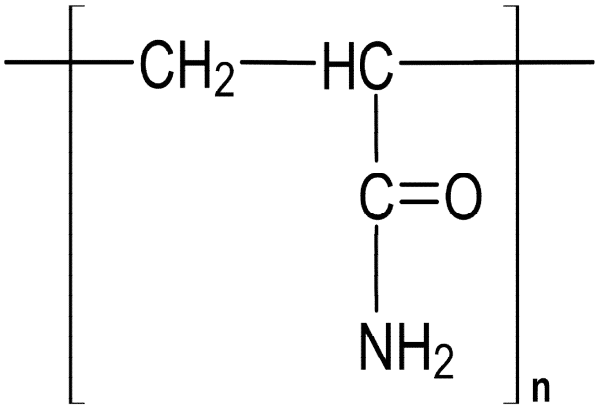

Figure 13: The structure of polyacrylamide used as flocculant in this study.

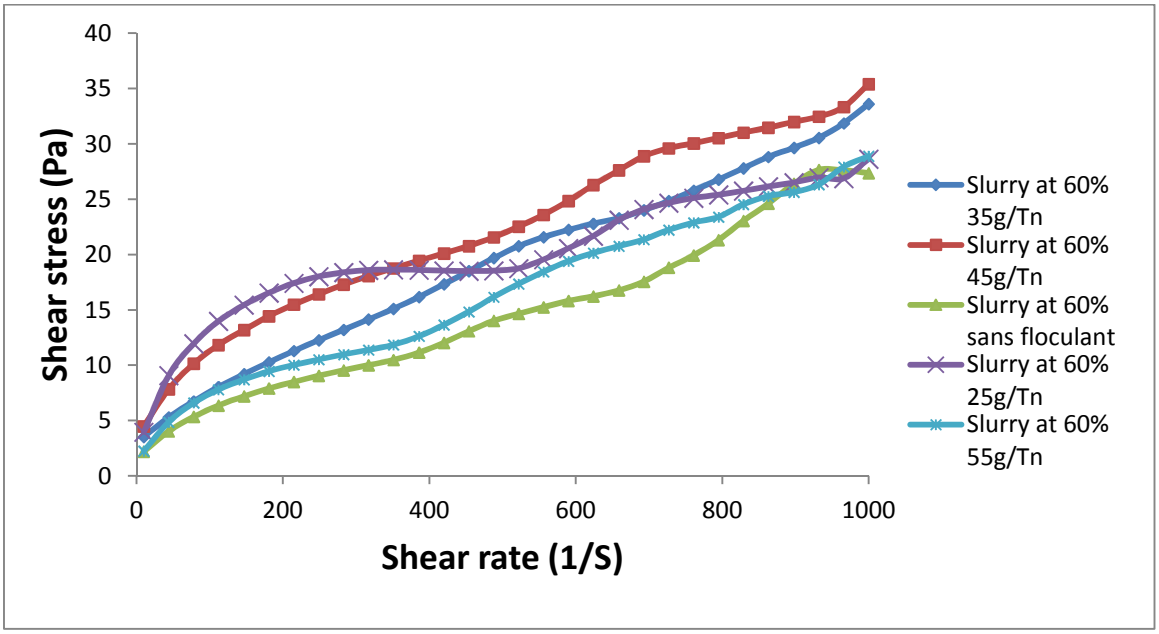

Figure 14: Effect of flocculant on the rheological behavior of phosphate slurry at 60% in solid rates.

We have prepared 5 samples of phosphate slurry at a solid rate of 60% and with the particle size distribution design, it should be noted that in this part the solid rate and the particle size distribution are always fixed, we will change the rate of flocculant in the slury.

We note from Fig. 14 that the flocculant rate has a remarkable impact on the rheological behavior of the phosphate slurry. From Fig.15 we set 3 (Shear rates) constant (600 1 / S, 400 1 / S, 200 1 / S) to show the effect of flocculant on the relative viscosity of the slurry.

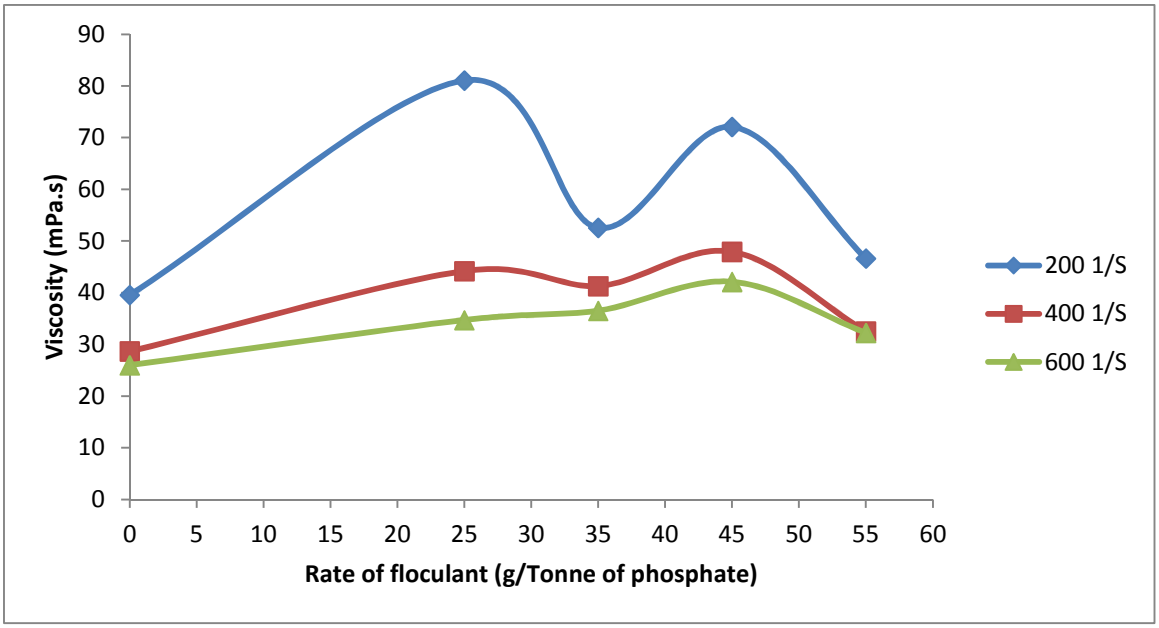

Figure 15: Impact of the flocculant rate on the viscosity of the slurry at different Shear rates.

The profile of the viscosity as a function of the flocculant rate has the same pace for all (Shear rates), only the amplitude of the curves that vary. In all that follows, the notation ('X' g / Tn) means ('X' gram of solid flocculant / Tonne of solid phosphate).

We can extract from the figure (15) that the viscosity of the phosphate slurry increases according to the flocculant rate up to the point (25g / Tn), it can be explained that the flocculant has increased the viscosity of the medium (water) but it did not act perfectly on the fine aggregates, that is to say that the flocculant has not yet reached the threshold so that it can combine all fine aggregates in the slurry. Between (25g / Tn) and (35g / Tn) the viscosity of the slurry has undergone a local decrease, this means that the flocculant rate at (35g / Tn) combines the fine aggregates well by forming large agglomerates in slurry which has lowered the viscosity, as it is well known in the literature, the more a suspension contains large grains the more it becomes less viscous.

Between (35g / Tn) and (45g / Tn) the flocculant has increased the viscosity of the medium, it has no remarkable impact on the aggregates.

It should be noted that the phosphate slurry contains 3 types of sizes of aggregates, fine, medium and large aggregates, at a flocculant level of (55g / Tn) we noticed that the viscosity of the slurry decreased again, this can be attributed to the fact that the flocculating rate (55 g / Tn) is the threshold for the medium-sized grains to form good agglomerates together, forming large agglomerates, which lowers the viscosity of the slurry. Hereinafter, optical microscopy of the phosphate slurry at different flocculant rates:

Figure 16: Optical microscope used in this study.

Figure 17: The scale used in microscopy (10 / 0.25) (160 / 0.17).

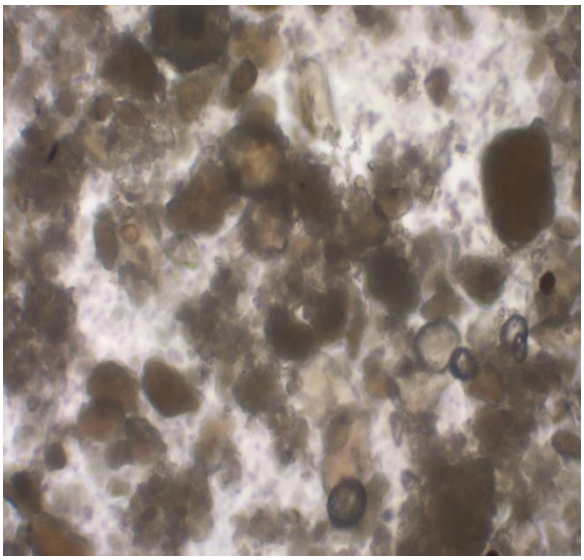

Figure 18: phosphate slurry at 60% in solid rate without addition of flocculant.

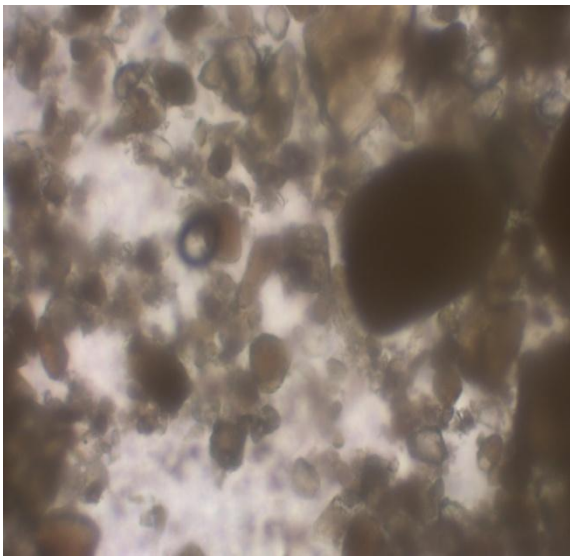

Figure 19: phosphate slurry at 60% in solid rate with the addition of (15 g / Tn) of flocculant.

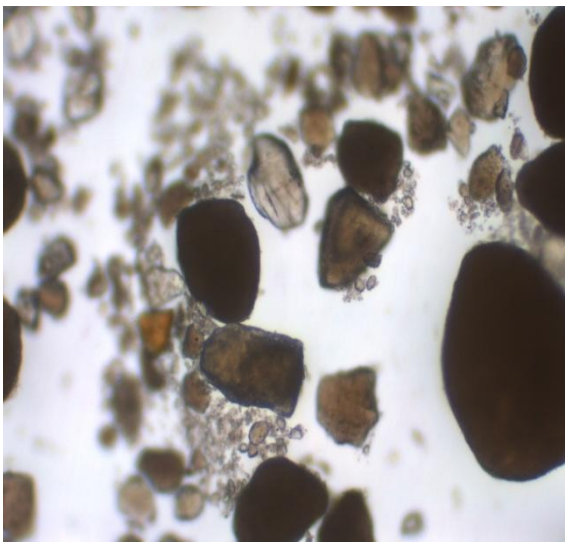

Figure 20 : phosphate slurry at 60% in solid rate with the addition of (25 g / Tn) of flocculant.

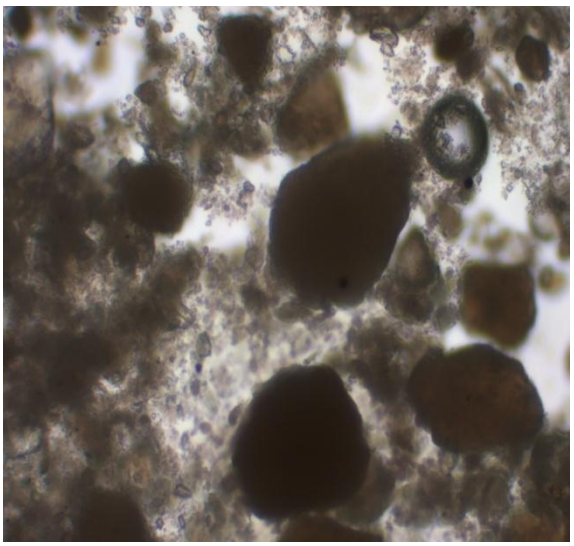

Figure 21 : phosphate slurry at 60% in solid rate with the addition of (35 g / Tn) of flocculant.

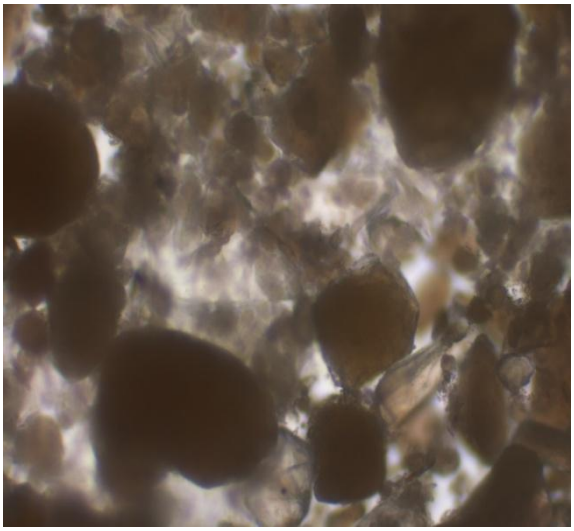

Figure 22 : phosphate slurry at 60% in solid rate with the addition of (45 g / Tn) of flocculant.

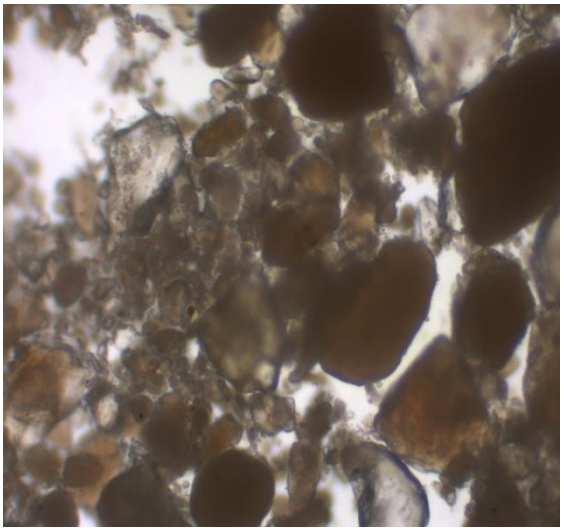

Figure 23: phosphate slurry at 60% in solid rate with the addition of (55 g / Tn) of flocculant.

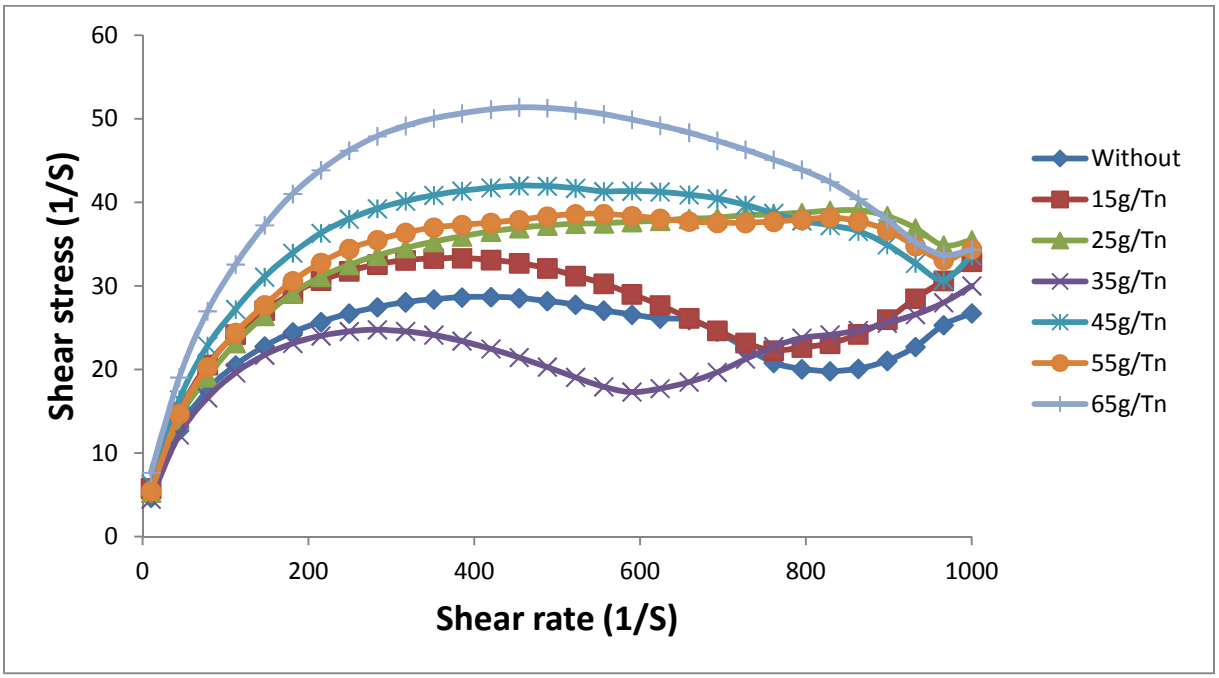

Figure 24: Effect of the flocculant on the rheological behavior of the phosphate slurry at 50% in solid.

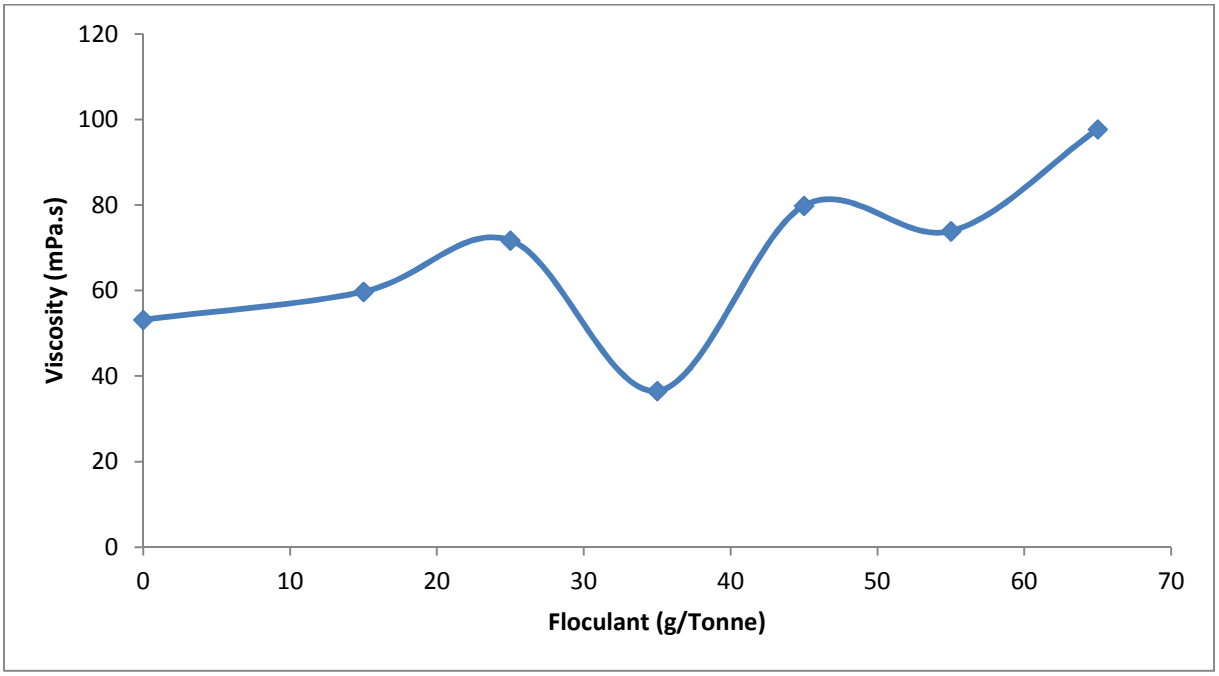

Figure 25: Impact of the flocculant rate on the viscosity of the pulp at a fixed Shear rate of 500 1 / S.

The same interpretations that we have concluded on the impact of the flocculant rate on the viscosity of the slurry at 60% in solid rates, are valid for the slurry at 50% in solid rates. The flocculant rate has the same effect for both cases.

We can conclude that the impact of the flocculant rate on the viscosity of the phosphate slurry is independent at the solids concentration, it is simply related to the particle size distribution of the phosphate particles in the slurry.

3. 2. Influence of Ester and Amine

During phosphate treatment operations at Khouribga, the crude phosphate undergoes a washing and flotation operation to remove impurities and enrich the phosphate. This operation consists in depressing the apatite by adding phosphoric acid H_3PO_4, collecting the carbonates by adding Ester and collecting the silicates by adding Amine. The problem is that the traces of these Esters and Amines still remain in the phosphate slurry, and surely they will impact the rheological behavior of this slurry.

The objective of this part is to study the impact of these Ester and Amine on the rheological behavior of phosphate slurry.

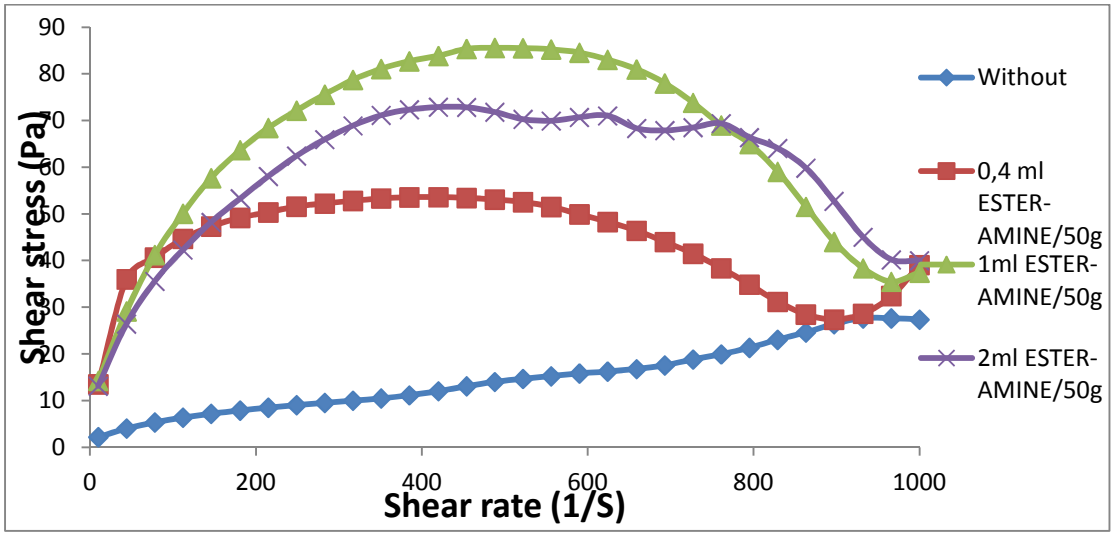

Figure 26: Effect of ester-amine on the rheological behavior of phosphate slurry. (1ml (ester-amine) means (1ml ester + 1ml amine))

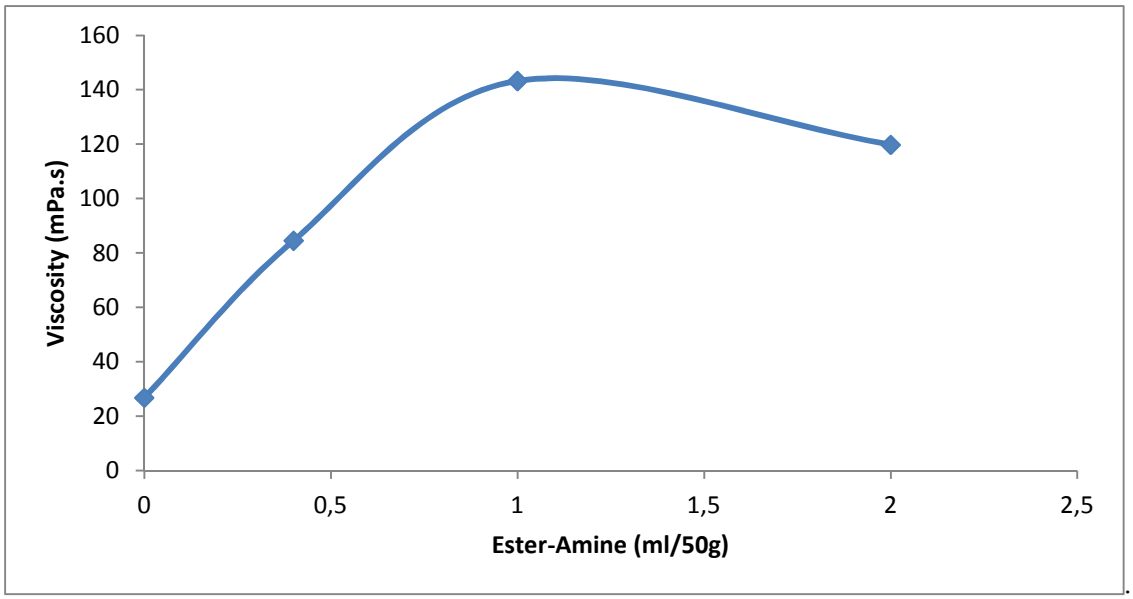

Figure 27: Impact of Ester and Amine on the viscosity of the slurry at a fixed Shear rate of 600 1 / S. (1ml (ester-amine) means (1ml ester + 1ml amine))

We have prepared 4 samples of phosphate slurry with the same solids concentration (60%) and the same size distribution (Design), the samples are composed of 50g of solid phosphate and 34g of water. We added different amounts of ester and amine in each sample. After passing samples to rheological measurements we noticed that the (Ester-Amine) content in the slurry has a very remarkable impact on the rheological behavior. Indeed, by taking a fixed (shear rate), the viscosity of the slurry increases in the interval (0 - 1 ml (ester-amine) / 50g of solid phosphate) and decreases in the interval (1 - 2 ml / 50g of solid phosphate).

It should be noted that (0.4 ml (ester-amine) / 50 g of phosphate solids) is equivalent to (8L(ester-amine) / Tonne of phosphate), and (1 ml (ester-amine) / 50 g of phosphate solids) is equivalent of (20L (Ester-Amine) / Tonne of phosphate).

3. 3. Influence of dispersant: Sodium Tri-Polyphosphate (STPP)

STPP (sodium tri-polyphosphate, an inorganic dispersant, chemical formula: ($Na_5P_3O_{10}$), is selected for the rheological studies of a variety of existing slurries. However, it was known that the strong adsorption of polyphosphate ions on solid matter ore-based slurries increased the repulsion between the mineral materials in the flotation process [70,79].

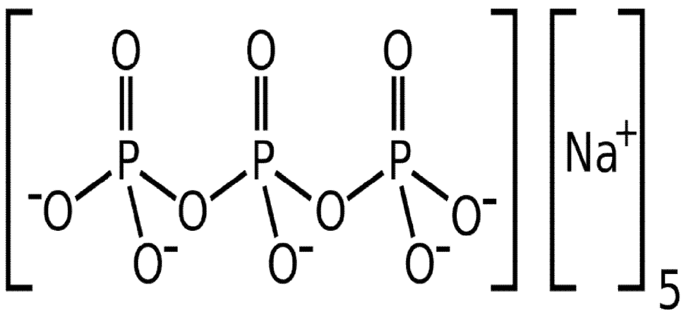

Figure 28: Structure of Sodium Tri-Polyphosphate (STPP)

In our study we will use sodium tri-polyphosphate as dispersant of particles contained in the phosphate slurry to lower the viscosity, and this to facilitate the flow by increasing the hydrodynamics and promoting the turbulence, and thus to optimize the energy required for pumping.

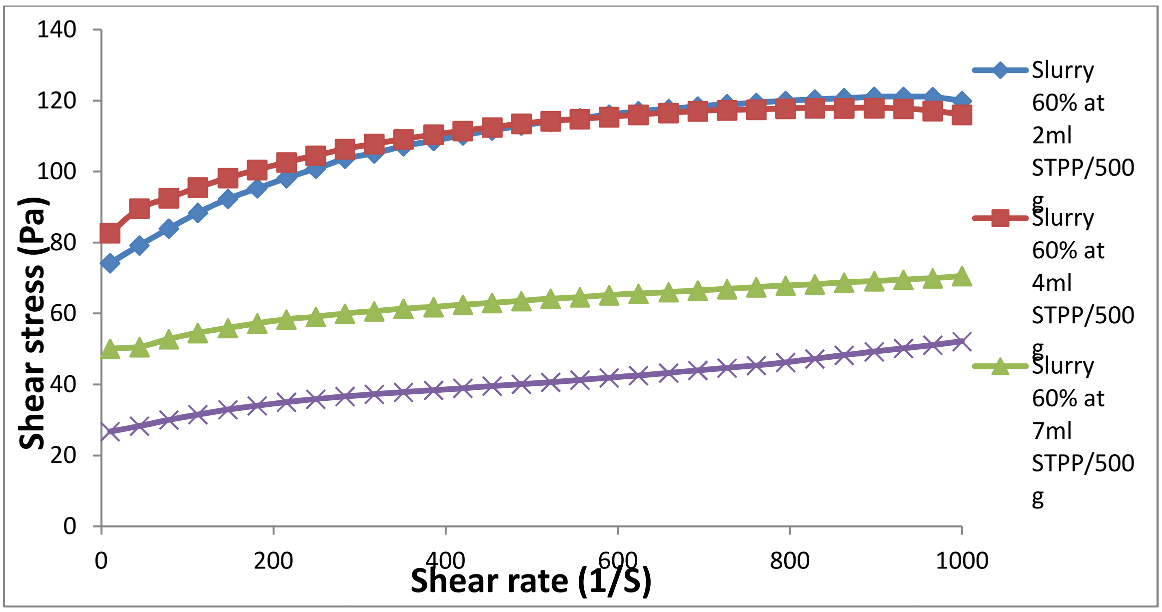

Figure 29: Effect of dispersant (STPP) on the rheology of phosphate slurry at 60% solids content.

Fig. 29 shows the effect of the dispersant (STPP) on the rheology of phosphate slurry at 60% solids, we note that the dispersant (STPP) acts perfectly on the rheological behavior of the phosphate slurry for quantities (7 ml STPP / of 500g slurry) and (10 ml STPP / of 500g slurry), but the addition of STPP with amounts of (2 and 4 ml STPP / 500g of slurry) has no impact remarkable on the rheological behavior of phosphate slurry. We thus notice that for the quantities (2 and 4 ml STPP / 500g slurry) the phosphate slurry has Pseudoplastic rheological behavior, but for the quantities (7 and 10 ml STPP / 500g of slurry) the rheological behavior is linear in nature (Bingham). We can also extract from fig. 29 that the STPP has a very important impact on the yield stress (elasticity). We can conclude that STPP lowers the viscosity and the yield point of phosphate slurry.

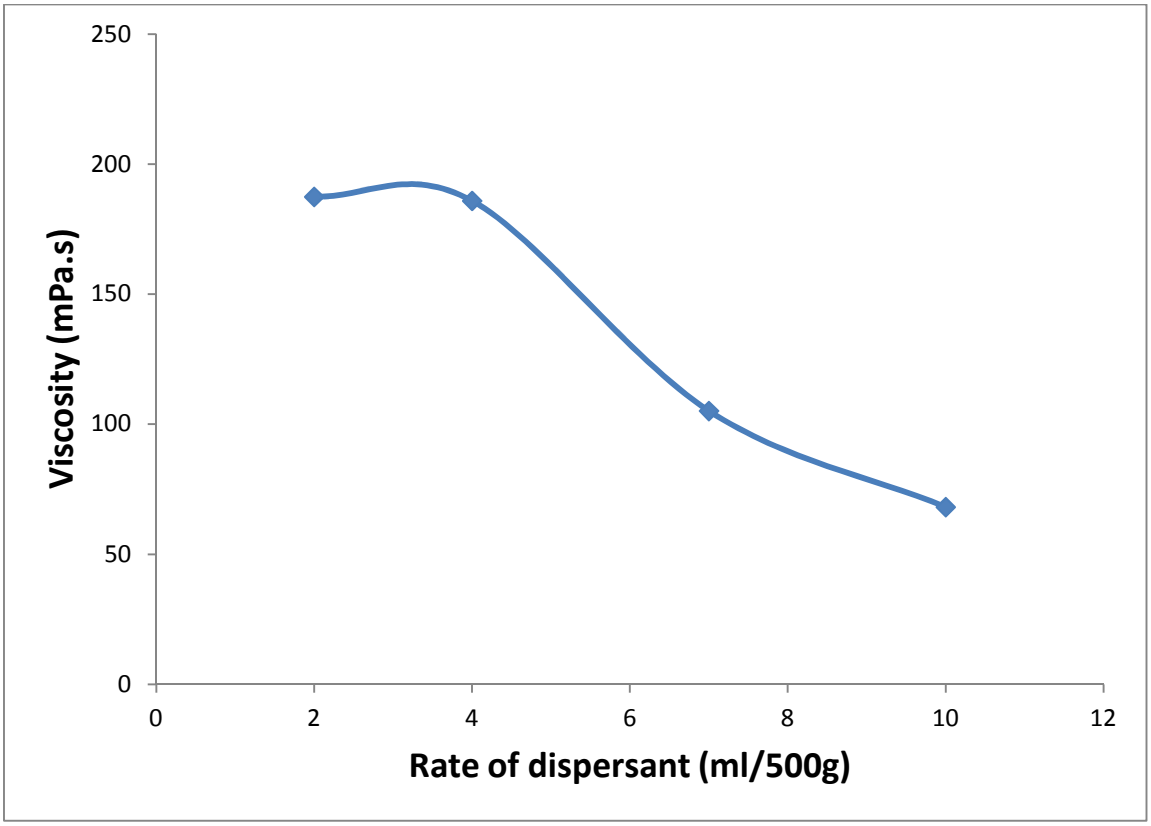

Figure 30: Viscosity versus amount of STPP in the phosphate slurry in (ml of STPP / 500g of slurry) at a fixed shear rate of 600 1 / S.

We note from fig. 30 that STPP does not have a remarkable impact on the viscosity for the amounts of STPP between (2 and 4 ml / 500g of slurry), but beyond 4ml, the STPP effect is quite remarkable on the viscosity of the phosphate slurry.

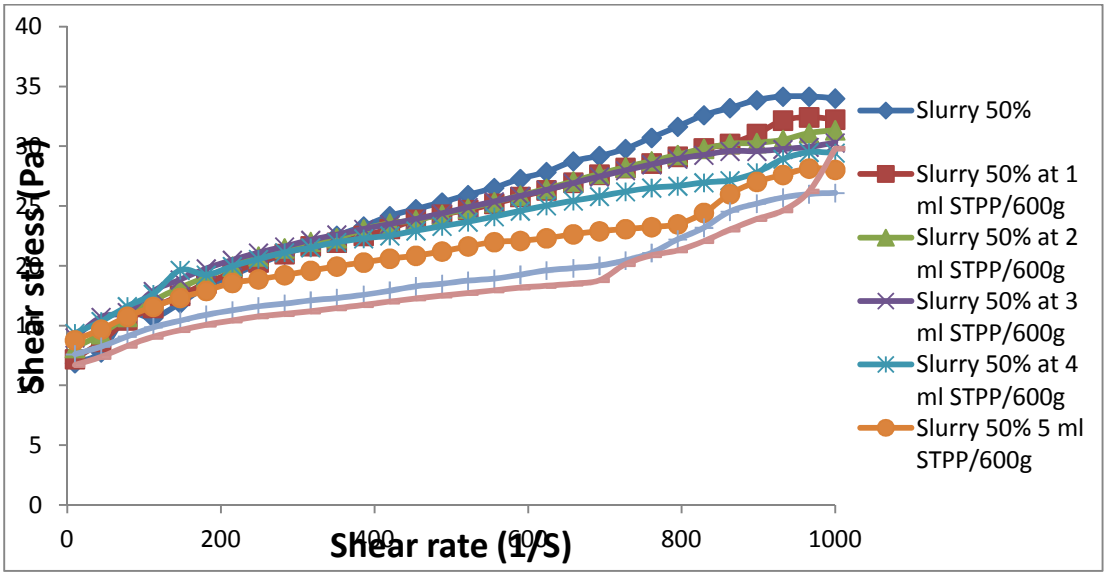

Figure 31: Effect of dispersant (STPP) on the rheology of phosphate slurry at 50% solids.

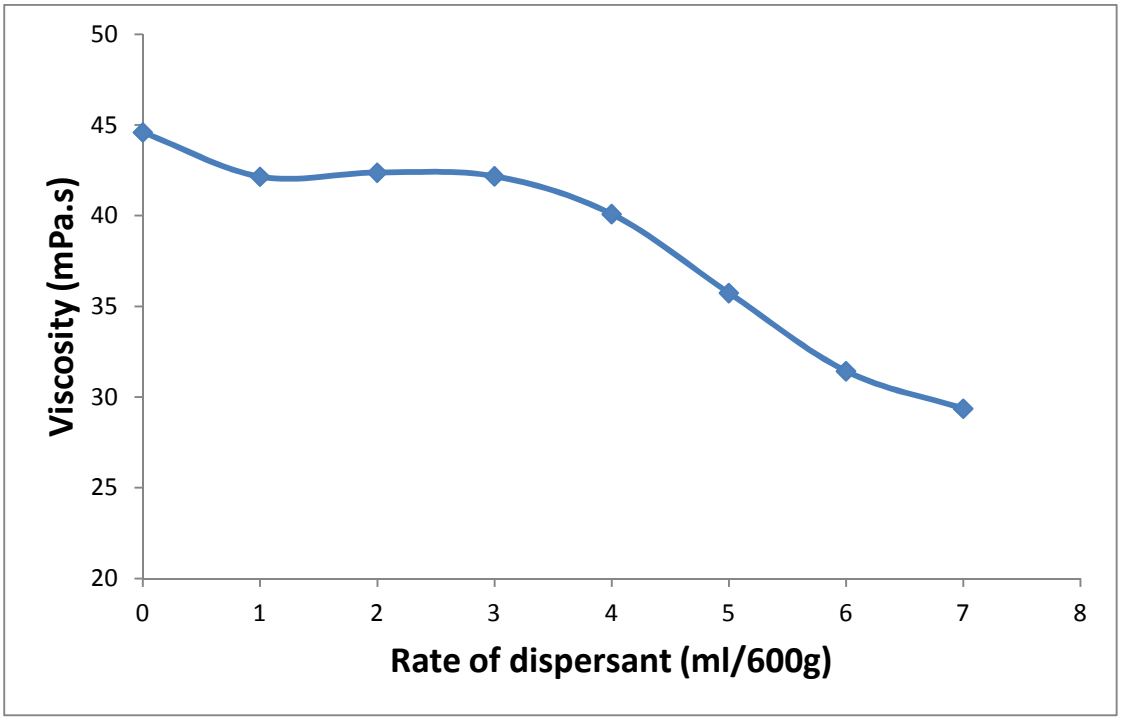

Figure 32: Viscosity versus amount of STPP in the phosphate slurry in (ml of STPP / 600g of slurry) at a fixed shear rate of 600 1 / S.

For the phosphate slurry at a solids content of 50%, we note that the STPP weakly decreases the viscosity of the slurry between (0 and 4ml of STPP / 600g of slurry) and strongly reduces the slurry viscosity between (4 and 7 ml of STPP / 600g of slurry), Fig. 32.

4. Modeling the rheological behavior of phosphate slurry

In the following, we are working on the B1 sample, the rheological data has been fitted to the Otswald-power law, Bingham, Herschel Buckley and Casson models to identify the rheological model that best describes the experimental data at each concentration index.

4. 1. Four models fitting

In this part we will try to adjust the experimental data obtained for sample B1, to the 4 models that we have mentioned, in order to know the most suitable model to describe the rheological behavior of the phosphate slurry at each index of concentration. Therefore, it is necessary to establish the parameters of optimal regressions of each model so as to have a trend curve which perfectly describes the curve obtained experimentally. The pipeline design indicated that the dynamic viscosity should be in the range (0,0066 – 0,0102 Pa.s) and yield stress in the range (1.56 - 3.8 Pa), In what follows, we look for the model which perfectly describes the rheological behavior of the phosphate slurry in the mathematical sense (it is necessary that the R^2 is close to 1), and at the same time it is necessary that this model generates values of viscosity and yield tress in the ranges design or close to these ranges.

4. 2. Models applications on phosphate slurry at 57 %, 52%, 46%, 34% concentration by mass

- Case of phosphate slurry at 57,27% concentration by mass

The adjustment of the rheogram obtained experimentally at a concentration of 57.27%, to the 4 rheological models gave the following results:

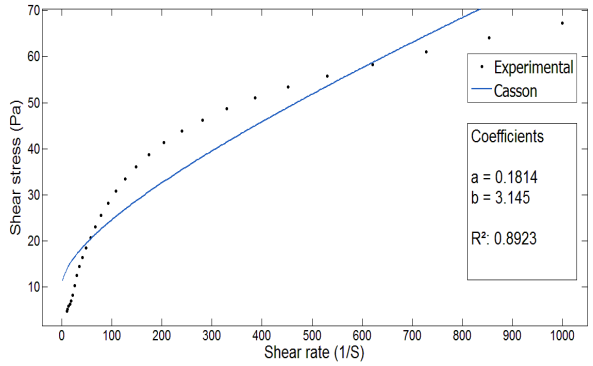

Fig 33 : Casson model $\sigma^{1/2} = 0{,}1814.\gamma^{1/2} + 3{,}145$

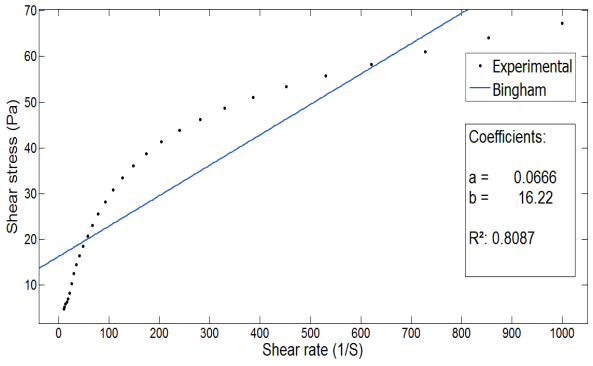

Fig 34: Bingham model $\sigma = 0{,}0666.\gamma + 16{,}22$

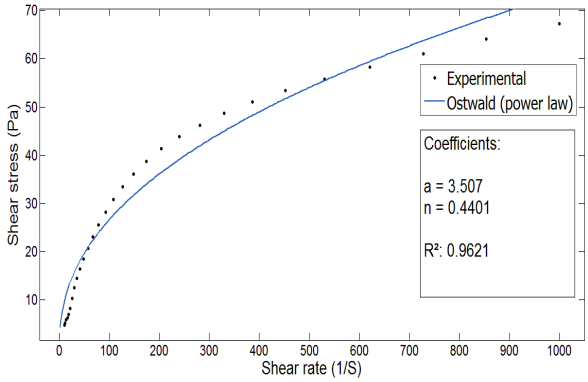

Fig 35: Ostwald model $\sigma = 3{,}507.\gamma^{0{,}4401}$

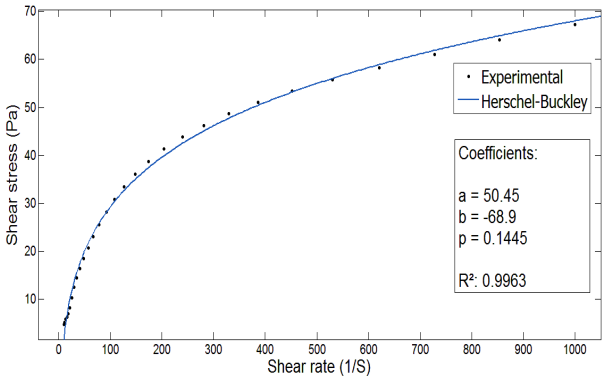

Fig 36: Herschel-Buckley $\sigma = 50{,}45.\gamma^{0{,}1445} - 68{,}9$

We note that the model which perfectly describes the rheological behavior of the phosphate slurry is the Herschel-Buckley model fig. 39 with an $R^2 = 0.9963$. The Ostwald model (Power-law), fig. 35 is also a suitable model for the description of the rheological profile at this concentration, with a $R^2 = 0.9621$. The Casson model seems to be adequate for the description of the rheological behavior for this concentration fig. 33, with a $R^2 = 0.8923$. The Bingham model fig. 34 is not suitable for describing the rheological behavior of phosphate slurry at the 57.27% concentration.

For a phosphate water slurry with a concentration of 57.27%, the Casson model does not perfectly describe its rheological behavior ($R^2 = 0.8923$), but it provides viscosity and yield stress values that seem logical and close to reality. For the case of fig. 33 the viscosity of Casson is $\nu = a^2 = 0.0329$ Pa.s and the yield stress is $b = 3.145$ Pa. These values are not the real values, but are approximate or relative values to the Casson model.

On the other hand, the Herschel-Buckley and Ostwald-power Law models perfectly describe the rheological behavior of the phosphate slurry at this concentration, but we generate viscosity and yield stress values that seem illogical (negative values of yield stress and high values of viscosity), and this is very far from the ranges of viscosity and yield stress for phosphate slurry at a concentration of 57.27 %. **[102]**

- Case of phosphate slurry at 52,32% concentration by mass

The adjustment of the rheogram obtained experimentally at a concentration of 52.32%, to the 4 rheological models gave the following results:

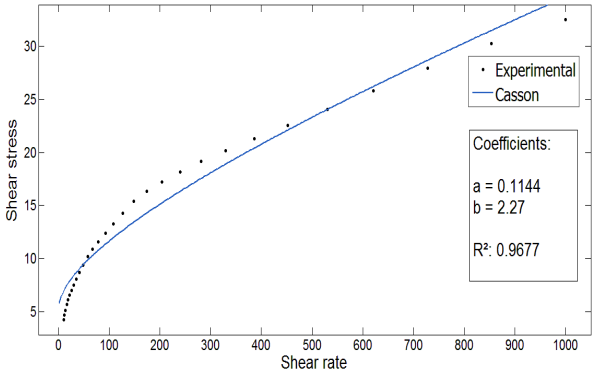

Fig 37 : Casson model $\sigma^{1/2} = 0{,}1144.\gamma^{1/2} + 2{,}27$

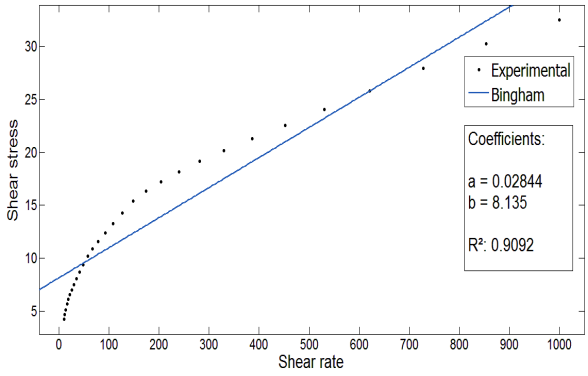

Fig 38 : Bingham model $\sigma = 0{,}02844.\gamma + 8{,}13$

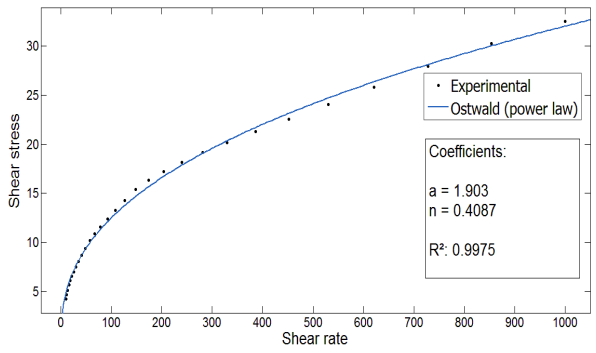

Fig 39: Ostwald model $\sigma = 1{,}903.\gamma^{0{,}4087}$

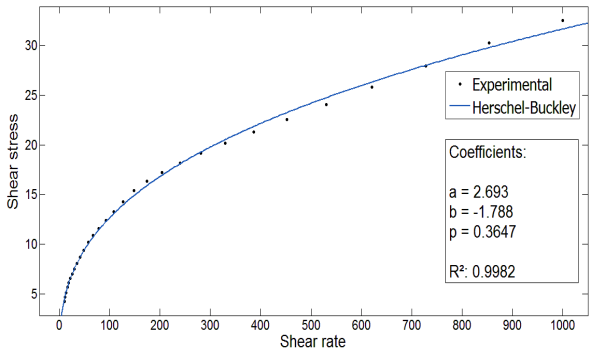

Fig 40: Herschel-Buckley $\sigma = 2{,}693.\gamma^{0{,}3647} - 1{,}788$

We note from fig. 49 and 40 that both the Ostwald and Herschel-Buckley models are suitable models for the description of the rheological profile of phosphate slurry at the concentration of 52.32%. The Casson model (fig. 37) also seems to be a suitable model for the description of the rheological behavior of phosphate slurry at this concentration, with a $R^2 = 0.9677$. The Bingham model is not a perfect model for describing the rheological behavior of phosphate slurry for this concentration.

The viscosity and yield stress values generated by the Casson model for this case are:

$\nu = a^2 = 0.013$ Pa.s and yield stress $b = 2.27$ Pa.

It should be noted that in this case where the concentration is 52.32%, the Casson model describes well the rheological behavior ($R^2 = 0.9677$) and the values of viscosity and yield stress seem logical and acceptable, because they are almost in the design ranges of viscosity and yield stress.

- Case of phosphate slurry at 46,03% concentration by mass

The adjustment of the rheogram obtained experimentally at a concentration of 46,03%, to the 4 rheological models gave the following results:

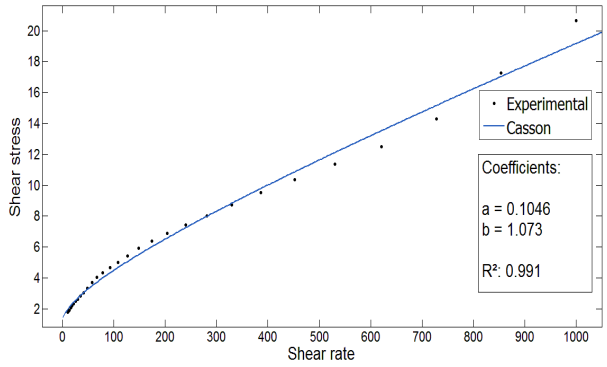

Fig 41 : Casson model $\sigma^{1/2} = 0,1046.\gamma^{1/2} + 1,073$

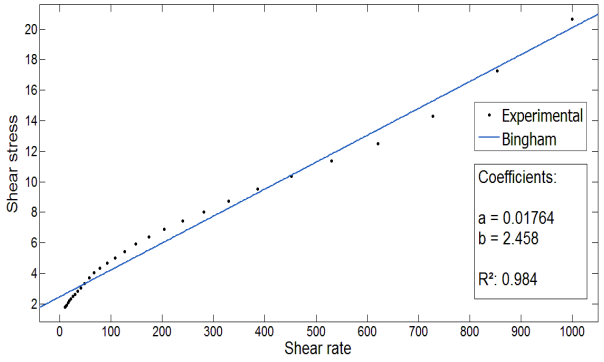

Fig 42 : Bingham model $\sigma = 0,01764.\gamma + 2,458$

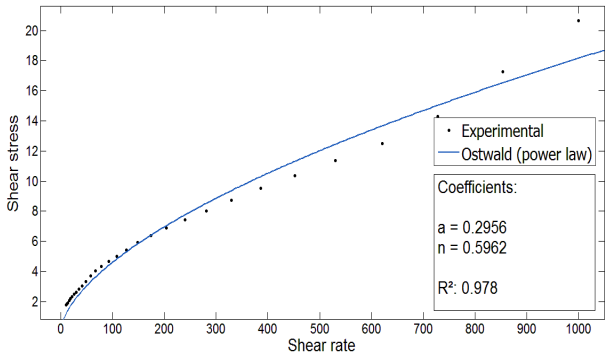

Fig 43: Ostwald model $\sigma = 0,2956.\gamma^{0,5962}$

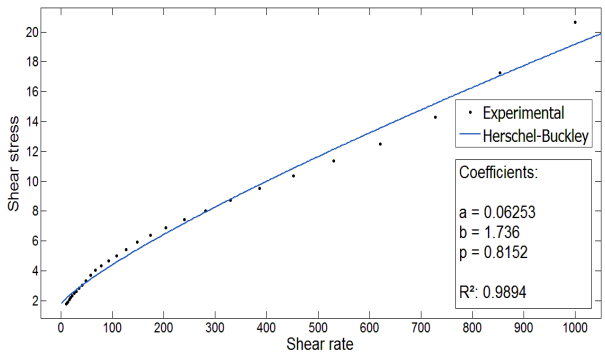

Fig 44: Herschel-Buckley $\sigma = 0,06253.\gamma^{0,8152} + 1,736$

For the case where the concentration of the slurry is 46.03%, we notice that all the models perfectly describe the rheological behavior of the phosphate water slurry. This proves what we have noticed experimentally in the paragraph (2. 4. 1. *The effect of the concentration of solids on the rheological behavior of phosphate water slurry*), we found that the 46.03% concentration point is a transition point between pseudoplastic behavior with threshold stress and Bingham behavior, for this reason all models have been suitable for this concentration. Among the four rheological models, the two Casson and Bingham models are the most suitable for describing the rheological behavior of the phosphate slurry at 46.03% concentration, with $R^2 = 0.991$ for Casson and $R^2 = 0.984$ for Bingham.

The viscosity and yield stress values for the Casson model are: $\nu = a^2 = 0.0109$ Pa.s and yield stress b = 1.073 Pa.

The viscosity and yield stress values for the Bingham model are: ν = a = 0.01764 Pa.s and yield stress b = 2.458 Pa.

Both models (Casson and Bingham) generated logical viscosity and yield stress values for a 46.03% concentration of phosphate slurry, but the most acceptable values are provided by the Casson model, because it has generated viscosity and yield stress values in the design ranges

- Case of phosphate slurry at 34,24% concentration by mass

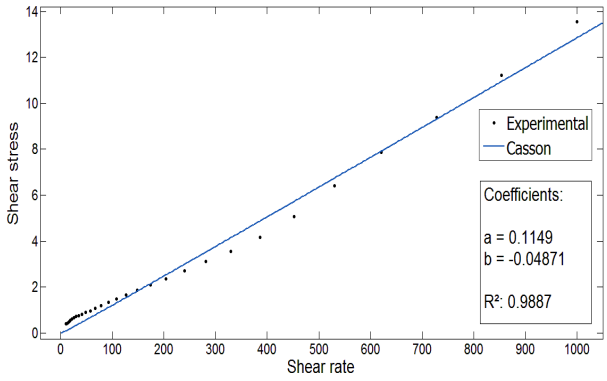

Fig 45 : Casson model $\sigma^{1/2} = 0{,}1149.\gamma^{1/2} - 0{,}04871$

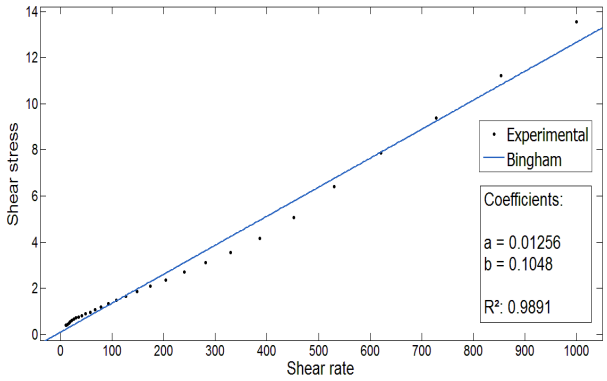

Fig 46 : Bingham model $\sigma = 0{,}01256.\gamma + 0{,}1048$

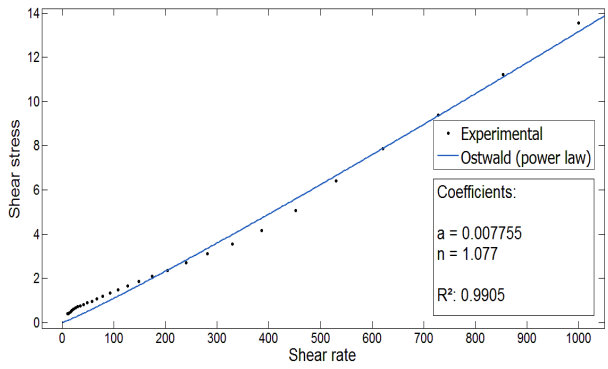

Fig 47: Ostwald model $\sigma = 0{,}007755.\gamma^{1{,}077}$

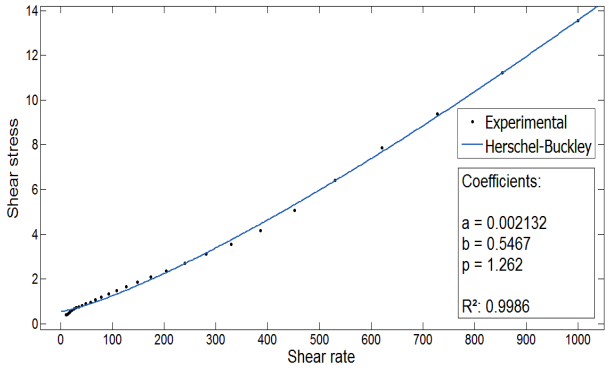

Fig 48: Herschel-Buckley $\sigma = 0{,}002132.\gamma^{1{,}262} + 0{,}546$

We note that the four rheological models perfectly describe the rheological behavior of the phosphate slurry at the 34.24% concentration. Between the four models, the two models Ostwald-power Law and Herchel Buckley are the models that perfectly describe this rheological behavior fig. 47 and 48, but the law of Ostwald is a law dedicated to Newtonian fluids, for our case there is always a threshold stress, so we adopt the Herschel-Buckley model at this concentration 34.24%.

The values of viscosity and yield stress according to the Herschel-Buckley model are ν = a = 0.0021 Pa.s and yield stress b = 0.546 Pa. These values seem logical and acceptable for the slurry at a concentration of 34.24%. .

It is well known in the literature that for the Herschel-Buckley equation, if the exponent P <1 the rheological behavior is pseudoplastic and if P> 1 the rheological behavior is dilatant, the same thing for the equation of Ostwald-power Law.

For our case fig. 20 and 21 the exponent of the Herschel-Buckley equation P = 1.26> 1 and the exponent of the Ostwald equation n = 1.077> 1, so for the concentration 34.24% the rheological behavior of the phosphate slurry is dilatant.

4. 3. Result and discussion

The regression parameters resulting from the modeling of the rheological behavior of the phosphate slurry through the four models for each concentration index are grouped together in Tables 3 and 4. The parameters **a** and **b** are successively viscosity and yield stress for each model, and the parameters n and p are the exponents of the models Ostwald and Herschel-Buckley.

	Casson model			**Bingham model**		
Concentration % by mass	**a² (Pa.s)**	**b (Pa)**	**R²**	**a (Pa.s)**	**b (Pa)**	**R²**
57,27%	0,0329	3,145	0,892	0,0666	16,22	0,808
54,50%	0,0194	2 ,711	0,929	0,04165	11,65	0,853
52,32%	0,013	2,27	0,967	0 ,02844	8,135	0,909
50,00%	0,0106	1,818	0,988	0 ,02182	5,459	0,952
46,03%	0,0109	1,073	0,991	0 ,01764	2,45	0,984
42,37%	0,0112	0,724	0,987	0,01578	1,471	0,99
38,45%	0,01272	0,1616	0,986	0,01355	0,3769	0,99
34,24%	0,0132	- 0,04871	0 ,988	0,01256	0,1048	0,989

Table 3: The regressions parameters of the Casson and Bingham models at each concentration.

	Ostwald-power Law model			Herschel-Buckley model			
Concentration % by mass	**a (Pa.s)**	**n**	**R²**	**a (Pa.s)**	**b (Pa)**	**p**	**R²**
57,27%	3,507	0,4401	0,962	50,45	- 68,9	0,1445	0,996
54,50%	2,708	0 ,413	0,985	13,52	- 18,64	0,2236	0,998
52,32%	1,903	0,4087	0,997	2,693	- 1,788	0,3647	0,998
50,00%	1,135	0,4409	0,993	0 ,5682	1,805	0,5336	0,995
46,03%	0,2956	0,5962	0,978	0 ,06253	1,736	0,8152	0,989
42,37%	0,1151	0,7158	0,972	0,01456	1,503	1,012	0,99
38,45%	0,01639	0,9783	0,984	0,003038	0,7945	1,221	0,996
34,24%	0,007755	1,077	0 ,99	0,002132	0,5467	1,262	0,998

Table 4: The regressions parameters of the Ostwald and Herschel-Buckley models at each concentration.

From the data in Tables 1 and 2 we can distinguish two forms of interpretation of the results, an interpretation from a mathematical point of view and an interpretation from a physical point of view.

5. Comparison between experimental and modeling results

5.1. Interpretation from a mathematical point of view

From a mathematical point of view, the model that has R² closer to 1 is the perfect model for the description of rheological behavior. Table 2 shows that the Herschel-Buckley model has an R² always close to 1 for all concentrations, so the Herschel-Buckley model is a perfect model of the description of the rheological behavior of phosphate slurry for the whole range of concentrations (34.24% - 57.27%), the Ostwald-power Law model is too.

The Casson model perfectly describes the rheological behavior over the concentration range (34.24% - 52.32%). The Bingham model perfectly describes the rheological behavior of the slurry on the range (34.24% - 46.03%).

5.2. Interpretation from a physical point of view

From a physical point of view, the R² must be close to 1 and in addition the model must generate viscosity and yield stress values in or near the design ranges, the Herschel-Buckley model perfectly describes the rheological behavior of slurry on the range (34.24% - 57.27%), but it provides logical values of viscosity and yield stress as for the concentration 38.45% and 34.24%.

Thus the Herschel-Buckley model is suitable for concentrations below 38.45%, it should be noted that for concentrations below 38.45% the rheological behavior of the phosphate slurry is dilatant (p> 1).

For the physical point of view we eliminate the Ostwald model, because it is a model dedicated to Newtonian fluids. It is quite remarkable from Table 1 that for the Casson model, the viscosity decreases with the dilution of the slurry, to the point of concentration 46.03% the viscosity begins to increase, which is contradictory with the physical logic, for this we can conclude that the Casson model is valid only for concentrations between (46.03% - 57.27%), it should be noted that the model Casson has values of R^2 acceptable and close to 1.

The Bingham model perfectly describes the rheological behavior of the phosphate-water slurry over the range of concentrations (34.24% - 46.03%) and we generate viscosity and yield stress values that we can consider acceptable and in the design ranges of viscosity and yield stress.

6. Conclusion

In this chapter, we proved that with dilution the viscosity of the phosphate slurry decreased and that the smaller the particle size in the slurry, the more it became viscous. We also showed the influence of the additives, flocculant, Ester, Amine and Dispersant (STPP) on the rheology of phosphate slurry. The temperature has a significant effect on the physico-chemical composition of the slurry, which has an impact on its rheological behavior. For modeling, we adjusted the experimental rheological behavior of the suspension for the four models (Casson, Bingham, Ostwald-Power Law and Heschel-Buckley). We concluded that the Herschel-Buckley model is suitable for describing the rheological behavior of the phosphate slurry and for calculating the apparent viscosity and the yield point for low concentrations (less than 38.45%). The Bingham model is suitable for the range of concentrations (34.24% to 46.03%). The Casson model is suitable for modeling the rheological behavior of the phosphate slurry and for calculating the viscosity and the yield stress for the concentration range (46.03% - 57.27%). We concluded from experimental results and modeling that with dilution, the phosphate slurry changes its pseudoplastic behavior towards Bingham behavior from the 46.03% concentration. Also it changes its Bingham behavior towards dilatant behavior from the concentration of 38.45%.

Chapter 5

CHARACTERIZATION AND RHEOLOGY OF MOROCCAN PHOSPHATE'S DERIVATIVES: PHOSPHOGYPSUM SLURRY AND SLUDGES

Chapter abstract

Phosphoric acid H_3PO_4 is a fundamental element for the manufacture of P-fertilizer, this acid is obtained through various processes. In this chapter we have interest to study the rheological behavior of the slurry generated during the attack of the phosphate by the sulfuric acid H_2SO_4. This slurry is a mixture between crystals of calcium sulphate dihydrate $CaSO_4.H_2O$ and phosphoric acid 29% in P_2O_5 and some impurities from crude phosphate **[80,81]**. We will carry out experiments to know the effect of solids concentration, crystal size, temperature and chemical composition on the rheology of phosphogypsum-slurry and the generated sludge. As far as modeling is concerned, we will try to adjust the experimental rheological behavior of the phosphogypsum slurry and sludge in the 4 rheological models, Casson, Bingham, Power Law and Herschel-Buckley. This is to identify the most appropriate theoretical model for the description of the rheological behavior of slurries and sludge. The adjustment of theoretical models to experimental rheological data allows us to predict the viscosity and elasticity of phosphogypsum slurry and sludge.

1. Processes for the manufacture of phosphoric acid

1.1. The production of phosphoric acid

Phosphoric acid is the main element in the phosphate industry, particularly for the production of fertilizers, and even the pharmaceutical and agri-food industries. It is obtained by transforming phosphates rocks rich in phosphorus, which is an essential element in life. Phosphoric acid is obtained either thermally or wet way **[80]**.

1. 1. 1. Thermal process

The thermal process consists of a reduction of the phosphate at high temperature leading to the sublimation of the phosphorus which is then oxidized by oxygen and recovered in the form of P_2O_5. Thus, the phosphoric acid is prepared by hydration of the P_2O_5 obtained. This process produces a high purity acid, however, the high energy cost limits its use [80]. The production of phosphoric acid thermally has the advantage of providing an acid with a high degree of purity, but its high energy consumption limits its use.

$$\mathbf{P4 + 5\ O2 \rightarrow P4O10 + 6\ H2O \rightarrow 4H3PO4}$$

1. 1. 2. Wet process

Phosphoric acid, or more correctly ortho-phosphoric acid H_3PO_4, results from the attack of natural phosphates by a strong acid (generally sulfuric acid, but nitric or hydrochloric acids can

also be used). With these latter two acids, soluble salts are formed which can make the separation of phosphoric acid difficult or economically impracticable [81,83]. The main reaction of the phosphate rock attack with sulfuric acid gives calcium sulphate as a by-product according to the following reaction:

$$Ca_{10}(PO_4)6F_2 + 10H_2SO_4 + 10nH_2O \rightarrow 6H_3PO_4 + 10CaSO_4, nH_2O + 2HF$$

The wet processes are widely used in the industrial world because they give a low cost acid. Any phosphoric acid process at the Jorf-Lasfar complex adopts the manufacture of wet phosphoric acid, based on phosphate slurry [86-91]. The manufacture of phosphoric acid involves 3 main operations:

- Preparation of the ore: which is either dry phosphate or phosphate-water slurry;
- Attack of the ore by sulfuric acid;
- Filtration for the recovery of phosphoric acid.

1. 2. Process of manufacture by sulfuric attack

A process which implements only one crystalline form of precipitated calcium sulphate, it should be noted that no such process satisfies at the same time all the objectives set ie high concentration of P_2O_5, minimum energy expended and high efficiency, for example the method Prayondihydrate and Rhone-Poulenc **[84].**

✓ **Process with formation of anhydrite: (n = 0)** ; $CaSO_4$ (40 at 50% P2O5 at 120-130°C)

Phosphate ore + H2SO4 → H3PO4 (40 à 50% en P205) + (CaSO4)

Ca3(PO4)2 + H2SO4 → 3CaSO4 +H3PO

With this type of process, the temperature of the reaction medium should be between 120 and 130 ° C. and the crude acid product can reach a concentration of 50% in P_2O_5.

✓ **Process with formation of hemihydrate :(n = 0.5)**; $CaSO_4.0.5H_2O$ (40 at 50% P_2O_5 at 90-110°C) :

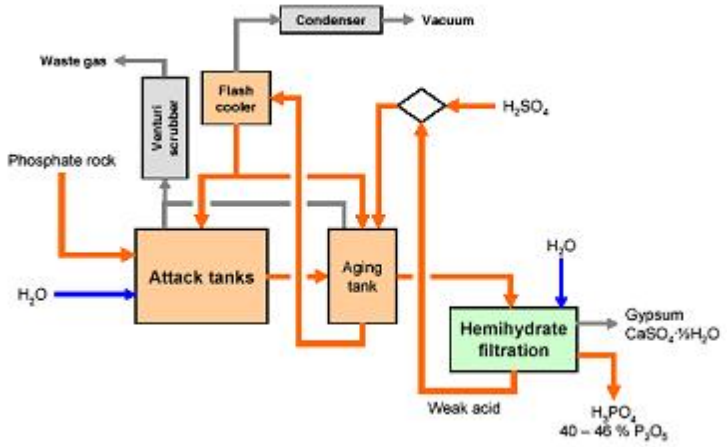

Figure 1: Process for producing phosphoric acid with formation of the hemihydrate [84].

Phosphate ore + H2SO4 → H3PH4 (40 – 46 % en P205) + (CaSO4)

Ca3(PO4)2 + 3H2SO4+3/2H2O → (3CaSO4,1/2 H2O)+2H3PO4

It remains a difficult process to control because the hemihydrate form of calcium sulfate tends to rehydrate. The acid obtained consists of more than 40% of P_2O_5, the level of impurities in the phosphogypsum being quite high.

- ✓ **Process with formation of dihydrate :(n = 2)** ; CaSO4.2H2O (26 – 32 % P_2O_5 at T <90°C).

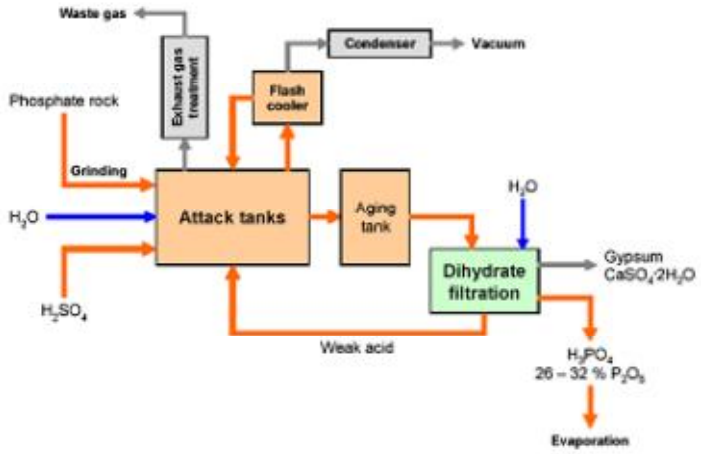

Figure 2: Process for producing phosphoric acid with formation of dihydrate [84].

The phosphoric acid production reaction according to the dihydrate process is:

$$Ca_{10}(PO_4)_6F_2 + 10H_2SO_4 + 20H_2O \rightarrow 6H_3PO_4 + 10CaSO_4.2H_2O + 2HF$$

The dihydrate process: leads to an acid with a P_2O_5 content ranging from 28 to 32%. Compared with the other methods previously described, the advantages of this method are multiple:

- ✓ Capital expenditure and lower production and maintenance costs;
- ✓ Possibility of using wet rocks without any qualitative limitation;
- ✓ Better processing capacity of various phosphate rocks;
- ✓ Production of more acid but phosphogypsum obtained quite impure (fluorinated compounds from 1.5 to 2.5%).

The last reaction above is a simplification of what actually happens in the reactor. It can be subdivided into three parallel and simultaneous reactions **[80]**:

1) Instantaneous ionization of the sulfuric acid from the dispersion in the reactor:

$$\mathbf{H_2SO_4 \rightarrow 2H^+ + SO4^{2-}}$$

2) Attacking rock particles phosphated by H + ions, dispersed in the reaction mixture:

$$\mathbf{Ca3\ (PO4)2CaF2 + nH^+ \rightarrow 2H_2PO_4^- + (n\text{-}6)H^+ + 4Ca^{2+} + 2HF}$$

3) Consequent crystallization after reaction of Ca^{2+} ions with $SO4^{2-}$ ions:

$$\mathbf{Ca^{2+} + SO4^{2-} \rightarrow CaSO_4.2H_2O}$$

In the case where the H_3PO_4/H_2SO_4 ratio is high in the reaction medium, it is considered that the overall reaction will be carried out in two stages **[81]**:

- ✓ Phosphate attack by phosphoric acid to give a solution of monocalcium phosphate:

$$\mathbf{Ca_3 + (PO_4)2 + 4\ H_3PO_4 \rightarrow 3CaH_4\ (PO_4)_2}$$

- ✓ The attack of monocalcium phosphate by sulfuric acid to lead to the formation of phosphoric acid and the precipitation of calcium sulphate:

$$\mathbf{3CaH_4\ (PO_4)_2 + 6\ H_2SO_4 + 6H_2O \rightarrow 3\ CaSO4,\ 2\ H_2O + 6H3PO4}$$

1. 3. Phosphoric acid manufacturing steps at (Line El Jorf-Lasfar plant)

The description of the phosphoric acid production process took place in the phosphoric plant of Jorf-lasfar and more precisely in (line E). This is the first industrial plant of the kind fed by phosphate-water slurry. The construction of this line dedicated to the production of phosphoric acid was based on a concentrate of technology used in the production of phosphate derivatives. With a daily production capacity of 1,400 tons of phosphoric acid, ie 450,000 tons per year, this industrial unit has a storage tank equipped with several units for thickening phosphate slurry, a reactor equipped with a maturation zone and several cooling and gas washing units. In addition to a significant increase in efficiency and productivity, line E is characterized by the efficiency of its industrial processes as well as their efficiency. Its technological and industrial equipment has undergone several tests and trials. Like the entire Slurry Pipeline device.

Figure 3: Photo of the attack section of line E

1. 3. 1. The attack

The phosphate slurry is pumped directly from the thickener to the tank by means of the reactor feed pump. This slurry is characterized by a solid content of 65%. The JACOBS process of line E uses an annular reactor equipped with several baffles, consisting of:

- 7 external annular compartments;
- A central compartment;
- A compartment to supply the cooling system;
- A small additional pump compartment, attached to the chiller supply compartment and serves as a reservoir for the supply of chiller circulation pumps.

Each compartment is equipped with an agitator, except the last one (which is used for pumping). The phosphate slurry containing 66% solids feeds the first compartment where it is diluted by a large volume of recycled feed from the maturation tank [84]. The phosphate slurry is stirred continuously to prevent the formation of a layer of phosphate in the bottom of the tank.

1. 3. 2. Vacuum cooling

The acidic attack reactions being exothermic, the slurry must be cooled in order to regulate the temperature within the attack and ripening tanks. The vacuum cooler (Flash-cooler) is a direct contact heat exchanger with a liquid ring pump which creates a partial vacuum assisted by a condenser, thus allowing the evaporation of water and the cooling of the slurry, the latter is transferred to the maturation tank, returns in excess to the tank by the overflow. Even if the cooling is only 3 ° C, the total energy dissipated is very important given the cooled flow rate.

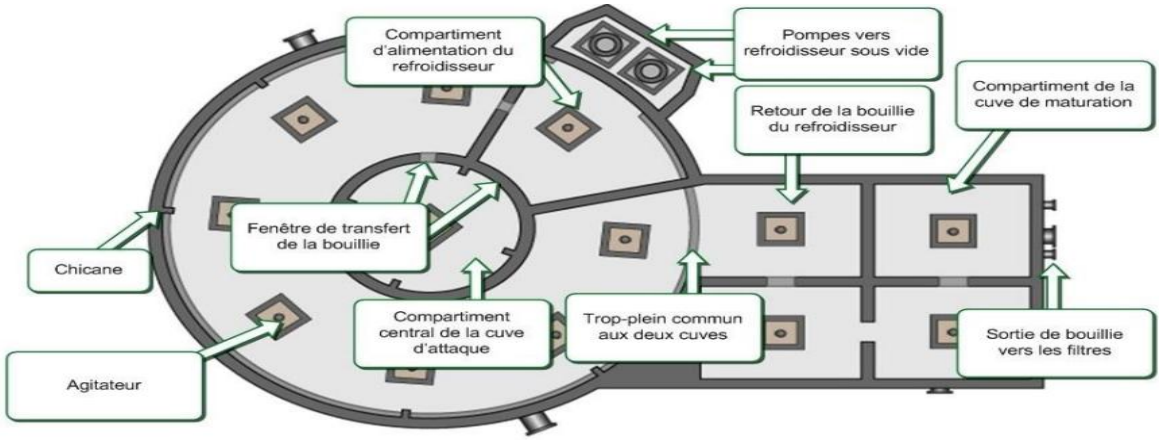

Figure 4: Main Components of the Reactor

The principle of operation of the vacuum cooler is to create a negative pressure (vacuum) and to force the continuous vaporization of water, causing the aspiration of fluorinated vapors and traces of phosphoric acids. This vaporization consuming energy (latent heat), the phosphogypsum slurry is thus cooled **[85]**.

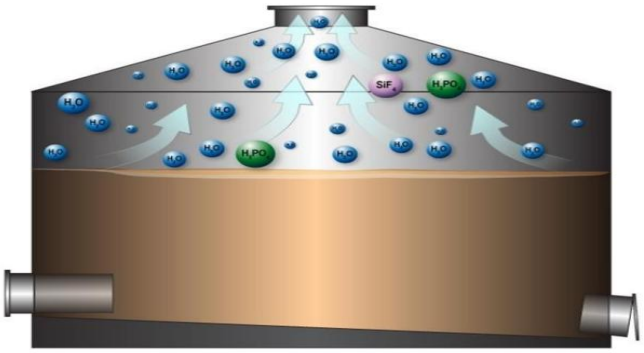

Figure 5: Configuration of Flash-cooler

Cooling also causes desaturation of the filter feed to reduce fouling in the filter. The cooler is mounted directly above the reactor to reduce the working pressure of the cooling pumps. The steam of the vacuum cooler is cooled in the pre-cooling condenser and the cooling condenser.

The pre-condenser preheats the recycled process water from the gas scrubber. The pre-condenser liquid is isolated and recovered in the insulation tank of the pre-cooling condenser. The pre-condenser pumps supply hot water to the filtration zone for washing the cake and the fabric. After the pre-condenser, most of the water vapor is condensed with the seawater in the cooling condenser. The cooling condenser liquid is discharged via a sealed closed pipe to the seawater discharge pipe which is an underground pipe.

1. 3. 3. Maturation

The maturation tank is a chamber with four compartments in series, equipped with stirrers. It is fed with mush from the Flash-cooler. The residence time is sufficient to allow the growth of gypsum crystals to a size for filtration **[80]**.

1. 3. 4. The filtration

The phosphogypsum-slurry from reactor to the filter is pumped to feed the compartments which distribute the slurry on the flat reversing filters which rotate below. The gypsum cake is formed in the trays. The liquid in it passes through the cake, the filter cloth and a pipe before entering the static vacuum chamber, inside the central valve located below the trays. For a reactor, two filtration lines (A & B) operate in parallel as shown in the following diagram:

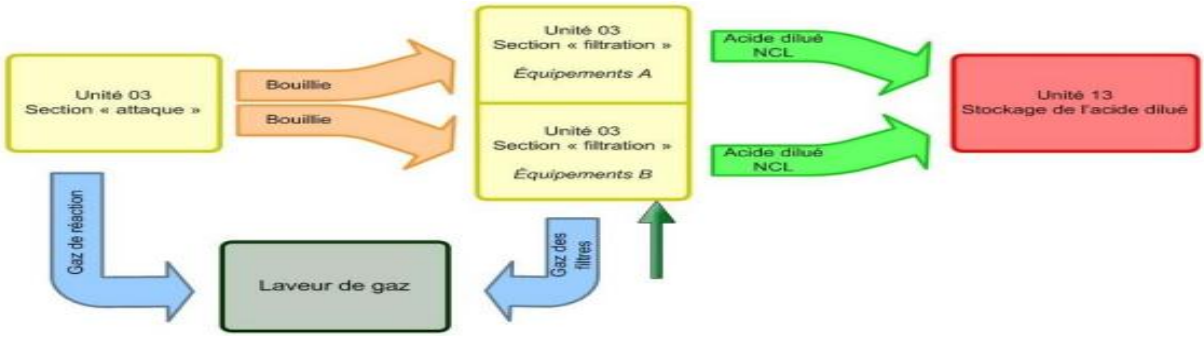

Figure 6: Phosphoric acid manufacturing process

After formation of the initial cake in the filter trays, the solid gypsum is washed three times on the filter to reduce the water-soluble P2O5 in the solids to less than 0.5% P2O5. The dilution of the acidity through the filter is of the order of less than 0.5% (from 28.5% to 28.0% P2O5). The acid product containing approximately 28% at 29% P_2O_5 and from the filter is pumped to the 29% acid clearing and storage zone. The washed gypsum is made muddy with seawater to be

discharged into an underground pipe leading to the sea. In the filtration section, two flat reversal filters separate the phosphoric acid and the gypsum. Both filters operate in parallel [93].

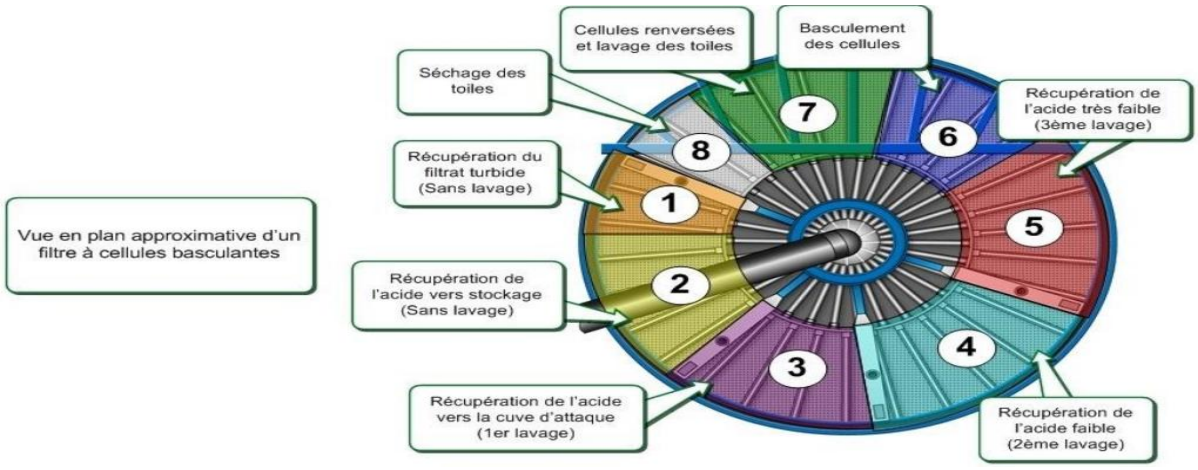

Figure 7: Principle of filtration operation

Finally, all phosphoric processes of the JorfLasfar complex have the same purpose: to produce wet phosphoric acid, starting with thickening (for processes using phosphate slurry) followed by phosphate attack and ending with filtration, while performing a washing of gases produced different reactions. However, different technologies are used for this production.

2. Description of crystallization phenomenon process

The gypsum formed in the reactor must crystallize to facilitate its subsequent separation, performed with filters. The crystallization of gypsum is a phenomenon whereby dihydrated calcium sulfate is organized into an ordered structure thus forming crystals.

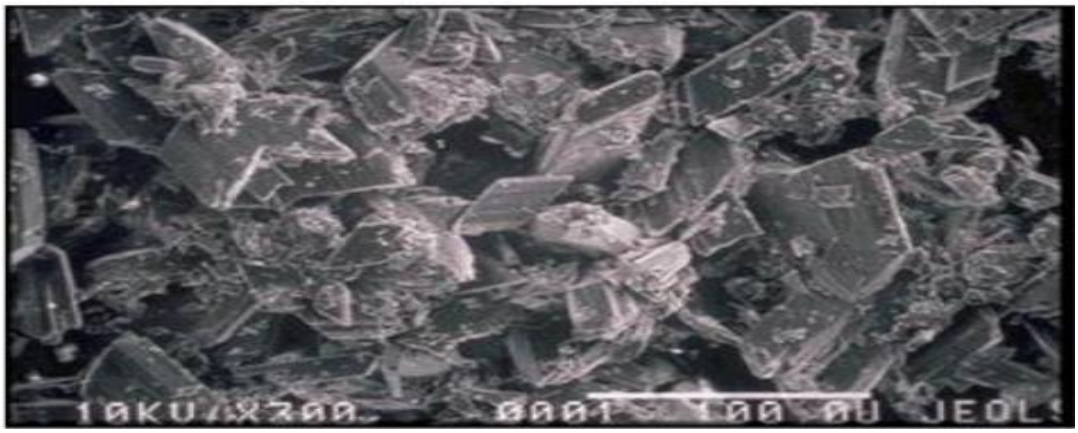

Figure 8: Microscopic view of gypsum crystals ($CaSO_4.2H_2O$)

The crystallization of the gypsum takes place in two stages: the nucleation, then the growth of the crystals. If the conditions of the gypsum can be caused by the surrounding conditions (for

example, a cooling). There can be crystallization of the gypsum and therefore, nucleation, only if the slurry is supersaturated in solute, in this case calcium sulfate dihydrate.

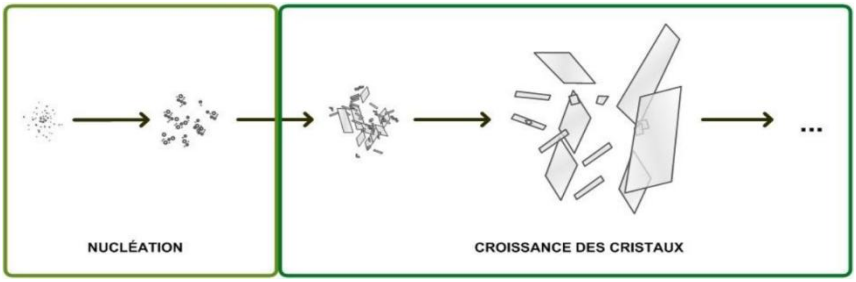

Figure 9: Schematic diagram of crystallization of gypsum.

A solution is supersaturated when it contains more solute dissolved than it can contain through external conditions (agitation, heating, etc...) This type of solution can easily precipitate following a disturbance (for example, An example of a supersaturated solution is a jar of water already saturated with salt in which additional salt is dissolved by vigorous mixing. And as shown in figure (9), the nucleation of gypsum is the phenomenon by which ions of calcium sulphates dihydrate form microscopic nascent crystals, called "germs".

These can be formed by using a surface as a support (for example, reactor walls, solid impurities in the slurry or existing crystals). These germs can also form spontaneously without the help of a carrier. In both cases, it is primary nucleation.

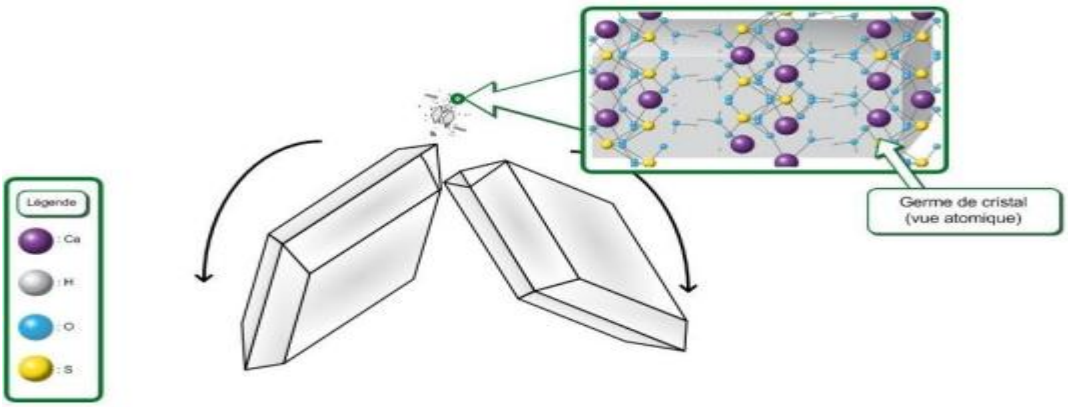

Figure 10: Schematic diagram of germination

Under favorable conditions, crystal seeds reach a critical size. Once this critical size is reached, the number of crystals stabilizes and their size increases. This step is called growth (Figure 10), it is carried out by diffusion of ions on the surface of the crystal, then by their integration in the crystal structure via a surface reaction.

Fig. 11 shows the variation in the velocity of two phenomena that are the formation of crystal seeds (nucleation) and the growth of crystals as a function of the saturation rate.

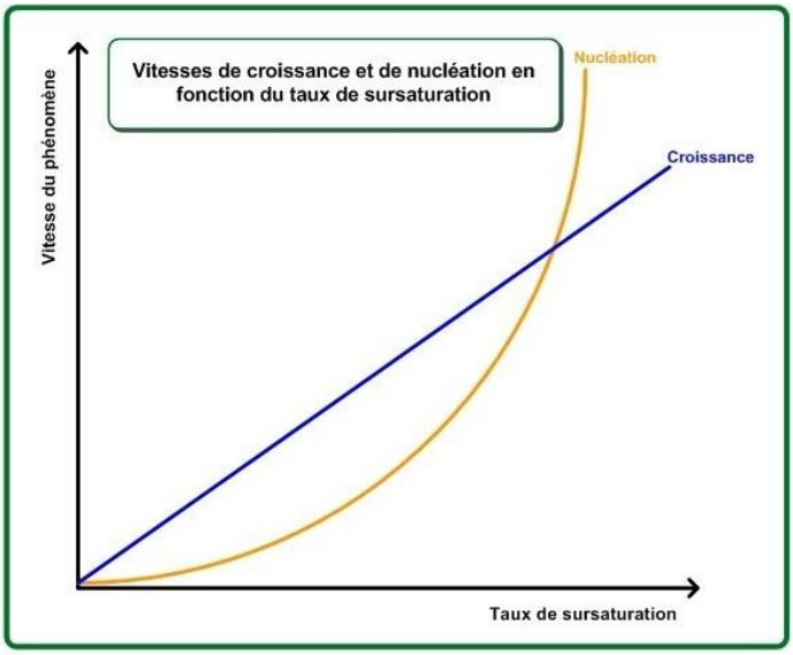

Figure 11: Growth and nucleation velocity versus supersaturation rate.

The higher the level of supersaturation, the higher the nucleation and growth velocity. In our case, the reactions that we described in the previous chapter show the state of hydration of calcium sulphate. Indeed, most processes precipitate this sulfate in the form of calcium sulfate bound to two molecules of water (gypsum - CaSO4.2 H2O). The gypsum crystals must then be separated from the phosphoric acid.

The operating conditions of the formation of gypsum are such that the acid obtained by these processes has 28 to 30% of P2O5 and contains various impurities (reflection of the phosphate treated). Other methods make it possible to obtain acid. Phosphoric acid at higher levels operating under conditions where the calcium sulfate is precipitated either in the form of anhydrite CaSO4, or in the form of hemihydrate $CaSO_4.1/2\ H_2O$. In the rest of the text, we will focus on the hydrate process (gypsum formation).

Crystallization or precipitation is induced by the super saturation of a solution. This super saturation occurs when Ca^{++} or SO_4^{--} ions are added to a saturated solution of these compounds.

When H_2SO_4 is added to CaO-containing slurry, the concentration of SO_4^{--} increases and then decreases rapidly following the precipitation of calcium sulfate. The content of SO_4 and CaO decreases proportionally.

In case of high super saturation the formation of calcium sulphate occurs spontaneously and not on the crystals existing in solution. There is nucleation. The figure below illustrates the phenomenon.

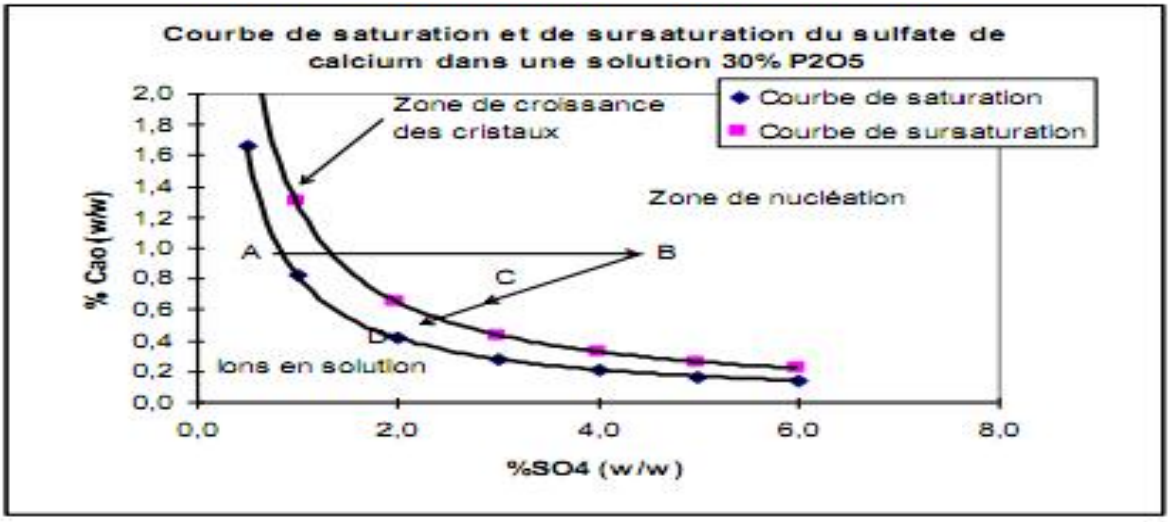

Figure 12: saturation curve and supersaturation of calcium sulphate in a 30% P_2O_5 solution.

The fig. 12 shows the typical curves of solubility and supersaturation of calcium sulphate. Point "A" represents the starting point. The SO_4^{2-} and Ca^{2+} ions are in equilibrium, to this solution is added sulfuric acid. The SO4 content will increase (point B) and then decrease rapidly (change from B to C). The supersaturation is important there is nucleation. During the transition from C to D the ion contents continue to decrease but there is no formation of nucleons. There is growth of existing crystals. Point D represents the new equilibrium. The best conditions of attack impose the formation of large crystals. They are also those of the best wash of the gypsum cake. It is done by diluting the phosphoric acid that accompanies the cake with water. The effectiveness of the dilution is better as the crystallization is good. Crystallization is a complex phenomenon. Some factors influencing its velocity are listed below.

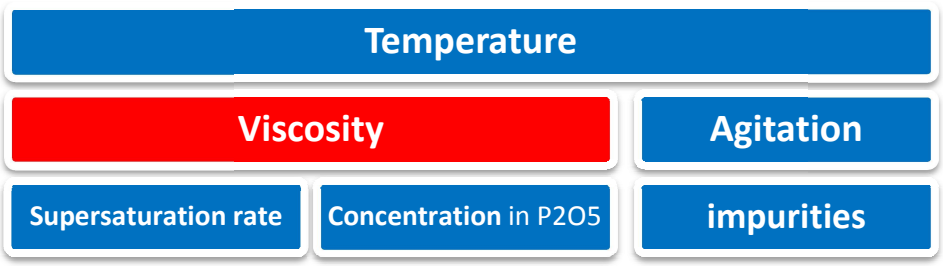

Figure 13: Factors Influencing the Quality of Crystallization

For example, some impurities will slow down the development of gypsum crystal. Since we speak of the velocity of crystallization, time remains indirectly an important variable of the overall

process. The operation leading to the formation of gypsum (calcium sulfate dihydrate, $CaSO_4.2H_2O$) is preferred to that (calcium sulfate hemihydrate, $CaSO_4.\ 1/2H_2O$), among others because it fits well to different grades of rock.

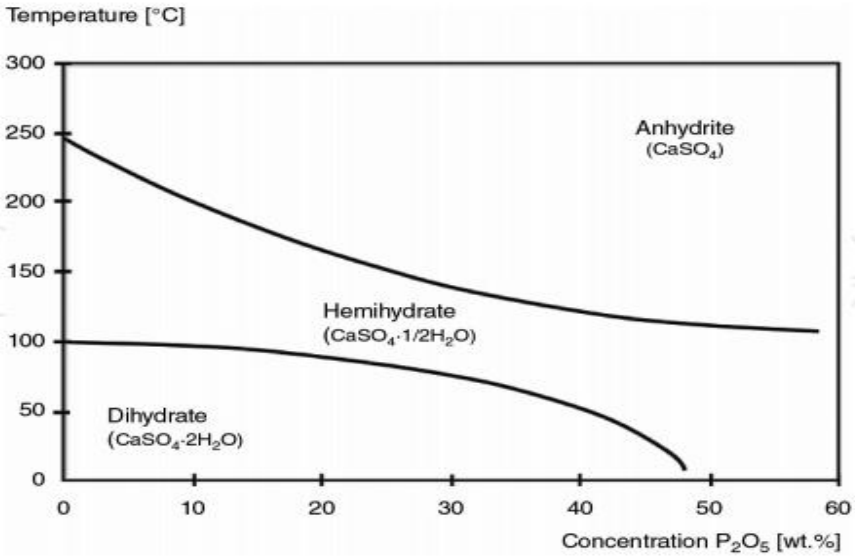

Figure 14: Form of calcium sulfate crystals ($Ca.SO_4$).

However, the velocity of chemical reactions increases exponentially with temperature according to Arrhenius law. This is why the reactor is operated between 78 ° C and 80 ° C., ie in the dihyrate zone, at the limit of the hemihydrate domain, whereas the velocity of the attack reactions remains relatively high.

3. Materials and rheological measurements

We studied the rheological behavior of the samples of phosphogypsum-slurry, taken from the tank of attack from the(line E) within the phosphoric plant, the catch was at a temperature of 80 ° C and with a rate of solid in general between (30% and 35%) and a density between 1550 Kg / m3 and 1600 Kg / m^3. The rheological behavior of (sludges '54' and '29') produced during storage and concentration of phosphoric acid was also studied.

3. 1. Physicochemical characterization of phosphogypsum-slurries and sludges

We have characterized 6 samples of Phosphogypsum (by X-ray fluorescence) to know the average chemical composition of Phosphogypsum, the characterized samples are named (B23, B29, B25, B28, B35, B37). The sludge '54' and sludge '29' samples were characterized by chemical analysis methods in the laboratory.

We notice that ACP means phosphoric acid and, for example, ACP 54 means acid phosphoric clarified 54% in P_2O_5.

Table 1: X-Ray Fluorescence Analysis of Phosphogypsum Samples.

Compound	**B25**	**B28**	**B35**	**B37**	**B29**	**B23**
MgO	0,17%	936,2ppm	0,19%	0,10%	0,10%	753,8ppm
Al2O3	0,27%	0,24%	0,38%	0,25%	0,26%	0,20%
SiO2	0,34%	0,35%	0,38%	0,31%	0,30%	0,27%
P2O5	6,09%	4,72%	6,37%	5,71%	6,41%	5,26%
SO3	20,45%	16,27%	24,91%	19,98%	20,86%	17,27%
K2O	230,6ppm		386,8ppm	198,3ppm	228,4ppm	
CaO	19,57%	16,56%	23,51%	19,16%	20,56%	16,44%
TiO2	158,2ppm	141,4ppm	305,4ppm	149,3ppm	193,2ppm	131,5ppm
V2O5	66,2ppm	54,8ppm		71,8ppm	83,8ppm	72,4ppm
Cr2O3	63,4	63,8	45,1	81,5	80,4	71,7
Fe2O3	0,10%	909,5ppm	0,13%	979,7ppm	0,11%	942,3ppm
CuO	22,9ppm	22,1ppm	24,4ppm	26,2ppm	22,2ppm	22,6ppm
ZnO	132,2ppm	122,2ppm	140,4ppm	123,6ppm	120,7ppm	137,8ppm
As2O3	9,6ppm	8,9ppm	5,4ppm	11,8ppm	6,4ppm	10,1ppm
SrO	712,9ppm	763,9ppm	877,9ppm	821,1ppm	760,7ppm	694,6ppm
Y2O3	135,3ppm	143,1ppm	160,9ppm	143,9pm	160,6ppm	134,7ppm
ZrO2	16,2ppm	17ppm	25,4ppm	24,4ppm	20,4ppm	15,3ppm
Nb2O5	0	0	0	0	0	0
SnO2	55,7ppm			103,5ppm		76ppm
La2O3	148,7ppm	94,1ppm	898ppm			
Sm2O3	0	0		0	0	0
Yb2O3	6,8ppm	0	0	0	0	0
PtO2	1,8ppm			3,2ppm		
PbO	1,3ppm	2,9ppm	4ppm	1,2ppm	1,3ppm	1,7ppm
Re	2,1ppm	3ppm	0	4ppm	1ppm	0,1ppm
U	102,3ppm	108,5ppm	106ppm	115,6ppm	108,3ppm	110,5ppm
NiO			0		8,1ppm	12,5ppm
Pr2O3			0			
MnO				2,8ppm		
Ag2O					508,1ppm	
Nd2O3						23ppm

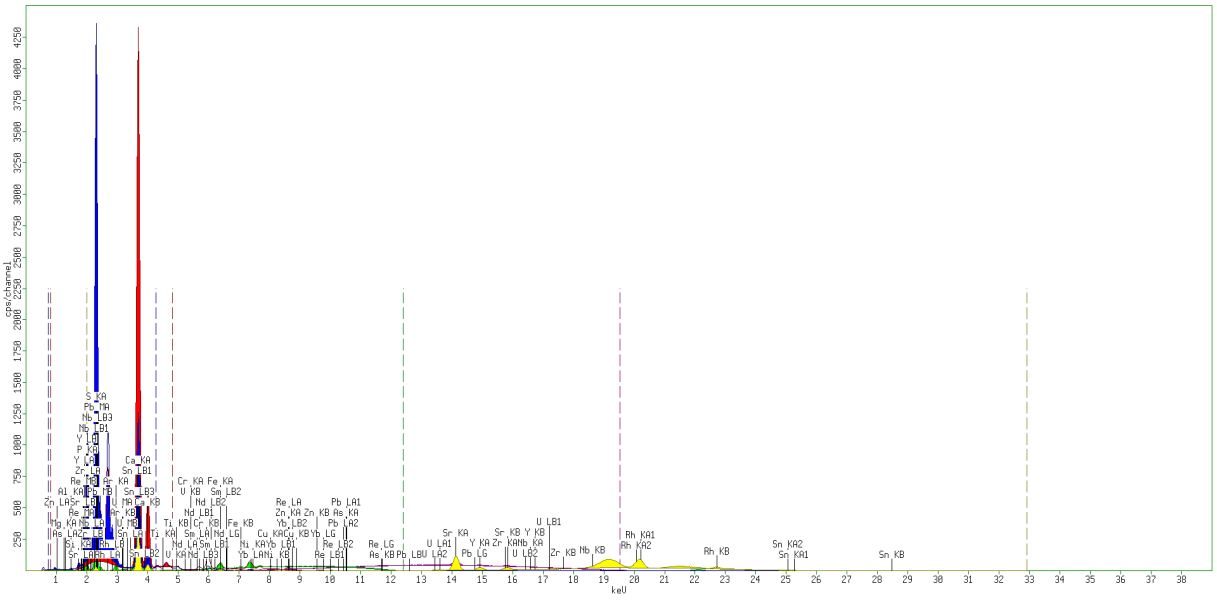

Figure 15: X-Ray Fluorescence spectrum of sample B25

In general, the chemical elements that predominate the composition of phosphogypsum are CaO (16% to 24%), and SO_3 (16% to 25%), and P_2O_5 (4% to 6.5%) this proportion in P_2O_5 is due to losses of H_3PO_4 acid during filtration, and H_3PO_4 co-crystallized with phosphogypsum. There are many other elements in the phosphogypsum with low proportions, are the mineral elements, clay substances such as Al_2O_3 and SiO_2, rare earths and radioactive elements.

3. 2. Chemical analysis of sludges '29' and '54'

	SO3	P2O5	MgO	Fe2O3	F	Cao	Al2O3
Sludge 54	10,05 %	23,34 %	0,08 %	0,17 %	8,78 %	18,71 %	0,63 %
Sludge 29	16,73 %	4,4 %	0,22 %	0,68 %	12,34 %	30,47 %	0,12 %

Table 2: Chemical analysis of sludges '29' and '54'

The sludge '29' occurs during the settling of the small sediments contained in the (ACP 29) during its storage [86], these small sediments came from the filtration operation of the phosphogypsum-slurry, they are particles of Phosphogypsum having a size lower than the diameter of the pores of the filter, in general these sludges are particles of calcium sulphate plus impurities. The sludge '54' occurs during the concentration of the (ACP 29%) to (ACP 54% in P_2O_5), the concentration actually at a temperature of 80°C under vacuum, the thermochemical conditions of this operation transform the sludge '29' into sludge '54'. The difference between the chemical composition of sludge '29' and '54' is quite remarkable on the (Table 2), we note that almost the

majority of ingredients in the table for sludge '29' are consumed during the operation of the concentration except for P_2O_5 and Al_2O_3, this is explained by the fact that, the elements (SO3, MgO, FeO3, F, CaO) interact with other impurities contained in the acid under the effect of the temperature, to give new compounds created in the sludge '54'. For the case of P_2O_5 we notice the contrary the content of P_2O_5 increases in the sludge '54' that sludge '29', normal thing, because the medium (the ACP 54) where the sludge '54' is created is rich in P_2O_5. [86]

3. 3. XRD characterization of Phosphogypse used in this study

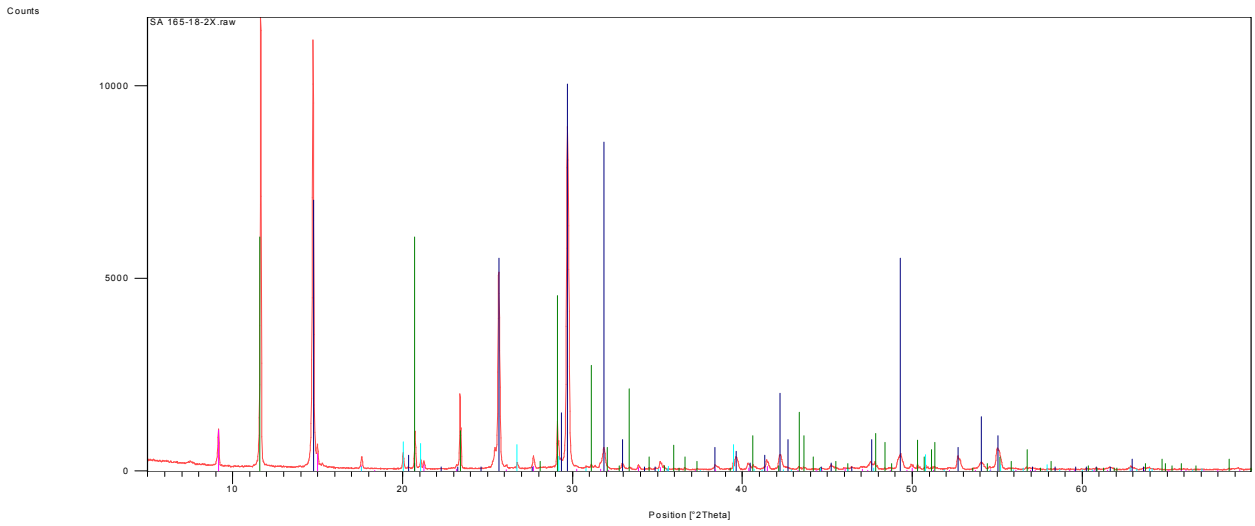

Figure 16: X-Ray Diffractogram of the Phosphogypsum Sample

Visible	Compound Name	Chemical Formula
++++	Bassanite, syn	Ca S O4.0.5 H2 O
++++	Gypsum, syn	Ca S O4 .2 H2 O
++++	Chukhrovite	Ca4 Al Si (S O4) F13 (H2 O)12
++++	Malladrite, syn	Na2 Si F6

Table 3: Phosphogypsum phases identified by (XRD)

We carried out this X-ray diffraction of Phosphogypsum used in this study at the analysis center that exists at the research and development department (OCP) in Jorf-Lasfar iorder to identify phases that exists in Phosphogypsum. We found that calcium sulphate dihydrate

($CaSO_4.2H_2O$) exists with a high fraction in our sample (streak in green), calcium sulphate hemihydrate ($CaSO_4.0.5H_2O$) exists with a low proportion (streak in blue), and the particles $Ca_4AlSi\ (SO_4)\ F_{13}\ (H_2O)_{12}$ and Na_2SiF_6 exist with very low proportions.

3. 4. Rheological measurements

The samples were stirred with a constant temperature. Measurement of the viscosity of the Phosphogypsum-slurry is carried out using a rotary rheometer (Anton Paar) series MCR 72.

The measuring device used is manufactured according to the most advanced technological concept, any type or combination of rheological tests, both in rotation and oscillatory mode, is possible.

The modularity of the system allows the integration of a wide range of temperature devices and application-specific accessories to guarantee absolute control at all times during rheological tests.

Figure 17: Rotary Viscometer (Anton-Paar)

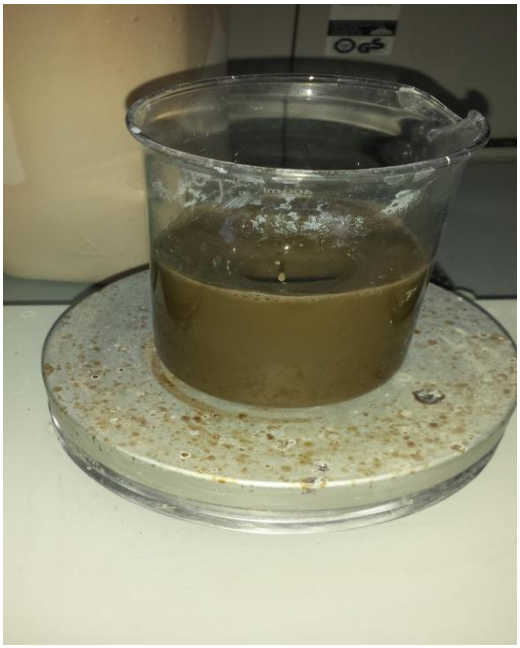

Figure 18: Phosphogypsum-slurry in agitation.

4. Results and discussions on experimental rheological behavior of Phosphogypsum Slurry and Sludges

We subjected 3 Phosphogypsum-Slurry samples named (1, 2 and 3) to rheological measurements over a range of shear rates (1 - 1000 s^{-1}), and at solid rates ranging from (31% to 36%), and temperatures ranging from (80 to 25 ° C). the samples are taken from the attack tank at

a temperature of 80 ° C. The method consists of taking rheological measurements on the same sample from the outlet temperature of the tank (80 ° C) to lower temperatures up to 25 ° C.

4. 1. Effect of temperature on the rheological behavior of the phosphogypsum-Slurry

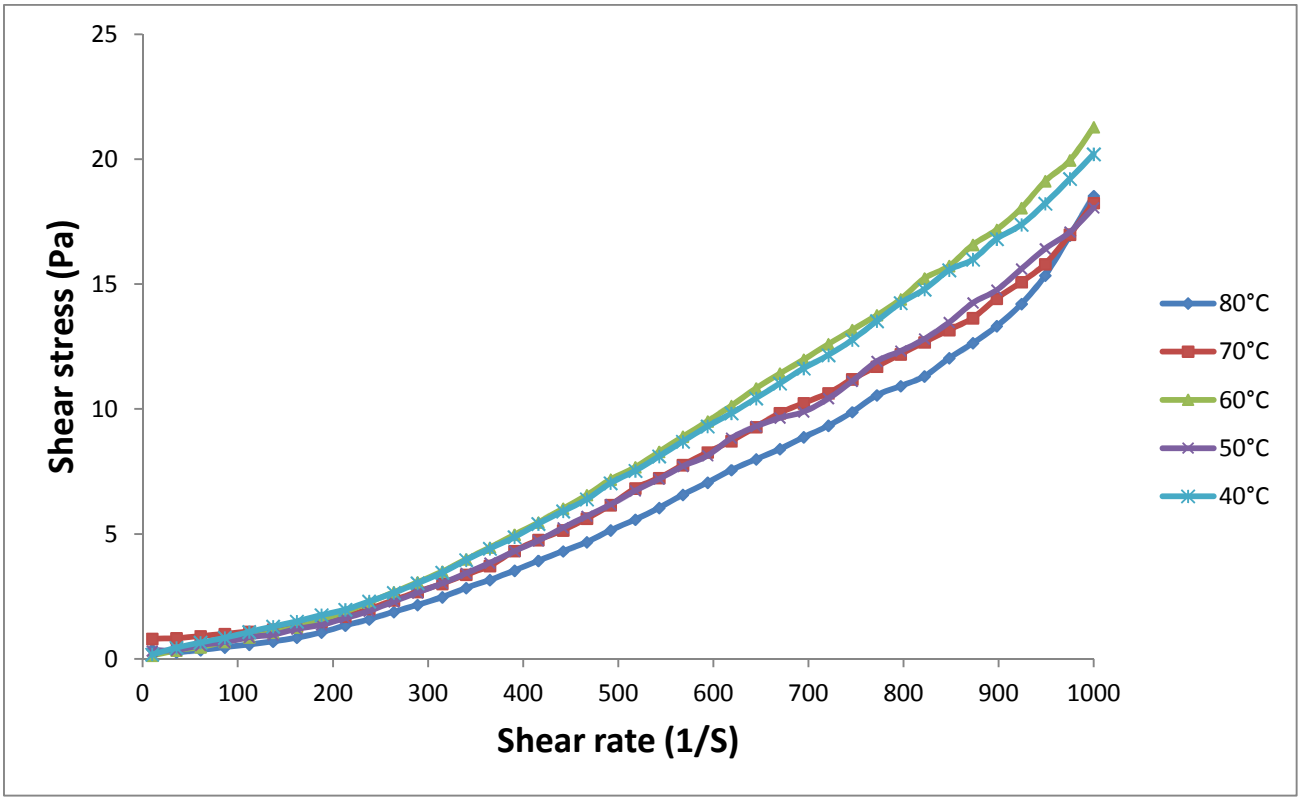

Figure 19: Rheology of the phosphogypsum-Slurry at different temperatures (sample 1) at 32% in solid rates.

From fig. 19 we can see that the rheological behavior of the slurry at all temperatures and at a solids rate of 32% is dilatant.

A fluid is said to be dilatant or (shearthickening) when it is characterized by an increase in viscosity with an increase in the rate of deformation. This behavior is often observed with solutions loaded with particles as in our case. As the particles become stressed, they become crowded and the resistance to flow increases.

The yield stress or elasticity is the point of intersection between the rheological curve and the ordinate axis, from the figures we can conclude that the flow threshold (yield stress) for the Phosphogypsum-Slurry is low and close to zero, so the yield stress may be negligible for the Phosphogypsum-Slurry.

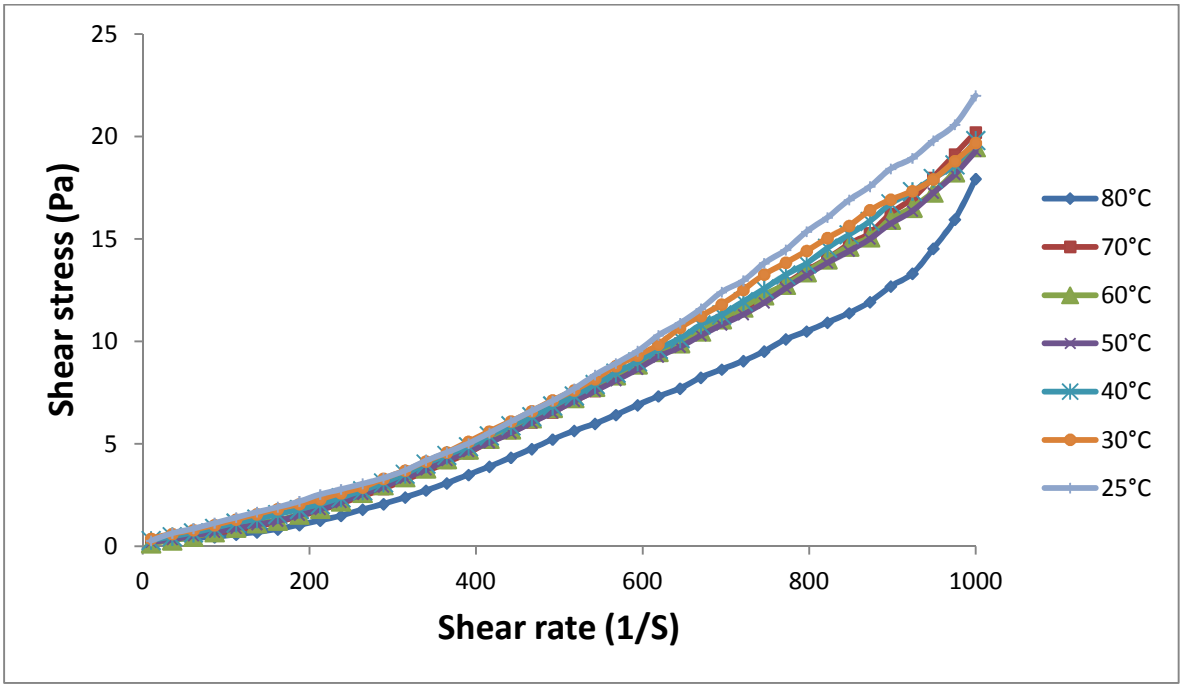

Figure 20: Rheology of the phophogypsum-Slurry at different temperatures. (sample 2) at 31% solids rate.

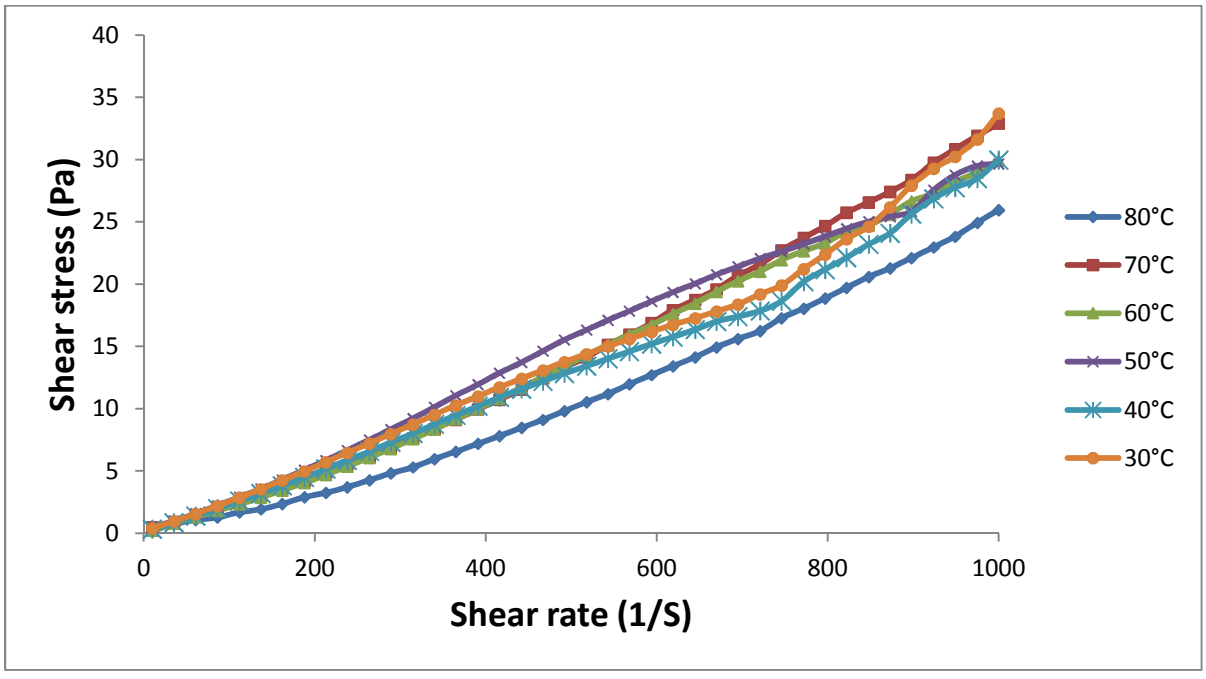

Figure 21: Rheology of the phosphogypsu-Slurry at different temperatures (sample 2) at 36% solids rate.

At a solid rate of 36% the phosphogypsum-slurry is more concentrated, during agitation the shock between the gypsum crystals increases, and the crystals begin to break, and the hydrodynamic and electrostatic interactions increase between the particles, causing the imbalance presented in fig. 21, we notice arbitrary variations in rheological behavior at each temperature.

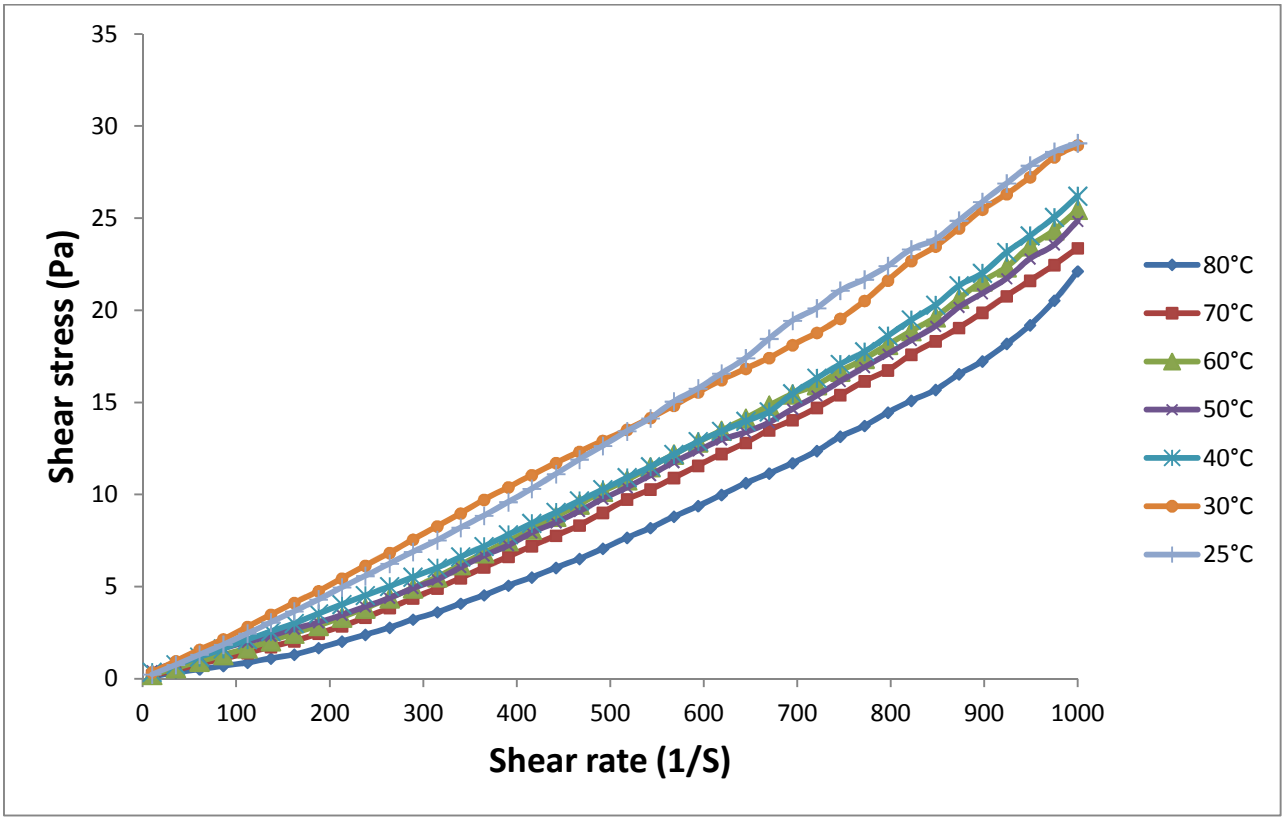

Figure 22: Rheology of the Phosphogypsum-Slurry at different temperatures (sample 3) 32% solid rate.

For sample (3) we see the same remarks raised for samples (1) and (2).

We can conclude from the 3 samples, that the rheological behavior of the Phosphogypsum-slurry is always dilatant (shear thickening), whatever the temperature (generally between 80 ° C and 25 ° C), the viscosity this slurry increases if we decrease the temperature between 80 ° C and 60 ° C, and decreases between 60 ° C and 50 ° C due to the change in particle sizes and agglomerations of small particles to each other, this affects the particle size distribution and therefore affects normal elevation viscosity as a function of temperature. Above 50 ° C the viscosity normally increases with temperature up to 25 ° C.

4. 2. Influence of the sizes of the gypsum crystals on the rheology of the phosphogypsum-Slurry

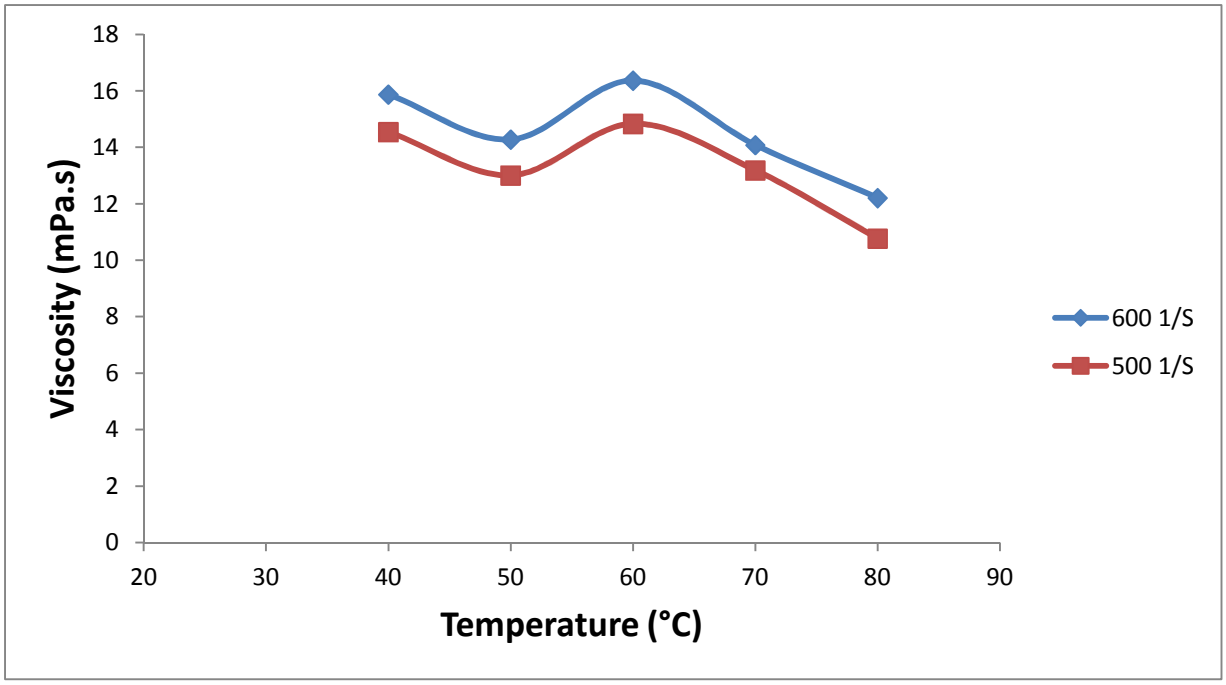

Figure 23: Viscosity as a function of Temperature (sample 1) at 500 1 / S and 600 1 / S fixed and at 32% in solid rate.

Setting the Shear rate at 500 1/S and 600 1/S, we noticed that the curve of viscosity as a function of temperature is the same for both (shear rates), the only difference is that the pace for (600 1 / S) is translated upward, normal thing because the more you increase the Shear rate the higher the viscosity increases.

In the fig. 23 is presented the variation of the viscosity as a function of the temperature, we note that the viscosity increases with the temperature decreases between 80°C and 60°C, between 60°C and 50°C the viscosity decreases, below 50°C the viscosity begins to increase again.

It is well known in the literature that the more the temperature of a fluid or a suspension decreases the more its viscosity increases, in Fig. 23 we notice an unexpected fluctuation in the variation of the viscosity between (60°C and 50°C) in this range the viscosity decreases with the lowering of temperature, this can be attributed to several phenomena. We can mention that between these phenomena, the modification of the texture or the morphology of the phosphogypsum in this temperature range (60°C and 50°C), or also the modification of particle size distribution, that is to say the size of the crystals of $CaSO_4.H_2O$ or the size of the agglomerations of these crystals. Indeed, as we have already discussed, the method consists in making rheological measurements on the same sample taken from the attack tank at 80°C, and we

begin to cool this sample to establish the rheological behavior of the phosphogypsum-slurry at any temperature. (80°C, 70°C, 60°C ... 25°C), during the cooling of the slurry the viscosity increases with the lowering of the temperature to the point of temperature 60°C, from this point the crystals begin to grow, and the small crystals begin to agglomerate together forming large particles, which causes this decrease in viscosity between (60°C and 50°C), at the bottom of 50°C the viscosity increases again with the decrease of the temperature under the effect of the increase of the viscosity of the medium (the ACP 29) but nothing happens at the level of the morphology or the sizes of the particles.

So we can deduce that the viscosity of the slurry increases between 80°C and 60°C under the effect of the increase of the viscosity of the medium, between 60°C and 50°C the viscosity of the slurry decreases under the effect of the increase of the size of the particles and agglomerations of the small crystals, beyond 50°C the viscosity of the slurry increases again under the effect of the lowering of the temperature of the medium.

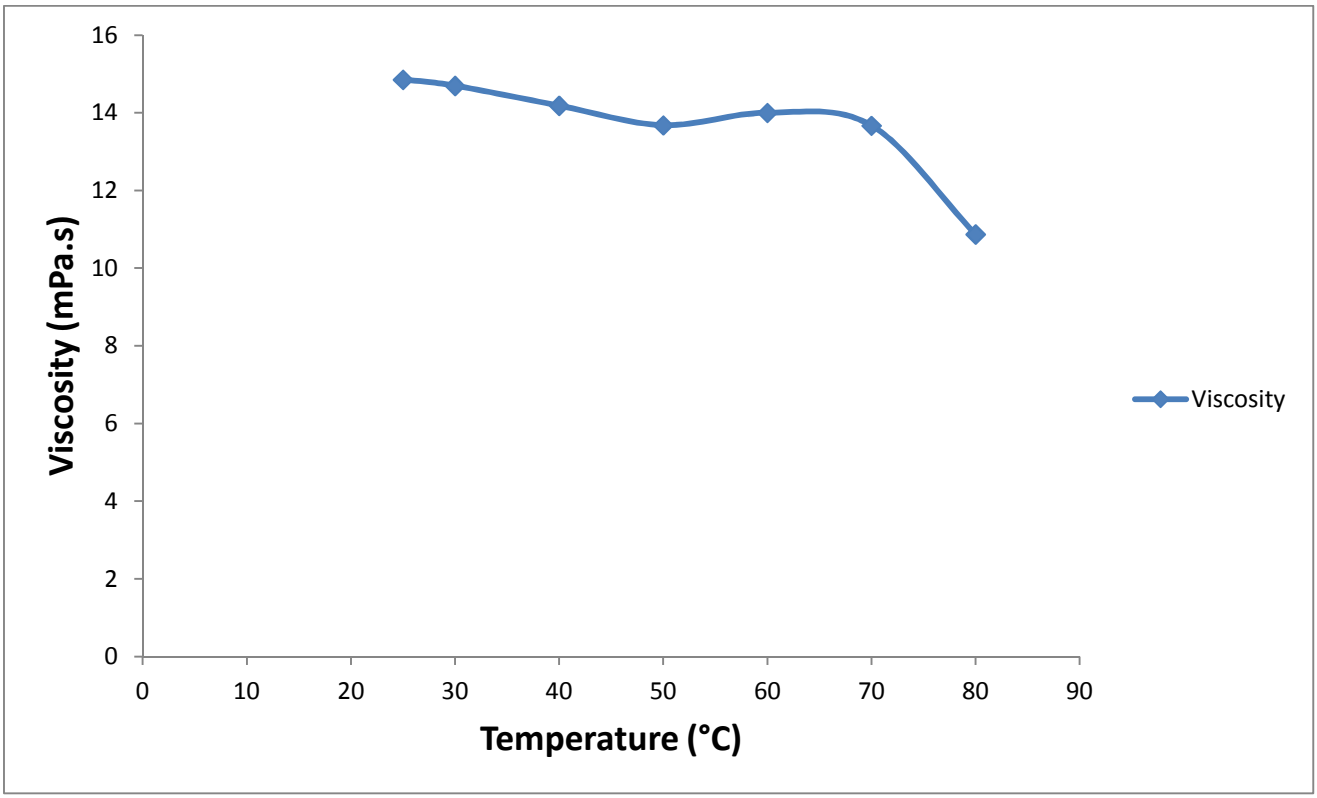

Figure 24: Viscosity versus Temperature (Sample 2) at 500 1 / S and at at 31% in Solids

For sample 2 we notice that the curve of viscosity as a function of temperature is little different than that of sample 1 Fig. 23, this is attributed to the difference in chemical composition and the particle size distribution between 2 samples, but the common point for all samples is the decrease in viscosity between 60°C and 50°C, this conclusion is almost capital.

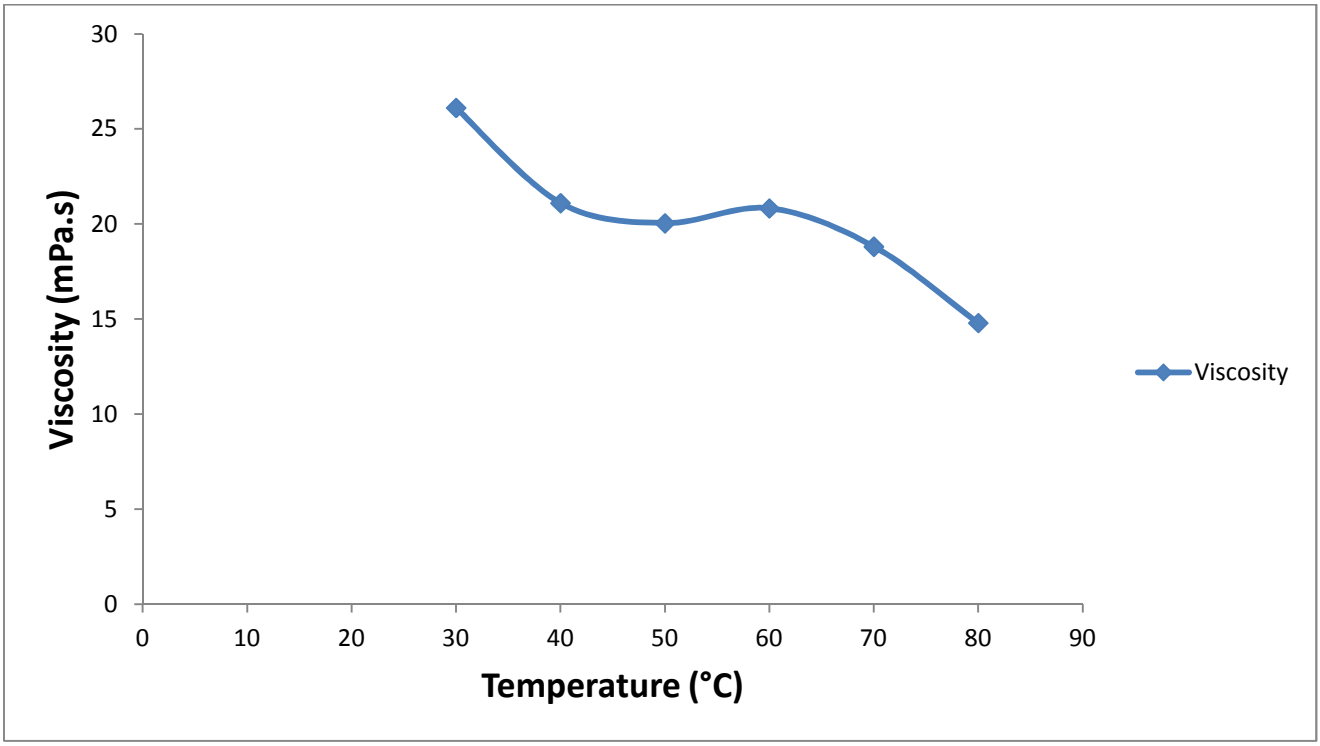

Figure 25: Viscosity vs Temperature at 500 1 S (Sample 3) at 32% Solid Rates

The remarks raised from figures 23, 24 and 25 illustrated by optical microscopy, is to see what happens to the morphology and the size of the gypsum crystals at each temperature index.

Figure 26: Optical microscope used in thi study.

Figure 27: The scale used in microscopy (10 / 0.25) (160 / 0.17).

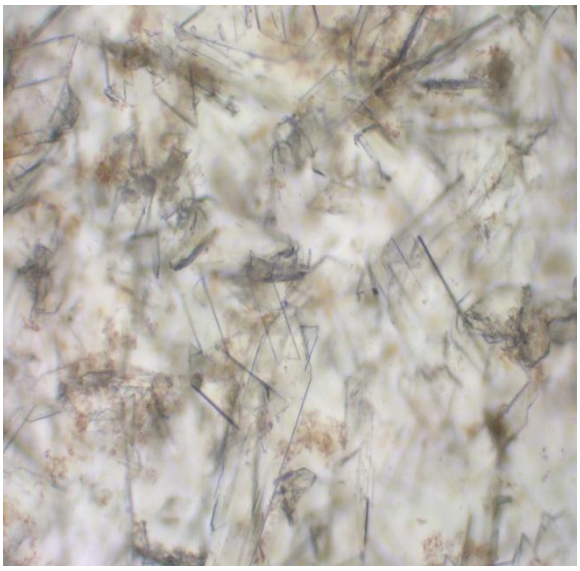

80°C

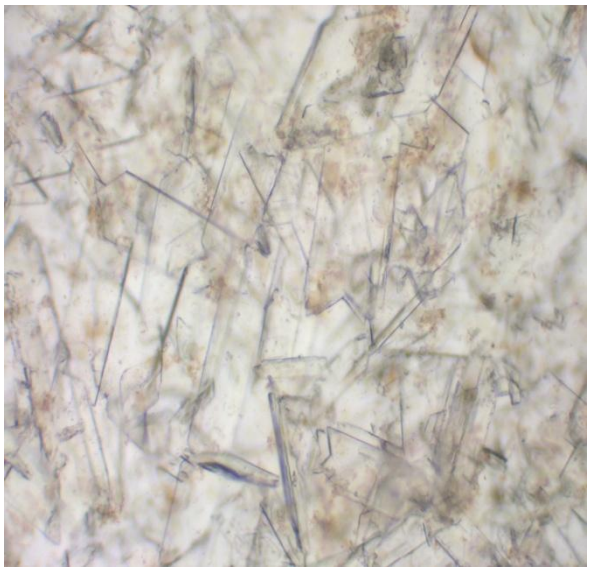

70°C

60°C

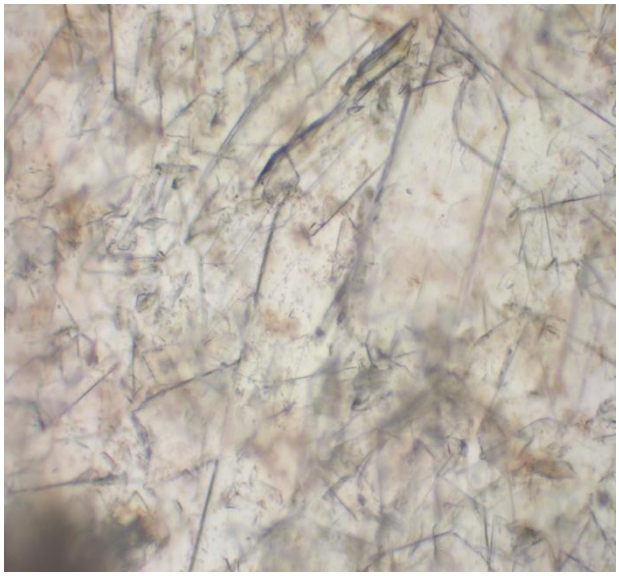

50°C

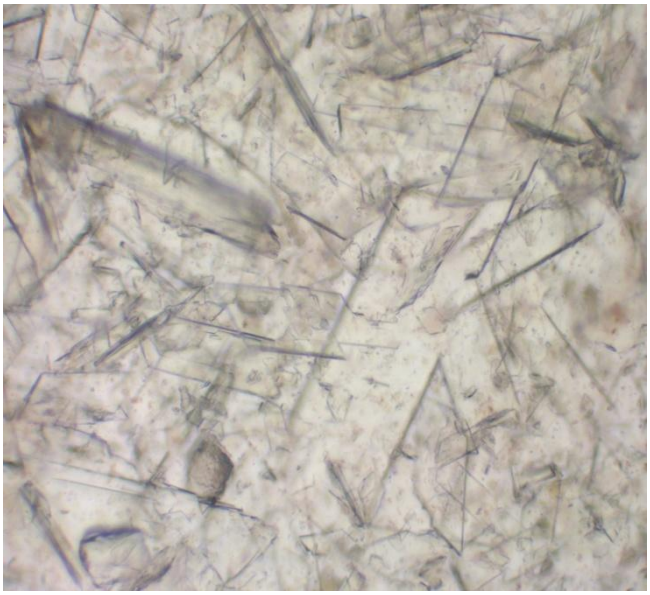

40°C **30°C**

We noticed that for 80°C and 70°C nothing happens at the particle sizes. For 60°C and 50°C the crystals grown and the small particles form agglomerates of large sizes, for 40°C and 30°C the particles keep the same sizes. This proves the hypotheses we have already proposed concerning the variation of the viscosity of the Phosphogypsum-slurry as a function of the temperature.

4. 3. Influence of the solid rate on the rheology of the Phosphogypsum-Slurry

By increasing the solids rate of the sample (2) to 33%, we notice that the rheological behavior of the Phosphogypsum-Slurry is still dilating at 80°C and 70°C as shown in fig. 28.

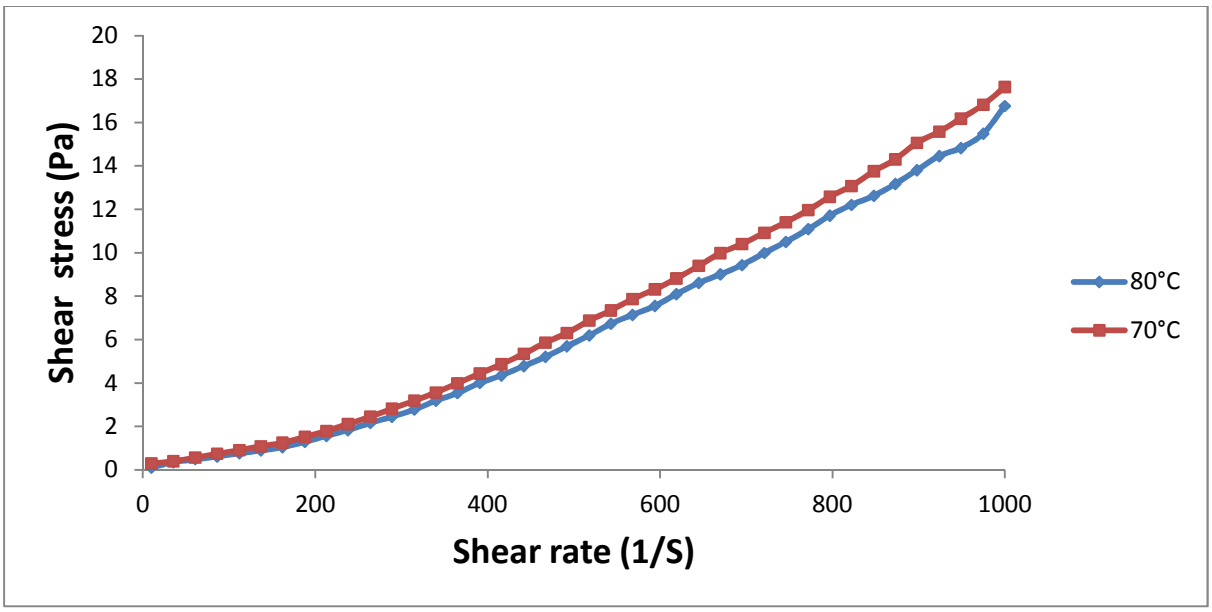

Figure 28: Rheology of the phosphogypsum-slurry (sample 2) at 33% solids rate at (80°C and 70°C)

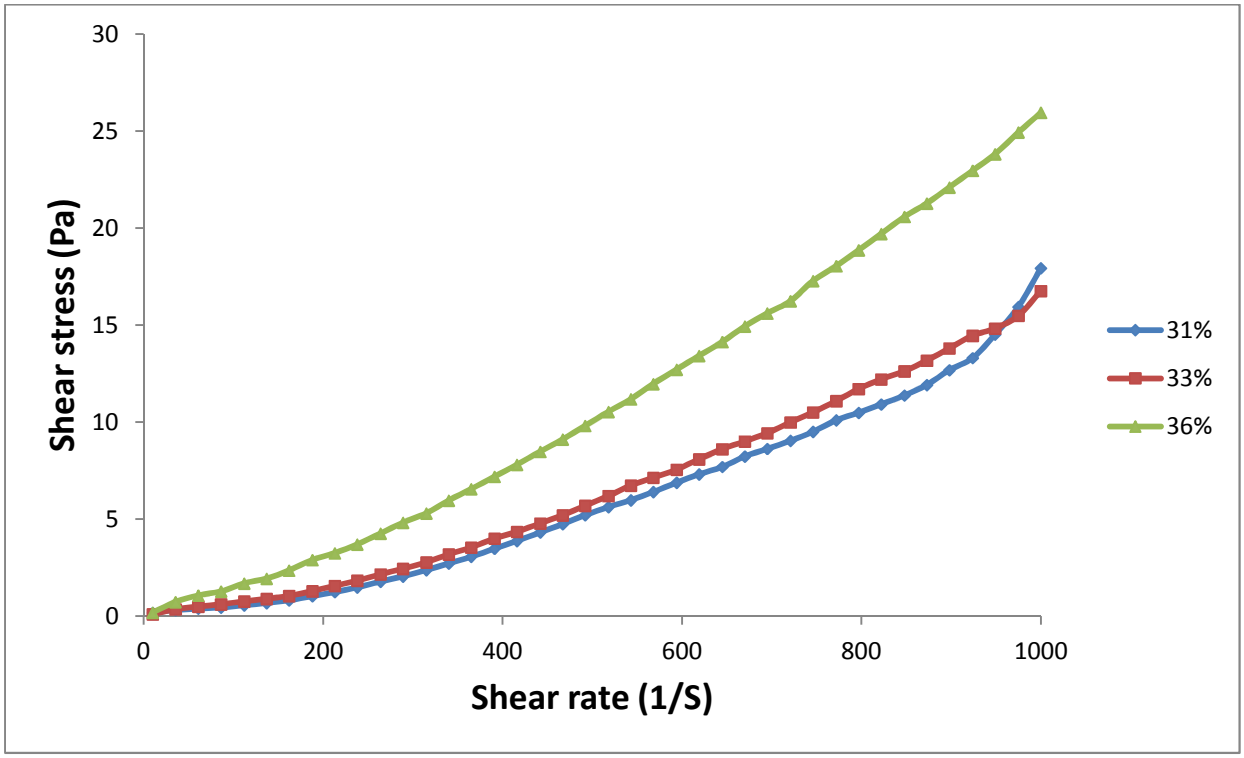

Figure 29: Rheology of the Phosphogypsum-Slurry (sample 2) at different solids rate at (80°C)

Fig. 29 shows the rheological behavior of sample 2 at solid rates of (31%, 33%, 33%), we did not aim to go far beyond the range of solid rates recommended by the designer of the process (30 to 35%). The viscosity of the slurry increases with the concentration of solids in the range (30% - 36%), the increase in the viscosity is slow between 30% and 33%, beyond 33% the viscosity increases strongly with the solid rate.

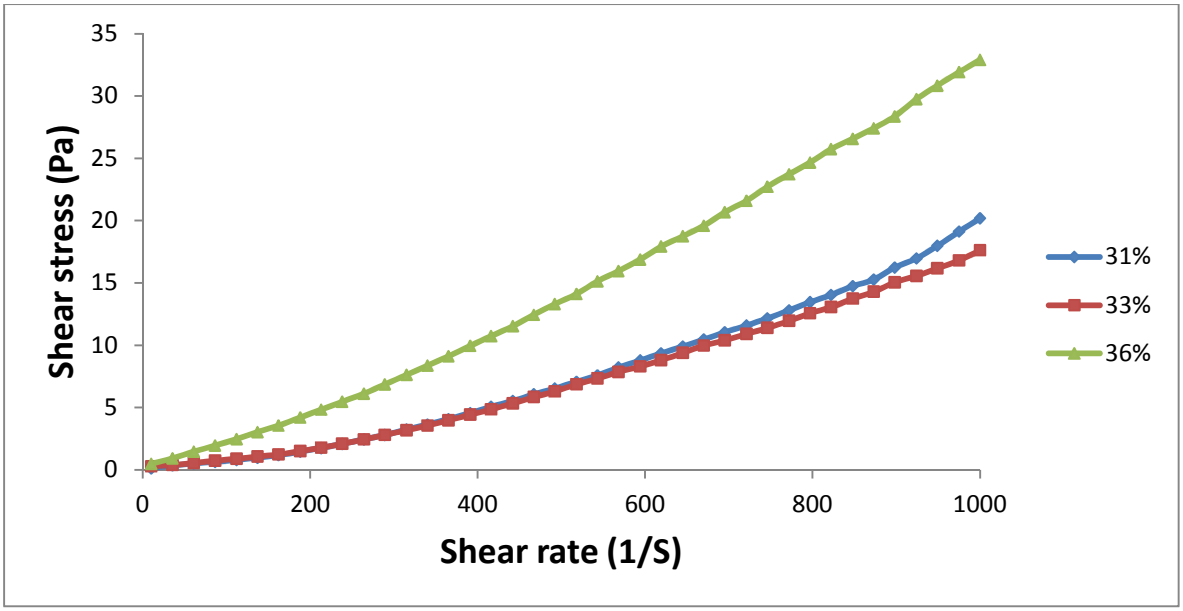

Figure 30: Rheology of the Phosphogypsum-Slurry (sample 2) at different solids rate at (70°C)

The same remarks raised for the case of the slurry at 80°C, as shown Fig. 29, are valid for the case of the slurry at 70°C. as regards the impact of the solids content on the rheology of the slurry.

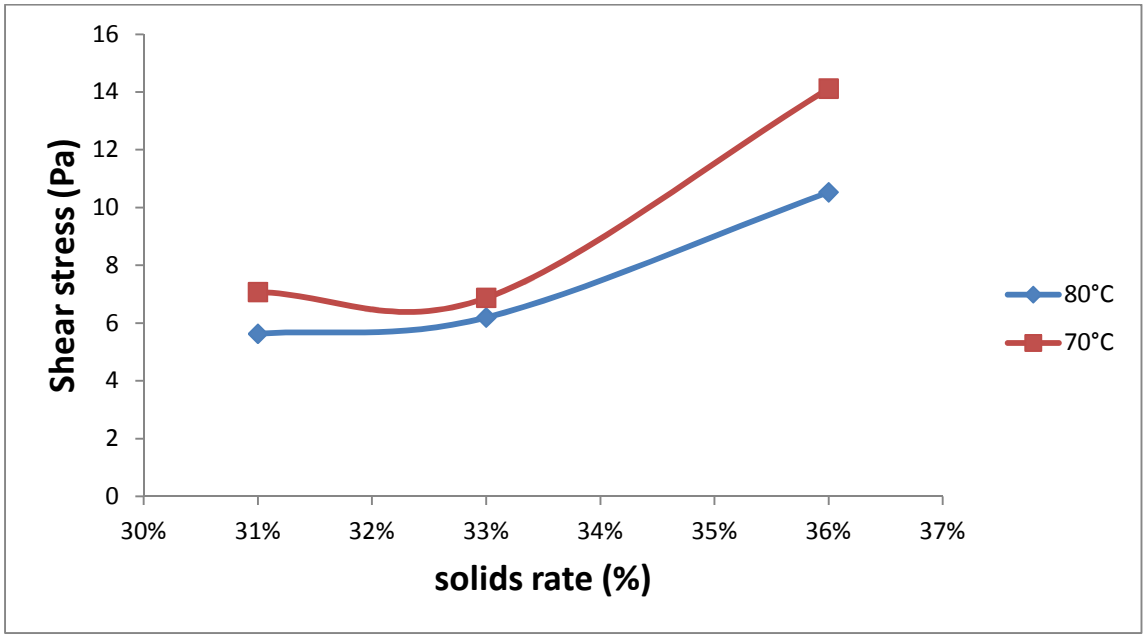

Figure 30: Shear stress versus solids rate (sample 2) at 70°C and 80°C

At a fixed shear rate (600 1 / S), the effect of the solids content of the Phhosphogypsum-Slurry on its viscosity is quite remarkable. Either at 80°C or 70°C the viscosity of the phosphogypsum-slurry begins to increase carefully between 30% and 33% in solid rates, beyond 33% the viscosity of the slurry increases exponentially.

4. 4. Rheology of the sludges types of "54" and "29" at various temperatures of 25°C – 80°C ranges

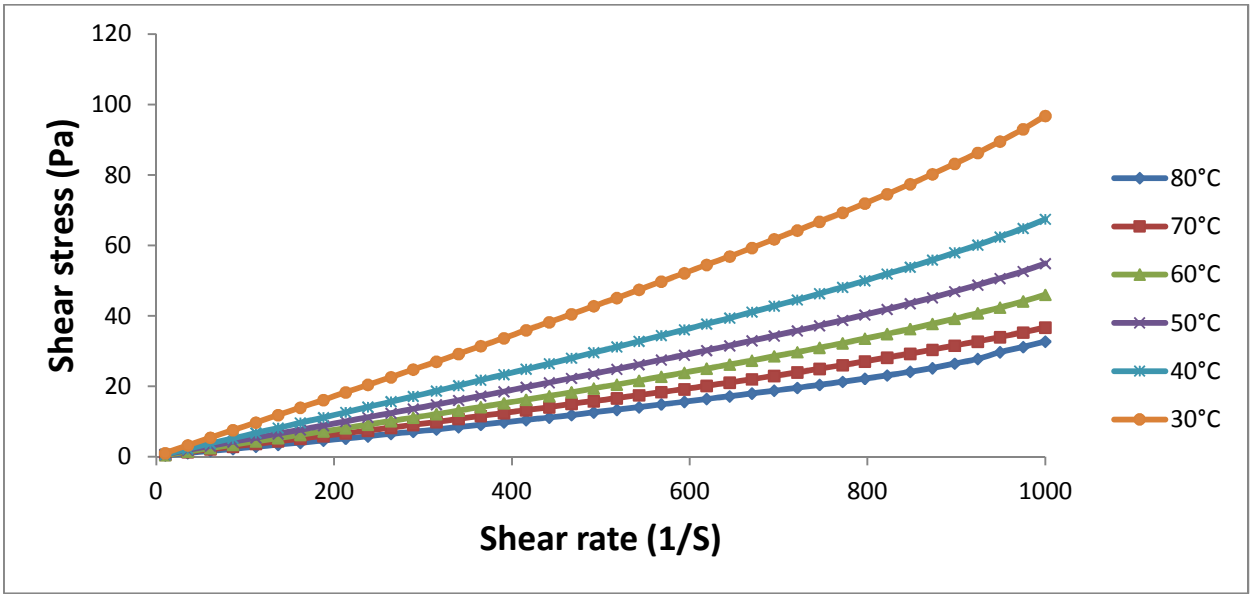

Figure 31: Rheology of the phosphoric Sludge '54' at Different Temperatures at (22% Solids Rate)

For sludge '54', we note that its rheological behavior is not very dilatant and close to a linear behavior without yield (Newtonian behavior) for the entire temperatures figure (31). In contrast to Phosphogypsum-Slurry, the viscosity of sludge '54' increases proportionally with decreasing temperature (Figure 32), which is normal, it is easy to detect from optical microscopy that nothing happens in terms of texture and size of sludge '54' particles with the lowering of the temperature.

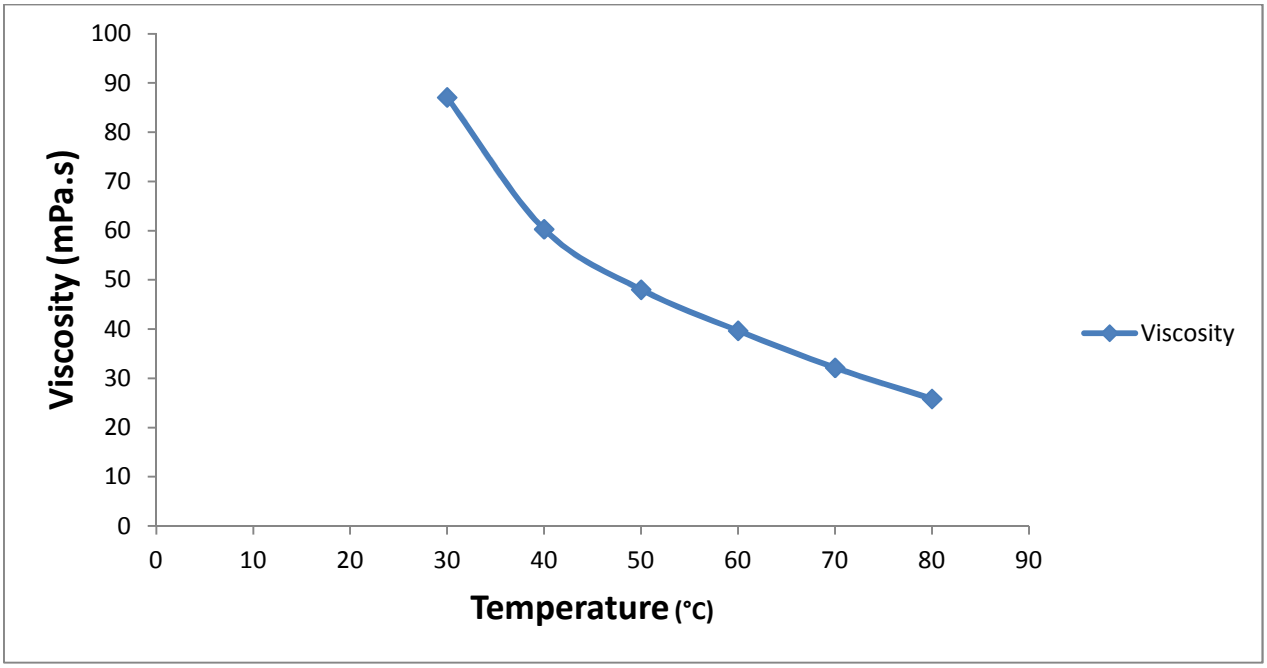

Figure 32: Viscosity as a function of the temperature of sludge '54' at (500 1 / S fixed)

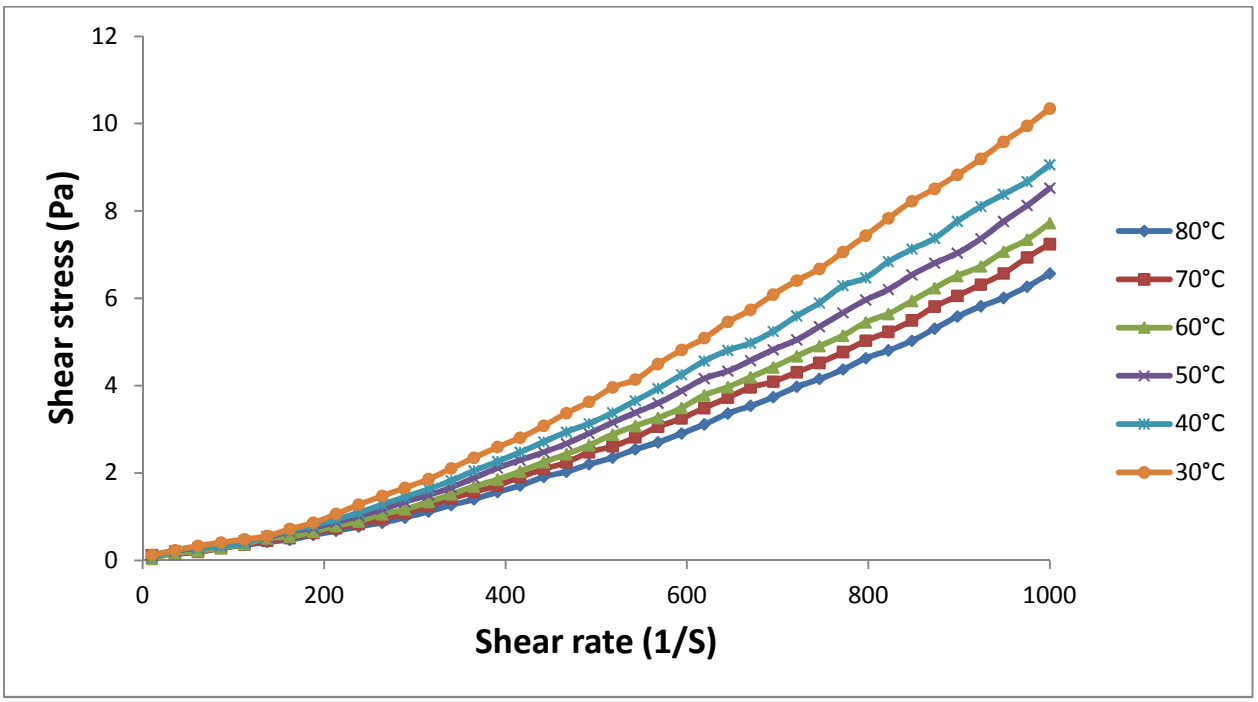

Figure 33: Rheology of the phosphoric sludge '29' at different temperatures (at 5% in solid rates)

4. 5. Morphological observation by the optical microscopy of sludge ″54″

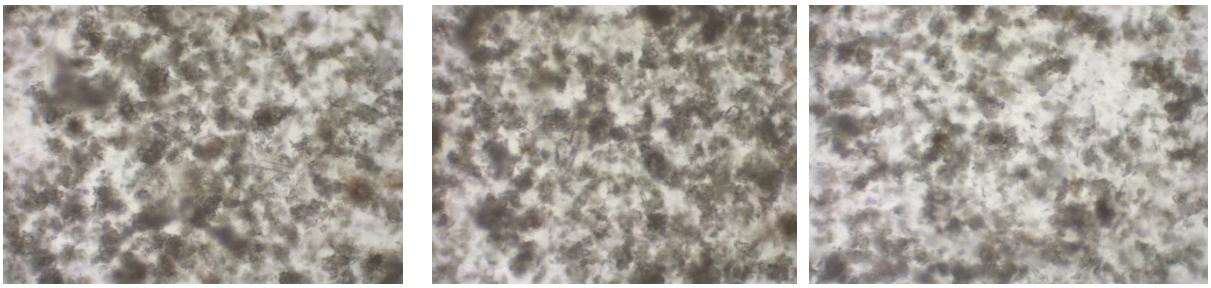

25°C 50°C 80°C

Figure 34: Optical microscopy of sludge 54.

We note that the rheological behavior of the sludge ‘54’ is not very dilatant and close to a linear behavior without threshold of flow for the entire temperatures fig. 31. In contrast to Phosphogypsum-Slurry, the viscosity of sludge ‘54’ increases proportionally with decreasing temperature Fig. 32, which is normal, it is easy to detect from optical microscopy that nothing happens in terms of texture and size of particles of the sludge ‘54’ with the lowering of the temperature.

The same interpretations made to the rheology of sludge ‘54’ are valid for sludge ‘29’, except that for sludge ‘29’ the rheological behavior is purely dilatant and less stable (subject to local fluctuations), and this is due to the fact that the solids content and the viscosity is low for sludge ‘29’, Fig. 33.

5. Modeling of the rheological behavior of the Phosphogypsum-slurry

In this part we will try to model the rheological behavior of the ample (2) with 31% in solids and this by adjusting the experimental rheological behavior to the Casson, Bingham, Herschel-Buckley, and Power-Law model. The purpose is to establish the relative viscosity values and yield stress related to each rheological model. The uses of these viscosity and yield stress values are numerous, for example there is thermal and hydrodynamic simulation software that requires us to enter the relative viscosity and yield stress values for a specific model before performing the simulation. Thus, in the design operations of reactors and pipelines, the knowledge of the rheological parameters relative to each model is paramount.

5.1. Adjustment of the rheological behavior of the Phosphogupsum-Slurry to the 4 rheological models at 80°C

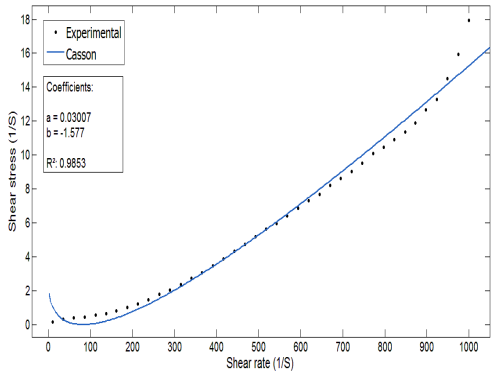

Fig 35 : Casson model $\sigma^{1/2} = (0{,}03007.\gamma)^{1/2} - 1{,}577$

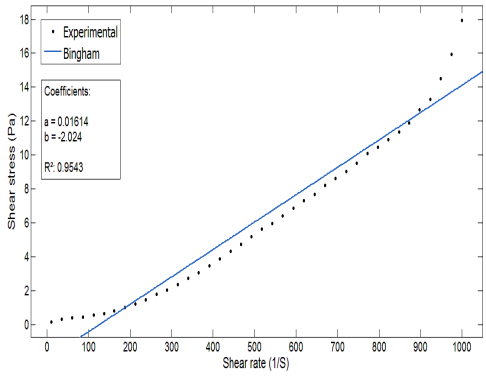

Fig 36 : Bingham model $\sigma = 0{,}01614.\gamma - 2{,}024$

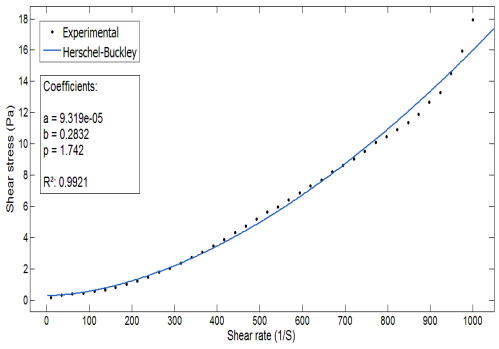

Fig 37 : Herschel-Buckley model $\sigma = 0{,}00009319.\gamma^{p} + 0{,}2832$

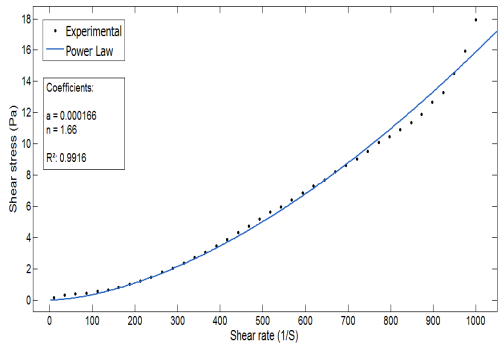

Fig 38 : Power Law model $\sigma = 0{,}000166.\gamma^{1{,}66}$

5. 2. Modeling the rheological behavior of Phosphogypsum-slurry through the 4 rheological models for temperatures: 80°C, 70°C, 60 ° C, ... 25 ° C

We will follow the same method for all temperatures (80°C, 70°C, 60°C, ... 25°C) by adjusting the flow curves generated experimentally to the four rheological models. The regression parameters of these curves to the theoretical models are grouped on the two following tables: (the parameters of regressions are the rheological parameters: viscosity and yield stress).

	Casson model			**Bingham model**		
Temperature (°C)	**a (Pa.s)**	**b (Pa)**	**R²**	**a (Pa.s)**	**b (Pa)**	**R²**
80	0,03007	-1,577	0,985	0,01614	-2,024	0,954
70	0.03449	- 1 ,52	0,995	0.01991	-2.289	0.971
60	0.03118	-1,28	0.997	0.01937	-2.01	0.979
50	0.03166	-1,36	0.996	0.01914	-2.039	0.976
40	0.03218	- 1,31	0.996	0.01981	-1.964	0.976
30	0.03101	- 1.18	0.996	0.02	-1.787	0.979
25	0.03701	-1.513	0.992	0.02171	-2.191	0.968

Table 4: Viscosity, yield stress and R² relative to the Casson and Bingham models.

	Ostwald-power Law model			**Herschel-Buckley model**			
Temperature (°C)	**a (Pa.s)**	**n**	**R²**	**a (Pa.s)**	**b (Pa)**	**p**	**R²**
80	0,000166	1,66	0,991	0,00009319	0,2832	1,742	0,992
70	0.0004226	1.554	0.998	0.0003137	0.2013	1.596	0,999
60	0.0007609	1.464	0.999	0.0006554	0.1071	1.485	0.999
50	0.0006161	1.494	0.999	0.0004704	0.1848	1.532	0.999
40	0.0007725	1.467	0.999	0.0004749	0.3482	1.535	0.999
30	0.001159	1.41	0.998	0.0007025	0.3818	1.48	0.999
25	0.0005982	1.519	0.997	0.0002401	0.6668	1.648	0.999

Table 5: Viscosity, yield stress and R² for Power Law and Herschel-Bulckley Models

In the previous tables are marked the viscosity, yield stress and R² values corresponding to each temperature of the sample, ranging from the highest temperature to the lowest. We have noticed that, from a mathematical point of view, the Herschel-Buckley model is the most suitable model for describing the rheological profile of the Phosphogypsum-slurry at all temperatures (R²

often close to 1), followed by the model of power-Law, and followed by the Casson model, and finally the Bingham model with R^2 little far from 1 compared to other models.

From a physical point of view, we notice that the Casson and Bingham models generate negative yield stress values, which is contradictory to the physical logic, and at the level of the rheological curves, it is quite remarkable that the rheological behavior of the phosphogypsum-slurry it has no flow threshold (yield) whatever the temperature.

7 - Conclusion:

In this chapter, we characterized physicochemically phosphogypsum and sludges generated during the manufacture of phosphoric acid at the industrial platform of Jorf-Lasfar. We have elaborated the rheological behavior of suspensions (Phosphogypsum-Slurries and sludges). Phosphogypsum-Slurry has a dilatant rheological behavior (shear-thickening) whatever the temperature. The viscosity of the Phosphogypsum-Slurry increases with the decrease of the temperature between 80°C and 60°C. Between 60°C and 50°C the viscosity decreases. Beyond 50 ° C the viscosity begins to increase again. This is due to the change in size of agglomerates of gypsum crystals. We thus evaluated the effect of the rate of crystal solids in the Phosphogypsum-Slurry on its rheological behavior, either at 80°C or 70°C. The viscosity of the phosphogypsum-slurry begins to increase carefully between 30% and 33% in solid rates, beyond, the viscosity of the Phosphogypsum-Slurry increases exponentially.

Modeling the rheological behavior of the Phosphogypsum-Slurry at different temperatures by the regression of the experimental rheological data to the empirical models, allowed us to identify the values of viscosity and yield stress (flow threshold).

Chapter 6

ELABORATION AND MODELING THE RHEOLOGICAL BEHAVIOR OF PHOSPHORIC ACIDS AND STUDY OF THE MgO IMPACT ON THEIR VISCOSITIES

Chapter abstract

The knowledge of the rheological behavior of phosphoric acids is so important. Its utility resides in pipe sizing operations and also in prediction of energy necessary for pumping these acids. The utility of knowledge the rheological behavior of the acids also lies in the software of modeling, hydrodynamic and thermal simulations. This software asks us to enter the rheological parameters of the material to carry out the simulation or the modeling (such as Ansys ...). Rheological information on phosphoric acids no longer exists in the literature. In this chapter we will elaborate experimentally the rheological behavior of all phosphoric acids produced in Jorf-Lasfar. Including the return acid 18% in P2O5 (this is the acid obtained during the third washing in the filtration operation of the Phosphogypsum cake), the phosphoric acids 29%, 42% and 54% in P_2O_5. Thus we will establish the rheological behavior of purified phosphoric acids. We studied the effect of temperature, density and shear rate on the rheological behavior of phosphoric acids. We studied also, the influence of magnesium monoxide (MgO) derived from phosphate rock, which has a very remarkable impact on the viscosity of phosphoric acids [94]. We also have interest in this study to establish the fluid-flow activation energy (Ea) corresponding to each acid. The activation energy is a parameter that characterizes the stability of the fluids. Finally we will end up modeling all the rheological profiles of the acids, this by the regression of these profiles to the empirical models of Casson, Bingham, Power-Law and Herschel-Buckley. This modeling allows us to identify the values of viscosity and yield stress related to each model.

1. Elaboration of the rheological behavior of phosphoric acids

1. 1. Description of the experimental procedure

We carried out rheological studies on the different phosphoric acids produced at the Jorf-Lasfar industrial platform, using the same rheometer (Anton-Paar) used in the previous chapters. The rheological profiles of these acids were studied over the range of shear rates (1 - 1000 S^{-1}). We studied the impact of temperature, density, shear rate, the proportion of (MgO) in acids and the phosphate diversity of these acids on their rheological behavior. Density measurements were made using a gravity bottle, temperature measurements were made using a temperature probe. To study the effect of (MgO) on the viscosity, we solubilize different amounts of the (MgO) solid in acids to see its impact on the viscosity, and this is done at a temperature of 50 ° C for all samples to facilitate the solubilization of (MgO) in phosphoric acids.

In the following, we consider the notation that ACP means the phosphoric acid and, for example, ACP 54 means clarified phosphoric acid 54% in P_2O_5.

Figure 1: Rheometer (Anton Paar) with Couette geometry.

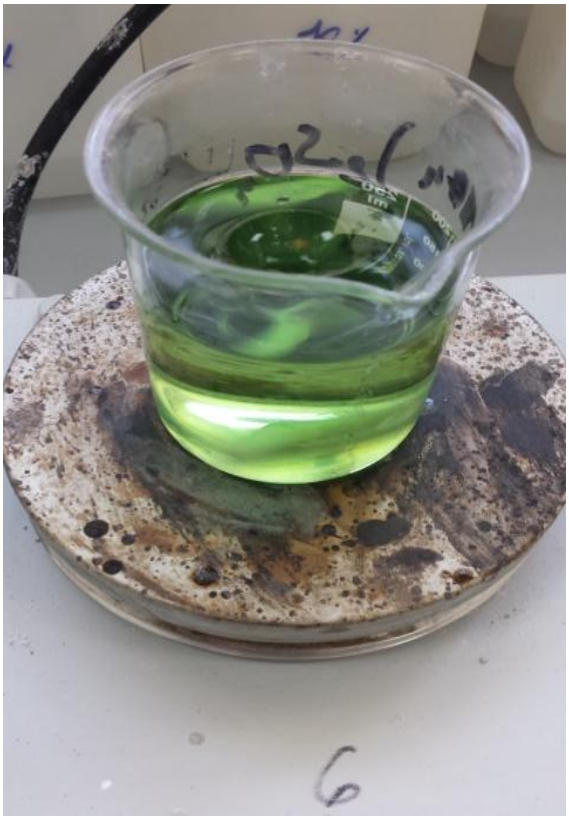

Figure 2: Phosphoric acid 29% P_2O_5, Density: 1225 g / l

Figure 3: Phosphoric acid clarified 54% in P2O5, Density: 1608 g / l (beaker on the left) Phosphoric acid purified 61% in P2O5, Density: 1720 g / l (beaker on the right)

Figure 4: Phosphoric acid clarified 54% in P2O5, from the Jorf-Lasfar platform (beaker on the right)
Phosphoric acid purified 54 %% in P2O5, from the Safi platform (beaker on the right)

1. 2. Effect of temperature of phosphoric acids on the rheology

We start our study with Phosphoric acid 54% in P_2O_5, from the Safi platform, to see the impact of temperature on its rheological behavior, and to compare the rheological behavior of phosphoric acids 54% of SAFI and JORF because the original phosphate of each is extracted from a different zone.

Phosphoric acid of JORF origin phosphate is extracted from the regions of KHOURIBGA and SAFI is extracted from the regions of BENGURIR and YOUSSOUFIA.

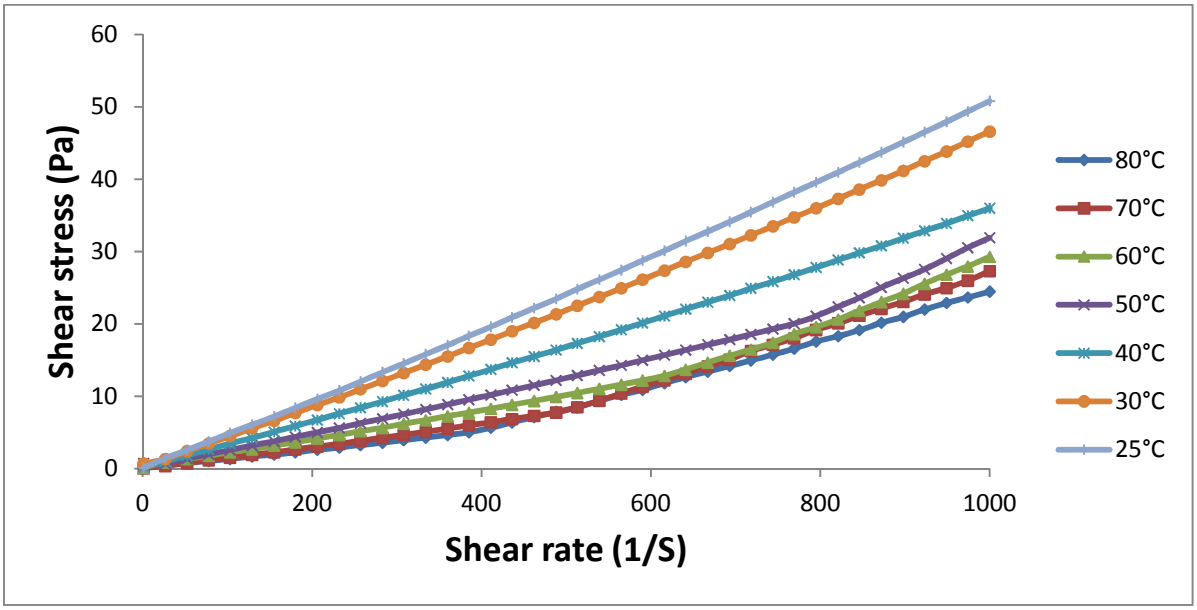

Figure 5: Rheology of phosphoric acid 54 (SAFI) at different temperatures (density: 1652 g / l)

The phosphoric acid 54% in P_2O_5 is obtained by passing phosphoric acid 29% to a concentration operation under vacuum to make it more concentrated. The first remark that we could extract from the fig. 5, is that the rheological behavior of phosphoric acid 54% of SAFI is dilating in the temperature range (80°C - 50°C) and Newtonian (linear) in the range (40°C - 25°C). The range (40°C - 50°C) presents a transition range of the rheological behavior of this acid from a dilatant behavior to a Newtonian behavior.

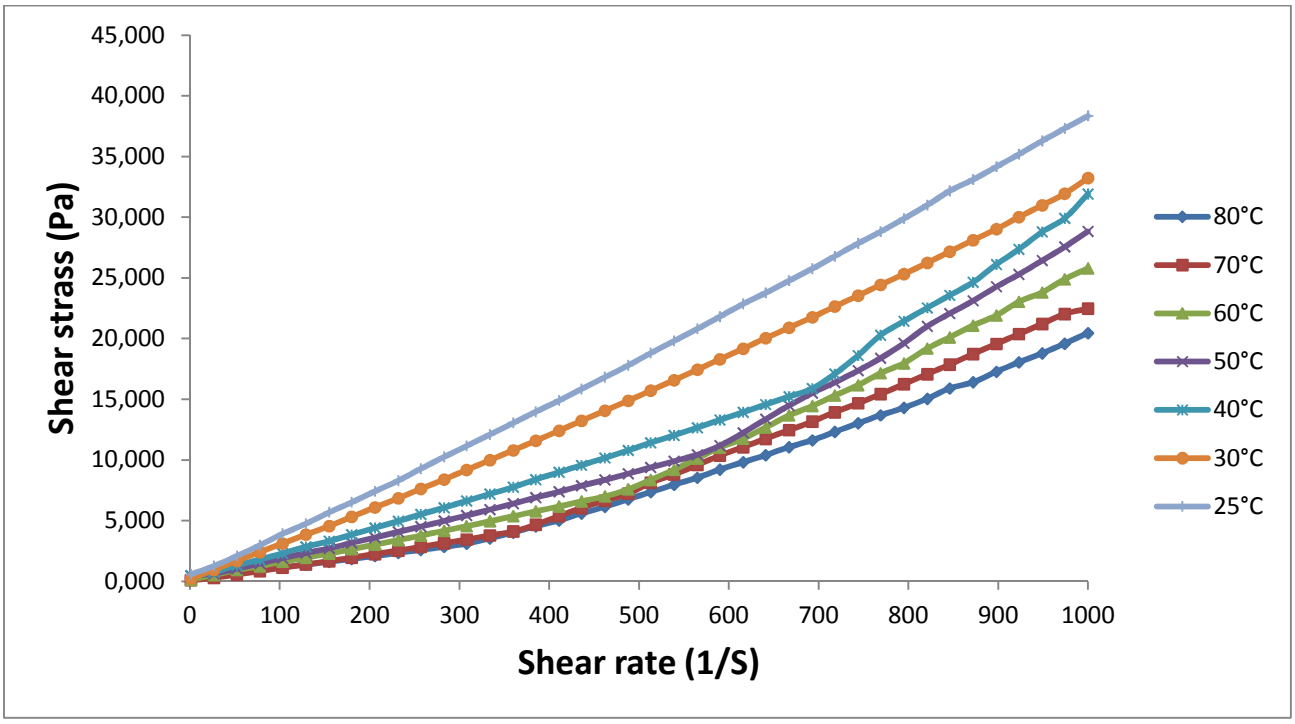

Figure 6: Rheology of phosphoric acid 54 (JORF) at different temperatures (density: 1608 g / l)

For phosphoric acid 54% of JORF-Lasfar with a density of 1,608 Kg / l the rheological behavior is dilatant over the range (40°C - 80°C) and Newtonian over (30°C - 25°C) the transition zone between the two natures of rheological behavior is (40°C - 30°C) unlike with SAFI acid, this can be attributed to the small difference between the densities of the 2 acids, and also to the impurity content in each acid, because the raw phosphate of manufacture of the phosphoric acid of SAFI is not extracted from the same place that Jorf-Lasfar.

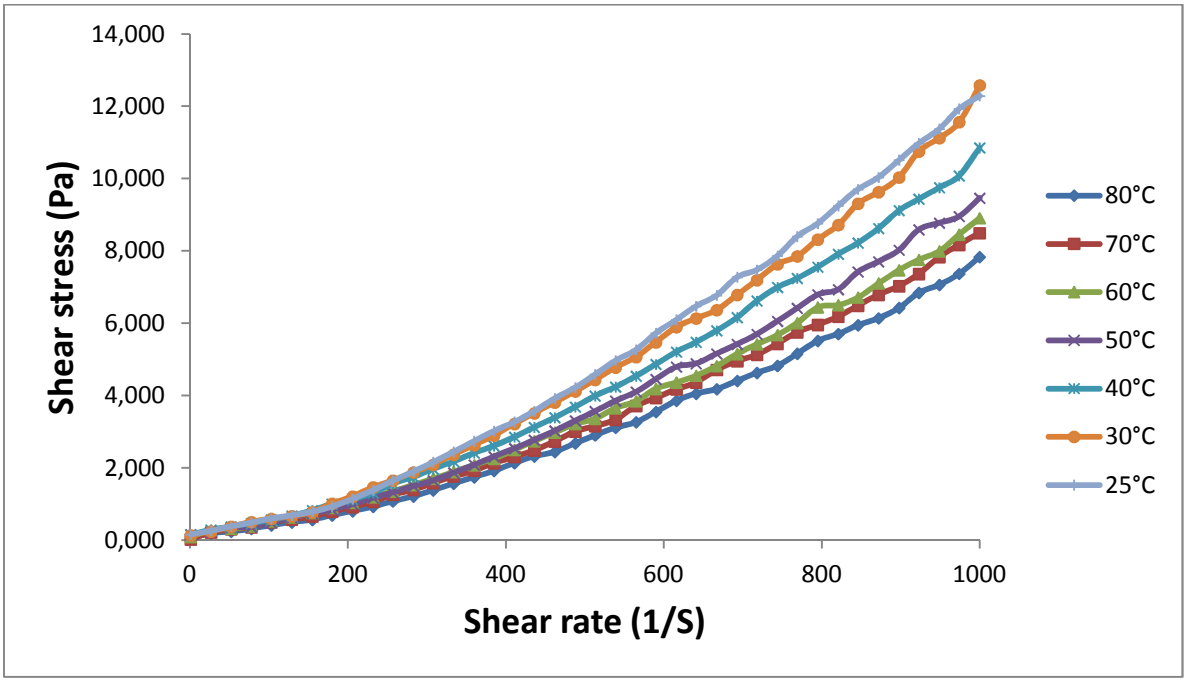

Figure 7: Rheology of phosphoric acid 29% (JORF) at different temperatures

Phosphoric acid 29% is the direct byproduct of the reaction of phosphate with sulfuric acid, obtaining this acid is through the filtration of the Phosphogypsum-slurry cake produced. In general, the density of the (ACP 29) is about 1225 g / l. Fig. 7 shows the rheological behavior of the (ACP 29) at different temperatures, we noticed that the viscosity of this acid increases proportionally with the decrease of the temperature, and that the nature of the rheological behavior is dilatant whatever the temperature. Unlike (ACP 54), the (ACP 29) still retains its dilatant rheological behavior with lowering of temperature. We also note that the rheological behavior of the (ACP 29) is stable month (the curves are not smooth), on the rheological curves there are fluctuations, that is to say that the fluid does not depend perfectly on the mechanical constraint applied by the cylinder, normal thing because the (ACP 29) is less dense and its viscosity is low, this is what causes the mechanical instability of the fluid noticed in the fig. 7.

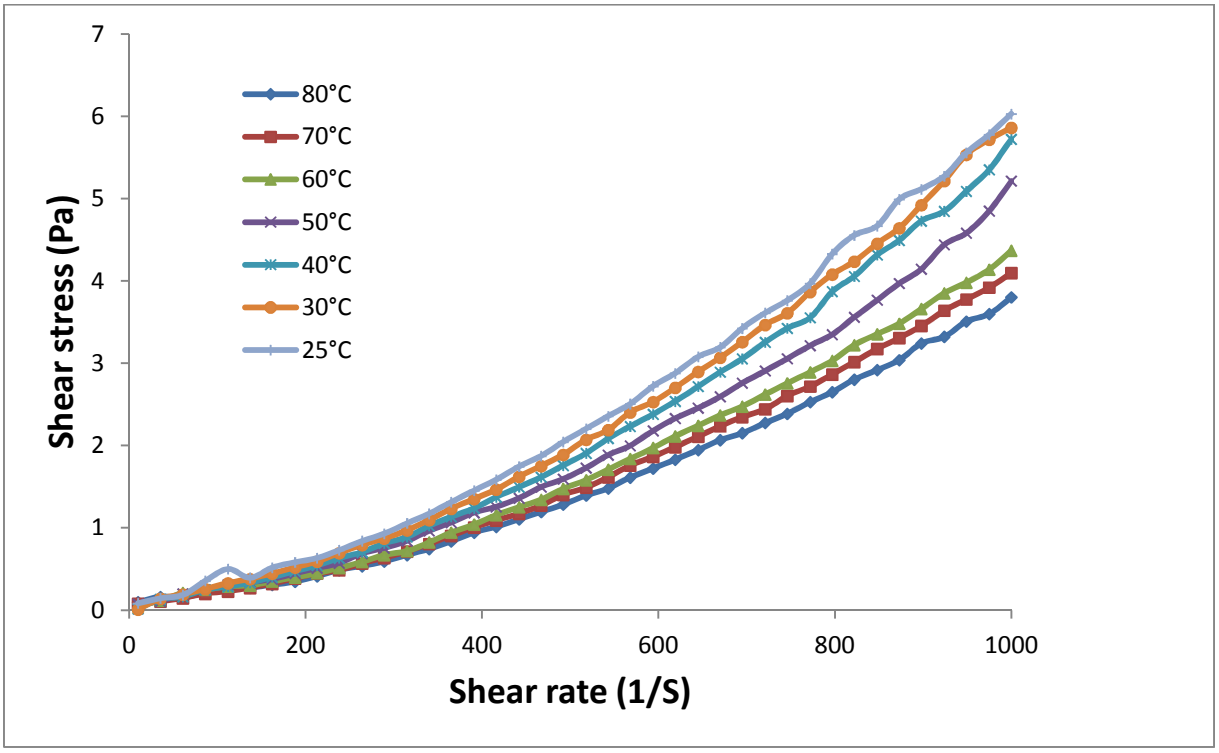

Figure 8: Rheology of phosphoric acid 18% (JORF) at different temperatures

The phosphoric acid 18% or (the return acid), will be obtained during the third wash of the phosphogype cake after filtration. The same remarks and interpretations made to the (ACP 29) are valid for the (ACP 18), except that the latter is less dense and less viscous than the (ACP 29), and consequently it is less stable than the ACP 29.

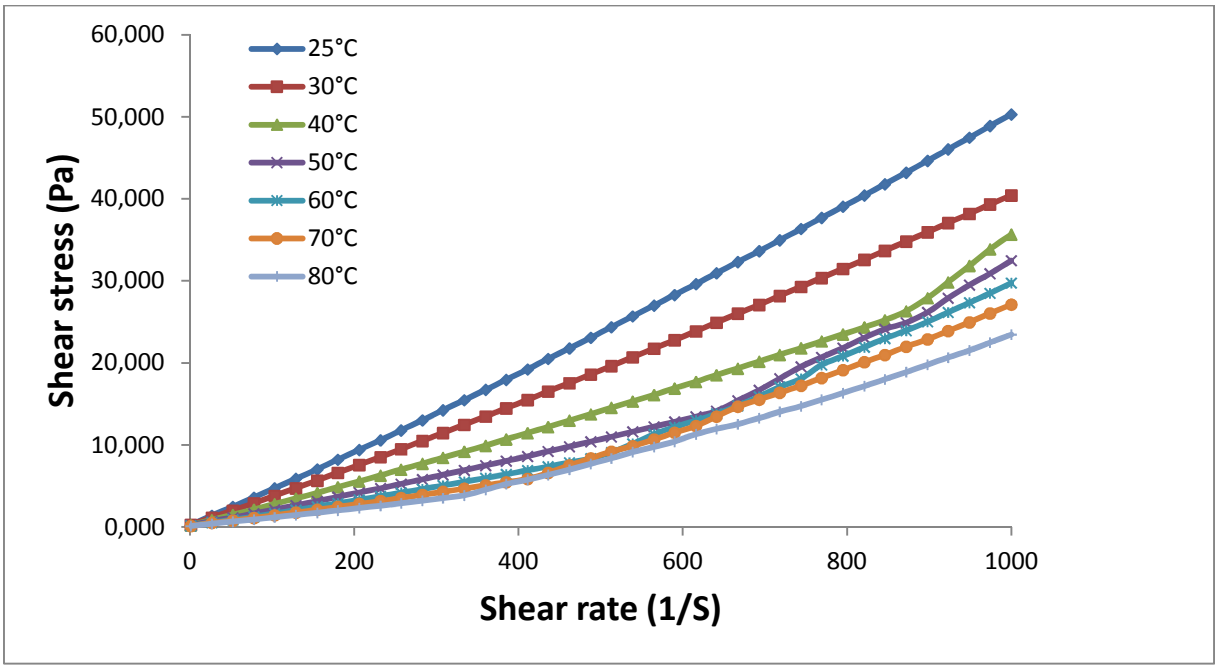

Figure 9: Rheology of purified phosphoric acid 61% in P_2O_5 at different temperatures (1720 g / l)

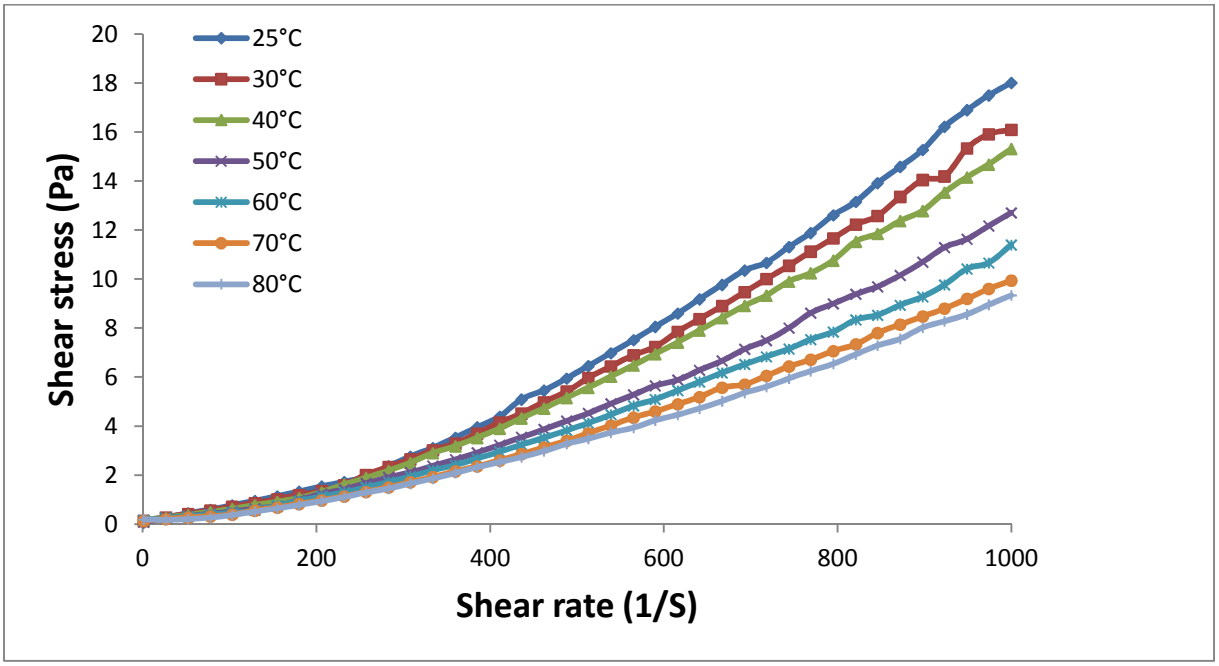

Figure 10 : Rheology of purified phosphoric acid 29% in P_2O_5 at different temperatures (1360 g/l)

The purified phosphoric acid is obtained by passing the clarified phosphoric acid through nano filtration via membranes, the rheological behavior of the purified phosphoric acid 61% in P_2O_5 named also (APP) over the range (40°C - 80°C) is dilatant. Below 40°C the rheological behavior is linear (Newtonian). For (APP 29%) the rheological behavior is always dilatant for all temperatures.

1. 3. Influence of phosphate origin diversity of phosphoric acids

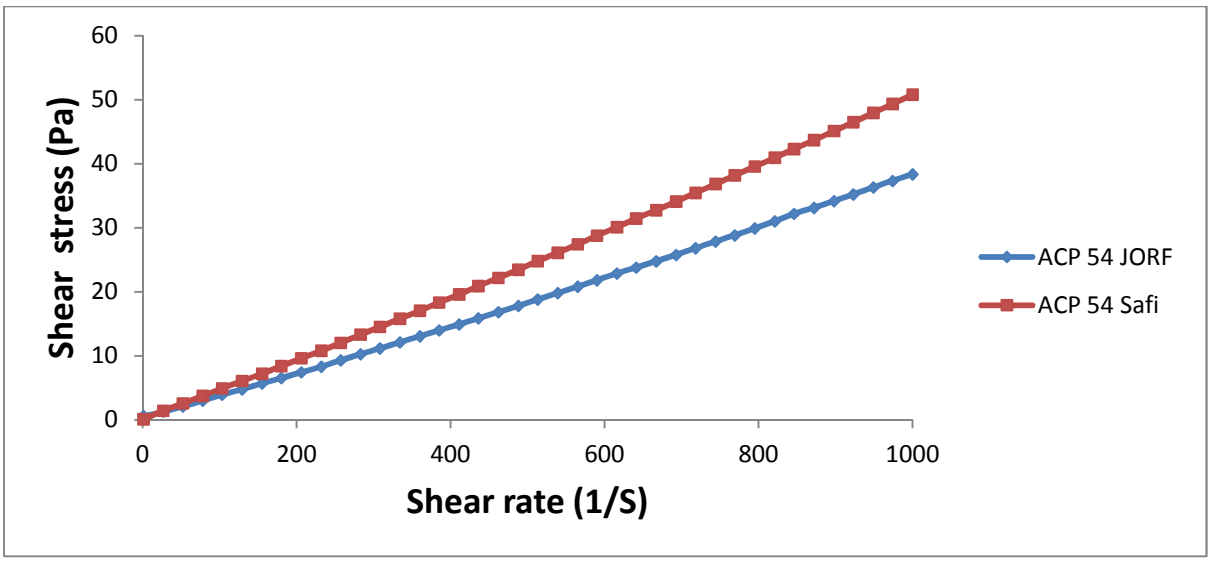

Figure 11: Rheology of phosphoric acids 54% (JORF and SAFI) at 25°C

In fig. 11 the rheological behaviors of the SAFI and JORF acids at 25°C are presented, fortunately the rheological behaviors for this temperature are Newtonian (linear without threshold stress), the elaboration of the viscosity of each one between they are done by determining the slope of the rheological curve. The viscosity of the (ACP 54 JORF) is μ = 0.038 Pa.S and the viscosity of the (ACP 54 SAFI) is μ = 0.050 Pa.S. The difference between the two viscosity values is due to the content of impurities in each of the acids, because the phosphate origins of these acids are not extracted from the same place. For this we carried out a chemical analysis of the two acids at the chemical analysis laboratory in the research and development department (O.C.P).

	SO_4^{2-} (g/l)	P_2O_5 (%)	MgO (%)	Fe_2O_3 (%)	F (%)	CaO (%)	Al_2O_3 (%)
Phosphoric Acid 54% (JORF)	33,32	53,6	1,2	0,41	0,16	0,02	0,23
Phosphoric Acid 54% (SAFI)	54,88	54,02	1,22	0,36	0,26	0,01	0,43

Table 1: Chemical Analysis of Phosphoric Acids 54% (JORF) and (SAFI)

The chemical analysis has shown that the proportions of impurities ($SO4^{2-}$, P_2O_5, MgO, FeO_3, F, CaO, Al_2O_3) are different between the two acids, this proves the difference between the rheological behavior of the two acids that we noticed in the fig. 11.

1. 4. Impact of density on the rheological behavior of phosphoric acid

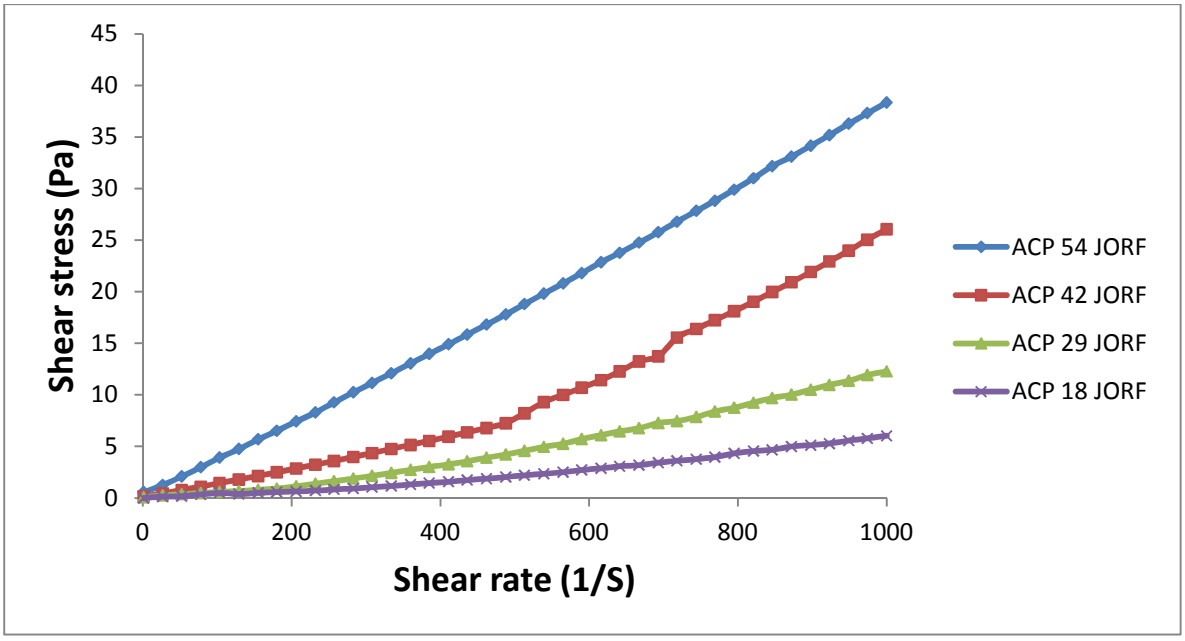

Figure 12: Comparison of rheological profiles of phosphoric acids 18%; 29%, 42%; 54 % (JORF) at 25 ° C .

Fig. 12 shows a comparison of the rheological behavior of the ACP 54%, 42%, 29% and 18% at 25°C. We have noticed that the higher the density of the phosphoric acid increases the more the viscosity increases, from the fig. 13 we can extract the interpretation that the viscosity of the phosphoric acid increases slowly between 1030 g / l and 1440 g / l, beyond 1440 g / l the viscosity begins to increase strongly.

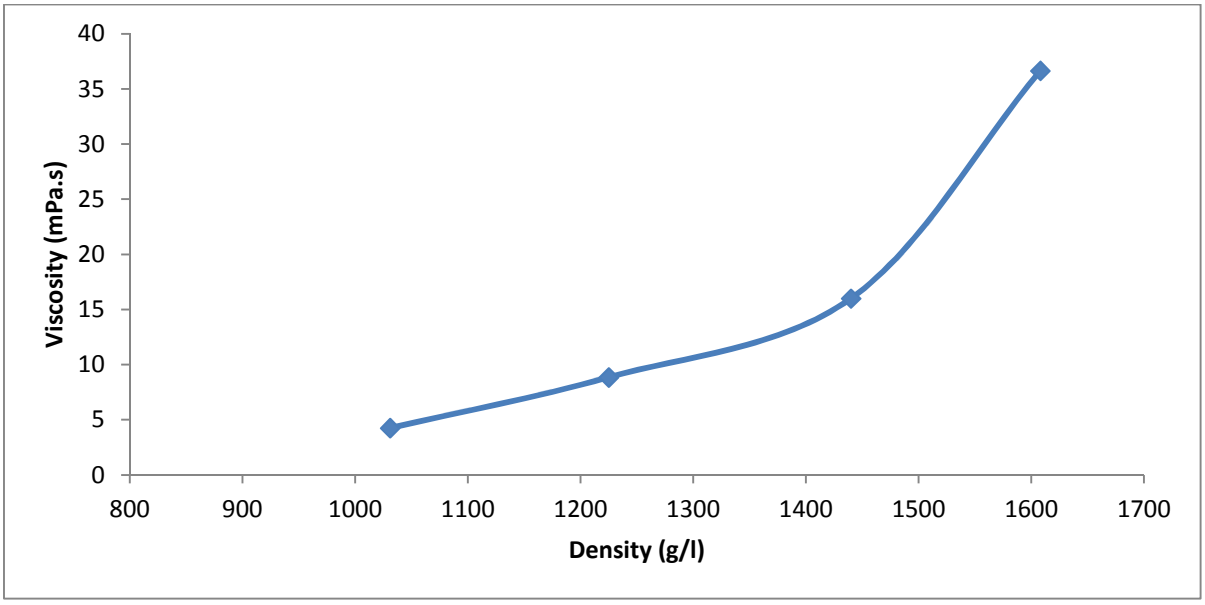

Figure 13: Viscosity as a function of the density of phosphoric acid (Jorf) at 25 ° C (Shear rate fixed 500 1 / S).

1. 5. Effect of Shear Rate on the Viscosity of Phosphoric Acids

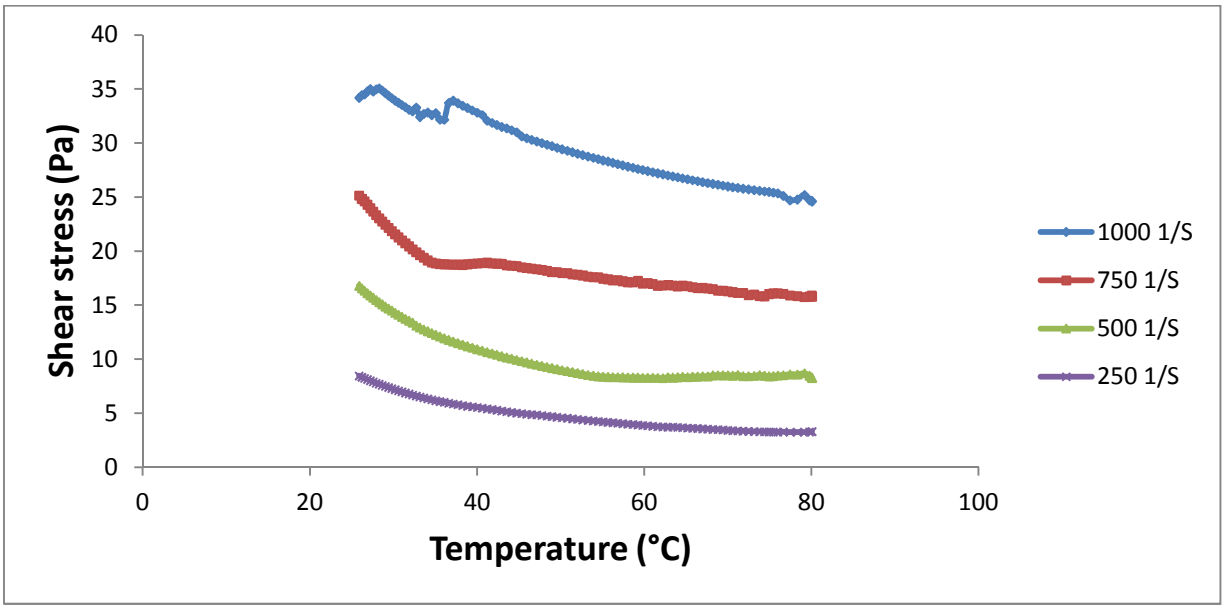

Figure 14: Viscosity as a function of temperature at constant shear rates (ACP 54 SAFI)

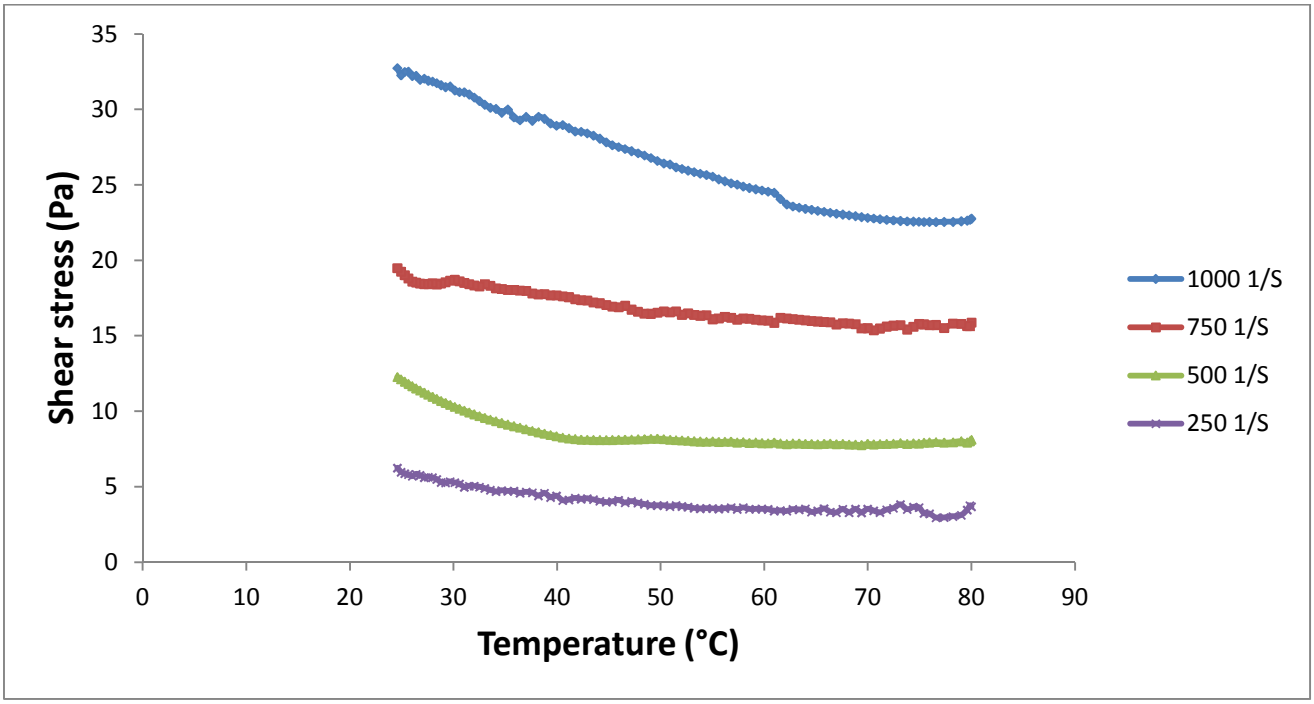

Figure 15: Viscosity as a function of temperature at constant shear rates (ACP 54 JORF)

We note from Figs 14 and 15 that the ACP 54 viscosity of JORF and SAFI increases as a function of temperature at constant shear rates (250 1 / S, 500 1 / S, 750 1 / S, 1000 1 / S), we found that the impact of temperature on viscosity is more remarkable for high shear rates (750 1 / S and 1000 1 / S), for low shear rates the impact of temperature on the viscosity is not very remarkable.

This is attributed to the fact that for high shear rates the velocity of flow of the acid during the rheological measurement is maximal, which favors the heat transfer in the acid and consequently its impact on the viscosity is very remarkable.

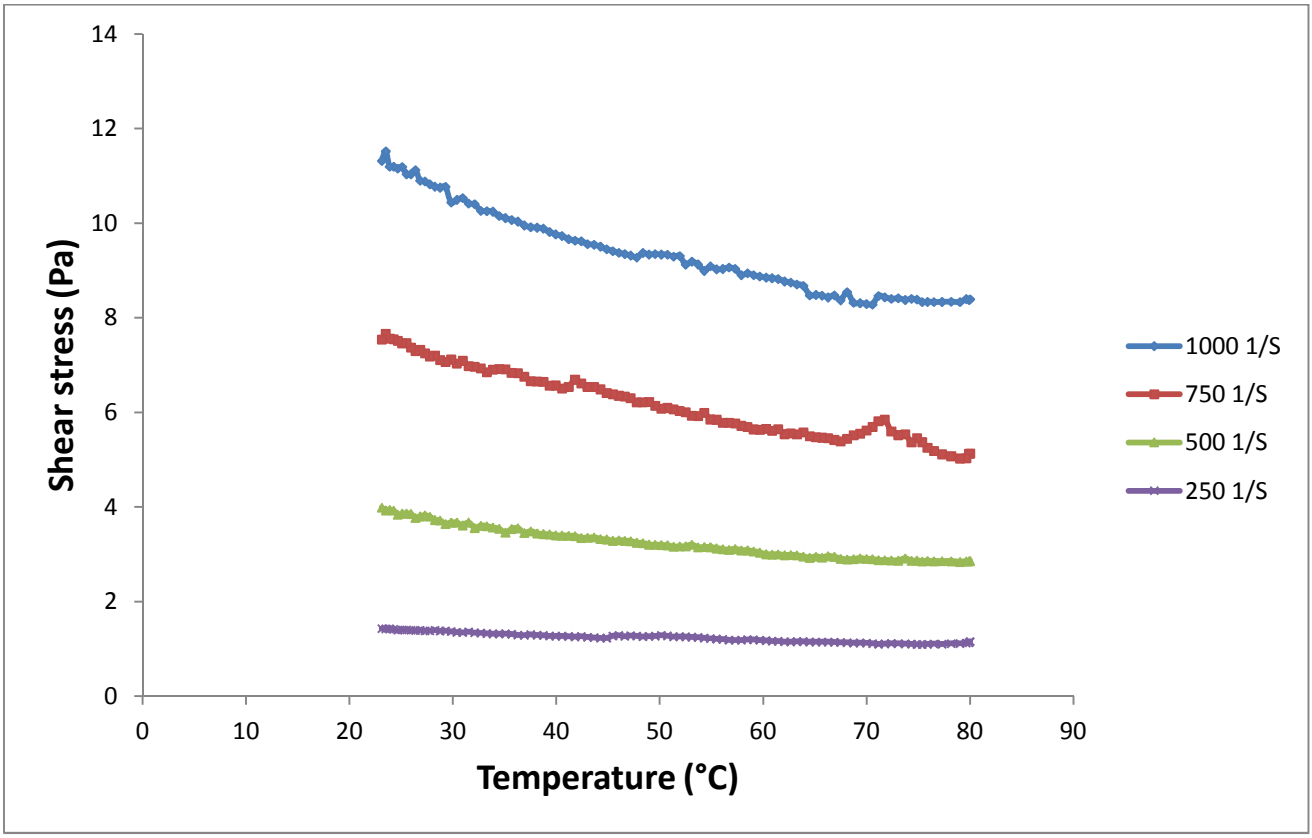

Figure 16: Viscosity as a function of temperature at constant shear rates (ACP 29 JORF)

If we take the two (ACP 54) JORF and SAFI at a fixed shear rate (500 1 / S), we notice that the viscosity increases slowly between 80°C and 45°C, from 45°C the viscosity begins to increase exponentially.

For the (ACP 29) fig. 16, the impact of the temperature on the viscosity is remarkable even for the high shear rates, this being due to the low density of the (ACP 29) compared to the (ACP 54), this means that water predominates the composition of the (ACP 29) and it is well known in the literature that the temperature has no remarkable impact on the viscosity of the water.

2. Effect of MgO compound on flow characteristics of phosphoric acids

2. 1. Impact of MgO on the rheology of Phosphoric acid 54% and 29% at (25°C)

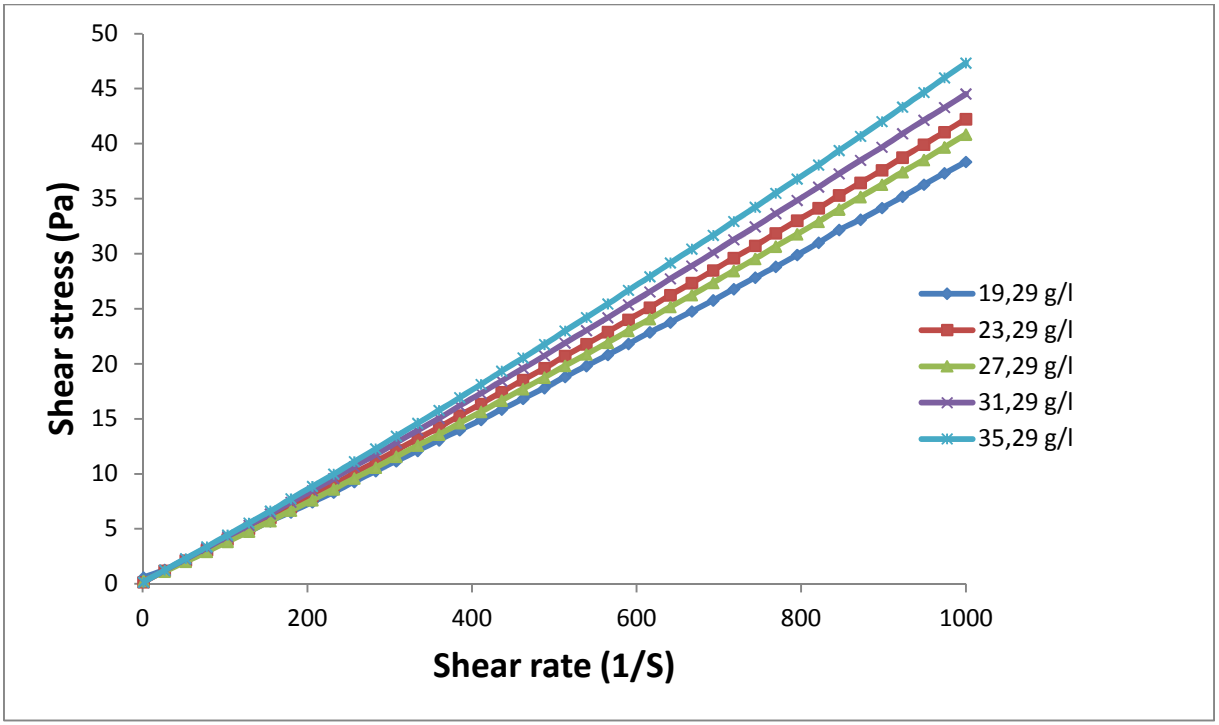

Figure 17: Impact of MgO on the rheology of (ACP 54) of JORF-Lasfar

We take a sample of (ACP 54) of Jorf-Lasfar at 25°C, which contains 19.29 g/L MgO, and we start adding the equivalent of 4 g/L MgO to this sample in each test to find out effect of MgO content in (ACP 54) on its rheological behavior.

To ensure a good solubilization of the MgO in the acid, we heat the acid to 50 ° C then we add the MgO and the solution and stirred well this solution. This step is repeated for all the tests, we wait for the sample to cool, to make the rheological measurements at 25°C.

According to the fig.17, we found that the rheological behavior of the (ACP 54) often keeps its linear rheological behavior (Newtonian) whatever the amount of MgO contained in the acid.

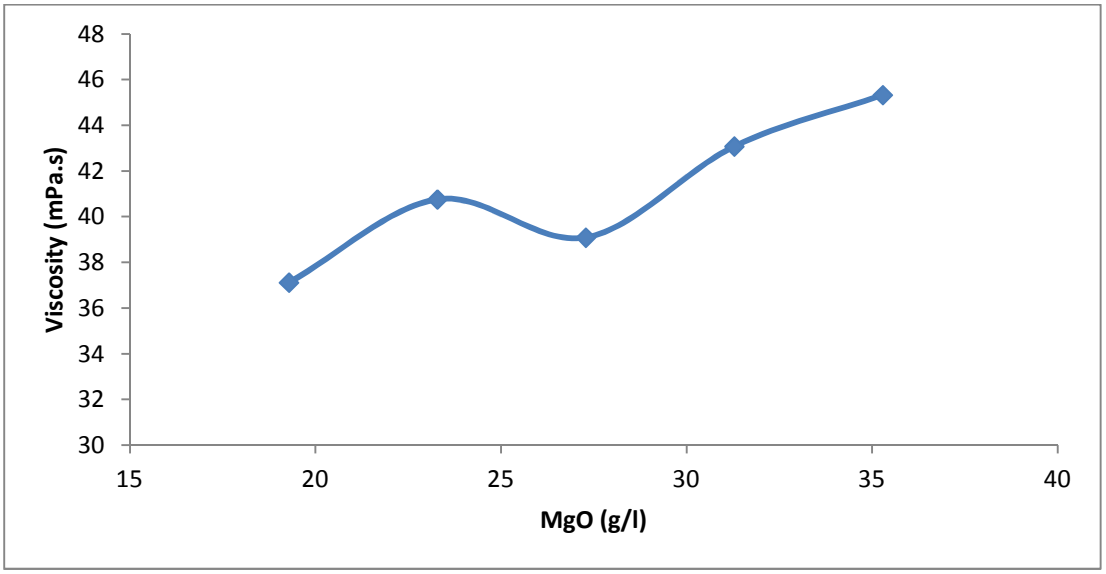

Figure 18: Impact of MgO on the viscosity of (ACP 54) JORF-LASFAR.

Fig. 18 shows the variation of the relative viscosity as a function of the MgO content at a fixed shear rate (600 1 / S), basically we note that the apparent viscosity of the ACP 54 increases with the increase in the MgO content, but there is some local fluctuation, the viscosity increases and decreases little during its growth, this is attributed to the creation of new particle in the ACP 54 such that ($MgSO_4$) and ($MgSiF_6$), the creation of these particles is due to the reaction of MgO with impurities mentioned in the table (1) contained in the (ACP 54).

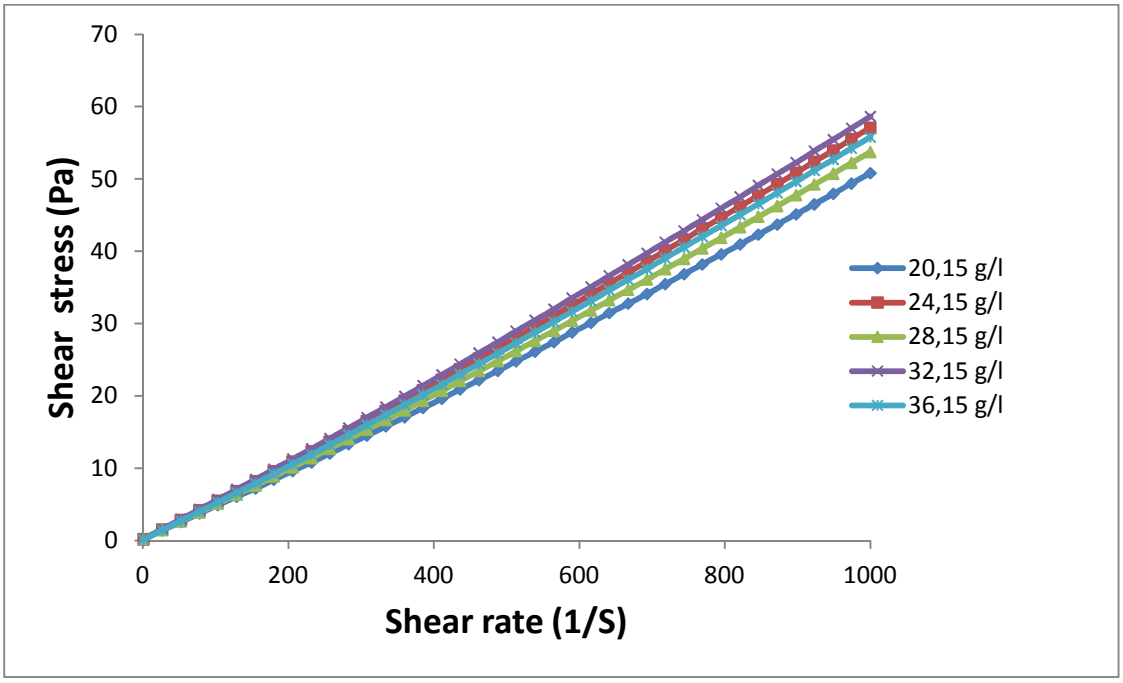

Figure 19: Impact of MgO on the rheology of (ACP 54) of SAFI

The same interpretations made to (ACP 54) of JORF are also noted for (ACP 54) of SAFI, except that the viscosity curve as a function of the amount of MgO is little different than that of (ACP 54) JORF, this can be attributed to the difference between the amounts of impurities in each acid, since the original phosphate of each acid is extracted from a different place.

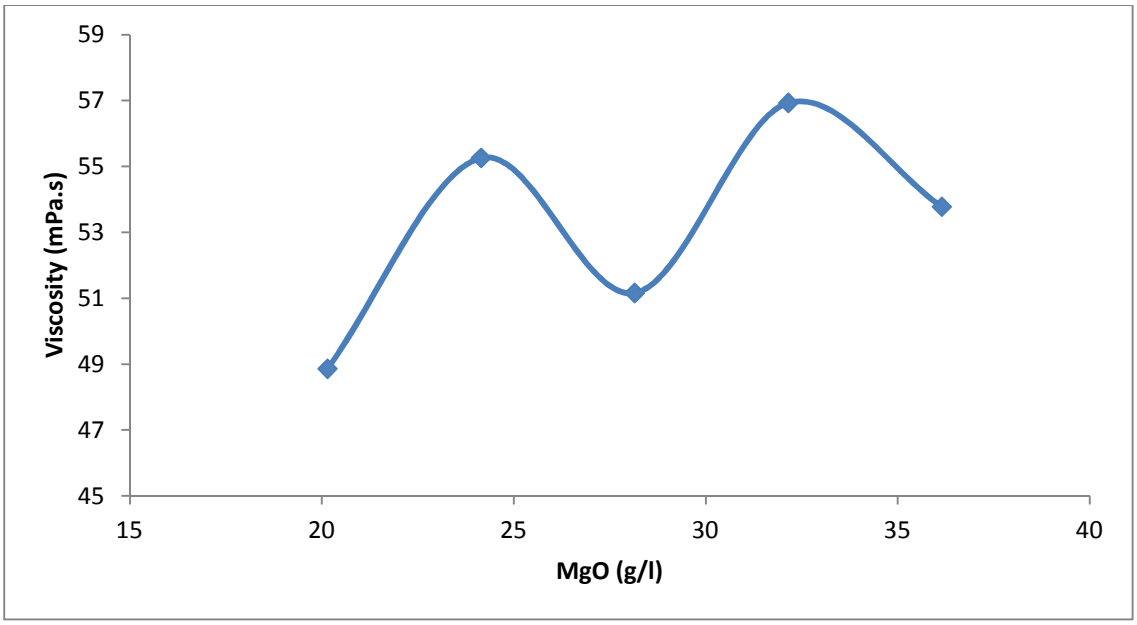

Figure 20: Impact of MgO on the viscosity of (ACP 54) SAFI

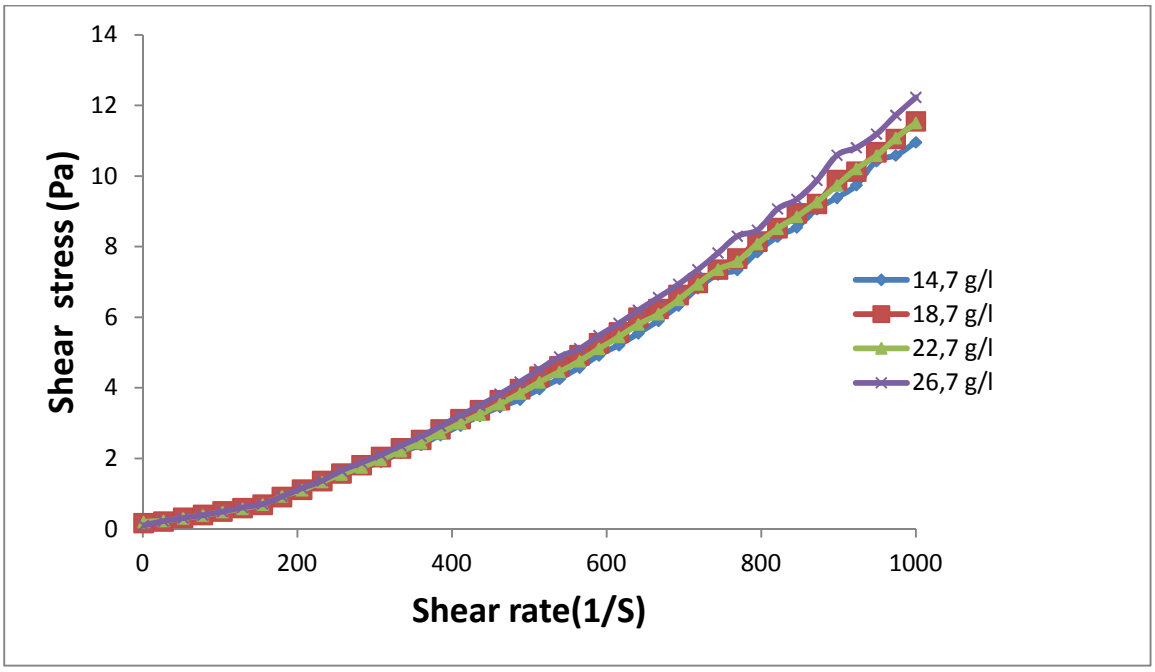

Figure 21: Impact of (MgO) on the rheology of the (ACP 29).

For phosphoric acid 29% (ACP 29) the particles created during the addition of MgO are in general ($MgAlF_5$) and (MgF_2).

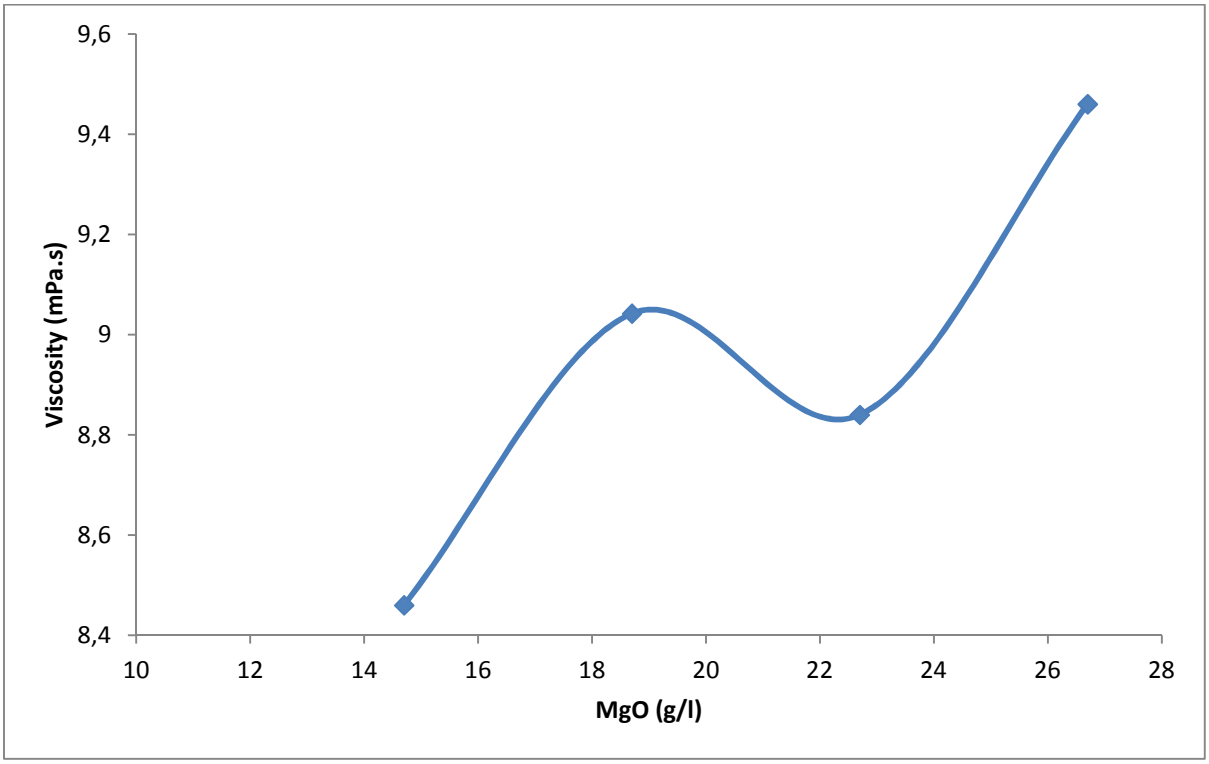

Figure 22: Impact of MgO on the viscosity of (ACP 29)

We can conclude that MgO has a very significant impact on the rheological behavior of phosphoric acids, in general the viscosity of phosphoric acids increase with the amount of MgO in these acids, except that there is other phenomenon related to stoichiometry which causes the appearance of the other crystalline particles in the acids because of the reaction of the MgO with the impurities contained in these acids under the effect of the temperature (50°C), which is what disturbs the normal growth of the viscosity as a function of the amount of MgO.

3. Modeling the rheological behavior of phosphoric acids

3. 1. Clarified phosphoric acid 54% P_2O_5 of JORF (Density: 1608 g / l)

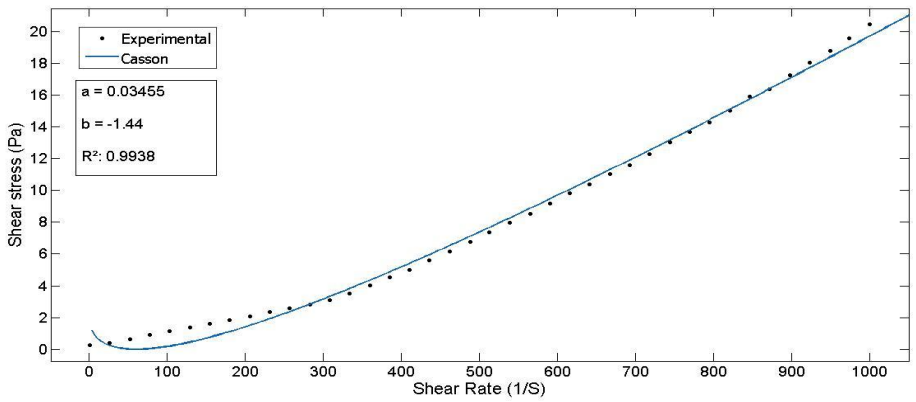

Figure 23 : Casson model $\sigma^{1/2} = (0{,}03455.\dot{\gamma})^{1/2} - 1{,}44$

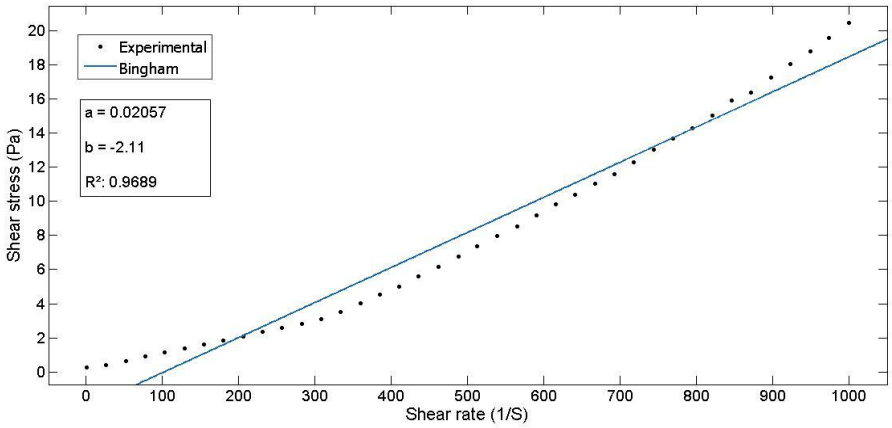

Figure 24 : Bingham model σ = 0,02057.γ – 2,11

Figs 23 and 24 show the regression of the experimental rheological behavior of phosphoric acid 54% at 80°C to the empirical models of Casson, Bingham, Ostwald Power-Law and Herschel Buckley, and this to identify the model the more suitable for the description of the rheological profile of phosphoric acid 54%, and thus to identify the values of viscosities and yield stress relative to each model. The regression is based on the least squares theorem and performs using Matlab.

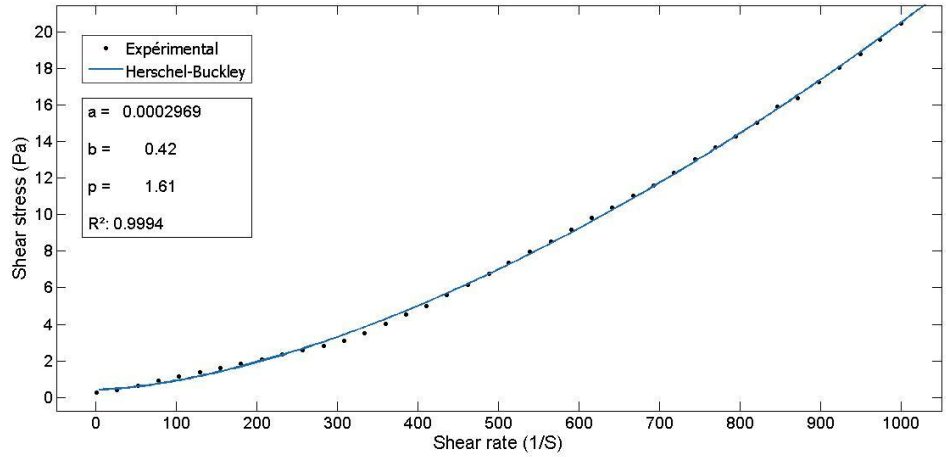

Figure 25 : Herschel-Buckley model σ = 0,0002969.γ^p + 0,42

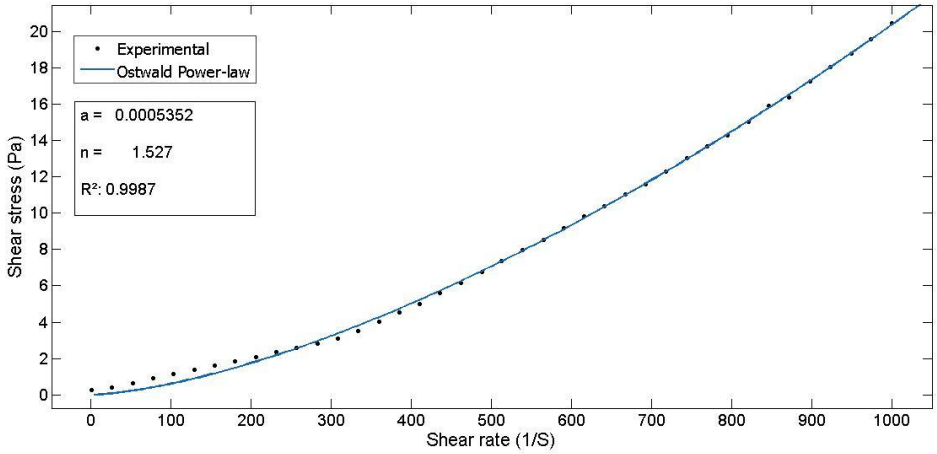

Figure 26 : Power Law model $\sigma = 0{,}0005352.\gamma^{1{,}52}$

From a mathematical point of view, we note that the Herschel-Buckley model is the most suitable model for describing the rheological behavior of phosphoric acid 54% at 80 ° C, with a $R^2 = 0.994$, followed by the Ostwald model (Power-Law) with $R^2 = 0.998$, followed by the Casson model with $R^2 = 0.993$, and finally the Bingham model with $R^2 = 0.96$ may be far from the experimental rheological behavior.

The rheological parameters identified through the regression of the experimental rheological profile of clarified phosphoric acid 54% to the empirical models at each temperature index are classified in Tables (2-7). These parameters are the viscosities, the yield stress points and the exponents relative to each model.

	Casson model			**Bingham model**		
Temperature (°C)	**a (Pa.s)**	**b (Pa)**	**R^2**	**a (Pa.s)**	**b (Pa)**	**R^2**
80	0.03455	-1.44	0.993	0.02057	-2.11	0.968
70	0.03984	-1.598	0.993	0.02342	-2.6	0.968
60	0.04376	-1.641	0.986	0.02567	-2.56	0.959
50	0.0467	-1.636	0.981	0.02776	-2.52	0.954
40	0.04433	-1.28	0.979	0.02953	-2.075	0.962
30	0.03582	-0.2925	0.999	0.03273	-0.6447	0.998
25	0.04016	-0.1752	0.999	0.03808	-0.3515	0.999

Table 2: Viscosity, yield stress and R^2 Relative to the Casson and Bingham Models.

	Ostwald-power Law model			Herschel-Buckley model			
Temperature (°C)	a (Pa.s)	n	R^2	a (Pa.s)	b (Pa)	p	R^2
80	0.0005352	1.527	0.998	0.0002969	0.42	1.61	0.999
70	0.0004879	1.558	0.998	0.0003548	0.2578	1.603	0.998
60	0.0005272	1.563	0.995	0.0001633	0.9635	1.729	0.998
50	0.0006456	1.547	0.991	0.0001088	1.514	1.8	0.996
40	0.001702	1.415	0.988	0.000249	1.865	1.688	0.993
30	0.01839	1.083	0.999	0.01368	0.5213	1.124	0.999
25	0.02741	1.048	0.999	0.01997	0.6792	1.092	1

Tableau 3 : Viscosity, yield stress and R^2 Relative to the Power Law and Herschel-Bulckley models.

In physics, there are no negative yield stresses. We notice, from the table 1-3, that the Casson and Bingham models generate negative values of yield stress but from the rheological curves fig. 6 we can easily extract that (phosphoric acid 54% clarified) has no flow threshold. The yield stress of phosphoric acid 54% is quite low, we can neglect it (b = 0), and if we neglect the yield stress (b) in the regression, this regression will not work properly. In the case of phosphoric acids we are interested only in viscosities, because we know that the yield stress are very low and considered null. So we extract from the tables the viscosity values for each model. From fig. 6 the rheological behavior of phosphoric acid 54% is Newtonian for the temperatures 25 ° C and 30 ° C, and Shear thickning (Dilatant) for the temperatures between (40 ° C and 80 ° C), for that the model of Bingham seems suitable for the temperatures (25 ° C - 30 ° C) with R^2 between (0.998 and 0.999).

3. 2. Clarified phosphoric acid 29% P_2O_5 of JORF (Density: 1225 g / l)

	Casson model			Bingham model		
Temperature (°C)	a (Pa.s)	b (Pa)	R^2	a (Pa.s)	b (Pa)	R^2
80	0.01213	-0.7621	0.995	0.007727	-0.7196	0.976
70	0.013	-0.7595	0.994	0.008441	-0.7508	0.977
60	0.01313	-0.7167	0.995	0.008759	-0.715	0.979
50	0.01515	-0.8675	0.995	0.009534	-0.8888	0.975
40	0.01693	-0.9084	0.995	0.0107	-0.9839	0.975
30	0.01973	-1.036	0.993	0.01212	-1.199	0.971
25	0.02024	-1.037	0.996	0.01256	-1.25	0.976

Tableau 4 : ***Viscosity, yield stress and R^2 Relative to the Casson and Bingham Models.***

	Ostwald-power Law model			Herschel-Buckley model			
Temperature (°C)	**a (Pa.s)**	**n**	**R²**	**a (Pa.s)**	**b (Pa)**	**p**	**R²**
80	0.0003404	1.45	0.998	0.000211	0.1356	1.517	0.999
70	0.0004322	1.428	0.998	0.0002549	0.1659	1.503	0.999
60	0.0005798	1.391	0.998	0.0003163	0.2027	1.477	0.999
50	0.0004074	1.454	0.998	0.0002461	0.1768	1.526	0.999
40	0.0004659	1.452	0.999	0.0002633	0.2233	1.533	0.999
30	0.0003864	1.497	0.998	0.0002158	0.2466	1.58	0.999
25	0.0004616	1.476	0.999	0.0003402	0.1408	1.519	0.999

Tableau 5:Viscosity, yield stress and R² Relative to the Power Law and Herschel-Bulckley models

In the case of phosphoric acid clarified 29% P_2O_5, it is quite remarkable in fig.7 that the rheological behavior of this acid is always Shear thickening for all temperatures. From a mathematical point of view, the Hershel-Buckley model is the most suitable for the description of the rheological profile of phosphoric acid 29% with $R^2 = 0.999$ for all temperatures. Followed by the Ostwal model (Power-Law) with R^2 between (0.998 and 0.999). Followed by the Casson model with R^2 between (0.993 and 0.996), and finally the Bingham model with R^2 in the vicinity of 0,97.

3. 3. Purified phosphoric acid 61% P_2O_5 (Density: 1720 g / l)

	Casson model			Bingham model		
Temperature (°C)	**a (Pa.s)**	**b (Pa)**	**R²**	**a (Pa.s)**	**b (Pa)**	**R²**
80	0.03983	-1.563	0.993	0.02368	-2.534	0.969
70	0.04774	-1.797	0.99	0.02738	-3.014	0.961
60	0.05193	-1.891	0.984	0.02942	-3.159	0.953
50	0.04891	-1.543	0.979	0.03053	-2.57	0.957
40	0.0399	-0.6664	0.987	0.03248	-1.322	0.983
30	0.04366	-0.2792	0.999	0.04043	-0.7135	0.998
25	0.05431	-0.3157	0.999	0.05025	-0.9075	0.998

Tableau 6 : Viscosity, yield stress and R² Relative to the Casson and Bingham Models.

	Ostwald-power Law model			Herschel-Buckley model			
Temperature (°C)	**a (Pa.s)**	**n**	**R²**	**a (Pa.s)**	**b (Pa)**	**p**	**R²**
80	0.0005544	1.542	0.999	0.000356	0.3618	1.604	0.999
70	0.0004527	1.593	0.997	0.0002248	0.627	1.692	0.998
60	0.0003973	1.624	0.995	0.0001156	1.106	1.8	0.997
50	0.0009928	1.498	0.989	0.0001595	1.739	1.758	0.995
40	0.008021	1.203	0.990	0.003101	1.331	1.336	0.992
30	0.0249	1.07	0.999	0.02057	0.4283	1.096	1
25	0.03069	1.071	0.999	0.02546	0.5199	1.097	1

Tableau 7 : Viscosity, yield stress and R² Relative to the Power Law and Herschel-Bulckley models

The purified phosphoric acid is obtained by passing the clarified phosphoric acid in nano filtration via membranes, the rheological behavior of this acid in the range (40°C - 80°C) is dilatant. Below 40°C the rheological behavior is linear (Newtonian). For this the three models, Hershel-Buckley, Ostwald, and Casson, seem suitable for the description of the rheological profile of purified phosphoric acid 61% for all temperatures (with R² in the vicinity of 0.99), except for the model of Bingham seems suitable only for temperatures below 40°C with R² between (0.983 and 0.998).

4. Deduction of values of the phosphoric acids viscosities at 80°C and 25°C

From the previous figures we have noticed that the (ACP 54%) of Jorf and Safi and the (APP 61%) have a linear rheological behavior without a yield at 25°C, at 80°C these acids have a dilatants rheological behavior and close at a linear behavior, this pushed us to report all the acids already mentioned to a linear behavior without yield to elaborate the value of the dynamic viscosity, the method is simple, it is enough to elaborate the slope of the linear trend curve approximated to the rheological curve.

Acids	Density en (g/l)	Dynamique viscosity at 25°C in (mPa.s)	Dynamique viscosity at 80°C in (mPa.s)
ACP 54% JORF	1608	37	17
ACP 54% SAFI	1652	49	21
ACP 29% JORF	1225	10	6
ACP 18% JORF	1031	5	3
APP 29%	1360	15	8
APP 61%	1720	48	19

Table 8: Viscosity values of all phosphoric acids at 25°C and 80°C.

(APP) means (purified phosphoric acid)

5. Fluid-flow activation energy of phosphoric acids

The activation energy of a fluid is a parameter that describes the mechanical stability of this fluid, the elaboration of this parameter is done through the regression of the Arrhenius equation to the experimental data of the variation of the viscosity according to the temperature.

Arrhenius equation: $\boldsymbol{\eta = A.\exp(\frac{E}{R.T})}$

With: η the relative viscosity, E: the activation energy, R: the perfect gas constant, T: the temperature, A: a coefficient of adjustment.

The regression of the Arrhenius equation to the viscosity curves as a function of the temperature of the (ACP 54) and the (ACP 29), we generate the values of activation energy.

Ea(ACP 54) = 9,262 Kj/mol

Ea(ACP 29) = 7,851 Kj/mol

The activation energy of the (ACP 54) is greater than that of the (ACP 29), which validates our previous assumptions that the (ACP 54) is more stable than the (ACP 29).

6. Conclusion

In this chapter, we have elaborated the rheological behaviors of various types of phosphoric acids and the impact of temperature on these rheological behaviors. We found that the rheological behavior of phosphoric acid 54% of SAFI is dilatant in the range temperatures (80 ° C - 50 ° C) and Newtonian in the range (40 ° - 25 ° C). For phosphoric acid 54% JORF, the rheological behavior is dilatant over the range (40 ° C - 80 ° C) and Newtonian over (30 ° C - 25 ° C). Phosphoric acid 29% often behaves dilatant whatever the temperature. With regard to the purified phosphoric acid (APP 61%), its rheological behavior is dilatant over the range (40 ° C - 80 ° C), down from 40 ° C the rheological behavior is linear (Newtonian). It has thus been noted that all these phosphoric acids have a rheological behavior without yield stress. As regards the effect of the density of phosphoric acid on the viscosity, it has been very remarkable that the viscosity of phosphoric acid increases slowly between 1030 g / L and 1440 g /L. Beyond 1440 g /L viscosity begins to increase exponentially. The diversity of the original phosphate on the rheological behavior of phosphoric acids has been studied in this chapter.

For the impact of the proportion of (MgO) in phosphoric acids, we found that MgO has a very remarkable influence on the rheology and viscosity of phosphoric acids. In general there is a non-proportionality between the addition of (MgO) in the acid and viscosity of this acid. This has been attributed to the creation of new particle in phosphoric acid such as $MgSO_4$, $MgSiF_6$, $MgAlF_5$ and MgF_2. This is due to a reaction of the (MgO) added with impurities contained in the phosphoric acid, and consequently it affects its rheology.

A modeling of the rheological profiles obtained experimentally was realized through the regression of these profiles to the empirical models of Casson, Bingham, Ostwald, and Hershel-Buckley. This is to identify the rheological parameters and viscosities relative to each model. We thus identified the activation energy of the fluid of various phosphoric acids through the Arrhenius equation.

General conclusion

In this thesis, we have carried out a modeling of phosphate slurry flow behavior through the Khouribga-Jorf-Lasfar pipeline in order to predict the behavior of head losses during the flow of phosphate slurry through the pipeline, based on the physical properties of the slurry that are: density, viscosity, flow rate and choke. We noticed that all these parameters had an important impact on the behavior of head losses which had done through the modeling and simulations that we have conducted.

We aimed to go further with the study of physical properties of phosphate slurry by elaborating a thorough rheological study of slurry. We had found interesting results in which the viscosity of the phosphate slurry has decreased with the dilution. Moreover, for smaller grain particles in the slurry, the solution became viscous. We found that the phosphate suspension changed its pseudoplastic behavior towards a Bingham behavior from the 46.03% concentration. It changed its Bingham behavior to a dilatant behavior from the 38.45% concentration. We also showed the influence of additives, flocculant, Ester, Amine and dispersant (STPP) on the rheology of phosphate slurry. Regarding modeling, we concluded that the Herschel-Buckley model is suitable for the description of the rheological behavior of phosphate slurry. Herschel-Buckley model is also suitable for the calculation of apparent viscosity and yield point for low concentrations (less than 38.45%). The Bingham model is suitable for the range of concentrations (34.24% to 46.03%). The Casson model is suitable for modeling the rheological behavior of this slurry and also for calculating the viscosity and the yield stress for the concentration range (46.03% - 57.27%).

Concerning products derived from phosphate slurry generated during the process of manufacture of phosphoric acid, which are (phosphogypsum-slurry, phosphoric acids and sludge). Phosphogypsum-Slurry has a dilatant rheological behavior (shear-thickening), whatever the temperature is. The viscosity of the Phosphogypsum-Slurry increases with the decrease of the temperature between 80°C and 60°C. Between 60°C and 50°C the viscosity decreases. Beyond 50°C the viscosity began to increase again. This is due to the change in size of agglomerates of gypsum crystals. We thus evaluated the effect of the rate of crystal solids in the Phosphogypsum-Slurry on its rheological behavior, either at 80°C or 70°C. The viscosity of the phosphogypsum-slurry began to increase carefully between 30% and 33% in solid rates. Beyond the viscosity of the Phosphogypsum-Slurry has decreased exponentially. We found that the rheological behavior of phosphoric acid 54% of SAFI is dilatant in the temperatures range (80°C - 50°C) and Newtonian

in the range (40°C - 25°C). For phosphoric acid 54% JORF, the rheological behavior is dilatant over the range (40°C - 80°C) and Newtonian over (30°C - 25°C). Phosphoric acid 29% often behaves dilatant whatever the temperatures is. With regard to the purified phosphoric acid (APP 61%), its rheological behavior is dilatant over the range (40°C - 80°C), down from 40°C the rheological behavior is linear (Newtonian). It has thus been noted that all these phosphoric acids have a rheological behavior without yield stress. Modeling using empirical rheological models was performed to identify the viscosity values relative to each model for the phosphogypsum-slurry and phosphoric acids.

REFERENCES

[1] M.E. Cates, S.J. Candau, J. Phys. Cond. Matter, 2, 6869, (1990)
[2] Poré, "Les dispersions aqueuses : suspensions, émulsions, mousses", Société des Publications Le Cuir, Paris, (1976).
[3] H. Mollet et A. Grubenmann "Formulation technology : Emulsions, suspensions, solid forms", Wiley-VCH, Weinheim, (2001).
[4] P. Coussot ant C. Ancey. "Rheophysical classification of concentrated suspensions and granular pastes", Phys. Rev. E, 59, 4445-4457, (1999).
[5] H. Lombois et al., "Sur le rôle ambigu de la lubrification dans la rhéologie des pâtes granulaires" Rhéologie, 7, 11-21, (2005).
[6] H. Van Damme, S. Mansoutre, P. Colombet, C. Lesaffre, D. Picart. "Pastes: lubricated and cohesive granular media". C.R. Physique, 3, 229-238, (2002).
[7] P. Somasundaran, S. Shrotri, Grinding aids "a review of their use, effects and mechanisms, Selected Topics in Mineral Processing", New Age International Publishers, India, pp. 47 – 70, (1995).
[8] M. Gao, E. Forssberg, "The influence of slurry rheology on ultrafine grinding in a stirred ball mill", 18th International Mineral Processing Congress, Sydney, CA (Conference Article), Australian, pp. 237 – 244, (1993).
[9] Y. Wang, E. Forssberg, "Dispersants in stirred ball mill grinding", Kona 13 67 – 77, (1995).
[10] Jie Zheng, Colin C. Harris, P. Somasundaran, "The effect of additives on stirred media milling of limestone", Powder Technology 9,1 173 – 179, (1997).
[11] G.A. Banini, R.A. Bearman, "Application of fuzzy cognitive maps to factors affecting slurry rheology", International Journal of Mineral Processing 52, 233–244, (1998).
[12] Hua-Gui Yang, Chun-Zhong Li, Hong-chen Gu, Tu-Nan Fang, "Rheological behavior of titanium dioxide suspensions", Journal of Colloid and Interface Science 236, 96–103, (2001).
[13] C. Bernhardt, E. Reinsch, K. Husemann, "The influence of suspension properties on ultra–fine grinding instirred ball mills", Powder Technology 105, 357 – 361, (1999).
[14] N. Mangesana, R.S. Chikuku, A.N. Mainza, I. Govender, A.P. van der Westhuizen, and M. Narashima, "The effect of particle sizes and solids concentration on the rheology of silica sand based suspensions", The Journal of The Southern African Institute of Mining and Metallurgy, (2008).
[15] Firouzi, J., Akbar Yousefi, A. & Langroudi, A.E., "Rheological Behaviour of Metal powder Suspensions under Dynamic loading", Iranian Polymer Journal, vol. 15(2), pp. 127-134, (2006).
[16] Pradipta Kumar Senapati, Dibakar Panda , Ashutosh Parida, "Predicting Viscosity of Limestone–Water Slurry", Journal of Minerals & Materials Characterization & Engineering, Vol. 8, No.3, pp 203-221, (2009).
[17] S. K. Mishra , P. K. Senapati & D. Panda, "Rheological Behavior of Coal-Water Slurry", Energy Sources, 24:159–167, (2002).
[18] C. Tangsathitkulchai, L.G. Austin, "Rheology of concentrated slurries of particles of natural size distribution produced by grinding", Powder Technology 56 293–299, (1988).
[19] C. Logos, Q.D. Nguyen, "Effect of particle size on the flow properties of a South Australian coal–water slurry", Powder Technology 88, 55–58, (1996).
[20] Hua-Gui Yang, Chun-Zhong Li, Hong-chen Gu, Tu-Nan Fang, "Rheological behavior of titanium dioxide suspensions", Journal of Colloid and Interface Science 236, 96–103, (2001).
[21] P. Somasundaran, Brij M. Moudgil (Eds.), "Grinding aids based on slurry rheology control, Reagents in Mineral Technology", Surfactant Science Series, New York, vol. 27, (1988).
[22] C. Tangsathitkulchai, "The effect of slurry rheology on fine grinding in a laboratory ball mill", International Journal of Mineral Processing 1587, 1 – 19, (2002).
[23] F.N. Shi, T.J. Napier-Munn, "A model for slurry rheology", International Journal of Mineral Processing 47, 103 – 123, (1996).
[24] Garcia, F., Bolay, N. le. & Frances, C., "Rheological behaviour and related granulometric properties of dense aggregated suspensions during an ultrafine comminution process", Powder Technology.130, 407-414, (2003).
[25] Tangsathitkulchai, C., Austin, L.G., "Rheology of concentrated slurries of of natural size distribution produced by grinding", Powder Technology, vol. 56, pp. 293- 299, (1988).

[26] T. Lemke, F. Bagusat, K. Kfhnke, K. Husemann, H.-J. Mfgel, "Time dependent viscosity of concentrated alumina suspensions, Colloids and Surfaces", A Physicochemical and Engineering Aspects 150, 283–287, (1999).
[27] Graeme L. Lane, "CFD modeling of a stirred bead mill for fine grinding", Second International Conference on CFD in the Minerals and Process Industries, Melbourne, Australia, pp. 449 – 454, (1999).
[28] Hua-Gui Yang, Chun-Zhong Li, Hong-chen Gu, Tu-Nan Fang, "Rheological behavior of titanium dioxide suspensions", Journal of Colloid and Interface Science 236, 96–103, (2001).
[29] P. Mikula´sˇek, R.J. Wakeman, J.Q. Marchant, "The influence of pH and temperature on the rheology and stability of aqueous titanium dioxide dispersions", Chemical Engineering Journal 67, 97–102, (1997).
[30] M. Gao, E. Forssberg, "The influence of slurry rheology on ultrafine grinding in a stirred ball mill", 18th International Mineral Processing Congress, Sydney, CA (Conference Article), Australian, pp. 237 – 244 (1993).
[31] Yamaguchi, K., M. Senna, and H. Kuno. "Effect of temperature on the flow properties of suspensions", J. Colloid Interface Sci. 70(3):584, (1979).
[32] Gao. M., Forsberg. E., "The influence of slurry rheology on the ultra-fine grinding in a stirred ball mill", Proceedings of XVIII International Mineral Processing Congress, Sydney, Australia, vol.2. pp. 237-244, (1993).
[33] T.H. Muster, C.A. Prestidge, "Rheological investigations of sulphide mineral slurries", Minerals Engineering 8, 1541 – 1555, (1995).
[34] C.A. Prestidge, "Rheological investigations of galena particle interactions", Colloids and Surfaces. A, Physicochemical and Engineering Aspects 126, 75–83, (1997).
[35] Clive A. Prestidge, "Rheological investigations of ultrafine galena particle slurries under flotation-related conditions", International Journal of Mineral Processing 51, 241–254, (1997).
[36] S. Vallar, D. Houivet, J. El Fallah, D. Kervadec, J.-M. Haussonne, "Oxide slurries stability and powders dispersion: optimization with zeta potential and rheological measurements", Journal of the European Ceramic Society 19, 1017–1021, (1999).
[37] P. Mikula´sˇek, R.J. Wakeman, J.Q. Marchant, "The influence of pH and temperature on the rheology and stability of aqueous titanium dioxide dispersions", Chemical Engineering Journal 67, 97–102, (1997).
[38] Stephen B. Johnson, George V. Franks, Peter J. Scales, David V. Boger, Thomas W. Healy, "Surface chemistry–rheology relationships in concentrated mineral suspensions", International Journal of Mineral Processing 58, 267 – 304, (2000).
[39] C.A. Prestidge, "Rheological investigations of galena particle interactions", Colloids and Surfaces. A, Physicochemical and Engineering Aspects 126, 75–83, (1997).
[40] Zhongwu Zhou, Peter J. Scales, David V. Boger, "Chemical and physical control of the rheology of concentrated metaloxide suspensions", Chemical Engineering Science 56, 2901 – 2920, (2001).
[41] Kaji, R., Y. Muranaka, H. Miyadera, and Y. Hishinuma. "Effect of electrolyte on the rheological properties of coal-water mixture". A glimpse into mineral matter in Indian coals. AIChE J. 33(1):11, (1987).
[42] Heimenz, P. C. "Principles of Colloids and Surface Chemistry", New York: Dekker, (1986).
[43] Boger, D. V., Y. K. Leong, G. B. Christie, and D. E. "Mainwaring. Flow behavior of high solids brown coal-water suspensions as liquid fuels". Proc. AusIMM Annual Conf. Coal Power ’87, New Castle, Australia (1987).
[44] Kaji, R., Y. Muranaka, H. Miyadera, and Y. Hishinuma. "Effect of electrolyte on the rheological properties of coal-water mixture". A glimpse into mineral matter in Indian coals. AIChE J. 33(1):11, (1987).
[45] Verwey, E. J. W. "Theory of the stability of lyophobic colloids". J. Phys. Colloid Chem. 51:631, (1947).
[46] Ismail, H. M. "Turbulent transfer mechanism and suspended sediment in closed channels". American Society of Civil Engineers, Transactions, 117:409-434, (1952).
[47] Vanoni, Vito A. "Transportation of suspended sediment by water". American Society of Civil Engineers. Transactions, 111:67-133, (1946).
[48] Chamberlain, A. R. "Effect of boundary form on fine sand transport in twelve-inch pipes". Colorado Agricultural and Mechanical College. Department of Civil Engineering. CBR No. SSARC 6 Colo, (1955).
[49] Wilson, W. B. "Mechanics of flow, with non-colloidal inert solids". American Society of Civil Engineers. Transactions, 107:1576- 1586, (1942).

[50] O'Brien, M. P. and Polsom, R. G. "The transportation of sand in pipe lines". California. University. Publications in engineering, 3:343-384, (1937).
[51] Craven, J. P. "The transportation of sand in pipes~ I. Full pipe flow". In Hydraulic Conference. Iowa City. proceedings,. (Iowa University. Studies in Engineering, Bulletin 34) S:67-77, (1953).
[52] Durand, R. "Basic relationships of the transportation of solids in pipes - experimental research", Minnesota International Hydraulics Convention. Proceedings, 19S3:89-l03.
[53] Ambrose, H. H. "The transportation of sand in pipes: II. Free surface flow", Hydraulics Conference, Iowa City. (Iowa University, Studies in Engineering, Bulletin 34) . proceedings 5:77-88, (1953).
[54] Chamberlain, A. R. "Effect of boundary form on fine sand transport in twelve-inch pipes". Colorado Agricultural and Mechanical College. Department of Civil Engineering. CBR No. SSARC 6, (1955).
[55] Ying Cheng ans al., "Cyber-physical integration for moving digital factories forward towards smart manufacturing: a survey", The International Journal of Advanced Manufacturing Technology, (2018).
[56] Andreja Zupancic, Romano Lapasin, Annika Kristoffersson, "Influence of particle concentration on rheological properties of aqueous a– Al2O3 suspensions", Journal of the European Ceramic Society 18 467–477, (1998).
[57] C. Tangsathitkulchai, "The effect of slurry rheology on fine grinding in a laboratory ball mill", International Journal of Mineral Processing 1587, 1 – 19, (2002).
[58] Richard Klimpel, "Laboratory studies of the grinding and rheology of coal–water slurries", Powder Technology 32, 267–277, (1982).
[59] T. Lemke, F. Bagusat, K. Kfhnke, K. Husemann, H.-J. "Mfgel, Time dependent viscosity of concentrated alumina suspensions, Colloids and Surfaces", A, Physicochemical and Engineering Aspects 150, 283–287, (1999).
[60] T.H. Muster, C.A. "Prestidge, Rheological investigations of sulphide mineral slurries", Minerals Engineering 8, 1541 – 1555, (1995).
[61] Jacobs, B.E.A., " Design of Slurry Transport Systems", pp. 285–286, (1991).
[62] Abulnaga, B. "Slurry Systems Handbook. McGraw-Hill", New York, (2002).
[63] Miedema, S.A.,"Slurry Transport: Fundamentals, a Historical Overview and The Delft Head Loss & Limit Deposit Velocity", Edited by Robert C. Ramsdell, (2016).
[64] Gray, J.Johann Heinrich Lambert, "mathematician and scientist", Hist. Math. 5(1), 1728– 1777, (1978)
[65] Moody, L.F, "Friction factors for pipe Flow". Trans. ASME 66(8), 671–684, (1944)
[66] Guyon, É., Hulin, J.-P., Petit, L, "Ce que disent les fluides", Belin, (2005)
[67] Saatdjian, E, "Les bases de la mécanique des fluides et des transferts de chaleur et de masse pour l'ingénieur". Éditions Sapientia, (2009).
[68] Rusconia, J., Lakhouajab, A., Kopuzc, M, "The design and engineering of the 187 km Khouribga to Jorf Lasfar Phosphate Slurry Pipeline", In: SYMPHOS 2015 - 3rd International Symposium on Innovation and Technology in the Phosphate Industry, Procedia Engineering, Elsevier, pp. 142–150., (2016)
[69] Baudez "Rheology of aging, concentrated, polymeric suspensions: Application to pasty sewage sludges", Journal of Rheology, (2001).
[70] He, M., Wang, Y. & Forssberg, E., "Slurry rheology in wet ultra-fine grinding of industrial minerals: a review", Powder Technology. Vol. 147, pp. 267-304, (2004).
[71] Henderson, C. B., R. S. Scheffee, and E. McHale. Energy Progr. 3:69, (1983).
[72] Firouzi, J., Akbar Yousefi, A. & Langroudi, A.E., "Rheological Behaviour of Metal powder Suspensions under Dynamic loading", Iranian Polymer Journal, vol. 15(2), pp. 127-134, (2006).
[73] Kim , D. C., S. H. Cho, S. K. Kang, and D. H. Shin, Proc. Fifth Int. Symp. Coal Slurry Combust. and Technol. , Tampa, FL, p. 757, (1983).
[74] Papachristodoulou, G., and O. Trass. "Coal slurry fuel technology". Can. J. Chem. Eng. 65:177, (1987).
[75] Swain, P., and D. Panda. "Rheology of coal-water mixture", Fuel Sci. and Technol. Int'l.14(9):1237, (1996).
[76] Tangsathitkulchai, C., Austin, L.G., "Rheology of concentrated slurries of natural size distribution produced by grinding", Powder Technology, vol. 56, pp.293-299, (1988).
[77] Casson N. "A flow equation for pigment oil suspension of the printhing ink type". In pergament presse, Edition New York, Vol. 24, (1959).
[78] Rauwendaal,C. 2001. "Polymer Extrusion", 4rd end. New York, USA :Hanser Gardner Press.

[79] Raleigh and Aplan. “The Use of Mineral Matter Dispersants and Depressants During the Flotation of Bituminous Coals”, Coal Science and Technology Volume 21, Pages 71-90 (1993).
[80] Becker, P., “Phosphates and phosphoric acid: raw materials, Technology and Economics of the Wet Processes” Marcel Decker Inc., New York, (1989).
[81] Slimane Manar, "Increasing the filtration rate of phosphor-gypsum by using mineral additives". “SYMPHOS 2015”, 3rd International Symposium on Innovation and Technology in the Phosphate Industry, Procedia Engineering, ELSEVIER, (2015).
[83] M.Roustan, J.C.Pharamond, et A.Line, J 3 800 , "Agitation. Mélange" , concepts théoriques de base. Technique de l’ingénieur, pp.7-11, (2002).
[84] Commission Européenne, "Grands volumes de produits chimique inorganiques ammoniac, acides et engrais", publiée par la Commission européenne, pages 262-287, (2007).
[85] Dimensionnement d’un réacteur agité, Application au transfert thermique, www.iut- tlse3.fr, consulté 17.05.2018.
[86] Peter M. Cole, "The recovery of rare earth oxides from a phosphoric acid by-product. Part 1: Leaching of rare earth values and recovery of a mixed rare earth oxide by solvent extraction", Hydrometallurgy, Pages 1-19, (1996).
[87] T.F. A1-Fariss and al, "Comparison between acidulation by sulfuric acid and by phosphoric acid for phosphate rock", Fertilizer Research, KluwerAcademic Publishers. Printedin the Netherlands, 29: 209-227, (1991).
[88] M. Lassis and al, "Dissolution of Djebel Onk phosphate ore using sulfuric acid, Environmental Nanotechnology", Monitoring & Management 4, 12–16, (2015).
[89] Khamaïs Brahim and al, "Effect of temperature on the attack of fluorapatite by a phosphoric acid solution", Scientific Research and Essay Vol. 3 (1), pp. 035-039, (2008).
[90] Roseli F.Gennari and al, "Phosphogypsum analysis: total content and extractable element cencentrations", 2011 International Nuclear Atlantic Conference - INAC 2011 Belo Horizonte,MG, Brazil, October 24-28, (2011).
[91] J Mulopo and D Ikhu-Omoregbe, "Phosphogypsum Conversion to Calcium Carbonate and Utilization for Remediation of Acid Mine Drainage", Chemical Engineering & Process Technology, (2012).
[92] Doudou Fam ans al, "Rheology and Flow of Phosphate Slurries (Mine Tailings) in Pipes", Chem. Eng. Technol. 10, 305-311, (1987).
[93] H. El-Didamony and al, "Treatment of phosphogypsum waste produced from phosphate ore processing", Journal of Hazardous Materials, 596–602 (2013).
[94] A. A. Sha ltout and al, "Developed Method for Spectroscopic Studies of Viscous Samples", Analytical Letters, 41: 3034–3048, (2008).
[95] J Kim and P Moin, "Application of a fractional-step method to incompressible Navier-Stokes equations", Journal of Computational Physics Volume 59, Issue 2, June 1985, Pages 308-323.
[96] KunXuKevin H.Prendergast, "Numerical Navier-Stokes Solutions from Gas Kinetic Theory", Journal of Computational Physics Volume 114, Issue 1, Pages 9-17, 1994.
[97] Thomas J.R.Hughes[a], Garth N.Wells , "Conservation properties for the Galerkin and stabilised forms of the advection–diffusion and incompressible Navier–Stokes equations", Computer Methods in Applied Mechanics and Engineering Volume 194, Issues 9–11, Pages 1141-1159, (2005).
[98] Desjardins, Benöit, "Regularity of weak solutions of the compressible isentropic navier-stokes equations", Communications in Partial Differential Equations Volume 22, Issue 5-6, (1997).
[99] Nigel Heywood and al, "Preliminary Design of 200mm and 300mm NB Distribution Pipelines for Phosphate Slurry at the Jorf Lasfar Terminal Facilities in Morocco", Proceedings of Hydrotransport 20 Conference, Melbourne, Australia, , pp 57 -72, (2017).
[100] Berry, M.C. Alaska pipeline. "The politics of oil and native land claims". United States: N. p,Web (1975).
[101] Belbsir H., El-Hami K."Modeling the Flow Behavior of Phosphate-Water Slurry Through the Pipeline and Simulating the Impact of Pipeline Operating Parameters on the Flow". In: Ezziyyani M. (eds) Advanced Intelligent Systems for Sustainable Development (AI2SD’2018). Advances in Intelligent Systems and Computing, vol 912. Springer, Cham, (2019).
[102] Belbsir, H., El-Hami, K., Soufi, A., "Study of the rheological behavior of the phosphate-water slurry and search for a suitable model to describe its rheological behavior". Int. J. Mech. Mechatron. Eng. IJMME-IJENS 18(04), 73–81, (2018).
[103] Hamza BELBSIR, Khalil EL-HAMI, Aziz SOUFI, "Modeling and simulation of the flow behavior of the phosphate slurry through the pipeline", ISTE Open Science, (2017).

ANNEXES: Scientific production during the course of my Ph.D thesis.

PUBLICATIONS

1. **Belbsir H**., El-Hami K, Mazouz H, "Study of the Rheological Behavior of Phosphate Slurry and Its Derivatives Products". In: Ezziyyani M. (eds) Advanced Intelligent Systems for Sustainable Development (AI2SD'2019). Advances in Intelligent Systems and Computing, vol 1104. Springer, (2020). [Scopus Indexation with Impact Factor].

2. **Belbsir H**., El-Hami K, "Modeling the Flow Behavior of Phosphate-Water Slurry Through the Pipeline and Simulating the Impact of Pipeline Operating Parameters on the Flow". In: Ezziyyani M. (eds) Advanced Intelligent Systems for Sustainable Development (AI2SD'2018). Advances in Intelligent Systems and Computing, vol 912. Springer, Cham, (2019). [Scopus Indexation with Impact Factor].

3. **Hamza BELBSIR**, Khalil EL-HAMI, Aziz SOUFI, "Study of the Rheological Behavior of the Phosphate-Water Slurry and Search for a Suitable Model to Describe its Rheological Behavior", International Journal of Mechanical & Mechatronics Engineering IJMME-IJENS Vol:18 No:04, (2018). [Scopus Indexation with Impact Factor].

4. **Hamza BELBSIR**, Khalil EL-HAMI, Aziz SOUFI, "Experimental investigations of rheological behavior of phosphate-water slurry", Sylwan Journal, Vol. 162, Issue 1, (2018). [Scopus Indexation with Impact Factor].

5. **Hamza BELBSIR**, Khalil EL-HAMI, Aziz SOUFI, "Modeling and simulation of the flow behavior of the phosphate slurry through the pipeline", ISTE Open Science, (2017).

COMMUNICATIONS AND PRESENTATIONS IN INTERNATIONAL AND NATIONAL CONFERENCES, CONGRESS

1. **Hamza BELBSIR**, Khalil EL-HAMI, Aziz SOUFI, "Modélisation du comportement de l'écoulement de la pulpe de phosphate à travers le pipeline". 5 ème édition de la « journée Doctorant », CEDoc Sciences et Techniques, FST Settat, 30 mars (2017).

2. **Hamza BELBSIR**, Khalil EL-HAMI, Aziz SOUFI, "Modeling and simulation of the flow behavior of the phosphate slurry through the pipeline with both continuous pompage and Batch cases" International Conference on Civil Engineering and Materials (ICCEM'2017), Al Hoceima Morocco, May, 11-12, (2017).

3. **Hamza BELBSIR**, Khalil EL-HAMI, Aziz SOUFI, "Study of the influence of the physical properties of phosphate water slurry on its rheological behavior", 6 ème édition de la « Journée Doctorant », CEDoc Sciences et Techniques, FST Settat, 5 Avril, (2018).

4. **Hamza BELBSIR**, Khalil EL-HAMI, Aziz SOUFI, "Modeling the rheological behavior of phosphate-water slurry", Third International Symposium on Dielectric Materials and Applications (ISyDMA'2018), Beni Mellal Morocco, April, 18-20, (2018).

5. **Hamza BELBSIR**, Khalil EL-HAMI, Hamid Mazouz, "Study of the rheological behavior of phosphate water slurry", Phosphate Days 2018 – International conference for research on Phosphate and Derivatives, Mohammed 6 Polytechnic University, Bengurir Morocco, November, 12-13, (2018).

6. **Hamza BELBSIR**, Khalil EL-HAMI, Aziz SOUFI, "Modeling the flow behavior of phosphate slurry through the pipeline and simulating the impact of pipeline operating parameters on the flow" – International conference for research on Phosphate and Derivatives, Mohammed 6 Polytechnic University, Benguerir, Morocco, November, 12-13, (2018).

7. **Hamza BELBSIR**, Khalil EL-HAMI, "Modeling the Flow Behavior of Phosphate-Water Slurry Through the Pipeline and Simulating the Impact of Pipeline Operating Parameters on the Flow", International Conference on Advanced Intelligent Systems for Sustainable Development, (AI2SD'2018), Tanger, Morrocco, July, 11 -14, (2018).

8. **Hamza BELBSIR**, Khalil EL-HAMI, Hamid MAZOUZ, "Study of the Rheological Behavior of Phosphate Slurry and Its Derivatives Products" International Conference on Advanced Intelligent Systems for Sustainable Development, (AI2SD'2019), Marrakech, Morrocco, July 8 – 11 (2019).

9. **Hamza BELBSIR**, Khalil EL-HAMI, Hamid MAZOUZ, "Study and modeling of the rheological behavior of phosphate slurry, phosphogypsum slurry and phosphoric acids", International Symposium on Innovation and Technology in the Phosphate Industry (SYMPHOS 2019), Mohammed 6 Polytechnic University, Benguerir, Morocco, October, 07 – 09, (2019).